Experimental and numerical analysis of ethanol fueled HCCI Engine

Harisankar Bendu

Department of Mechanical Engineering

National Institute of Technology Rourkela

Experimental and numerical analysis of ethanol fueled HCCI Engine

Dissertation submitted in partial fulfillment

of the requirements of the degree of

Doctor of Philosophy

In

Mechanical Engineering

By

Harisankar Bendu

(Roll Number: 512ME109)

based on research carried out

under the supervision of

Prof. S Murugan

July, 2017

Department of Mechanical Engineering

National Institute of Technology Rourkela

Department of Mechanical Engineering

National Institute of Technology Rourkela

July 12, 2017

Certificate of Examination

Roll Number: *512ME109*

Name: *Harisankar Bendu*

Title of Dissertation: *Experimental and numerical analysis of ethanol fueled HCCI Engine*

We the below signed, after checking the dissertation mentioned above and the official record book of the student, hereby state our approval of the dissertation submitted in partial fulfillment of the requirements of the degree of *Doctor of Philosophy* in *Mechanical Engineering* at *National Institute of Technology Rourkela*. We are satisfied with the volume, quality, correctness, and originality of the work.

S Murugan
Principal Supervisor

A Kumar
Member, DSC

S Mishra
Member, DSC

R K Sahoo
Member, DSC

A Avinash Kumar
External Examiner

K P Maity
Chairperson, DSC

Dayal Ramakrushna Parhi
Head of the Department

Department of Mechanical Engineering

National Institute of Technology Rourkela

Prof. S Murugan

Associate Professor

July 12, 2017

Supervisors' Certificate

This is to certify that the work presented in the dissertation entitled *Experimental and numerical analysis of ethanol fueled HCCI Engine* submitted by Harisankar Bendu, Roll Number 512ME109, is a record of original research carried out by him under oursupervision and guidance in partial fulfillment of the requirements of the degree of *Doctor of Philosophy* in*Mechanical Engineering*. Neither this dissertation nor any partof it has been submitted earlier for any degree or diploma to any institute or university inIndia or abroad.

S Murugan
Associate Professor

Declaration of Originality

I, *Harisankar Bendu*, Roll Number *512ME109* hereby declare that this dissertation entitled " Experimental and numerical analysis of ethanol fueled HCCI Engine" presents my originality work carried out as a doctoral student of NIT Rourkela and, to the best of my knowledge, contains no material previously published or written by another person, nor any material presents by me for the award of any degree or diploma of NIT Rourkela or any institution. Any contribution made to this research by others, with whom I have worked at NIT Rourkela or elsewhere, is explicitly acknowledged in the dissertation. Works of other authors cited in this dissertation have been duly acknowledged under the sections "Reference" or "Bibliography". I have also submitted my original research records to the scrutiny committee for evaluation of my dissertation.

I am fully aware that in case of any non-compliance detected in future, the Senate of NIT Rourkela may withdraw the degree awarded to me on the basis of the present dissertation.

July 12, 2017

NIT Rourkela *Harisankar Bendu*

Acknowledgment

The journey of reaching any milestone is never easy without a determined ambition, sincere dedication and a perfect person who can torch your path of ignorance. I am obliged to my supervisor Prof. S. Murugan, Associate professor, Department of Mechanical Engineering for being an embodiment of the constant source of inspiration and knowledge. Under the guidance, I have learnt the art of doing research and the real value of life.

I sincerely thank Prof. S.K Sarangi, former Director, NIT Rourkela for his motivational speeches at regular interval of my tenure. I also sincerely thank Prof. Amitesh Biswas, Director, NIT Rourkela for his support in submitting the thesis.

I express my sincere thanks to Prof. S.S. Mohapatra, former HOD, Department of Mechanical Engineering, NIT Rourkela for providing me the necessary facilities in the department. I also thank Prof. Dayal Ramakrushna Parhi, HOD, Department of Mechanical Engineering, for his support in submitting the thesis. I take this opportunity to express my deep sense of gratitude to the members of my Doctoral Scrutiny Committee members, Prof. K.P. Maity (Chairman), and Prof. R.K. Sahoo, Department of Mechanical Engineering, and Prof. A.Kumar, Department of civil engineering, and Prof. S. Mishra, Department of Chemical Engineering, for their constant encouragement and valuable suggestions while carrying out my research.

At the same time, I am thankful to the teaching staffs of the department, whose valuable suggestion at the right time helped me reaching the goal.

I sincerely acknowledge the helping hand of the laboratory staffs and other nonteaching staffs of NIT Rourkela, for their timely help and support. My friends, whose consolation during the bad days and encourage words, helped me maintain the equilibrium during the course of fulfilling my ambition.

Lastly, I must thank the invisible force which we define as the almighty god for giving me patience and driving me towards never ending process of learning.

July 12, 2017

NIT Rourkela *Harisankar Bendu*

Abstract

Presently, the research on the homogeneous charge compression ignition (HCCI) engines has gained importance in the field of automotive power applications due to its superior efficiency and low emissions compared to the conventional internal combustion (IC) engines. In principle, the HCCI uses premixed lean homogeneous charge that auto-ignites volumetrically throughout the cylinder. The homogeneous mixture preparation is the main key to achieve high fuel economy and low exhaust emissions from the HCCI engines. In the recent past, different techniques to prepare homogeneous mixture have been explored. The major problem associated with the HCCI is to control the auto-ignition over wide range of engine operating conditions. The control strategies for the HCCI engines were also explored. This dissertation investigates the utilization of ethanol, a potential majorcontributor to the fuel economy of the future.Port fuel injection (PFI) strategy was used to prepare the homogeneous mixture external to the engine cylinder in a constant speed, single cylinder, four stroke air cooled engine which was operated on HCCI mode.Seven modules of work have been proposed and carried out in this research work to establish the results of using ethanol as a potential fuel in theHCCI engine.Ethanol has a low Cetane number and thus it cannot be auto-ignited easily. Therefore, intake air preheating was used to achieve auto-ignition temperatures.

In the first module of work, the ethanol fueled HCCI engine was thermodynamically analysed to determine the operating domain. The minimum intake air temperature requirement to achieve auto-ignition and stable HCCI combustion was found to be 130 ℃. Whereas, the knock limit of the engine limited the maximum intake air temperature of 170 ℃. Therefore, the intake air temperature range was fixed between 130-170 ℃ for the ethanol fueled HCCI operation.

In the second module of work, experiments were conducted with the variation of intake air temperature from 130-170 ℃ at a regular interval of 10 ℃. It was found that, the increase in the intake air temperature advanced the combustion phase and decreased the exhaust gas temperature. At 170 ℃, the maximum combustion efficiency and thermal efficiency were found to be 98.2% and 43% respectively. The NO emission and smoke emissionswere found to be below 11 ppm and 0.1% respectively throughout this study. From these results of high efficiency and low emissions from the HCCI engine, the following were determined using TOPSIS method. They are (i) choosing the best

operating condition, and (ii) which input parameter has the greater influence on the HCCI output.

In the third module of work, TOPSIS - a multi-criteria decision making technique was usedto evaluate the optimumoperating conditions. The optimal HCCI operating condition was found at 70% load and 170 °C charge temperature.The analysis of variance (ANOVA) test results revealed that, the charge temperature would be the most significant parameterfollowed by the engine load. The percentage contribution of charge temperature and load were63.04% and 27.89% respectively.

In the fourth module of work, the GRNN algorithm was used to predict the output parameters of the HCCI engine. The network was trained, validated, and tested with the experimental data sets. Initially, the network was trained with the 60% of the experimental data sets. Further, the validation and testing of the network was done with each 20% data sets.The validation results predicted that, the output parameters those lie within 2% error.The results also showed that, the GRNN models would be advantageous for network simplicity and require less sparse data. The developed new tool efficiently predicted the relation between the input and output parameters.

In the fifth module of work, the EGR was used to control the HCCI combustion. An optimum of 5% EGR was found to be optimum, further increase in the EGR caused increase in the hydrocarbon (HC) emissions. The maximum brake thermal efficiency of 45% was found for 170 °C charge temperature at 80% engine load.The NO emission and smoke emission were found to be below 10 ppm and 0.61% respectively.

In the sixth module of work, a hybrid GRNN-PSO model was developed to optimize the ethanol-fueled HCCI engine based on the output performance and emission parameters.The GRNN network interpretive of the probability estimate such that it can predict the performance and emission parameters of HCCI engine within the range of input parameters. Since GRNN cannot optimize the solution, and hence swarm based adaptive mechanism was hybridized.A new fitness function was developed by considering the six engine output parameters. For the developed fitness function, constrained optimization criteria were implemented in four cases. The optimum HCCI engine operating conditions for the general criteria were found to be 170 °C charge temperature, 72% engine load, and 4% EGR. This model consumed about 60-75 ms for the HCCI engine optimization.

In the last module of work, an external fuel vaporizer was used to prepare the ethanol fuel vapour and admitted into the HCCI engine. The maximum brake thermal efficiency of 46% was found for 170 °C charge temperature at 80% engine load.The NO emission and smoke emission were found to be below 5 ppm and 0.45% respectively.

Overall, it is concluded that, the HCCI combustion of sole ethanol fuel is possible with the charge heating only. The high load limit of HCCI can be extended with ethanol fuel. High thermal efficiency and low emissions were possible with ethanol fueled HCCI to meet the current demand.

Keywords: HCCI, Ethanol, performance, combustion, emission, TOPSIS, GRNN, PSO.

Contents

List of Figures

List of Tables

Abbreviations

ADC	Analog to digital converter
ACO	Ant colony optimization
AHP	Analytic hierarchy process
ANN	Artificial neural networks
ANP	Analytical network process
ARC	Activated radical combustion
ATAC	Active-thermo atmosphere combustion
AKI	Antiknock index
BPNN	Back propagation neural networks
BMEP	Brake Mean Effective Pressure
CO_2	Carbon dioxide
CO	Carbon monoxide
CAD	Crank angle degree
CI	Compression ignition
DAS	Data acquisition system
DRE	Destruction or removal Efficiency
DEE	Diethyl ether
DME	Di-methyl ether
EGR	Exhaust gas recirculation
ECS	Energy conversion system
ECU	Electronic control unit
EU	European Union
EC	External combustion
FTP	Federal Test Procedure
GA	Genetic algorithm
GRNN	Generalized regression neural network
HTHR	High temperature heat release
HiMICS	Homogeneous charge intelligent multiple injection combustion system
IMEP	Indicated mean effective pressure
IC	Internal combustion
JFET	Junction field effect transistor
GHG	Global greenhouse gas
GHGs	Greenhouse gases
HCCI	Homogeneous charge compression ignition
LIVM	Low Impedance Voltage Mode
LTHR	Low temperature heat release
LTC	Low-temperature combustion
MON	Motor Octane Number
MOSFET	Metal-oxide semiconductor field-effect transistor
MVEG	Motor Vehicle Emissions Group-
MK	Modulated kinetics
MULDIC	Multiple stage diesel combustion
MCDM	Multi criteria decision making
NADI	Narrow angle direct-injection
NDIR	Non-dispersive infrared
NVO	Negative valve overlap
N	Nitrogen
NO_x	Oxides of nitrogen

NMHC	Non-methane hydrocarbon
N_2	Diatomic molecular nitrogen
OI	Octane Index
PSO	Particle swarm optimization
PM	Particulate matter
PCCI	Premixed charge compression ignition
PREDIC	Premixed lean diesel combustion
PAN	Peroxyacetyl nitrates
PFI	Port fuel injection
RBF	Radial basis function
RON	Research Octane Number
SCCI	Stratified charge compression ignition
SCSI	Stratified charge spark ignition
SI	Spark ignition
TOPSIS	Technique for order preference by similarity to ideal solution
TTL	Transistor-Transistor Logic
TDC	Top dead centre
THC	Total hydrocarbon
TS	Toyota-Soken
UNIBUS	Uniform bulky combustion system
UHC	Unburned hydrocarbon
VCR	Variable compression ratio
VVA	Variable valve actuation
WOT	Wide open throttle

Chapter 1

Introduction

1.1. General

Worldwide, the demand for energy is increasing exponentially with the increase in the population and improvement in living standards. The source of energy for almost in all the sectors including domestic, transportation etc. is still fossil fuels. The huge consumption of the fossil fuels is contributing the global greenhouse gas (GHG) emissions which cause an adverse effect on the public health and climate change. Internal combustion (IC) engines used in transportation, power generation, and commercial sector are one of the significant contributors to the air pollution. in order to overcome this situation, energy efficient combustion technologies are being explored and employed. Additionally, renewable alternative fuels might help in the reduction of global carbon emissions. This chapter discusses on the different energy conversion systems, air pollution and climate change, IC engines, emissions from the transportation sector, different alternative fuels used in transportation, and advanced combustion technologies.

1.2. Energy consumption and GHG emissions

The demand for energy increases with the growth in the economic and industrial development. Today, the combustion of fossil fuels in most of the countries accounts for more than two-thirds of its energy consumption which accounts two-thirds of the world's primary energy utilization [1]. Fig. 1.1 shows the world energy consumption by country and fuel source. China consumes 23% (approx. one-fourth) of the world's total energy consumption followed by the US consumes 17.3%. India consumes 5.6% of the total energy consumption. The fossil fuels contribute to the majority of the fuel consumption with sources of are oil, natural gas, and coal. It is apparent from the figure that, fossil fuel accounts 86% of the total energy consumption.

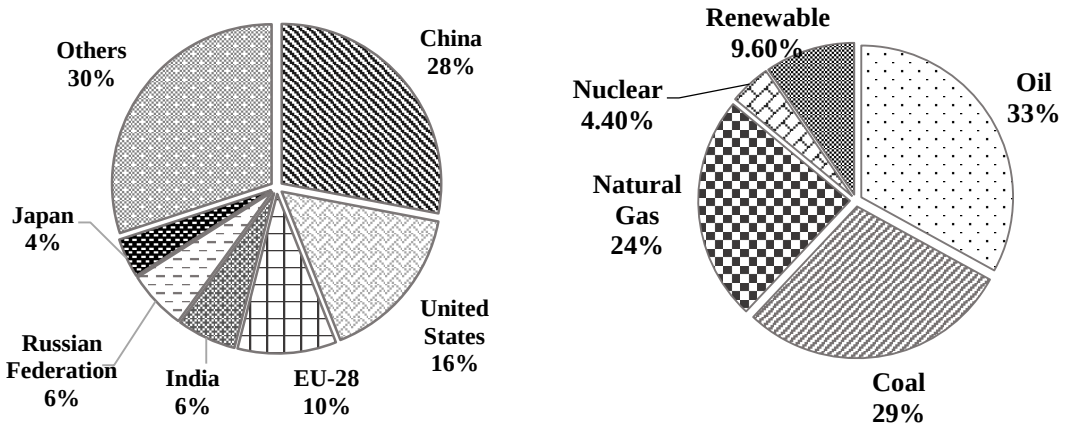

Fig. 1.1. World energy consumption (2015) by country and source [2].

The main concerns of the future energy strategies include the growing global population, the increasing population mobility, the increasing production and consumption of goods, and the goods transportation. Therefore, the need for efficient, clean, and inexpensive energy sources is perceived in contrast to the environmental and health issues connected with the use of fossil fuels. Fig. 1.2 shows the anthropogenic global green house gas (GHG) emissions by gas. Carbon dioxide (CO_2)is the main constituent in the GHG emissions by about 76%. F-gases refers to fluorinated gases, which include hydrofluorocarbons (HFCs), perfluorocarbons (PFCs), and sulfur hexafluoride (SF_6).

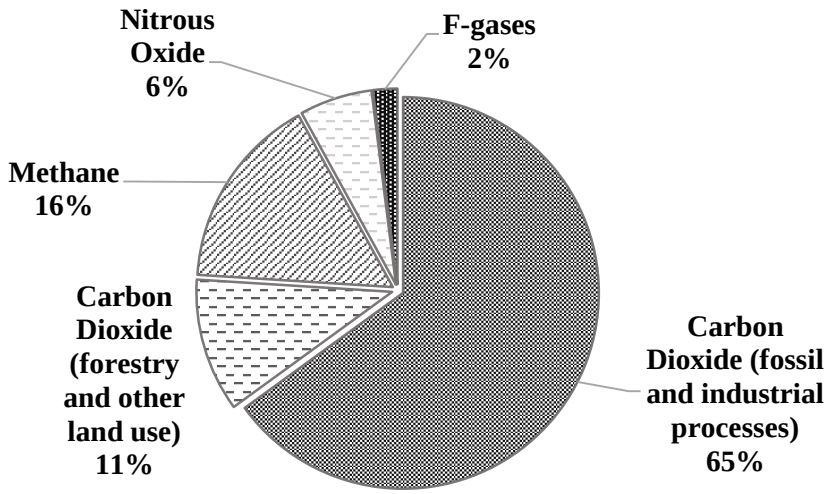

Fig. 1.2. Global GHG emissions by gas in 2010 [3].

The major sectors in which energy is consumed predominantly are; (i) power generation, (ii) transportation, (iii) agriculture, (iv) industrial, and (v) households. Fig. 1.3 shows the anthropogenic GHG emissions by economic sectors. The major GHG emission contributing sectors from the figure are electricity generation, agriculture, and industry. The transportation sector contributes 14% of the GHG emissions involve fossil fuels burned for the road, rail, air, and marine transportation. Almost all (95%) of the world's transportation energy comes from petroleum-based fuels, largely gasoline, and diesel.

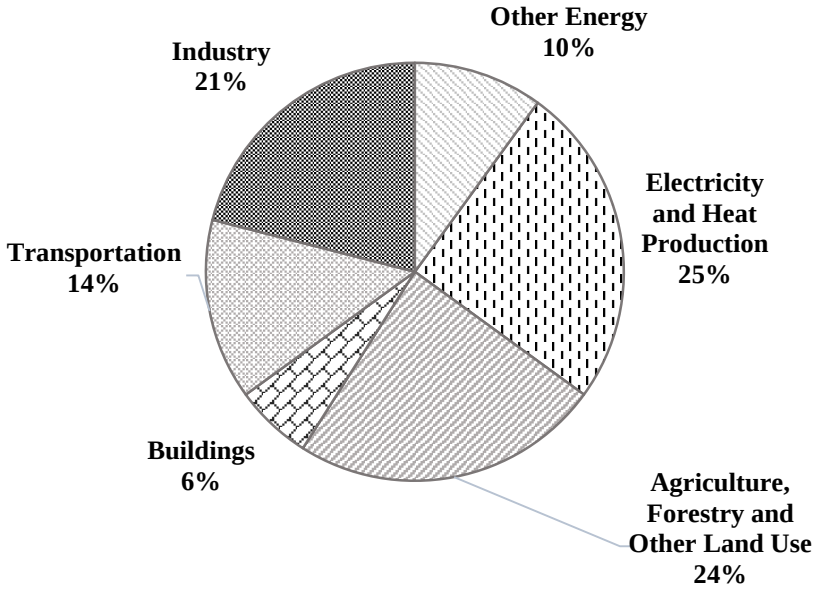

Fig. 1.3. GHG emissions by economic sectors in 2010 [3].

1.3. Air pollution and climate change

Poor air quality and climate change are two different phenomena, but having common causes of air pollutants from a variety of sources and activities. Fossil fuel combustion is the primary source of the both. Taking actions to reduce the pollution from fossil fuel burning will help improving air quality, and climate change. Air quality issues, such as ground-level ozone, particulate matter (PM), the release of other air contaminants and acid rain largely occur in the lowest part of the atmosphere which carries the air we breathe. Global climate change refers to changes in the climate of the earth as a whole, caused by human activities releasing an surplus of greenhouse gases (GHGs) into the atmosphere. This abnormal buildup of GHGs is warming the earth's atmosphere. Global atmospheric warming, in turn, is triggering major alterations in the global climate. A worldwide rise in

sea level associated with melting ice sheets and glaciers, and thermal expansion, is occurring. This is expected to accelerate in the fourth coming years.

1.4. Energy conversion systems

According to the first law of thermodynamics, energy can be converted from one form to another form. A system that transforms one form of energy to the human required energy form is termed as an energy conversion system (ECS). Fig. 1.4 shows the schematic representation of energy conversion system.

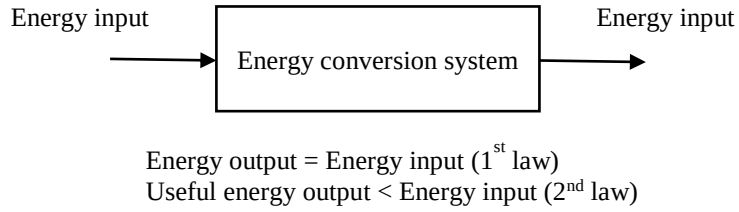

Fig. 1.4. Schematic representation of energy conversion system.

A heat engine is a device/machine which derives heat/chemical energy from the combustion of the fuel and converts into useful mechanical work. Based on the combustion of the fuel, heat engines are classified as external combustion (EC) and internal combustion (IC) engines. Fig. 1.5 shows the classification of heat engines. The advantages of IC engines over EC engines are compact, high power to weight ratio, safe to use, immediate startup, and high efficiency.

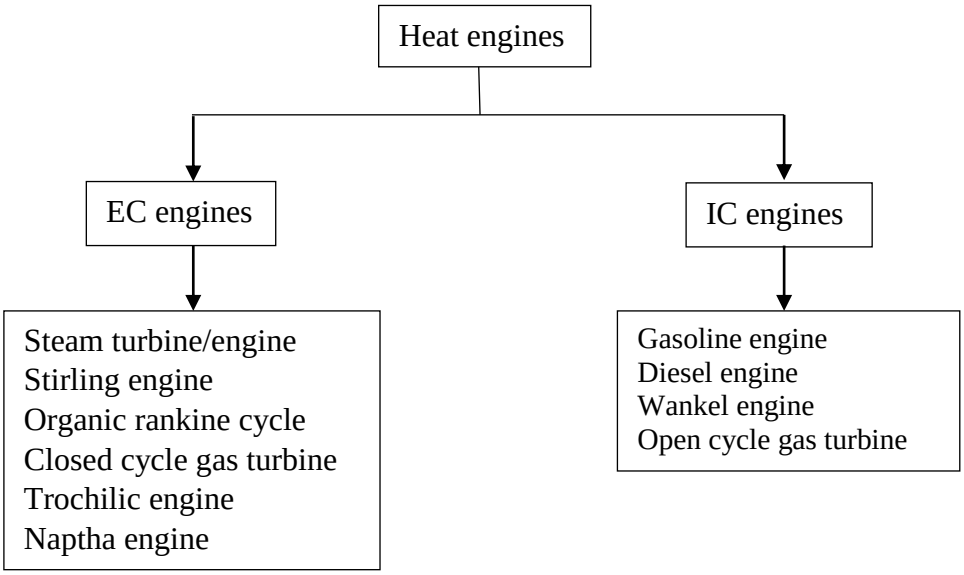

Fig. 1.5. Classification of heat engines.

1.5. IC engines

IC engines are the primary power horses in the automotive industries. Engines develop power by consuming an enormous amount of fuel by combustion, and emit harmful exhaust emissions such as unburned hydrocarbon (UHC), carbon monoxide (CO), carbon dioxide (CO_2), oxides of nitrogen (NO_x), and particulate matter (PM) [4]. The main advantage of spark ignition (SI) engines are low smoke emissions due to homogeneous air/fuel mixture preparation, peppy drive (smooth, light and easy to drive), low maintenance cost, small initial investment, top speed, short gears, and silent drive. The disadvantages of SI engines are low torque, low volumetric efficiency, low thermal efficiency, worst idling performance, and frequent servicing. The main advantage of compression ignition (CI) engines was high thermal efficiency due to its high compression ratio. Other advantages are high torque, high power, reliable, low CO emissions, and high part load efficiency. The disadvantages of CI engines are high noise, low speed, impossible retrofitting, high cost, and tradeoff emissions.

The majority of the automotive vehicles run on IC engines that consume huge fossil fuel consumption. The spark ignition (SI) and compression ignition (CI) engines under IC engines cause severe air pollution by releasing a variety of emissions into the atmosphere. Emissions that are released directly into the atmosphere from the tailpipes of automotive vehicles are the primary source of vehicular pollution. But, they also pollute the air during the processes of manufacturing, refueling, and from the emissions associated with oil refining and distribution of the fuel they burn [5].Primary pollution from motor vehicles is pollution that is emitted directly into the atmosphere, whereas secondary pollution results from chemical reactions between pollutants after they have been released into the air. The gases that contribute to global warming are related to the chemical composition of the Earth's atmosphere. Some of the gases in the atmosphere function like the panes of a greenhouse. These gases let some radiant heat in from the sun but do not let it all back out, thereby helping to keep the Earth warm. One of these important heat-trapping gasses is carbon dioxide (CO_2).

1.6. Emissions from transportation sector

The transportation sector includes the movement of people and goods by cars, trucks, trains, ships, airplanes, and other vehicles. The majority of GHG emissions from transportation are CO_2 emissions resulting from the combustion of fossil fuels in IC

engines. Despite many emission legislation policies and advanced combustion technologies, transportation sector remains as one of the major sources of air pollution. The emissions from the incomplete combustion of the petroleum fuels cause the deterioration of air quality and human health due to the formation of harmful pollutants such as oxides of nitrogen (NO_x), carbon monoxide (CO), particulate matter (PM) and soot. Transport is responsible for around half of all energy-related nitrogen oxide emissions (56 Mt in 2015) and is a major source of primary particulate matter (accounting for around 10% of total energy-related primary $PM_{2.5}$ emissions). Road transport is the largest source of the transportation sector's NO_X and primary PM emissions (58% and 73% of the total). In urban areas, the emission concentration from automotive vehicles is relatively higher than other sources due to intensive popullation. Also, the individual's exposure to the automotive emissions are high due to their exhaust pipes are close to the ground [1].

Table 1.1 EU emission standards for passenger cars [6].

Tier	**Date**	**CO**	**THC**	**NMHC**	**NO_x**	**HC+NO_x**	**PM**
Diesel							
Euro1	July 1992	2.72	-	-	-	0.97	0.14
Euro2	January 1996	1.0	-	-	-	0.7	0.08
Euro3	January 2000	0.64	-	-	0.50	0.56	0.05
Euro4	January 2005	0.50	-	-	0.25	0.30	0.025
Euro5	September 2009	0.50	-	-	0.180	0.230	0.005
Euro6	September 2014	0.50	-	-	0.080	0.170	0.005
Petrol (Gasoline)							
Euro1	July 1992	2.72	-	-	-	0.97	-
Euro2	January 1996	2.2	-	-	-	0.5	-
Euro3	January 2000	2.3	0.20	-	0.15	-	-
Euro4	January 2005	1.0	0.10	-	0.08	-	-
Euro5	September 2009	1.0	0.10	0.068	0.060	-	0.005
Euro6	September 2014	1.0	0.10	0.068	0.060	-	0.005

CO–carbon monoxide; THC–total hydrocarbon; NMHC–non-methane hydrocarbon

Crude oil accounts for more than 90% of transport energy demand (in final energy terms), with different oil products serving various modes of transportation, with differing implications for emissions. Over time, the share of diesel vehicles in some national light-duty vehicle fleets has grown. This phenomenon, which is referred to as dieselisation, is most pronounced in the countries of the European Union (EU). In European countries, policies that make diesel cars cheaper to purchase and operate than gasoline cars, including lower vehicle purchase and fuel tax rates, have contributed to this development.

Table 1.1 provides the emission standards for diesel and gasoline passenger cars. India has been following European emission norms for vehicles and fuels.

1.6.1. Nitrogen oxides (NO_x)

Diatomic molecular nitrogen (N_2) is a relatively inert gas that makes up about 80% of the air. However, the chemical element nitrogen (N), as a single atom, can be reactive and have ionization levels (referred to as valence states) from plus one to plus five. Thus nitrogen can form several different oxides. The family of NO_x compounds and their properties are listed in Table 1.2.

Table 1.2 Nitrogen oxides (NO_x).

Formula	**Name**	**Nitrogen valence**	**Properties**
N_2O	nitrous oxide	1	colorless gas water soluble
NO N_2O_2	nitric oxide dinitrogen dioxide	2	colorless gas slightly water soluble
N_2O_3	dinitrogen trioxide	3	black solid water soluble, decomposes in water
NO_2 N_2O_4	nitrogen dioxide dinitrogen tetroxide	4	red-brown gas very water soluble, decomposes in water
N_2O_5	dinitrogen pentoxide	5	white solid very water soluble, decomposes in water

Emissions of NOx from combustion are primarily in the form of NO. According to the Zeldovich equations, NO is generated to the limit of available oxygen (about 200,000 ppm) in air at temperatures above 1,300 °C. At temperatures below 760 °C, NO is either generated in much lower concentrations or not at all. Combustion NO is generated as a function of air to fuel ratio and is more pronounced when the mixture is on the fuel-lean side of the stoichiometric ratio (the ratio of chemicals which enter into reaction). The Zeldovich equations are:

$N_2 + O \rightarrow NO + N$

$N + O2 \rightarrow NO + O$

$N + OH \rightarrow NO + H$

In all combustion there are three opportunities for NOx formation. They are:

- **Thermal NOx** - The concentration of "thermal NOx" is controlled by the nitrogen and oxygen molar concentrations and the temperature of combustion. Combustion at temperatures well below 1,300 °C (2,370°F) forms much smaller concentrations of thermal NO_x.
- **Fuel NO_x** - Fuels that contain nitrogen (e.g., coal) create "fuel NO_x" that results from oxidation of the already-ionized nitrogen contained in the fuel.
- **Prompt NOx** - Prompt NOx is formed from molecular nitrogen in the air combining with fuel in fuel-rich conditions which exist, to some extent, in all combustion. This nitrogen then oxidizes along with the fuel and becomes NOx during combustion, just like fuel NOx. The abundance of prompt NO_x is disputed by the various writers of articles and reports - probably because they each are either considering fuels intrinsically containing very large or very small amounts of nitrogen, or are considering burners that are intended to either have or not have fuel-rich regions in the flame.

Table 1.3 NO_x Control Methods [7].

S.No.	**Emission Control Principle or Method**	**Successful Technologies**	**Pollution Prevention Method (P) or Addon Technology (A)**
1	Reducing peak temperature	Flue Gas Recirculation (FGR) Natural Gas Reburning Low NOx Burners (LNB) Combustion Optimization Burners Out of Service (BOOS) Less Excess Air (LEA) Inject Water or Steam Over Fire Air (OFA) Air Staging Reduced Air Preheat Catalytic Combustion	P P P P P P P P P P P
2	Reducing residence time at peak temperature	Inject Air Inject Fuel Inject Steam	P P P
3	Chemical reduction of NOx	Fuel Reburning (FR) Low NOx Burners (LNB) Selective Catalytic Reduction (SCR) Selective Non-Catalytic Reduction (SNCR)	P P A A
4	Oxidation of NOx with subsequent absorption	Non-Thermal Plasma Reactor Inject Oxidant	A A
5	Removal of nitrogen	Oxygen Instead of Air Ultra-Low Nitrogen Fuel	P P

6	Using a sorbent	Sorbent in Combustion Chambers Sorbent In Ducts	A A
7	Combinations of these Methods	All Commercial Products	P and A

Many new combustion systems incorporate NO_x prevention methods into their design and generate far less NO_x then similar but older systems. As a result, considering destruction or removal Efficiency (DRE) for NO_x may be inappropriate. Comparing estimated or actual NOx emissions from a new, well-designed system to NO_x emitted by a similar well-controlled and operated older system may be the best way of evaluating how effectively a new combustion system minimizes NO_x emissions. Table 1.3 lists principles or methods that are used to reduce NO_x. Basically there are six principles, with the seventh being an intentional combination of some subset of the six.

1.6.2. Particulate matter (PM)

The unburned carbon particles, engine oils, debris, soot andash particulates are known as particulate matter (PM). This diesel particulate matter (DPM) is the visible cloud of blacksmoke that appears from engine start-up and continues to appearwhen the engine is running. PM_{10} are particles from 2.5microns to 10 microns, $PM_{2.5}$are particles less than 2.5microns.

A Diesel Particulate Filter (DPF) is a device that traps the exhauststream particulate matter by means of physical filtration. Thisprocess is an established, efficient and effective way of removingDPM from the exhaust stream. Once captured, the accumulatedDPM must then be dealt with in a safe and secure manner.There are two solutions to this problem. One is to remove andreplace the filter with a fresh one; the second method is toregenerate the filter so it can be reused.

1.7. Potential liquid alternative fuels

The ECS can use both non-conventional and conventional sources of energy. The energy generated by using wind, tides, solar, geothermal heat and biomass are known as renewable energy. All these sources are renewable or inexhaustible and do not cause environmental pollution. The main problems associated with the non-conventional sources of energy are the uncertainty over a period of availabilityand the difficulty of transporting

this form of energy to the place of its end use. Fig. 1.6 shows the conventional and renewable sources of energy.

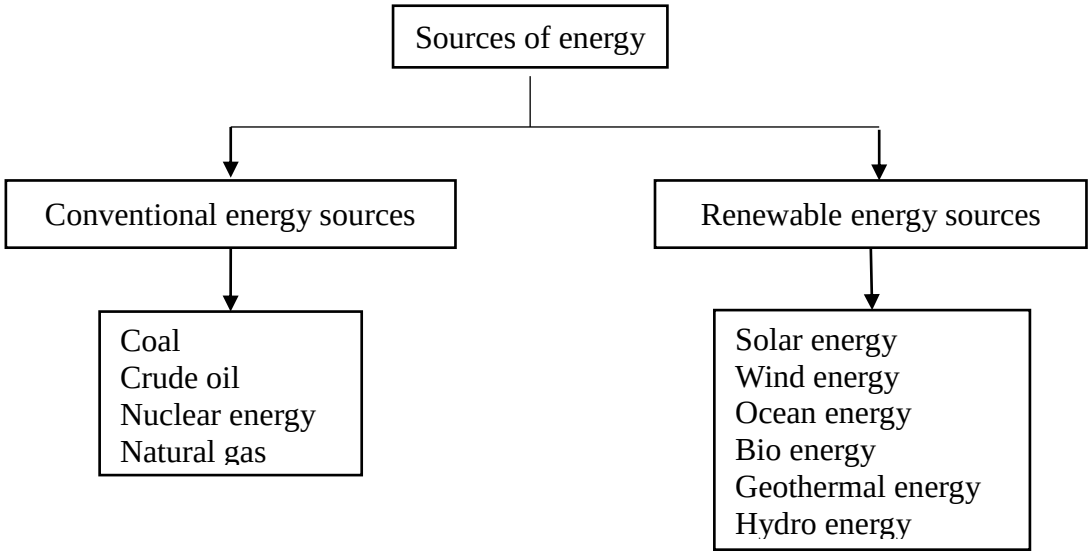

Fig. 1.6. Non-conventional and conventional sources of energy.

The reserves of the crude oils are depleting exponentionally due to the increase in the energy demand. The sustainable development is possible with the utilization of "green energy" obtained from the alternative fuel sources. The transformation for the utilization of alternative energy sources in the transportation sector is difficult with respect to its energy efficiency, and clean combustion process remains an important research topic. The influencing factors for the transformation of the alternative energy sources are (i) energy independence, (ii) possible decreases in the emissions of CO_2, soot, and unburned hydrocarbons (UHC), and (iii) fuel sources like agricultural residue, food waste, scrap tyres [8] and algae biomass. The use of alternative liquid fuels in IC engines causes conflict with the modern exhaust gas treatment systems. The subsequent subsections discuss the commonly used liquid alternative fuels such as biodiesel, ethanol, and methanol that are used in the transportation sector.

1.7.1. Biodiesel

Biodiesel is an alternative fuel produced from organic substances that are composed of fatty acids. Triglyceroids present in these feedstock are converted into mono esters by using transesterification processes. The potential feedstocks are edible and non-edible oils, animal fats, and algae. Biodiesel's physical properties are similar to those of petroleum diesel, but it is a cleaner-burning alternative [9]. Biodiesel has better-lubricating properties

and much higher cetane ratings [10]. Biodiesel is the non-petroleum fuel that can be blended with petroleum diesel to form a biodiesel blend. Biodiesel is simple to use, biodegradable, nontoxic, and essentially free of sulfur and aromatics. It can be used in diesel engines without any significant modifications.The use of biodiesel in a CI engine results in substantial reductions of UHC, carbon monoxide, and particulate matter compared to emissions from diesel fuel. The biggest problems associated with biodiesel are (i) poor oxidation stability, (ii) higher viscosity and density, and (iii) cold flow property. A biodiesel life cycle study (1998), jointly sponsored by DOE and the U.S. Department of Agriculture, concluded that biodiesel reduces net CO_2 emissions by 78% compared to petroleum diesel. This is due to biodiesel's closed carbon cycle. The biodiesel should be stored in a clean, dry, dark environment. Acceptable storage tank materials include aluminum, steel, fluorinated polyethylene, fluorinated polypropylene, and Teflon. Copper, brass, lead, tin, and zinc should be avoided.

1.7.2. Alcohols

Utilization of alcohol based fuels are of interest for several reasons because, they are easily produced and transported and utilized much like conventional fossil fuels. The first four aliphatic alcohols are primarily considered for fuel: methanol, ethanol, propanol, and butanol. Methanol and ethanol are both relatively simple to produce and can both be created from carbon dioxide, which could reduce their net contribution to greenhouse emissions. Methanol and ethanol are the two promising alcohol fuels for IC engines. As a fuel, methanol and ethanol both have advantages and disadvantages over fuels such as petrol (gasoline) and diesel fuel. In SI engines, both alcohols can run at a much higher exhaust gas recirculation rates and with higher compression ratios. Both alcohols have a high octane rating, with ethanol at 109 RON (Research Octane Number), 90 MON (Motor Octane Number), which equates to 99.5 (antiknock index) AKI [11]. As a CI engine fuel, both alcohols emit very little particulates, but their low cetane number means that an ignition improver like glycol must be mixed into the fuel with approx. 5%.

1.7.2.1. Methanol

As the most basic alcohol, methanol is an affordable alternative transportation fuel due to its efficient combustion, ease of distribution and wide availability around the globe. Methanol is a high octane fuel that enables very efficient and powerful performance in SI engines. Engines optimized for methanol could provide an energy based efficiency gain of

50% over a standard (port fuel injected, non-turbo) gasoline engine in a light-duty vehicle. The power-producing qualities of methanol are well-known, and it is used in several motorsports. While methanol has a low cetane rating, it also can be used in CI engines as a diesel fuel substitute. Dual-fuel heavy-duty engines operating on diesel and methanol fuels can improve efficiency, and dramatically reduce emissions for trucks, buses, and off-road vehicles. Methanol, also known as wood alcohol, can be used as an alternative fuel in flexible-fuel vehicles that are designed to run on M85, a blend of 85% methanol and 15% gasoline. Methanol could become a major alternative fuel in the future as a source of the hydrogen needed to power fuel-cell vehicles. Automakers are no longer manufacturing methanol-powered vehicles.

1.7.2.2. Ethanol

Ethanol is an alcohol with two carbon atoms, between which there is a single bond (empirical formula C_2H_5OH). Other terms, such as ethyl alcohol, spirit or grain alcohol are also used. Ethanol produced from biomass is also described as bioethanol. Ethanol is one of the most widely used biofuels today. As a transportation fuel ethanol in the form of E-diesel (ethanol blend with 15−20% in conventional diesel), and gasohol (90% of gasoline and 10% ethanol blend). In gasoline engines, ethanol is used as E85 (85% ethanol blend) and gasohol in many countries. The largest production of ethanol fuel was in the United States, followed by Brazil. Table 1.4 provides the world's ethanol production by country and year. The global ethanol production was approximately doubled from 2007 to 2015.

Table 1.4 Countrywide ethanol fuel production (Million Gallons) by year [12].

Country	**2007**	**2008**	**2009**	**2010**	**2011**	**2012**	**2013**	**2014**	**2015**
USA	6,521	9,309	10,938	13298	13948	13300	13300	14300	14806
Brazil	5,019	6,472	6,578	6921.54	5573.24	5577	6267	6190	7093
Europe	570	734	1,040	1208.58	1167.64	1179	1371	1445	1387
China	486	502	542	541.55	554.76	555	696	635	813
Canada	211	238	291	356.63	462.3	449	523	510	436
Rest of World	315	389	914	984.61	698.15	752	1272	1490	1147
Total	13,123	17,644	20,303	23310.9	22404.091	21812	23429	24570	25682

1.8. Advanced combustion technologies

The automobile population is increasing exponentially due to the rapid growth in the population. Year over year the emission legislations are also becoming stringent. The main task for the scientists, researchers, engineers, and academicians are to find solutions to minimise the engine exhaust emissions and effective utilisation of energy. Since last two decades, many automotive industries introduced several modern automotive vehicles, mainly to increase fuel economy, minimise the emissions, and to utilise different alternative fuels. The novel combustion technologies are vital for improving engine efficiency, reducing pollution and cost efficient conversion techniques. The advanced combustion technologies that have been introduced to achieve such solution homogeneous charge compression ignition (HCCI), stratified charge compression ignition (SCCI), stratified charge spark ignition (SCSI), and low-temperature combustion (LTC) due to superior thermal efficiencies and ultra-low emissions of NO_x and soot [4,13–16]. In HCCI engines, a lean homogeneous air-fuel mixture is used for auto-ignition. Whereas in SCCI engines, hetrogeneous mixture is used for auto-ignition. In SCSI engines, the hetrogeneous air fuel mixture is ignited with spark. The overall cylinder air fuel mixture is also lean in SCCI and SCSI engines. Among these, the HCCI engines have a potential to meet the stringent emission standards (EURO VI) and CO_2 emission standards [17,18]. The HCCI that has the capability to adopt multi-fuels, the use of biofuels as alternative neat fuels or additives is possible [19]. The recent developments of advanced combustion technologies are described in Chapter 2.

The main focus of this research study was to use ethanol in an HCCI engine.

1.9. Organisation of thesis

The reminder of the thesiscomprises the following chapters;

Chapter 2 Literature Review

A comprehensive review of research works pertaining to the development of HCCI engines and methods of utilizing ethanol in IC engines are the up to date. The various issues related to combustion, performance and emission parameters of the HCCI engine fueled with the ethanol are also discussed in this chapter. The research gaps observed after reviewing the articles are also given in this chapter.

Chapter 3 Experimental materials and methods

This chapter provides the necessary information on the HCCI engine experimental test rig and various instruments used in this study. The method of measuring various engine parameters and the procedure to calculate the instrument uncertainties were also included at the end of this chapter. The experimental methodologies that were followed to convert CI engine to run on the HCCI mode are also discussed in this chapter. The calculation of important parameters that are related to the combustion, performance, and emission characteristics are discussed.

Chapter 4 Thermodynamic modelling, GRNN prediction and PSO optimization

The correlations and equations used for the thermodynamic modelling, generalized regression neural network (GRNN) prediction and particle swarm optimization (PSO) optimization are provided here.

Chapter 5 Results and Discussion

This chapter discusses the preliminary results that were obtained in a thermodynamic analysis of the HCCI engine examined in this study. It also discusses the experimental results obtained for the ethanol fueled HCCI engine on the three major parameters evaluated were (i) combustion, (ii) performance, and (iii) emission. The experimental results were further predicted with the GRNN tool and optimized with the PSO algorithm.

Chapter 6 Conclusions

The conclusions of the investigation to evaluate the ethanol as an alternative fuel for an HCCI engine are provided. It also mentions the important findings of the research and the scope of future work.

Chapter 2

Literature Review

2.1. General

Homogeneous charge compression ignition (HCCI) technology is believed to be a promising one to be applied in both spark ignition (SI) and compression ignition (CI) engines in the near future. However, problems associated with combustion phase control, controlled auto-ignition, operating range, homogeneous charge preparation, cold start and emissions of unburned hydro carbon (UHC), and carbon monoxide (CO) need to be solved for a successful operation of HCCI engines. Extensive research on HCCI combustion with a homogeneous fuel-air mixture preparation is going on throughout the world. In this chapter, the strategies of different external and in-cylinder mixture preparation methods that are proposed and adopted in the HCCI are presented. Further, different strategies of controlled auto-ignition by HCCI combustion are also discussed. The content of this chapter has been published in a reputed international journal "Renewable and sustainable energy reviews", which is mentioned in the list of papers published in the end of the thesis.

2.2. Basics of HCCI combustion

The HCCI operation is alike to SI engine which utilizes the homogeneous charge for combustion and alike to CI engine that has the auto ignition of the mixture. Thus, HCCI is the hybrid nature of SI and CI combustion processes [20]. In SI engines, three zones of combustion namely burnt zone, unburned zone and a thin flame reaction zone in-between for turbulent flame propagation through the cylinder. In CI engines, fuel is diffused into the cylinder and a definite diffusion flame travels with in the cylinder. In HCCI engine combustion, spontaneous ignition of whole cylinder charge takes place without any diffusion flame or flame front propagation [21,22]. Table 2.1 compares the different parameters influencing the combustion processes in SI, CI, and HCCI engines.

Engines are operated in the region of lower equivalence ratios to improve efficiency and reduce emissions. Due to enormous increase in the vehicle population, the lean combustion technology is employed mainly in IC engines. The NO_x emission can be reduced only by reducing the flame temperature of combustion. Lean burn engines

produce lower temperatures, which is the key factor to reduce the formation of thermal oxides of nitrogen. The excess air employed in lean burning results in a more complete combustion of the fuel which reduces both the UHC and CO emissions. Moreover, the heat transfer losses in the IC engine can be decreased only minimising the combustion temperature. The HCCI combustion is one in which the low temperature combustion (LTC) is used to reduce the heat transfer losses, and the heat of fuel is completely released in a few crank angles near top dead centre (TDC).

The auto-ignition of the fuel by CI engines can handle wide range of the fuels for combustion. The HCCI engines are operated to auto-ignite the fuel by the compression as the piston proceeds to the TDC. The engine has to be operated on a variable compression ratio (VCR) to adjust the auto-ignition of the cylinder charge near the TDC. A wide range of fuels can be burnt easily by adopting the VCR method [23–26]. Some of the other methods for fuel flexibility for the given engine are charge heating [15,27,28], boost pressure [26,29–33], exhaust gas recirculation (EGR) [34–36], variable valve actuation (VVA) [37–40] etc.

Table 2.1 Comparison of SI, CI and HCCI combustion engines.

Engine type	**SI**	**HCCI**	**CI**
Ignition method	Spark ignition	Auto-ignition	
Charge	Premixed homogeneous before ignition		Heterogeneous
Ignition point	Single	Multiple	
Throttle loss	Yes	No	
Compression ratio	Low	High	
Speed	High	Low	
Combustion flame	Flame propagation	Multi-point auto-ignition	Diffusive flame
Fuel economy	Good	Comparable to CI	Better
Max. efficiency	30%	>40%	40%
Major emissions	HC, CO and NO_x	HC and CO	NO_x, PM and HC
Injection type	Port injection	Both port and direct injection	Direct injection
Equivalence ratio	1	<1	
Fuel injection method	Direct injection		
	Indirect injection		

Fig. 2.1 shows the region of HCCI combustion well above the UHC/CO oxidation limit and escapes the formation of both NO_x and soot. The HCCI combustion is considered to be one of the best combustion technologies to be adopted wider in the market near future, as it offers wide range of fuel flexibility [41–43] with a higher thermal efficiency, and low emissions. Fuel flexibility is also cited as a potential benefit [44]. The preparation of lean homogeneous mixture and low temperature combustion (LTC) are adopted in HCCI

technology to suppress the NO_x and soot emissions from the engine [45]. In HCCI engines, a lean homogeneous flammable mixture (fuel-air equivalence ratio $\Phi<1$) is prepared, before the start of ignition and auto ignited as a consequence of temperature rise in the compression stroke.

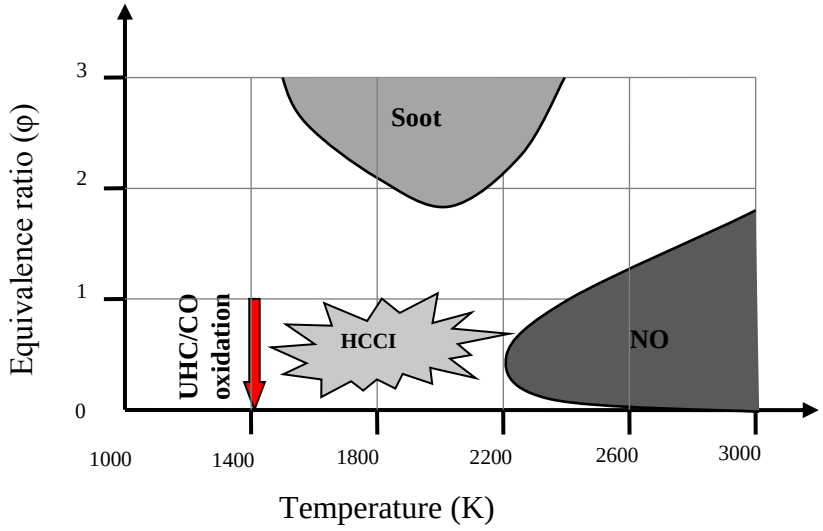

Fig. 2.1. HCCI combustion: simultaneous reduction of NO_x and soot.

2.3. Challenges of HCCI combustion

Before implementing the benefits of the HCCI combustion engines, it has to overcome some of the barriers for mass production. The challenges of the HCCI combustion include: i) combustion phase control, ii) controlled auto-ignition, iii) operation range, iv) cold start, v) emissions of UHC and CO, and vi) homogeneous charge preparation [46]. Among these challenges, the homogeneous mixture preparation and combustion phase control play vital role in determining the efficiency and emissions.

2.3.1 Combustion phase control

The main challenge of the HCCI engine is to control ignition timing, which influences the power and efficiency. The conventional engines have a direct mechanism to control the start of combustion. Unlike, spark timing in SI engines and fuel injection timing in CI engines, the HCCI engine lacks start of combustion controlled by auto-ignition. The fuel-air mixture is premixed homogeneously, before the start of combustion initiated by the auto-ignition of time-temperature history. This phenomenon of auto-ignition leads to the main combustion control which is affected by the few factors [46,47]: fuel auto-ignition chemistry and thermodynamic properties, combustion duration, wall temperatures,

concentration of reacting species, residual rate, degree of mixture homogeneity, intake temperature, compression ratio, amount of EGR, engine speed, engine temperature, convective heat transfer to the engine, and other engine parameters. Hence, the HCCI combustion control over a wide range of speeds and loads is the most difficult task. Controlling combustion is the most important parameter, because it affects the power output and the engine efficiency. If combustion occurs too early, power drop in terms of efficiency and serious damage to the engine occurs, and if combustion occurs too late, the chance of misfire increases. Most of the researchers believe on the fact that HCCI combustion is governed by chemical kinetics [14,48,49].

2.3.2 Abnormal pressure rise with noise

The instantaneous heat release which is caused by auto-ignition of the whole homogeneous charge simultaneously during compression stroke. The instantaneous heat release results in abrupt rise in temperature followed by abrupt pressure rise, and then high levels of noise. Controlling this sudden heat release is extremely important, because it is the main source of pressure rise, which may cause a severe damage to the engine. The acceptable pressure rise limit is approximately 8 bar/CA for noise [50].

2.3.3 Domain of operation

The operating range of the HCCI engine is a limited one compared to the conventional engines, which is another hurdle for a commercial success in the market. Controlling the ignition timing over a wide load and speed range is a difficult task [51,52]. The operating range is influenced mainly by the auto-ignition properties of fuel and engine geometry. Extending the HCCI operation to full/higher load also limits the part/light load operation, due to lack of ignition energy to auto-ignite the lean mixture at the end of compression stroke. The flammability limits the fuel-air mixture during very lean HCCI operation. In addition to this, the UHC and CO emissions also increase near the idle operation, as a result of inefficient combustion efficiency. Hence, the domain of operation of the HCCI engines is in a limited range.

2.3.4 High levels of UHC and CO

Heywood [53] reported that the UHC and CO emissions in an IC engine are due to combustion of either rich or very lean to stoichiometric mixtures. The temperature of the lean mixture limits of inflammability, while the rich mixture suffers from lack of oxidant

in the combustion chamber. The efficiency of combustion is improved only, if the exhaust contains low levels of UHC emissions. The lean operation of the HCCI combustion produces high levels of UHC and CO emissions. Kraft et al. [54] indicated that the unburned hydrocarbon emission in HCCI engines is mainly due to the incomplete oxidation of fuel through an excess oxidant, which is available for combustion. Some other reasons of UHC are crevice volumes present in the combustion chamber, valve overlapping, wall deposit absorption etc. The exhaust gas temperature is too low to oxidize UHC and CO to CO_2 and H_2O completely, even during exhaust stroke. Due to low temperature combustion process, catalytic converters are also inefficient to oxidize these pollutants. The efficiency of combustion in HCCI is greatly improved by the complete oxidation of the fuel lastly by power stroke.

2.3.5 Cold start

The cold start problem in the HCCI engines is another hurdle in most of the geographically cold regions. The compressed charge looses more heat to the cold combustion chamber walls at the cold start operation. This problem can be overcome by starting the engine by the conventional mode for a short warm-up period, and then switch to the HCCI mode.

2.3.6 Homogeneous charge preparation

The mixture preparation is the key to achieve high fuel economy and low exhaust emissions from the engine. The thermodynamic cycle time of IC engines takes a very short span and within that, the homogeneous mixture preparation time for combustion is much lower. The degree of homogeneity of the fuel-air mixture is greatly improved only by increasing the time for mixture preparation. Some other benefits of effective mixture preparation are control of wall wetting and oil dilution. Low temperature combustion (LTC) is employed in many combustors like IC engines, and gas turbines mainly to decrease NO_x emissions as they are responsible for peroxyacetyl nitrates (PAN) formation.

2.4. Homogeneous charge preparation strategies

The preparation of the homogeneous mixture is the main factor in reducing the particulate matter (soot) emissions, and local fuel rich regions to minimise oxides of nitrogen. The local fuel-rich regions can be decreased by an effective mixture preparation. However, the

preparation of the homogeneous mixture for the cycle-to-cycle variation of speed and load is a difficult task due to less time availability of mixture preparation. The effective mixture preparation for the HCCI combustion includes both the fuel-air homogenisation and temperature control over in combustion. The strategies for mixture preparation are either in-cylinder direct injection, or external mixture which is shown in Fig. 2.2. Both the preparation methods have their own disadvantages that the external mixture has a low volumetric efficiency and in-cylinder mixture is prone to an oil dilution. Table 2.2 gives the various names of HCCI which are listed in the literature.

Table 2.2 Overview of HCCI acronyms from literature.

Reference	**Acronym**	**Meaning**	**Location**
Onishi [21]	ATAC	Active thermo-atmosphere combustion	Nippon Clean Engine Research Institute
Noguchi [22]	TS	Toyota-Soken combustion	Toyota/Soken
Thring [55]	HCCI	Homogeneous charge compression ignition	Southwest Research Institute (SwRI)
Ishibashi [56]	ARC	Active radical combustion	Honda
Gatellier [57]	NADI^{TM}	Narrow Angle Direct Injection	Institut Français Du Pétrole (IFP)
Kimura [58]	MK combustion	Modulated kinetics combustion	Nissan
Takeda [59]	PREDIC	Premixed diesel combustion	New ACE
Hashizume [60]	MULDIC	Multiple stage diesel combustion	New ACE
Yokota [61]	HiMICS	Homogeneous charge intelligent multiple injection combustion system	Hino
Yanagihara [62]	UNIBUS	Uniform bulky combustion system	Toyota
Iwabuchi [63]	PCI	Premixed compression ignited combustion	Mitsubishi
Aoyama [64]	PCCI	Premixed Charge Compression Ignition	Toyota

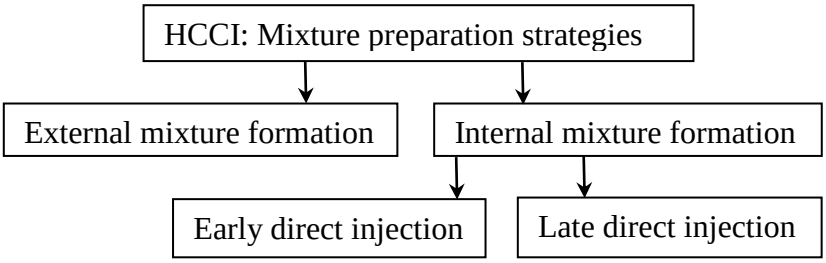

Fig. 2.2. Strategies for mixture preparation.

2.4.1 External mixture preparation

The homogeneous mixture which is prepared external to the engine cylinder is the most effective due to more mixing time availability, before the start of combustion. This method of preparation is more suitable for high volatile fuels like gasoline and alcohols. The mixture preparation strategies are port fuel injection (PFI), manifold induction, fumigation, wide open throttle (WOT) carburetion etc. However, the low volatile fuel like diesel can also be used by using fuel vaporiser. The gaseous fuels are ready to mix with the air and preparation of homogeneous mixture externally is pretty simple, but the engine may suffer with the volumetric efficiency, if the calorific value of the gas is low. The gaseous fuels are mixed mostly in the intake manifold and some early implementations are acetylene [27,65], biogas [66–68], hydrogen [69–72] etc. Fig. 2.3 illustrates the different methods of external mixture preparation by researchers.

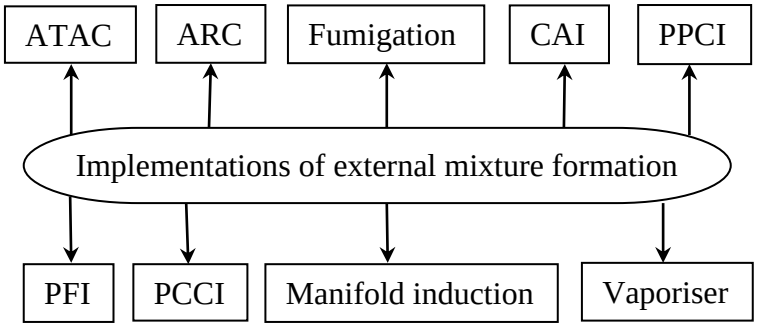

Fig. 2.3. Early implementations of external mixture formation.

A first study on the HCCI combustion process was performed on two stroke engines by Onishi et al. in 1979 [21]. There was no flame propagation, as in a conventional SI engine instead, the whole mixture burned slowly at the same time. They called it as "active-thermo atmosphere combustion" (ATAC) [73–75]. The same combustion was demonstrated at the Toyata Motor Co. Ltd. and named as "TS (Toyota-Soken) combustion" [22]. Noguchi et al. [22] demonstrated the same combustion process in an opposed-piston two stroke engine. Later, Honda R&D Co., Ltd.investigated on activated radical combustion (ARC) on two stroke gasoline engines [56,76–79]by winning the fifth place in Granada-Dakar rally competition. The premixed charge compression ignition (PCCI) engine developed by the Toyota Central Research [64] in which combustion of premixed lean mixture arose from a multi-point ignition which could be very promising and necessary for achieving both higher efficiency and lower nitrogen oxide (NO_x) emission. The premixed charge compression ignition (PCCI) engine operated stably in the

air-fuel ratio range of 33-44 and ignition occurred spontaneously at unspecified points as it does in diesel engines. Table 2.3 presents the external the mixture preparation strategies used in HCCI engines.

Some researchers introduced an electronically controlled fuel vaporizer for low volatile and high boiling point fuel such as diesel [80–83]. The diesel vaporiser formed a very light and dispersed aerosol with a very fast evaporation due to a very high surface to volume ratio. The smoke emission was reported to be negligible, and the EGR was used for combustion control and the NO_x emission. The operation temperature of vaporizer was above the boiling point of fuel for successful external mixture preparation [84]. Some researchers used a high intake air temperature [28,43,85–87] to vaporise the fuel in the intake manifold. The common disadvantage reported by them was the electric power consumption for vaporisation of diesel. Another study was reported by the researchers on the effect of premixed ratio in diesel engine with the partially premixed charge compression ignition (PPCI) combustion using diesel fuel [88–90]. An investigation [23] of diesel fuel with a port fuel injection with variable compression ratios reported that, the compression ratios need to be reduced in order to avoid knock in the HCCI combustion. The cool-combustion chemistry of diesel fuel led to auto-ignition at approximately 800K during compression stroke [91].

The port fuel injection (PFI) is the simplest method of external mixture preparation, in which injector is mounted in the intake manifold, very close to the intake valve. This system improves the volumetric efficiency and fuel distribution over carburetion. The mixture enters into the cylinder during engine suction and the turbulence created by intake flow improves further homogenization. This method of mixture formation has been reported to be successful with gasoline and alcoholic fuels [20,92–98]. The main drawback of this strategy is injection timing which cannot influence the start of ignition. Furthermore, heavy fuels with lower volatility of PFI results in poor vaporization with increased wall impingements.

Table 2.3 Overview of external mixture preparation strategy implemented in gasoline-fueled HCCI engines.

Reference[a]	**HCCI acronym**	**Key features**	**Advantages**	**Disadvantages**
Onishi [21]	ATAC	Uniform mixing between residuals and fresh charge. No flame propagation as in the case of SI engines. High EGR rates are used to achieve auto-ignition of gasoline.	Remarkable reduction in emissions and high fuel efficiency.	Limited to part load operation.
Noguchi [22]	TS	Stable spontaneous auto-ignition with port fuelling in presence of active radicals.	Smooth combustion with low HC emissions and improved fuel consumption.	Limited to part load operation.
Thring [55]	HCCI	The operating regime was function of air/fuel equivalence ratio and external EGR rates.	High fuel efficiency and low emissions.	Restricted to part load operation and control of auto-ignition timing is problematic.
Ishibashi [56]	ARC	Active radicals in the exhaust gases were controlled by changing the exhaust valve axis movement.	Two-stage auto-ignition combustion is observed at lower load. Fuel economy was improved by 57% while HC emission reduction by 60%.	Idling with auto-ignition was not possible with AR combustion.
Saqaff [99]	ARC	Reduced exhaust port area in the range of 1-8%	Exhaust gas temperature decreased by about 16.7% to 22.5% while the fuel consumption reduced by about 11.1% to 49.8%.	Idling with auto-ignition was not possible with AR combustion.
Aoyama [64]	PCCI	Spontaneous ignition occurred at unspecified points as it does in diesel engines. The flame then developed rapidly throughout the combustion chamber.	Low NO_x emission was noticed than in diesel engines.	Intake air heating and supercharging were necessary to extend the range of stable combustion.

[a] Only the first author is listed, all papers have multiple authors.

2.4.2 In-cylinder mixture preparation

The demerits associated with low volatile fuels (like diesel) by the port fuel injection can overcome with the internal mixture formation. Two strategies; i) early direct injection and ii) late direct injection for in-cylinder mixture formation have been adopted by the researchers. The injection timing for an early direct injection was set during compression stroke, for a late direct injection it was set after TDC. High injection pressures with a large number of small nozzle holes adopted to increase the spray disintegration which forms homogeneous mixture.

2.4.2.1 Early direct injection

The fuel injection process in the HCCI combustion is charge homogeneity, which is influenced by injection timing. Early injection method is mostly used method of achieving HCCI diesel combustion. The early injection allows a longer ignition delay along with the low temperatures to homogenize the diesel-air mixture. Unlike conventional diesel, direct injection in diesel engines, pulsed injection strategy is used. The total amount of fuel per cycle is injected in many pulses as shown in Fig. 2.4.

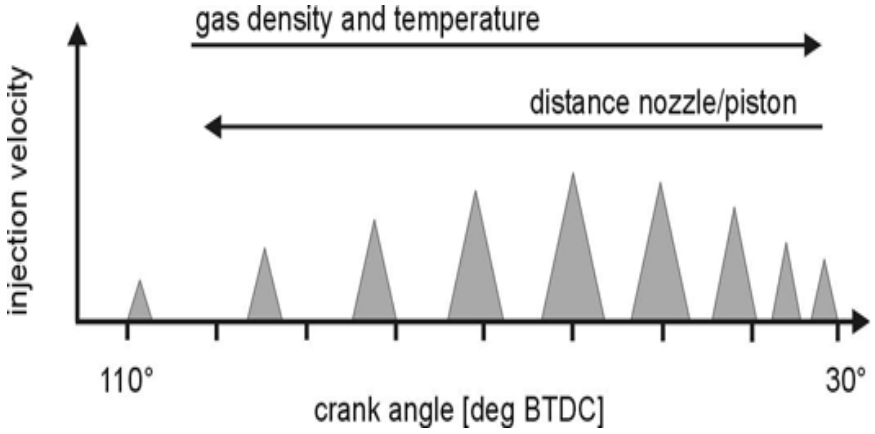

Fig. 2.4. Pulsed injection strategy for early in-cylinder injection [100].

The early direct fuel injection during compression stroke results in wall wetting due to over-penetration of diesel as a result of poor volatility and low air density during early CAD compression stroke. A piezoelectric controlled common rail injector is capable to control injection with high injection pressures for performing variable pulsed injections. The area below the curve represents the fuel mass belonging to each pulse.The low gas density at the beginning of injection requires short pulses with the reduced injection velocities, and the time interval between the pulses is relatively large. As the piston moves

up, density and temperature in the cylinder increase and penetration is reduced. The pulse durations can be prolonged, while the time intervals between subsequent pulses are decreased. At the end of the pulsed injection the distance between nozzle and piston reduces significantly, and the mass injected per pulse must be reduced again in order to prevent fuel deposition on the piston [100]. The in-cylinder mixture preparation strategies used in HCCI engines are listed in Table 2.4.

The early in-cylinder implementations used in diesel-fueled vehicles are PREDIC, MULDIC, HiMICS, UNIBUS and MULINBUMP. Fig. 2.5 illustrates different direct in-cylinder strategies adopted in recent years.

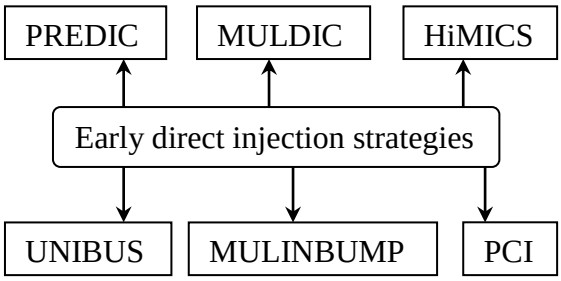

Fig. 2.5. Early in-cylinder diesel direct injection strategies.

The fuel is injected during early compression stroke, which becomes partly homogeneous mixture and combustion starts closer to the TDC. This concept is called premixed lean diesel combustion (PREDIC) [101,102]. Takeda et al. [59] from New ACE institute, Japan reported low NO_x and soot emissions, while the UHC emission is more due to poor combustion efficiency. The injection strategy was modified such that, two side injectors whose nozzle diameter was reduced from 0.17 mm to 0.08 mm and the number of holes was also increased from 6 to 16. The operating region is limited to part load only. Nishijima et al. [103] used an early injection timing and found a problem that the fuel spray reached the cylinder wall, which caused a higher HC emission and fuel consumption. Iwabuchi et al. [63] from the Mitsubishi Motors corporation used early injection strategy, where premixed compression ignited (PCI) combustion system adopted in a four stroke, single cylinder, diesel engine. The PCI combustion limited to part load and found more HC emission with low NO_x emission.

Table 2.4 Overview of in-cylinder direct injection strategies used in diesel-fueled HCCI engines.

Reference[a]	**Strategy**	**HCCI acronym**	**Key features**	**Advantages**	**Disadvantages**
Takeda [59]	Early in-cylinder direct injection	PREDIC	Two side injectors whose nozzle diameter was reduced from 0.17 mm to 0.08 mm and the number of holes increased from 6 to 16.	Low NO_x and soot emissions.	The UHC emission was more due to poor combustion efficiency. Limited to part load operation only.
Nishijima [103]	Early in-cylinder direct injection	PREDIC	Two sprays, one injected from each side injector diagonally, impinged each other at the center of the cylinder to create an air-fuel mixture.	Adequate water split injection pattern could retard fuel injection timing by keeping low NO_x and UHC emission levels.	Due to wall impingement of the fuel spray, higher UHC emission and fuel consumption.
Iwabuchi [63]	Early in-cylinder direct injection	PCI	Used an impinged-spray nozzle which realized the low penetration, high-dispersion, and high injection rates.	NO_x emissions reduced.	Limited to part load operation and found more UHC emissions.
Hashizume [60]	Early in-cylinder direct injection	MULDIC	Two stage injections: the first stage combustion corresponds to the premixed lean combustion, and the second stage combustion corresponded to diffusion combustion under the high temperature and low oxygen conditions.	Reduce NO_x emissions at high load conditions.	UHC emissions were higher.
Yokota [61]	Early in-cylinder direct injection	HiMICS	Two injector tips were needed, a multi-hole (30 holes each 0.10 mm) tip for early injection and a conventional injector tip for near TDC injection.	NO_x reduction from approximately 800 to 200 ppm.	UHC increased from 3000 to 8000 ppm.
					Continued to next page
Hasegawa [62]	Early in-cylinder	UNIBUS	A double injection technique was used. The first injection was used as an early	Low NO_x and smoke emissions were possible.	Limited to low loads and at high loads

	direct injection		injection for fuel diffusion whereas the second injection was used as an ignition trigger for all the fuel.		conventional diesel combustion was used.
Su [104,105]	Early in-cylinder direct injection	MULINBUMP	A flash mixing technology was used with BUMP combustion chamber, while multi-pulse injections to limit the spray penetration.	Near zero NO_x and smoke emissions.	For higher power output injection mode must be carefully designed.
Kimura [58]	Late direct injection	MK combustion	Three features in MK combustion: Late fuel injection timing starts from 7^o BTDC to 3^o ATDC, high levels of EGR and high swirl ratio.	NO_x emissions were reduced to about 50 ppm without an increase in PM.	The operating range was limited to one-third of peak torque and half-speed.
Kimura [106]	Late direct injection	MK combustion	In addition to the above, piston bowl diameter was increased from 47 to 56 mm. This reduced UHC emissions significantly.	ULEV (ultra-low emission vehicle) standards can be met with a 5-way catalyst. NO_x < 0.07 g/mile and PM < 0.01 g/mile.	The operating range was limited to half torque and three-quarters speed.
Gatellier [57,107,108]	Early in-cylinder direct injection	NADI^{TM}	The fuel injection angle was narrowed such that wall wetting was eliminated.	At part load near zero particulate and the NO_x emissions while very good fuel efficiency.	Conventional diesel combustion was observed at full load.

[a] Only the first author is listed, all papers have multiple authors.

The strategy of multiple injections in the HCCI mode is used instead of a single injection strategy, in order to run at high load. The multiple stage diesel combustion (MULDIC) and homogeneous charge intelligent multiple injection combustion system (HiMICS) uses the first injection during early compression stroke and the second injection is just before the TDC. The uniform bulky combustion system (UNIBUS) developed by the Toyota Motor Corporation in the Japanese market (1KD-FTV, 3 liter-4cylinder) in August 2000 [62]. A double injection technique was used. The first injection was used as an early injection for fuel diffusion and to advance the changing of fuel to lower hydrocarbons (i.e. low temperature reaction). The second injection was used as an ignition trigger for all the fuel. It is reported, that the ignition of the premixed gas could be controlled by the second injection, when the early injection was maintaining a low temperature reaction. This system is limited to low loads and at high loads conventional diesel combustion is used.

The MULINBUMP is a compound combustion technology of premixed combustion and "lean diffusion combustion" in a DI diesel engine [104]. The premixed combustion is achieved by the technology of multi-pulse fuel injection. The start of pulse injection, injection-pulse number, injection period of each pulse and the dwell time between the injection pulses are controlled. The objective of controlling the pulse injection is to limit the spray penetration of the pulse injection, so that the fuel will not impinge on the cylinder liner, and to enhance the mixing rate of each fuel parcel by promoting the disturbance to the fuel parcels. The last or main injection pulse was set around the TDC. A flash mixing technology was developed from the design of a so-called BUMP combustion chamber, which was designed with some special bump rings. The combustion of fuel injected in the main injection proceeded under the effect of the BUMP combustion chamber at a much higher air/fuel mixing rate than it does in a conventional DI diesel engine, which leads to "lean diffusion combustion". The pulse injection mode modulation was investigated by variation of control signals; a series of injection modes were realized based on the prejudgment of combustion requirement. The designed injection modes included, so called even mode, staggered mode, hump mode and progressive increase mode with four, five and six pulses respectively. The experimental results indicated that, the HCCI diesel combustion was extremely sensitive to the injection mode. There were many ways to reach near zero NO_x and smoke emissions, but the injection mode must be carefully designed for higher power output [105].

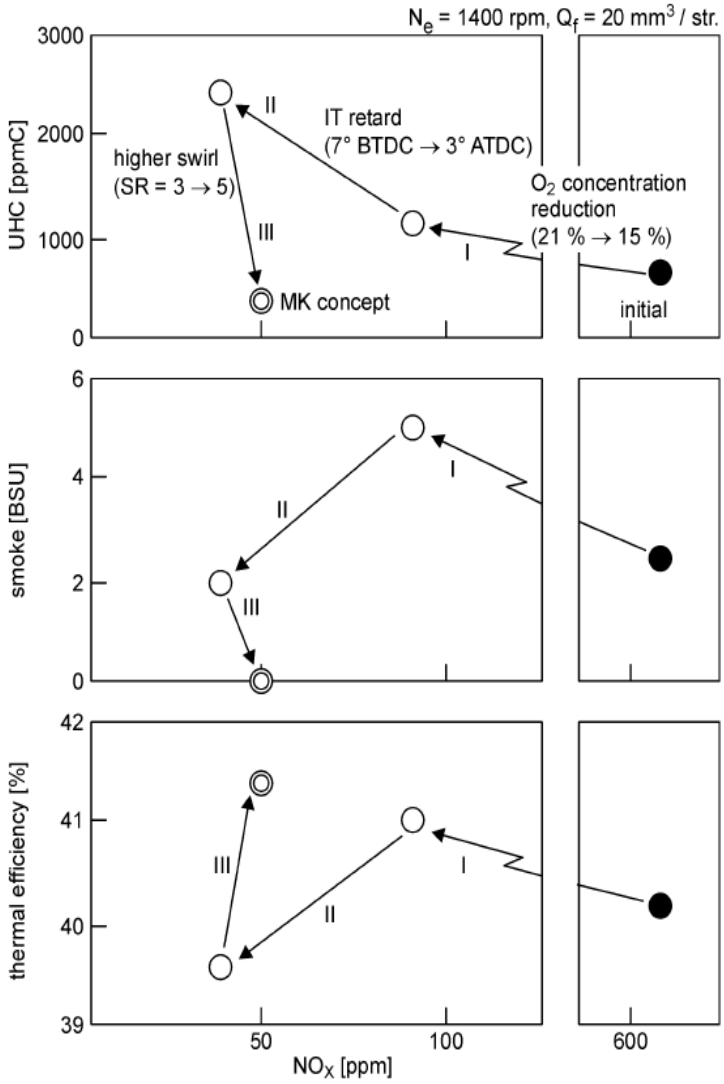

Fig. 2.6. Nissan MK-concept: Effects of EGR, retarded injection timing (IT) and increased swirl on exhaust emissions and thermal efficiency [106].

2.4.2.2 Late direct injection

The development of diesel-fueled late DI HCCI system is the modulated kinetics (MK) combustion system developed by the Nissan Motor Co., Ltd. [58,109]. A schematic diagram of the Nissan MK-concept is illustrated in Fig. 2.6 [106]. This system combines two mutually independent intake ports, one of which is a helical port for generating an ultra-high swirl ratio and the other is a tangential port for generating a low swirl ratio. The tangential port incorporates a swirl control valve that controls the swirl ratio (3.5 -10) by varying the flow rate. To achieve the premixed combustion, the fuel-air mixture homogeneity before ignition is required in MK combustion that can be achieved by increasing the ignition delay longer and rapid mixing with a high swirl. In the MK system,

there are three features; (i) late fuel injection timing starts from 7º BTDC to 3º ATDC, (ii) high levels of EGR and (iii) high swirl ratio. The formation of NO_x emissions can be suppressed by high EGR rates (reduces oxygen concentration from 21% to 15%) and low temperature combustion. The ignition delay was increased by decreasing the compression ratio to 16:1.

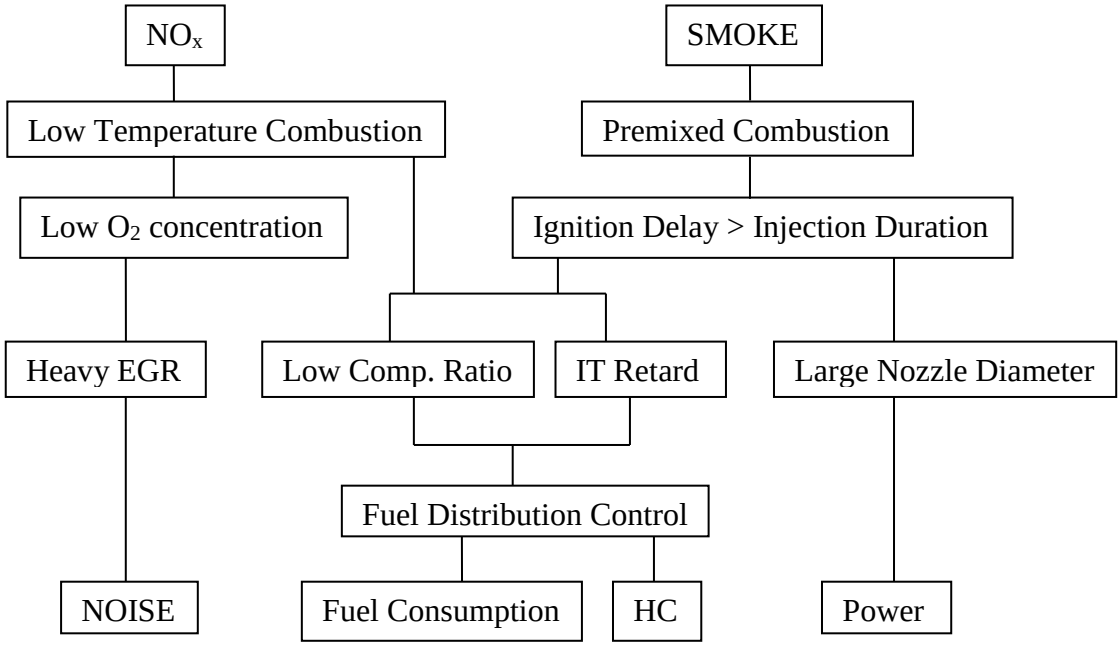

Fig. 2.7. Schematic of the MK combustion concept [110].

Kawamoto et al. [111] found that low compression ratio was effective in expanding the MK combustion region on the high-load side. The basic concept of MK combustion is explained schematically in Fig. 2.7 [110]. Kimura et al. [112] examined the effects of combustion chamber insulation on the heat rejection and the thermal efficiency. The combustion chamber was insulated by using a silicon nitride piston cavity that was shrink-fitted into a titanium alloy crown. The application of heat insulation reduced the angular velocity of the flame in the combustion chamber by about 10∼20%. This reduction in the angular velocity of the flame was found to be one cause of combustion deterioration when the heat insulation was applied to the combustion chamber. The main advantage of the late direct injection system is the combustion control by the injection timing over the port fuel injection and the early direct injection systems.

2.4.3 Narrow angle direct injection NADI™

In order to prevent fuel deposition on the cold cylinder liner, the angle between the spray must be reduced. The concept of narrow angle direct-injection (NADI) was suggested by Walter and Gatellier [57,107,108] to keep the fuel target within the piston bowl and avoid the interaction of the spray with the liner at advanced injection timing. The results indicated that the liquid fuel impingement on the bowl wall led to fuel film combustion which was called "pool fire". Because of the rich air–fuel mixture and low temperature on the wall surface, the pool fire resulted in incomplete combustion and high soot formation for all early injection cases.

A narrow fuel spray angle and a dual injection was examined by Myung et al. [113]. In their investigation, the fuel injection angle was narrowed from 156^{o} of conventional diesel engine to 60^{o}, while the compression ratio was reduced from 17.8:1 to 15:1 to prevent the early ignition of the mixture. The results showed that the NO_x emissions were greatly reduced as the injection timing was advanced beyond 30^{o} BTDC and the IMEP indicated a modest decrease although the injection timing advanced to 50-60^{0} BTDC in the case of the narrow spray angle configuration. Fig. 2.8 portrays the narrow spray adoption in early in-cylinder direct injection. In early in-cylinder fuel injection, the spray direction adaption is important, because the volume between the injector nozzle and piston is larger.

Tiegang et al. [114], investigated the effects of two spray injection angles (i.e., 150^{o} and 70^{o}) on the combustion process in an HSDI optical diesel engine employing multiple injection strategies with high injection pressures (600 and 1000 bar). The premixed combustion was observed for the 150^{o} tip with the high injection pressure, while other cases showed diffusion flame combustion features. A non-luminous flame was seen for the first injection of the 150^{o} tip, while two types of flames were seen for the first injection of the 70^{o} tip including a non-luminous flame and a luminous film combustion flame. The flame was observed more homogeneous for the 150^{o} tip with the higher injection pressure, namely a combustion process close to the PCCI-like combustion, with a little soot formation. More soot luminosity was observed for the 70^{o} tip due to fuel-wall impingement. The fuel film combustion led to the lower NO_x emissions due to its rich mixture nature. For both the injection angles and higher injection pressures resulted in higher NO_x emissions, because of the leaner air-fuel mixture and higher in-cylinder temperatures for the increased injection pressures.

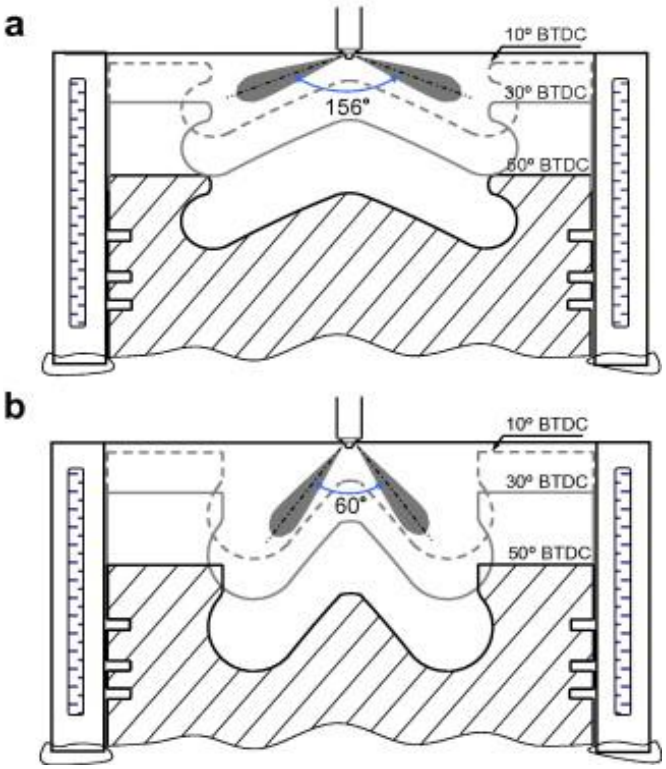

Fig. 2.8. Schematic diagrams of the (a) Conventional diesel engine. (b) NADI^{TM} for an early injection[113].

The French Institute of Petroleum, IFP [107] has developed a combustion system that was able to reach near zero particulate and NO_x emissions, while maintaining the performance standards of the DI diesel engines. A Narrow Angle Direct Injection (NADI™) was applied to this dual fuel mode engine which applied HCCI at part load, and switched to conventional diesel combustion to reach full load requirements. At part load (including Motor Vehicle Emissions Group-MVEG-and Federal Test Procedure-FTP- cycles), the HCCI combustion mode allows near zero particulate and the NO_x emissions, and maintained a very good fuel efficiency. At 1500 and 2500 rpm, NADI™ reached 0.6 and 0.9 MPa (6 and 9 bar) of indicated mean effective pressure (IMEP) with the emissions of NO_x and particulate under 0.05 g/kWh, which were found to be lower by 100 and 10 times respectively than a conventional diesel engine. At full load, NADI™ system is consistent with future diesel engine power density standard. Lately, IFP [115] has also developed a near-zero NO_x and particulate combustion process, the NADI™ concept, a dual-mode engine application switching from a novel lean combustion process at part load to conventional diesel combustion at full load. It was assumed that narrow spark cone angle injection can reduce liner wetting problem, when the fuel is injected at early CAD for the HCCI combustion.

2.5. HCCI combustion control strategies

The combustion phase in HCCI engines is controlled either by altering time-temperature history or by altering the mixture reactivity [116]. Fig. 2.9 illustrates the methods of controlling HCCI combustion. The first group indicates the purpose of which is to alter the time-temperature history of the mixture. It includes fuel injection timing, variation of intake air temperature, variation of compression ratio (VCR) and variable valve timing (VVT). The second group attempts to control the reactivity of the charge by varying the properties of the fuel, the fuel-air ratio or the amount of oxygen by EGR. However, the homogeneous mixture preparation, before the start of ignition is the main objective of HCCI combustion which can be controlled a) by increasing the degree of homogeneity; and b) delaying auto-ignition. The important strategies for controlling HCCI combustion phase are listed in Table 2.5.

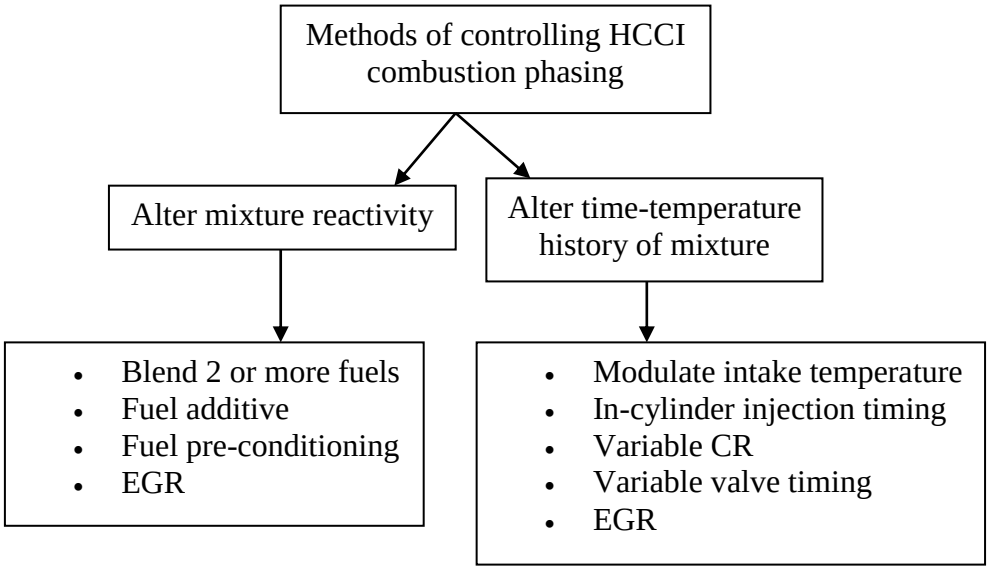

Fig. 2.9. Methods for controlling HCCI combustion phasing [116].

2.5.1 Control strategies to increase the mixture homogeneity

There are a few control strategies proposed and implemented by researchers to increase the mixture homogeneity in HCCI engines, which are reviewed and discussed in the following subsections.

2.5.1.1 Ultra high injection pressure with small nozzle holes

The atomisation of the fuel inside the combustion chamber can be improved greatly by using high injection pressures (high velocity of the jet) and by decreasing the nozzle hole diameter. Xiangang et al. [117] investigated the effects of ultra-high injection pressure (300 MPa) and micro-hole nozzle (d = 0.08 mm) on flame structure and soot formation of impinging diesel spray. A larger flame structure and week soot formation were detected with a micro-hole nozzle at injection pressures of 200 and 300 MPa. There was no liquid wetting for a micro-hole nozzle. They suggested that, fuel-air mixture homogeneity could be increased by increasing the injection pressures (high velocity of the jet) and by decreasing the diameter of nozzle hole.

2.5.1.2 High swirl ratio

The swirl of air in the combustion chamber also improves the mixing rate. The BUMP combustion chamber in MULINBUMP combustion system uses a high swirl ratio (3-5) with bump rings improves the mixing rate of fuel and air and high swirl is essential for the quick homogeneous mixture preparation for combustion.

2.5.1.3 Pulsed fuel injection

The early in-cylinder fuel injection requires multiple pulsed injections of the total fuel. The lower air density during early CAD injection during compression stroke causes over penetration of the fuel. The MULDIC combustion system uses a two stage fuel injection in which the first injection is used for premixed lean combustion, while the second injection is meant for diffusion combustion. The multi-stage fuel injection during early compression stroke is used by the HiMICS and MULINBUMP combustion systems, where fuel-air mixing was enhanced.

Table 2.5 Control strategies for HCCI combustion.

Reference[a]	**Control strategy**	**Key features**	**Advantages**
Su [104]	High swirl ratio	Specially designed BUMP combustion chamber used swirl ratios 3-5 with bump rings.	Improves the mixing rate of fuel and air, and high swirl is essential for the quick homogeneous mixture preparation.
Xiangang [117]	Ultra high injection pressure with small nozzle holes	Ultra-high injection pressure (300 MPa) and micro-hole nozzle (d = 0.08 mm) were used.	Mixture homogeneity increases. A larger flame structure and week soot formation. There is no liquid wall wetting.
Christensen [118]	High boost pressure	Increase the indicated mean effective pressure.	Low UHC and NO_x were observed with boost pressure and engine load.
Olsson [52]	High boost pressure	Extended the high load operation.	High loads up to 16 bar brake mean effective pressure, and ultra-low emissions.
Law [119]	Variable compression ratio (VCR)	Active valve train was used to trap the exhaust gases.	Low NO_x emissions.
Christensen [23]	VCR	HCCI fuel flexibility was demonstrated by using primary reference fuels.	By changing the compression ratio any fuel can be burnt in HCCI engines.
Flowers [120]	Intake charge temperature	Increased the combustion efficiency by charge heating.	Emissions of hydrocarbons and carbon monoxide tend to decrease with increasing intake temperature.
Hatim [121]	Charge temperature and equivalence ratio	Start of combustion was varied with mixture reactivity.	High inlet temperature decreases ignition delay and accelerates the overall kinetics.
Martinez [122]	Heat exchanger	The intake air was heated by waste thermal energy in the exhaust gases.	Reduced the requirements of intake heating.
Gerardo [123]	Exhaust gas recirculation (EGR)	Increases ignition delay and to reduce NO_x emissions.	Longer ignition delay improved mixture homogeneity.
Fang [124]	EGR	Variable EGR and ignition timings were used.	Lower EGR rate and delayed ignition timing should be applied at higher load and vice versa to avoid knocking.
Jan-Ola [125]	EGR	The combustion efficiency at low load conditions was improved.	Cold EGR improved combustion efficiency of turbocharged HCCI engine at all conditions.

Mohamed [68]	Fuel additive	Di-methyl ether (DME), formaldehyde (CH_2O) and hydrogen peroxide (H_2O_2) were used as additives.	H_2O_2 addition was effective in advancing the ignition timing.
Hiraya [126]	Engine speed	Extending the engine operating regime.	As the speed increases, ignition delay becomes longer, which requires high intake temperatures. Hence, lower speeds are suitable for high load HCCI combustion.
Murase [127]	Pulsed flame jet	To enhance ignition reliability and burning rate.	Direct ignition timing control of HCCI combustion is possible with pulsed flame jet.
Hashizume [60], Yokota [61]	Split injection	The combustion process was optimized via fuel injection timing.	Split injection strategy can optimize the combustion process and control emissions.
Christensen [128]	Water injection	Controlling the auto-ignition timing.	Low NO_x emissions and delays auto-ignition timing.

[a] Only the first author is listed, all papers have multiple authors.

2.5.1.4 High boost pressure

Supercharging or turbocharging is used in HCCI engines to extend the domain of operation [26,129]. Supercharging in HCCI combustion increases the Indicated Mean Effective Pressure (IMEP) to 14 bar [118]. Supercharging has the capacity to deliver increased charge density and pressure at all engine speeds, while turbocharging depends upon the speed of the engine. The in-cylinder density and volumetric efficiency can be improved with a high boost pressure. The evaporation of the fuel is increased with a high intake pressure due to high in-cylinder temperatures. The mixing time can be decreased with the boost pressure is advantageous with all early injection systems. The combustion efficiency can be marginally improved at high boost levels, and cooled EGR rates was introduced [130]. But, Taewon et al. [131] found, that the increase of intake boost pressure shortened ignition delay which is not favourable for the MK combustion. Olsson et al. [52] extended the operating range of 6-cylinder truck engine modified to turbocharged HCCI engine to achieve high loads up to 16 bar Brake Mean Effective Pressure (BMEP), and ultra-low NO_x emissions.

2.5.2 Control strategies to delay the auto-ignition

2.5.2.1 Variable compression ratio (VCR)

The start of ignition (SOI) can be delayed by decreasing the compression ratio of the diesel engine, but it should not be decreased to much as it suffers from the thermal efficiency. Many researchers worked on variable compression ratio (VCR) engines to delay auto-ignition of the fuel and to utilize many alternative fuels in HCCI engines. To achieve HCCI combustion decreasing inlet temperatures and lambdas, higher compression ratios were need to maintain correct maximum brake torque and suggested that VCR can be used instead of inlet heating [119]. Christensen et al. [23] demonstrated a low octane (n-heptane) fuel or a high octane (iso-octane) fuel or a medium octane fuel which is the most suitable for the HCCI operation, regarding fuel efficiency and emissions. Increasing the compression ratio from 10:1 to 28:1, achieved fuel flexibility of HCCI engine. Fig. 2.10 (a) and 2.10 (b) depict the cylinder pressure and the heat release for zero octane and 100 octane fuels. By changing the compression ratio any fuel can be burnt successfully in an HCCI engine.

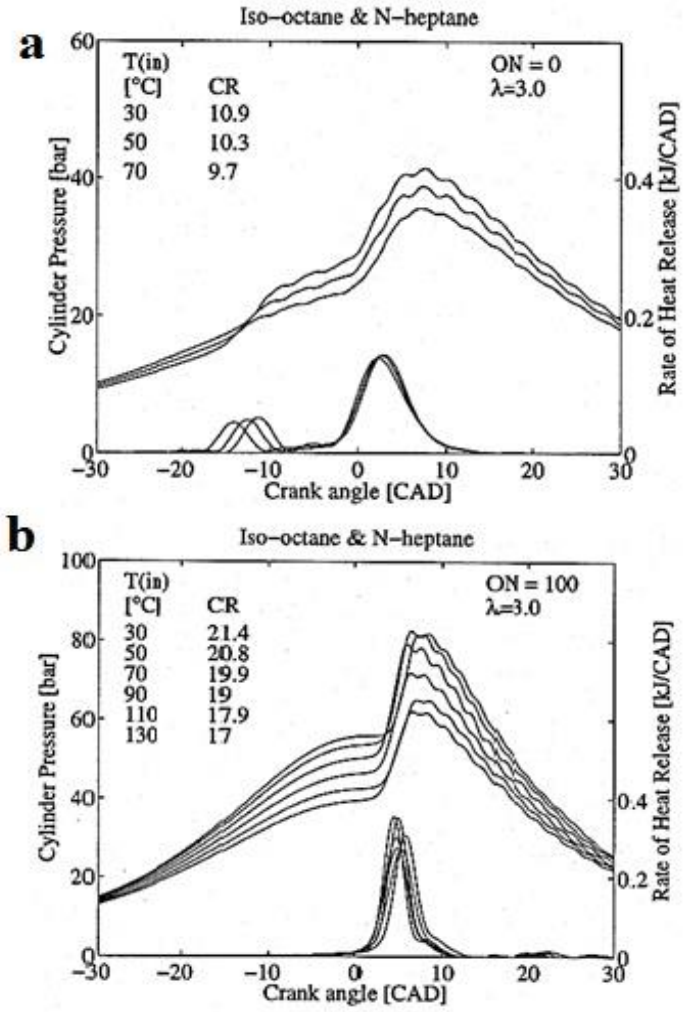

Fig. 2.10. Cylinder pressure and heat release for (a) PRF (n-heptane) (b) PRF (iso-octane) [23].

2.5.2.2 Charge temperature and equivalence ratio

The auto-ignition of fuel-air mixture is a very sensitive to intake air temperature changes, as small as 5-10 ^{o}C [132,133]. Hence, the combustion control is very difficult task in order to achieve high efficiency without any knock. Diesel fuel does not require any charge heating, as it can be burnt easily with a compression ratio of 16. For low cetane fuels, modulate intake air temperature would be necessary to reach its auto-ignition temperature near the TDC for combustion. A higher intake temperature advances combustion, but the engine volumetric and thermal efficiency can be largely reduced, due to the fact that, if ignition is advanced into the compression stroke, it will cause a significant negative work on the piston. Flowers et al. [120] studied cylinder-to-cylinder effects on the variable intake temperature and propane fuel flow rate. Hatim et al. [121] analysed the influence of the inlet temperature, equivalence ratio and compression ratio on the HCCI auto-ignition process of primary reference fuels. The SOI can delay by increasing the ignition delay

also. Fig. 2.11 and 2.12 depict the ignition delays as function of the inlet temperature and equivalence ratio respectively for primary reference fuels.

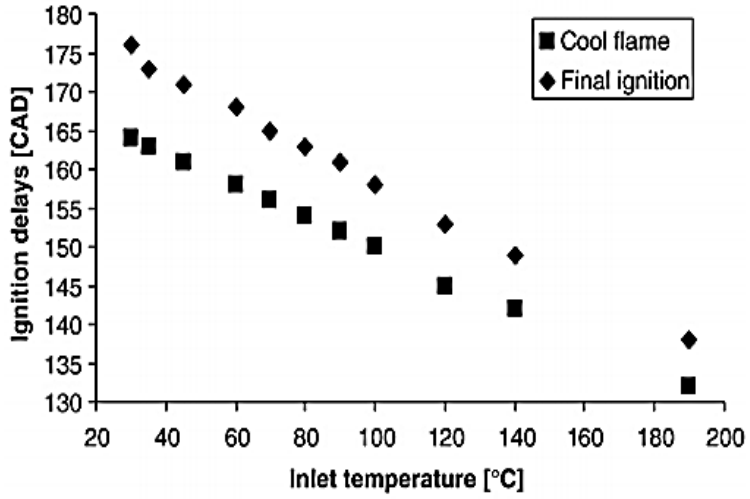

Fig. 2.11. Ignition delays as a function of the inlet temperature for n-heptane [121].

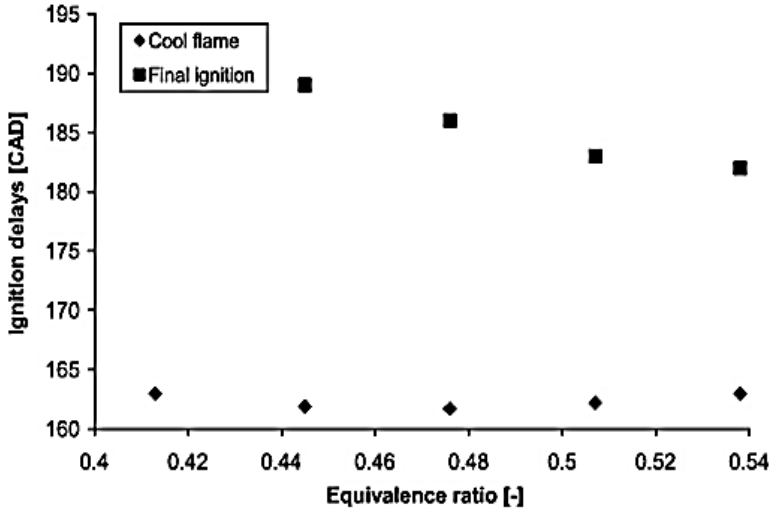

Fig. 2.12. Ignition delays as a function of the equivalence ratio for iso-octane [121].

2.5.2.3 Exhaust gas recirculation (EGR)

The technology of EGR is widely used in HCCI combustion due to its high potential of controlling the auto-ignition of time-temperature history and enhancement of NO_x emission reduction. The EGR can be categorised into internal and external EGR. Internal EGR is acquired by the exhaust gas trap (EGT) using the negative valve overlap (NVO) and variable valve timing (VVT) methods. The most practical means to delay the auto-ignition in an HCCI engine is through the addition of high levels of EGR into the intake.

The inert gases present in the EGR can be used to control the heat release rate due to its impact on chemical reaction rate, which can delay the auto-ignition timing. Hence, EGR reduces the heat release rate, and thus also lowers the peak cylinder temperature due to the constituents of EGR (mainly CO_2 and H_2O) having higher specific heat capacities.

The MK combustion system uses a high EGR to reduce the NO_x emissions up to 98% less than conventional diesel engine. Gerardo et al. [123] studied the effect of EGR on the ignition delay and emissions which are; i) reducing oxygen concentration at the intake, ii) lowers the adiabatic flame temperature, iii) increases the ignition delay with a slower pressure rise rate that also improves the combustion noise, iv) decreases NO_x emissions, and v) a high EGR rate decreased volumetric efficiency and increased smoke emissions. Saxena et al. [134] used an exhaust gas recovery device coupled with an HCCI engine to heat the input energy to ignite the wet ethanol. Ganesh et al. [81] reported that, the EGR has two primary effects on the HC emission (a) the intake of some un-burnt HC with exhausted gas into the next cycle leads to a decrease in HC emissions, and (b) the decrease of combustion temperature in the cylinder led to an increase in HC emissions. Fang et al. [124] investigated on the dual effects of EGR on the BSFC and reported that, the EGR can reduce the pumping loss, and it would lead to slowing the flame propagation speed, making the combustion process far from TDC and decreasing work efficiency of combustion in cylinder. Sjöberg et al. [135] investigated the effect of varying the flow rates of EGR on the auto-ignition chemistry of ethanol fueled HCCI engine. The results indicated that the EGR lowered the oxygen concentration and ethanol exhibit single stage ignition. Fig. 2.13. shows the consequences of intake charge temperature on varying the EGR flow rates.

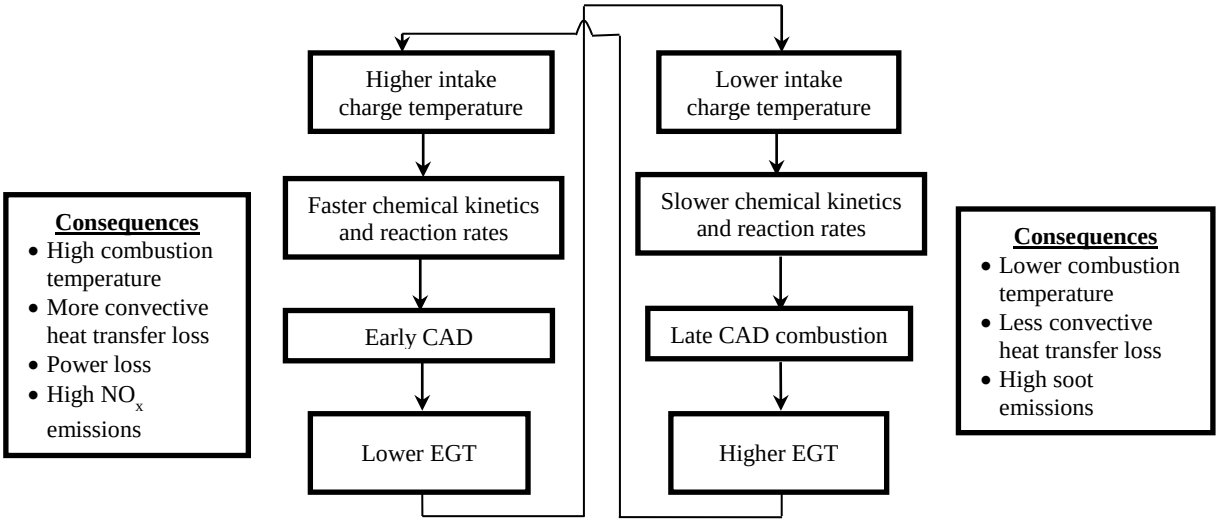

Fig. 2.13. Consequences of intake charge temperature and EGR in HCCI engine.

The combustion limit towards leaner air-fuel mixture and the tolerance to the EGR can be significantly extended. The low heating value of lean mixtures and the high heat capacity of EGR can lower the peak temperature of combustion, thus reduce NO_x emission. Up to 95% reduction in NO_x emission was obtained experimentally [136,137]. At low load, the combustion efficiency is the most important one in HCCI combustion which is improved by EGR [125]. The EGR also used to control the HCCI auto-ignition. The hot EGR advances the combustion timing, while the cold EGR method retards the combustion timing.

2.5.2.4 Fuel modification

The auto-ignition characteristics of the fuel-air mixture can be controlled with fuel blending or/and additives. For HCCI combustion volatility, and auto-ignition characteristics of the fuel are important [138]. Fuel requirements for the HCCI engine operation was investigated by Rayn et al. [139] using constant volume combustion bomb experiments. The experimental results indicated that the primary properties of fuel relate to the distillation characteristics and the ignition characteristics. Research octane number (RON) is a measure of fuel resistance to knock while motor octane number (MON) is a measure of how the fuel behaves at low loads. Kalghatgi [140,141] developed an Octane Index (OI) (function of MON and RON) for measuring the auto-ignition or anti-knock quality of a practical fuel at different operating conditions. Kalghatgi's lower OI shows an earlier combustion phasing. Shibata et al. [142,143] showed a relationship between RON and low temperature heat release (LTHR) which has a strong impact on high temperature heat release (HTHR). He studied 12 hydrocarbon constituents for an HCCI combustion in which olefins and aromatics (except benzene) have a function to retard combustion phasing (LTHR), while iso-paraffins and n-paraffins have a function to advance combustion (HTHR). The effects of cetane number (CN) on the HCCI performance, auto-ignition, and emissions were investigated by some researchers [144–148]. Aroonsrisopon et al. [149] found that, HCCI combustion is a strong function of fuel composition and cannot be predicted by octane number. Maurya et al. [150] used a port fuel injection technique and elevated air temperatures to prepare a homogeneous air/fuel mixture. They found that, a stable ethanol HCCI operation was achieved for equivalence ratios of 2.0–5.0 at 1500 rpm. Shibata et al. [142] demonstrated that, the fuel chemistry directly affected by LTHR and the subsequent main combustion stage (HTHR). Bunting et al. [151,152] found that, high cetane fuels have stronger LTHR behaviour, and do not require high intake

temperature for auto-ignition. They concluded that, low Cetane fuels would be more desirable for better HCCI combustion [153]. The HCCI combustion of high octane fuel (iso-octane) showed a single stage ignition, while the fuel blends showed a two-stage ignition [50]. Fig. 2.14 depicts the single and two-stage heat release rates for iso-octane and PRF80.

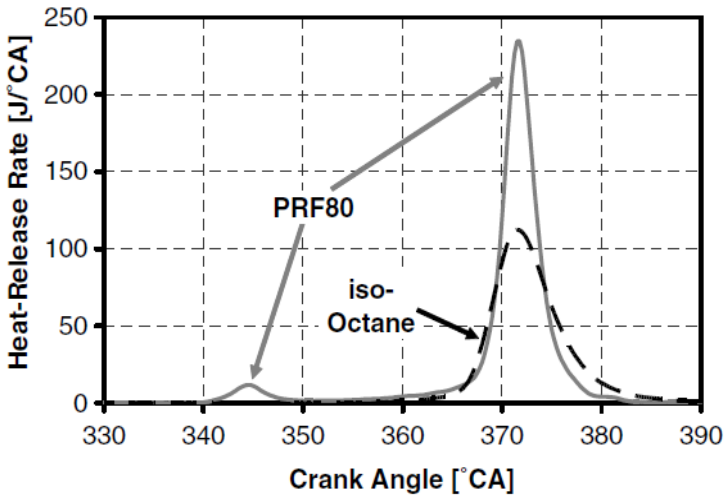

Fig. 2.14. Heat-release traces for iso-octane and PRF80 [50].

The HCCI auto-ignition can also be controlled with fuel additives. An additive fuel in HCCI combustion has the ability to promote or inhibit the kinetics of auto-ignition chemistry. Di-methyl ether (DME) has good characteristics of auto-ignition and combustion with a low flame temperature, and exhibit two-stage heat release [154]. Mosbach et al. [155] used numerical simulation of ethanol and diethyl ether (DEE) by means of a stochastic reactor model. Mohamed et al. [68] studied the effect of additives such as di-methyl ether (DME), formaldehyde (CH_2O) and hydrogen peroxide (H_2O_2) for the control of ignition in natural gas HCCI engines. The study revealed that, high octane fuels require auto-ignition promoters in HCCI combustion engines such as natural gas [133,156,157], LPG [158–160] and ethanol [161]. Mack et al. [162] have demonstrated the use of wet ethanol in HCCI engine, and reported that a stable operation would be possible up to 40% water. The fuel inhibitors extend the ignition delay and promote low temperature oxidation [163,164]. Clothier et al. [165] studied the effect of fuel additives during cold start conditions. He found that the addition of DEE to diesel fuel significantly inhibited its ignition. The fuel additives in HCCI engines control the start of ignition or extend the maximum load limit.

2.6. Thermodynamic modelling of HCCI engines

Khaliq et al. [166] investigated the first and second law analyses for a wet ethanol fueled HCCI engine. They reported that the exergy destruction in the turbocharger pressure ratio was more significant than compressor efficiency and ambient temperature. Many researchers used air-standard cycle models to perform thermodynamic analysis of IC engines. In these studies, the working fluid (i.e., air) was considered to behave as an ideal gas with constant specific heats [167–171]. These air-standard models were used for the comparison of engine parameters and fluid properties. This assumption was found to be inaccurate due to high rise in combustion temperature. Some of the other studies presented the linear variation of the temperature dependent specific heats on the various air-standard cycles such as Otto, Diesel, and Miller [172–174]. However, these linear models are valid for moderate temperature ranges. For the large temperature changes and accuracy, the temperature dependent specific heats are required for a realistic approach.

2.7. Multi criteria decision making (MCDM) approach based on TOPSIS method

Sakthivel et al. [175] used the technique for order preference by similarity to ideal solution (TOPSIS) method for the selection of the best fish oil blend. They found that, the 20% blend was optimum among the six biodiesel blends which they used in their study. Sakthivel et al. [176] also proposed analytical network process (ANP)-TOPSIS model for the selection of the best biodiesel blend, and reported that 20% blend was found optimum. Garcia et al. [177] studied a linguistic multi criteria decision making (MCDM) problem for the selection of a cleaning system for engine maintenance. Soufi et al. [178] used MCDM approach for a bio-lubricant selection for two-stroke petrol engines. They produced bio-lubricants based on a castor oil, palm oil, and waste cooking oil. Etghani et al. [179] optimized the performance and emission features of a diesel engine fueled with castor oil biodiesel based on the TOPSIS method. They simultaneously considered six objectives, maximization of brake power and minimization of BSFC, PM, NO_x, CO and CO_2 emissions. Garcia and Lamata [180] evaluated the maintenance decision problem using TOPSIS in an IC engine factory for production, sale and maintenance to obtain the ranking of alternatives in linguistic terms. Sarkar [181] used analytic hierarchy process (AHP) to perform the evaluation of CO_2, NO_x, efficiency, capital cost, operation and

maintenance costs, service life and produced electricity cost for electrical energy generation. He used the TOPSIS method for the evaluation of the best generation technology and reported the order of performance among them as; natural gas fueled solid oxide fuel cells > natural gas combined cycle > natural gas fueled phosphoric acid fuel cells > natural gas internal combustion engine > hydrogen fueled solid oxide fuel cells > hydrogen internal combustion engines > hydrogen combustion turbines > hydrogen fueled phosphoric acid fuel cells > and natural gas turbine.

2.8. Application of GRNN for prediction of engine parameters

Validating experimental results using artificial neural networks (ANN) is an evolutionary approach which does not use any complex mathematical equations for explaining the non-linear and multi-dimensional systems. During training, the ANN predicts the experimental data and validates with an independent set of data. For any new data, the ANN has the ability to improve the engine performance [186,197]. ANN models have been extensively used to predict the performance and emission characteristics of conventional engines [187,188,195]. Rezaei et al. [182] developed two different ANN models namely radial basis function (RBF) and feed forward (FF) to predict the engine performance metrics. The validation results indicated that, there was less than 4% error for butanol and ethanol-fueled engines. Boliviana et al. [198] used generalized regression neural network (GRNN) to control the diesel engine vibration based on the cylinder pressure. Soufi et al. [184] developed back-propagation neural network (BPNN) for predicting the performance and emissions of a 200 cc two stroke engine. They related the input and output parameters, and suggested that the ANN application would be useful for prediction. The HCCI auto-ignition using ANN was developed using a multi-input single-output (MISO) model for the prediction of the start of combustion [199]. The MISO ANN model was used for a misfire detection in the HCCI engines [87]. They detected that the HCCI engine misfire with 100% accuracy. Piloto et al. [200] predicted the Cetane number of biodiesel using ANN with an accuracy of 92%. Many researchers predicted the performance and emissions using various ANN models other than GRNN, which is currently used in this study. Table 2.6 provides the comparison of the results obtained by different researchers using ANN models.

Table 2.6 Comparison of results obtained by different researchers using ANN models.

Reference	**Fuel used**	**Engine emission parameters**				**Performance parameters**	
		NO_x	**Smoke**	**UHC**	**CO**	**EGT**	**BTE**
Rezaei [182]	Ethanol and butanol	√	X	√	√	X	X
Taghavifar [183]	n-heptane	√	√	X	X	X	X
Soufi [184]	Biolubricants	√	X	√	√	X	X
Haghighi [185]	Diesel and biodiesel blend	√	√	X	X	X	X
Özener [186]	Diesel	√	√	√	√	X	X
Yusaf [187]	CNG-diesel	√	X	X	√	√	√
Najafi [188]	Ethanol and gasoline blends	√	X	√	√	X	√
Sayin [189]	Gasoline	X	X	√	√	√	√
Hossein [190]	Diesel	√	X	√	√	X	X
Roy [191]	Diesel	√	√	X	X	X	√
Çay [192]	Methanol	X	X	X	X	√	X
Mohamed [193]	Diesel and biodiesel blends	√	X	√	√	X	X
Çay [194]	Methanol and gasoline	X	X	√	√	X	X
Deh [195]	Ethanol and gasoline blends	√	X	√	√	X	X
Hosoz [196]	Diesel and biodiesel blends	√	X	√	√	√	√
This work	Ethanol	√	√	√	√	√	√

✓ specific parameter considered in the past research work.
X specific parameter not considered in the past research work.

Many research studies were carried out on the optimization of IC engines which are classified as (a) geometry optimization and (b) optimization of operating conditions. Geometry optimization uses an optimization algorithm to find the best cylinder geometry that minimizes certain fitness functions [201]. The optimization study [202] on the cylinder geometry of a DI diesel engine using with three fitness functions (UHC, NO_x, and soot) and two operating conditions (load and speed). They observed a reduction in NO_x emissions with the combustion chamber of narrow and deep shape. Park [203] focused on reduction of the specific fuel consumption with stoichiometric diesel combustion. The emissions were not considered as optimization objectives due to the claim that they are manageable with after treatments. Wickman et al. [204] optimized diesel engine combustion chamber geometry using genetic algorithm (GA). They found a reduction in the exhaust emissions (UHC, NO_x, and soot) and fuel consumption. Kesgin [205] used GA-NN methods to optimize the engine efficiency and NO_x emissions of a natural gas

engine. The results showed an increase in the efficiency, while the amount of NO_x emissions being kept under the constraint value of 250 mg/Nm^3 for stationary engines. Hiroyasu et al. [206] optimized diesel engine using GA to minimize specific fuel consumption, NO_x, and Soot. They used multiple injections to decrease the trade-off emissions. Mohammadhassani et al. [207] were combined ANN and ant colony optimization (ACO) to predict and reduce exhaust emissions with 294 data sets. They reduced the NO_x and soot emissions, and also optimized fuel flow rate and intake air temperature. Mousa et al. [208] have proposed hybrid PSO-GA algorithm for a local search optimization. Mozaffari and Azad [209] have optimized EGT and UHC emissions during cold start with hybrid PSO and fuzzy logic. This heuristic multi-objective algorithm can solve crucial automotive problems. Roy et al. [210] were optimized the CNG operated performance and emission tradeoff behavior to reach Tier 4 emissions with the inherent design of PSO.

2.9. Summary

From the literature review, it is understood that, the HCCI combustion engines has advantages over conventional SI and CI engines. The HCCI combustion closely follows Otto cycle that causes high thermal efficiency by saving fuel. Also, achieving ultra-low NO_x and smoke emissions would be possible. The homogeneous mixture preparation and spontaneous auto-ignition are the main key features of these tremendous advantages of the HCCI engines. The automobile manufacturers mainly focus on the fuel economy and low emissions from the HCCI engines. Hence, many researchers explored the potential of using renewable liquid fuels mainly to reduce emissions and also to meet the energy demand. The gasoline (and diesel) fuel variation is one of the key factors preventing the HCCI engine for practical applications. Maybe the consistency of ethanol could be an advantage. One of the possible alternative fuel is ethanol due to its clean combustion characteristics. Therefore, the present research is mainly focused on the effective utilization of the ethanol in the HCCI engines.

2.10. Objectives of the present study

In the first objective, improving HCCI power output, experimental tests were conducted that explore increasing the high load limit of HCCI operating conditions. The experimental results were examined for a better understanding of the HCCI operation, and what conditions the engine can lead to high power output, better efficiency and minimal

emissions. The best operating points for the ethanol fueled HCCI engine are suggested, and detailed operating characteristics are explored.

In the second objective, prediction and optimization of ethanol fueled HCCI engine, two topics were explored. The first was to predict the HCCI output parameters for any input conditions. This could saves time and cost of conducting experiments at each and every operating condition. The second was to choose the best HCCI operating condition using optimization based on the flexible and user defined weights.

2.11. Dissertation contributions

This dissertation aims to the understanding of the ethanol fueled HCCI combustion through the utilization of experimental and optimization techniques. A few key contributions to the scientific community are highlighted below.

- Utilization ethanol in a high compression ratio HCCI engine to improve thermal efficiency and reduce exhaust emissions.
- Thermodynamic modelling of the HCCI engine to investigate the preliminary results of combustion, performance, emissions and load limits.
- The use of ethanol in an HCCI engine with charge heating and PFI technique to evaluate the combustion, performance and emission behaviour.
- Application of TOPSIS method to determine the optimum charge temperature and load using multicriteria decision making technique.
- The prediction of the HCCI output parameters using GRNN for any input criteria.
- The use of EGR in the ethanol fueled HCCI engine with charge heating and PFI technique to control the combustion, and to evaluate the combustion, performance and emission behaviour.
- The best operating condition of the ethanol fueled HCCI engine was optimized using hybrid GRNN-PSO.
- To evaluate the combustion, performance and emission behaviour of a HCCI engine with charge heating and fuel vaporizer.

Chapter 3

Experimental materials and methods

3.1. General

Before carrying out a research, a basic idea on the properties of the materials that have to be used in the study is essential. Also, a thorough knowledge is required on the fundamentals or basic principles of the instruments that are to be used. This chapter provides the details of the experimental setup used in this research study. Further, it describes the instrumentation adopted for the research study. The procedure for conducting the HCCI engine experiments along with the loading device and emission measuring instruments are discussed. This chapter also provides information on the accuracies and uncertainties of the instrumentation adopted in this study.

3.2. Materials for this investigation

In order to evaluate the combustion, performance and emission parameters of the HCCI engine at various engine operating conditions, the following equipment/instruments are required before starting the investigation.

- A high compression ratio engine preferably diesel engine is required to be modified such that an HCCI combustion mode is achieved. In this thesis, external mixture formation technique was used to convert the existing diesel engine into HCCI mode by adopting port fuel injection technique.

- An Arduino board preferably electronic control unit (ECU) for controlling the injector and pump electronically.

- A dynamometer to apply sufficient resistance to the HCCI engine.

- A high resolution pressure transducer to record the cylinder pressure data of the HCCI engine. Also, crank position sensor to record the speed and position of the piston.

- The instruments for measuring the fuel flow and air flow to calculate the performance parameters of the HCCI engine.

- The emission measurement instruments to record the emission parameters.

The detailed description of the above mentioned equipment/instruments are given in the following subsections.

3.3. HCCI engine experimental setup

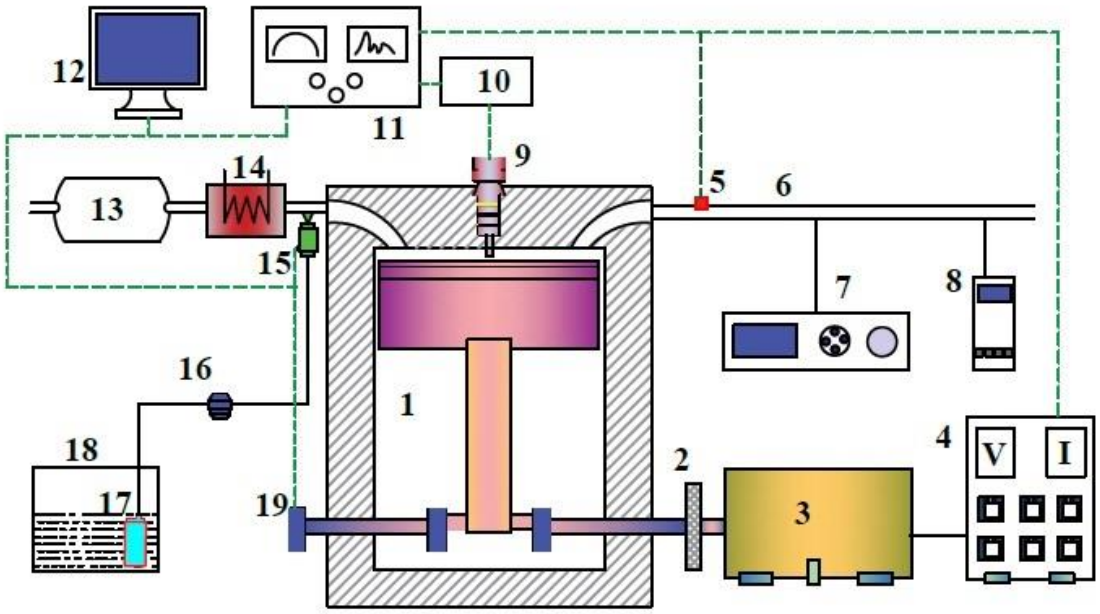

Fig. 3.1. Schematic diagram of the experimental setup.

1. Engine
2. Flywheel
3. AC alternator
4. Resistive load cell
5. EGT sensor
6. Exhaust manifold
7. Exhaust gas analyzer
8. Smoke meter
9. Pressure transducer
10. Charge amplifier
11. Data acquisition system
12. Computer
13. Intake plenum
14. Air heater
15. Port fuel injector
16. Pressure regulator
17. Fuel pump
18. Fuel tank
19. Crank position sensor

The test engine used in this thesis was a single cylinder, four-stroke, air-cooled, constant speed diesel engine (make: Kirolaskar and model: TAF1) with 661.5 cc displacement volume and 4.4 kW rated power. The technical specifications of the engine are given in Appendix A1. For the research study, the diesel engine was converted to run on the HCCI mode by adopting external mixture formation technique. The flush mounted pressure transducer on the cylinder head records the in-cylinder pressure of the HCCI engine. The intake air was preheated to achieve auto-ignition temperature of the ethanol. The intake air temperature was varied from 130 to 170 °C insteps of 10 °C at a regular interval and admitted into the test engine. The reason for selecting the minimum and maximum temperature for preheating is given in Chapter 5. A temperature sensor and a temperature controller were used to monitor and control the electrical heating.A k-type thermocouple

was used to measure the exhaust gas temperature (EGT). The schematic diagram of the experimental setup is shown in Fig. 3.1. An electrical dynamometer connected to a resistive load bank was coupled to the engine, which provided a necessary load to the engine. The engine has a fixed valve timing. This might be another reason that residual EGR was not used for controlling the HCCI combustion process since it requires adjusting the valve timings in real-time.

3.4. Air flow measurement

Air flow can be measured with the following techniques [211].

- Pitot tubes
- Mechanical anemometers
- Heated-element anemometers
- Orifice meters
- Venturi meters
- Capture hoods

Anemometers ate the commonly used for air flow measurement. The term is derived from the Greek word anemos, which means wind, and is used to describe any wind speed measurement instrument used in meteorology [212].The following are different types of the anemometers.

- Cup anemometers
- Vane anemometers
- Hot-wire anemometers
- Laser doppler anemometers
- Ultrasonic anemometers
- Plate anemometers
- Tube anemometers

The vane anemometer is one of the mechanical velocity anemometer. It may be described as a windmill or a propeller anemometer. The axis on the vane anemometer must be parallel to the direction of the flow and therefore horizontal. The speed of the fan is measured by a rev counter and converted to a windspeed by an electronic chip. Hence, volumetric flowrate may be calculated if the cross-sectional area is known.The photographic view of the digital anemometer is shown in Fig. 3.2.This instrument is used because its hand-held digital anemometer. The fresh intake air was metered with a digital anemometer (make: Lutron, model: AM-4200). A large surge tank (60 times displacement volume) was used to minimize the damping in the pressure pulse during the suction stroke. The mass flowrate of air is calculated using Eq. 3.1.

$$m_a = \rho_a \times A \times v_a \tag{3.1}$$

Where m_a, ρ_a and v_a are the mass flowrate, density and velocity of the air respectively, A is the area of the intake manifold.

The theoretical mass of air is calculated using Eq. 3.2. It is the product of density of air and swept volume of the cylinder.

$$m_T = \rho \times V_s \tag{3.2}$$

Further, volumetric efficiency was calculated using Eq. 3.3. It is the ratio of the mass of air trapped in the cylinder to the theoretical mass of air.

$$\eta_V = \frac{m_a}{m_T} \tag{3.3}$$

Fig. 3.2. Photographic view of the digital anemometer.

Fig. 3.3 depicts the variation of the volumetric efficiency with the intake air temperature. It is evident from the figure that the volumetric efficiency decreases with the increase in the intake air temperature. This is due to the decrease in the density of air with the increase in the intake air temperature. For a constant speed engine, the volumetric efficiency is constant at all the engine operating loads.

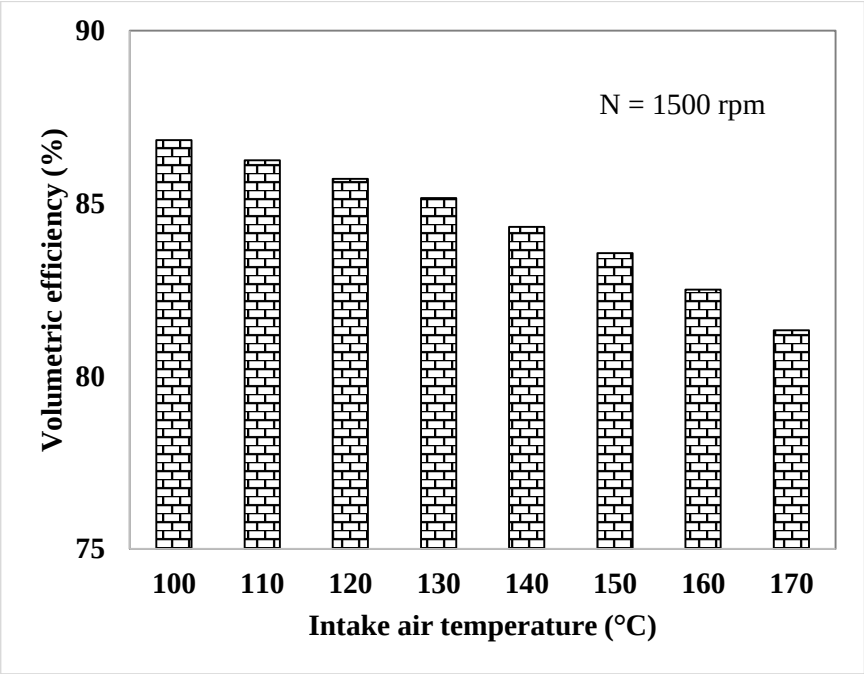

Fig. 3.3. Variation of the volumetric efficiency with intake air temperature.

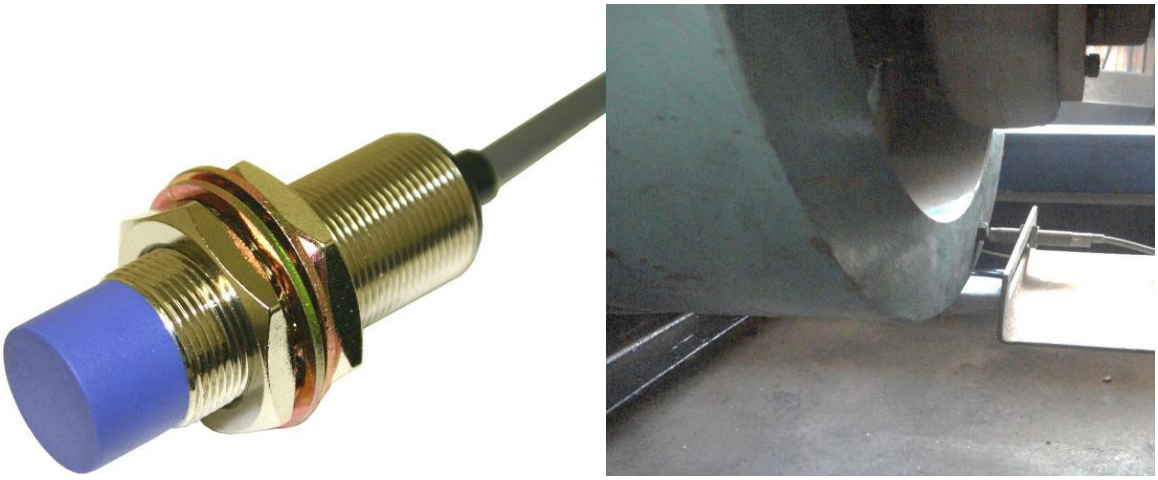

Fig. 3.4. Photographic view of PNP sensor (left), and TDC marker and deflector (right).

3.5. Speed measurement

A non-contact PNP (positive, negative, positive) type sensor (make: Kistler, model: 5015A1000) was connected near the flywheel of the engine to measure the engine speed. The pulse frequency output of PNP sensor from each revolution of the crank shaft was converted into voltage output. A standalone frequency to voltage converter was used for signal conditioning. Fig. 3.4 shows the photographic view of PNP sensor, and TDC marker and deflector. The PNP sensor wiring for speed measurement is shown in Fig. 3.5.

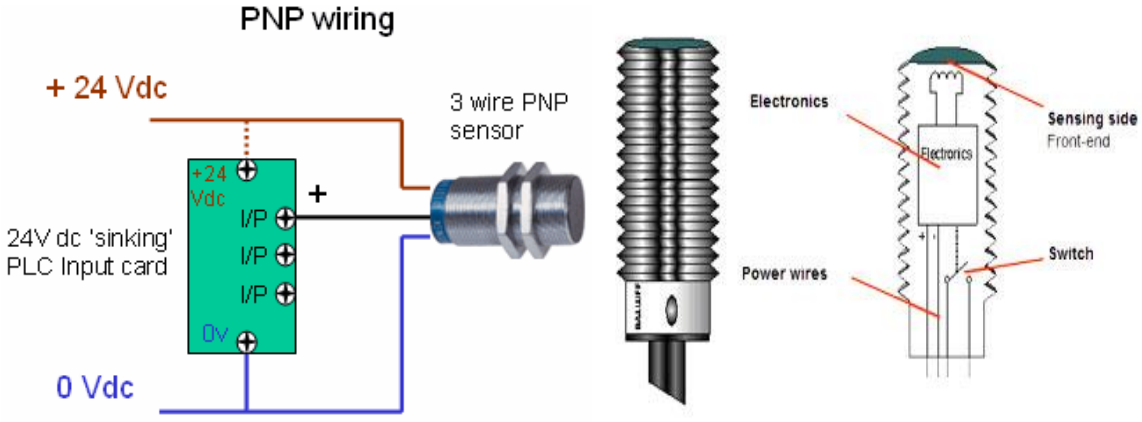

Fig. 3.5. PNP sensor wiring for speed measurement.

3.6. Fuel flow measurement

The fuel was injected into the custom intake manifold with a port fuel injector (PFI). The injector was controlled by an electronic control unit (ECU) that in turn synchronized with a crank angle sensor. Fig. 3.6 shows the photographic view of port fuel injector and pump.

Fig. 3.6. Photographic view of port fuel injector (left) and pump (right).

Fig. 3.7 portrays the flow chart of the electronic fuel injection. The fuel injection is the static flow capacity, corresponds to the volume flow rate based on the pulse time. The solenoid of the PFI will be energized to allow the fuel to inject. Therefore, the pulse injection time was controlled for accurate fuel injection. Initially, speed of the engine was recorded and checks for constant speed of 1500 rpm. If the speed exceeds 1500 rpm then,

1 ms pulse time will be reduced. On the other hand, speed is less than 1500 rpm then, 1 ms pulse injection time will be increased. The increase/decrease in the pulse time is based on the engine speed. If the engine reaches the constant speed of 1500 rpm then the pulse time was maintained constant for that load. The amount of fuel injected per cycle was recorded for further calculations.

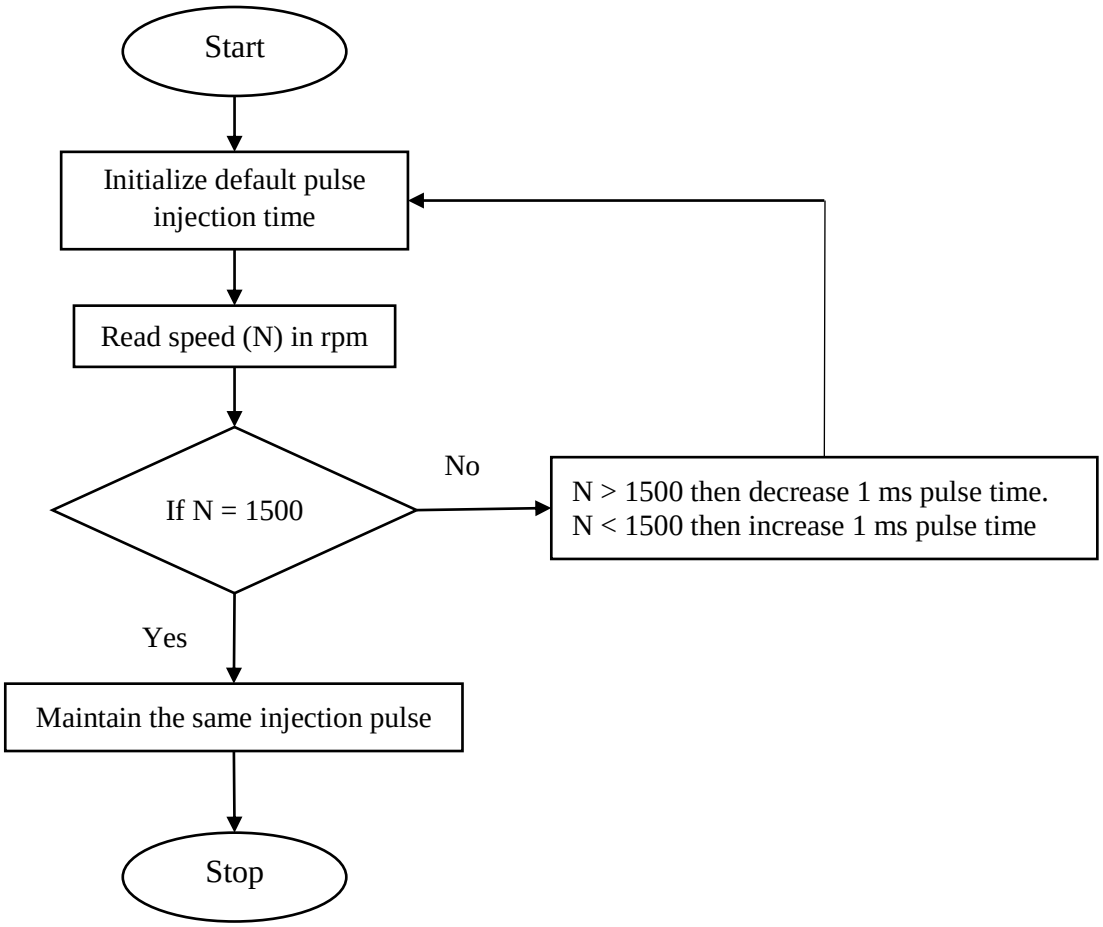

Fig. 3.7. Flow chart of the electronic fuel injection.

3.7. In-cylinder pressure measurement

An air-cooled piezoelectric quartz transducer (make: KISTLER, model: 5395A) was mounted on the cylinder head and used to measure the in-cylinder pressure with a resolution of 0.5 crank angle degree (CAD) interval with the signal triggered by the crankshaft encoder. Fig. 3.8 shows the photographic view of Kistler pressure transducer. The exploded view of the piezoelectric transducer is shown in Fig. 3.9. Appendix A2 provides the technical specifications of the pressure transducer. Fins were attached to the pressure transducer body to provide the cooling medium. A total of 200 consecutive

engine cycles were recorded to avoid the occurrence of cycle-to-cycle variations. These recorded pressure traces were then averaged, and post processed using a combustion diagnostic software. A 12 bit analog to digital converter (ADC) was used to convert analog signals to digital signals. The analog to digital card had both an external and internal trigger facility. The pressure and crank angle data were collected in an excel spreadsheet installed in the data acquisition system (DAS).

Fig. 3.8. Photographic view of Kistler pressure transducer.

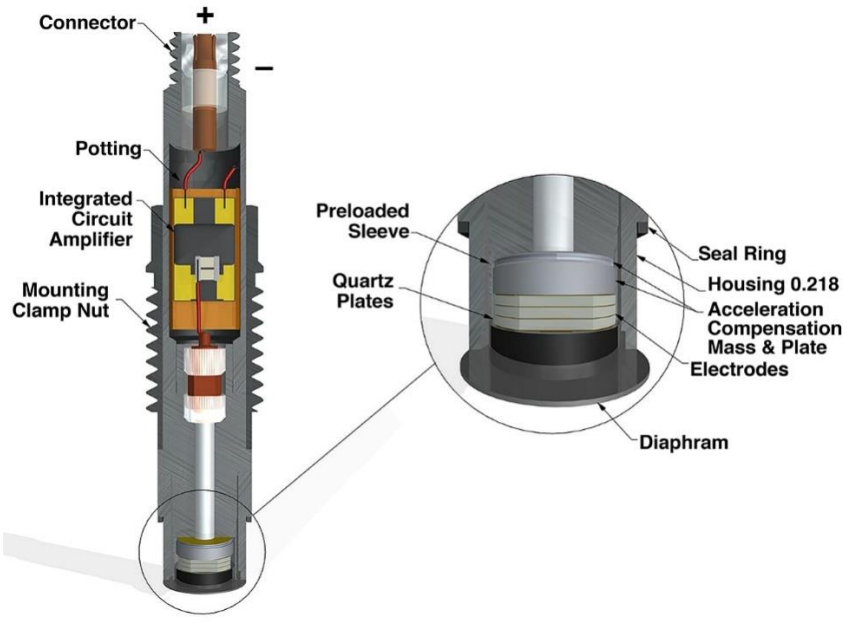

Fig. 3.9. Exploded view of piezoelectric transducer.

The charge amplifier (make: KISTLER, model: 365C) was in conjunction with the piezoelectric pressure transducer was integrated in the circuit. The charge amplifier converted the electric charge signals generated by the piezoelectric pressure transducer to

voltages and sent to data recording equipment. The charge amplifier could operate with a power supply of 7-32 V DC with a range of 0-100 bar pressure. The signal conditioning task is a part of the measurement system is to couple information, contained within the small amount of electrical charge generated by the crystals, to the outside world without dissipating it or otherwise changing it. The quantity of charge generated by the piezo element was measured in units of picocoulombs (pC), which was 1 x 10^{-12} coulombs. The two types of signal-conditioning systems most often used were the charge-Mode system using charge amplifiers and the Low Impedance Voltage Mode (LIVM) System typically using a junction field effect transistor (JFET) or metal-oxide semiconductor field-effect transistor (MOSFET). Fig. 3.10 shows the circuit diagram of piezoelectric pressure transducer along with the charge amplifier. Appendix A3 lists the technical specifications of the charge amplifier.

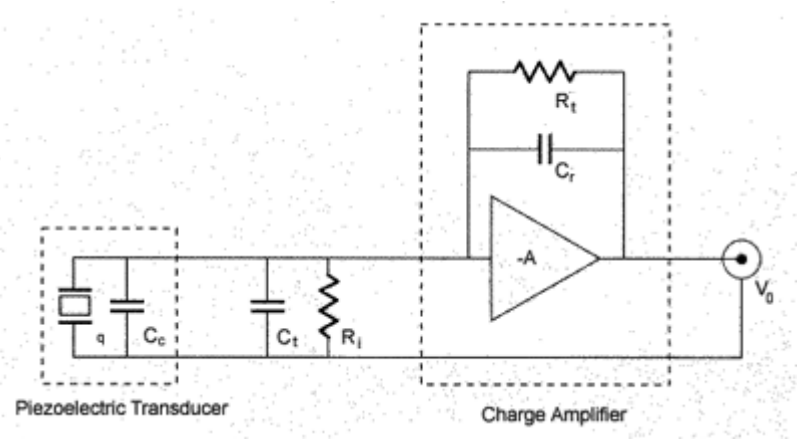

Fig. 3.10. Circuit diagram of piezoelectric pressure transducer and the charge amplifier.

Where C_t = transducer capacitance, C_c= cable capacitance, C_r = range (or feedback) capacitor, R_t = time constant resistor (or insulation of range capacitor), R_i = insulation resistance of input circuit (cable and transducer), q = charge generated by the transducer, V_o = output voltage, and A = open-loop gain.

Charge amplifiers are typically made up of a high-gain inverting voltage amplifier with a MOSFET or JFET high-impedance input to achieve high insulation resistance. The input stage of the charge amplifier used a capacitive feedback circuit to balance or "null" the effect of the applied input charge signal. The feedback signal is then given as a measure of input charge. This amplifier present essentially infinite input impedance to the sensor and thus measured its output without changing it - the goal of all measurement processes. The gain (transfer function) of the basic charge amplifier is dependent only upon the value of

the feedback capacitor C_f and is independent of input capacitance, an important feature of the charge amplifier. The charge amplifier gain is independent of input capacitance, therefore system sensitivity is unaffected by changes in input cable length or type, an important point when interchanging cables. Neglecting the effects of R_t and R_i results in the output voltage as given in Eq. 3.4.

$$V_0 = \frac{-q}{C_r} \times \frac{1}{1 + \frac{1}{AC_r}\left(C_t + C_r + C_c\right)} \tag{3.4}$$

For sufficiently high open-loop gain, the cable and transducer capacitance can be neglected and the output voltage depends only on the input charge and the range capacitance.

$$V_0 = \frac{-q}{C_r} \tag{3.5}$$

3.8. Engine control

The combustion control is the most challenging task in the HCCI engines for a wide range of operation. The primary controller of combustion timing is intake air temperature. This is maintained using electric heater.

3.9. Diagnostics

The experimental procedures used in this dissertation paid attention to some important metrics: in-cylinder pressure, intake temperature, heat release, combustion duration, combustion timing, thermal efficiency, and emissions.

3.9.1. In-cylinder pressure measurement

The transient pressure in the cylinder was measured with the piezoelectric pressure transducer. The pressure traces were measured for each half degree crank angle. The pressure data was filtered using least square polynomial curve fitting technique. This pressure data was used to compute many engine operating parameters such as heat release rates, CA50, and ringing intensity. This dissertation shows the averaged in-cylinder pressure traces of 200 consecutive thermodynamic cycles during steady state operation.

The variations of the pressure trace profiles obtained during the steady state operation were lower.

3.9.2. Intake temperature

The auto-ignition temperature of ethanol is higher than diesel due its low Cetane number. Therefore, high intake air temperatures are required to facilitate the auto-ignition process. combustion timing advances with the increase in the intake temperature. An electric heater of 600W was used to preheat the intake air before entering into the cylinder. The temperature of the air was maintained with the help of a highly sensitive temperature controller.

3.9.3. Heat release

The heat release rate during combustion process was determined with the help of in-cylinder pressure traces. The first law of thermodynamics was applied to calculate the heat release rate.

$$dQ = dU + dW \tag{3.6}$$

The ideal gas equation can be expressed as:

$$PV = mRT \tag{3.7}$$

Differentating Eq. (3.7) we get, $PdV + Vdp = mRdT$ (3.8)

$$dU = mC_v(\theta)dT \tag{3.9}$$

By substiting dU in Eq. (3.9) into Eq. (3.8) we get

$$dU = \frac{C_v(\theta)}{R}\left(PdV + VdP\right) = \frac{1}{\gamma - 1}\left(PdV + VdP\right) \tag{3.10}$$

By substiting dU in Eq. (3.10) into Eq. (3.6) we get

$$dQ = \frac{1}{\gamma - 1}\left(PdV + VdP\right) + PdV$$

$$\frac{dQ}{d\theta} = \frac{\gamma}{\gamma - 1}P\frac{dV}{d\theta} + \frac{1}{\gamma - 1}V\frac{dP}{d\theta} \tag{3.11}$$

where Q, θ, γ, P, and V represents heat release, crank angle, ratio of specific heats,

pressure and volume respectively. $\frac{dV}{d\theta}$ is defined and $\frac{dP}{d\theta}$ is the experimental pressure traces.

3.9.4. Combustion duration

The crank angle at which 5% and 95% of the cumulative heat release occurs is termed as start and end of combustion respectively. The combustion duration is the time between the start and end of combustion.

3.9.5. Combustion timing (CA50)

The crank angle at which 50% of the cumulative heat release occurs is termed as combustion timing.

3.9.6. Brake power (BP)

Brake power is the output power measured from the crank shaft. An electric dynamometer is used for loading the engine.

3.9.7. Air standard efficiency

The ideal cycle efficiency using air as working fluid with assumption of isentropic compression and expansion is termed as air standard efficiency. It is defined as the work output divided by the heat addition and calculated using Eq. 3.12.

$$\eta = 1 - \left(\frac{1}{CR}\right)^{k-1} \tag{3.12}$$

Where CR is the compression ratio and k is the ratio of specific heats, $k = C_p / C_v$.

It is understood from the above expression that, high compression ratios lead to higher efficiencies. Therefore, CI and HCCI engines are most efficient than SI engines.

3.9.8. Brake thermal efficiency

Brake thermal efficiency is defined as break power of a heat engine as a function of the thermal input from the fuel. It is used to evaluate how well an engine converts the heat from a fuel to mechanical energy. It can be calculated using Eq. 3.13.

$$\eta_{bth} = \frac{BP}{m_f \times LHV} \tag{3.13}$$

Where m_f is the mass of the fuel and LHV is the lower heating value of the fuel.

3.10. Emission measurements

The exhaust emissions from the HCCI engine tailpipe were sampled using an AVL 444 Digas analyzer and followed ASTM D6522 for measurement. The smoke opacity was measured by an AVL 437 diesel smoke meter. The basic principles of operation of the gas analyzer and the smoke meter are described in the following subsections. The description of the gas analyzer and smoke opacity are also further discussed in the subsequent subsections.

3.10.1. NDIR principle for UHC and CO emissions measurement

An NDIR sensor is one of the simple spectroscopic sensor often used as a gas detector [213]. It is nondispersive in the sense of optical dispersion since the infrared energy is allowed to pass through the atmospheric sampling chamber without deformation. The measurement of UHC and CO emissions from the engine exhaust using non-dispersive infrared (NDIR) principle. Fig. 3.11 illustrates the NDIR principle for emission measurement. The main components of an NDIR sensor are an infrared source (lamp), a sample chamber or light tube, a light filter and an infrared detector. The IR light is directed through the sample chamber towards the detector. In parallel, there is another chamber with an enclosed reference gas, typically nitrogen. The gas in the sample chamber causes absorption of specific wavelengths according to the Beer–Lambert law, and the attenuation of these wavelengths is measured by the detector to determine the gas concentration. The detector has an optical filter in front of it, eliminates all light except the wavelength that the selected gas molecules can absorb.Ideally other gas molecules do not absorb light at this wavelength, and do not affect the amount of light reaching the detector however some cross-sensitivity is inevitable [214]. Beer's Law describes the exact relationship between IR light intensity and gas concentration as in Eq. 3.14.

$$I = I_0 e^{kP} \tag{3.14}$$

Where I = the intensity of light striking the NDIR detector, I_0 = the measured intensity of an empty NDIR sample chamber, k = a system dependent constant and P = the concentration of the gas to be measured.

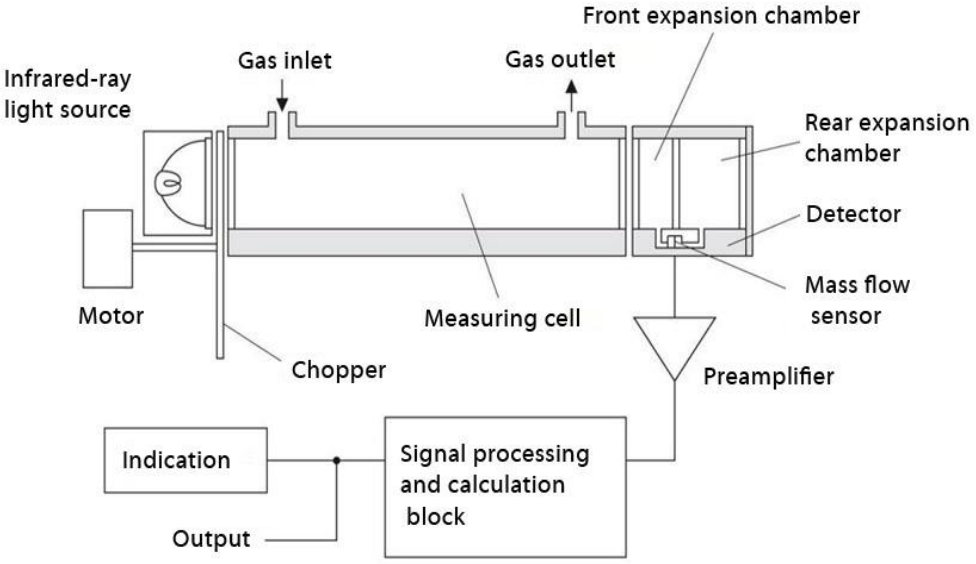

Fig. 3.11. Pictorial layout of NDIR principle.

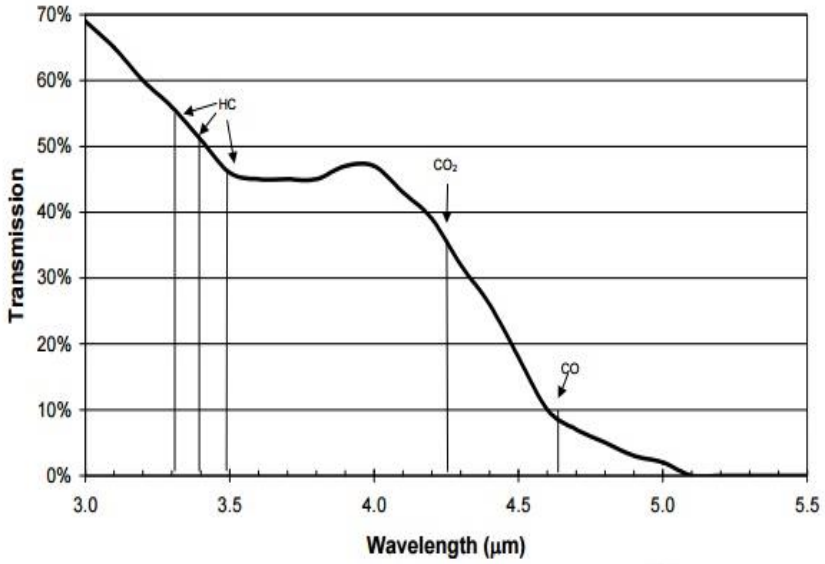

Fig. 3.12. Spectral transmission of the glass envelope for IR lamps and absorption wavelengths for HC, CO_2 and CO gases [214].

The NDIR gas sensor needs an infrared source for the excitation of the gas molecules. Thermal radiators (IR lamps) are often employed for this task. Their operating temperature should be as high as possible to obtain a large output intensity and detector signal. Glass envelope lamps operate at higher filament temperatures when compared to other filament

or ceramic heating elements. The envelope can be a gas-filled or a vacuum. However, the transmission of the glass envelope limits the useful spectral range and constrains the types of gas molecules that can be measured by NDIR.The transmission characteristics of a typical lamp glass are illustrated in Fig. 3.12 with the center wavelength of some common gas absorption bands. The intensity of the IR light decreases significantly above 4 mm with a cutoff wavelength located at 5 mm. A IR lamp is a very cost-effective component for an NDIR sensor, but it has a limited IR range. For carbon monoxide (CO), carbon dioxide (CO_2) and hydrocarbon (HC) detection, it is an ideal technique.

The most desirable NDIR lamp characteristics are (a) high IR output, (b) accurate filament position, (c) small size, (d) long lifetime, and (e) low thermal time constant.

3.10.2. Electrochemical principle for the NO measurement

Electrochemical method of detection is one of the direct methods for NO detection. These electrochemical sensors use amperometry measurement technique for quantitative analysis. In amperometry, the chemical species are subjected to a potential through an electrode system for quantitative analysis. Fig. 3.13 portrays the gas detection system featuring an electrochemical gas sensor. A bias circuit (Potentiostat) is required by the electrochemical gas sensor so that the appropriate bias potential can be maintained between the reference and the sensing electrodes. The output current produced by the gas sensor is in proportion to the gas concentration. The small currents generated from the electrochemical cell are converted into measureable voltages by a trans-impedance amplifier.The trans-impedance amplifier output is sampled by the analog to digital converter (ADC), generating a digital reading for the level of voltage. The microprocessor uses this value for computing the concentration of the target gas. A zero setting and a gain setting correction will be required at some point of stage in the system. This could be done at the trans-impedance amplifier or within the microprocessor. An analog reading of gas concentration can be directly obtained from the voltage output of the trans-impedance amplifier. The NO species is oxidized on the sensor which consists of a working and Ag/AgCl reference electrode pair. A potential (approx 900 mV) is applied to the working/measuring electrode, relative to a reference electrode, and the resulting small redox current due to the oxidation of NO according to the following reaction, is measured by an amplifier system and recorder:

$$NO + 4OH^- \rightarrow NO_3^- + 2H_2O + 3e^- \quad (3.15)$$

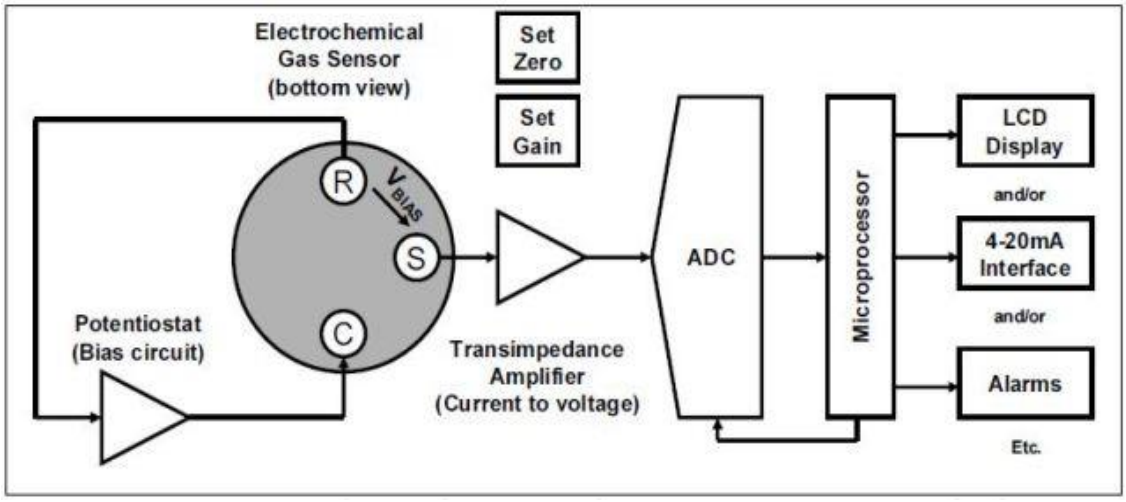

Fig. 3.13. Block diagram of gas detection system using an electrochemical gas sensor [215].

3.10.3. AVL 444 Digas Analyser

The different samples of exhaust gases from the HCCI engine were analysed in a gas analyzer (make: AVL India, model: 444). The analyser was fitted with a DiGas sampler, conforming to ARAI certification: ARAI/TA(4GRV)/AVL/DiGas 444/0910-12. The principle for measuring the CO, UHC emissions was the NDIR, and for the NO was electrochemical. The CO emission was measured in volume percentage, while the UHC was measured in ppm (vol.) of n-hexane equivalent, and the NO emission was measured in ppm (vol.) during each run of the engine operation. The photographic view of the AVL 444 Digas analyzer is shown in Fig. 3.14. The complete technical specification of the AVL 444 Digas analyzer is given in Appendix A4.

The analyzer was interfaced through its RS 232C communication bus to an in-house developed emission data acquisition platform, which recorded the emissions over a span of 120 s in 20 s consecutive intervals, which was greater than the instrument response time of 15 s, for each case of the engine operation. The exhaust gases were tapped from a T joint between the exhaust gas outlet, and the smoke meter tapping point. A fine filter to remove the adverted particulates and a condensate trap were incorporated, after the main exhaust gas cooler so that the exhaust inlet temperature to the analyzer was maintained ≤ 40 °C as per the instruction manual. Stray condensates, if any, were tackled by the condensate separator inbuilt in the analyzer, which was flushed before every case of data recording. Leak check, UHC residue test, zero adjustment and condensate purging of the analyzer, were carried out before each observation. It is to be noted that, the analyzer was

calibrated with the recommended calibration gas mixture, before the start of the entire range of experimentation. The detector in the gas analyser was made up of Selenium photocell with a diameter of 45 mm. Its maximum sensitivity in light was within the frequency range of 550-570 nm. Below 430 nm and above 680 nm, the sensitivity of the instrument was less than 4% related to the maximum sensitivity. Emission tests were carried out by inserting a probe into the engine's exhaust tube by opening the ball valve. Before taking the emission test, a leak check was conducted in the digital gas analyser, to discharge the residual gases by closing the probe's nozzle manually.

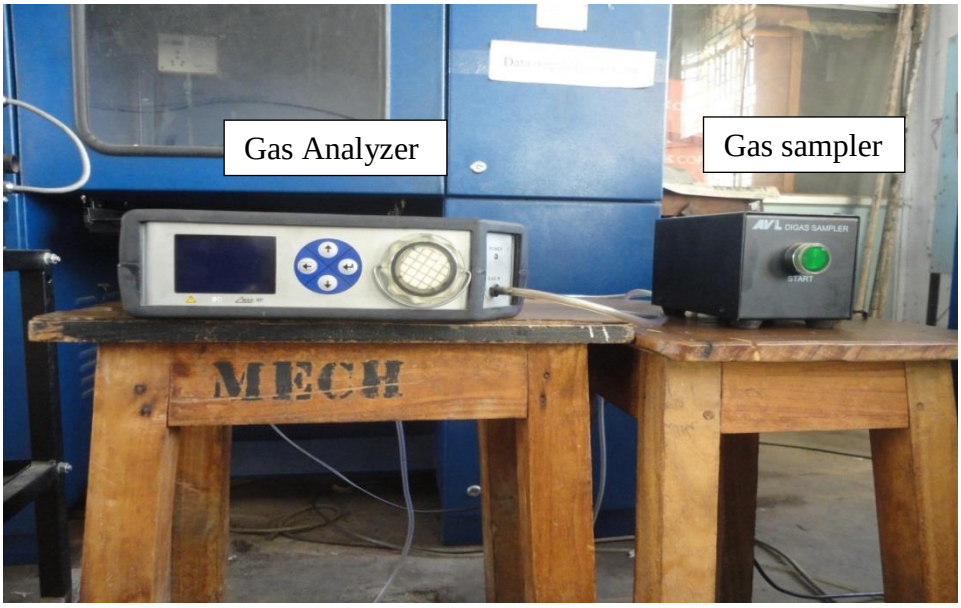

Fig. 3.14. Photographic view of the AVL Digas 444 analyzer.

The gas analyser was calibrated prior to the emission test with calibration gases certified to ±2% accuracy as per the EPA test methods in 40 CFR 60 and the ISO 3930, 1976 test method. Three calibration gases (zero, mid and high) for CO, NO, and NO_2 were used. The purified ambient air was used as the zero gas. The mid-level gas concentration was 40% to 60% of the high range calibration gas. A high-level gas concentration of the high range calibration gas was not higher than 125% of the expected concentration n nor less than 90% of the expected concentration. The high level gas was equal to the calibration span. The analyser calibration error was not greater than ±5% of the calibration span value for the mid and high range calibration gases, or 5 ppm, whichever is less restrictive.The calibration error was calculated as follows:

$$\% \text{ Difference} = \frac{\text{Analyzer response} - \text{Gas concentration}}{\text{Calibration span}} \times 100 \qquad (3.16)$$

For the zero gas, the calibration error shall be no more than 10 ppm:

Difference in ppm = Analyser response – Zero gas concentration.

The following steps were adopted for calibration of the gas analyzer:

Step 1: Allow the analyser to purge the calibration gases prior to beginning the emissions test.

Step 2: A test shall consist of three runs, with each run at least 20 minutes in length.

Step 3: Record the readings for HC, CO and NO, at 2 minute intervals for 20-minute run.

After a maximum of three valid 20-minute emission tests, conduct a post-test calibration as

follows for the HC, CO and NO calibration gases:

Step 1: Allow the analyser to purge the gas sample until a stable zero reading is observed. Record the zero reading.

Step 2: Introduce the high range calibration gas to the analyser and allow it to reach a stable

reading. Record the analyser reading.

Step 3: Introduce the mid-range calibration gas into the analyser and allow it to reach a stable

reading. Record the analyser reading.

Calculate the difference with the pre-test calibration value. If the difference is greater than ±5% or 5 ppm, whichever is less restrictive, the emission test runs are invalid, and must be repeated.

3.10.4. Smoke measurement

The smoke emission was sampled with AVL (Austria) 437 diesel smoke meter. This smoke meter was certified by ARAI, Pune, India, as per ARAI/TA(SM-RV)/AVL/437/1011-02. Fig. 3.15 illustrates the schematic diagram of the smoke measurement. The operating principle is based on the attenuation of a light beam caused by the exhaust gases in a measuring chamber of defined measuring length, and nonreflecting surface filled homogeneously with the exhaust gas. The loss of light intensity between the light source and a receiver is measured and reported in % opacity, the calculation being based on the Beer- Lambert law. The absorption coefficient “k” was also reported by the smoke meter, in accordance with the ECE-R24/ISO 3173. Condensation inside the instrument is avoided, as the measuring chamber is thermostatically heat controlled at 70 ± 5 ^{o}C. To ensure accuracy and repeatability observations were recorded, at each case of the engine operation, for a span of 120 s at

intervals of 20 s, which was greater than the instrument measurement value resolution time of 10 s. The photographic view of the AVL 437C diesel smoke meter is shown in Fig. 3.16. The technical specification of AVL 437C diesel smoke meter are given in Appendix A5.

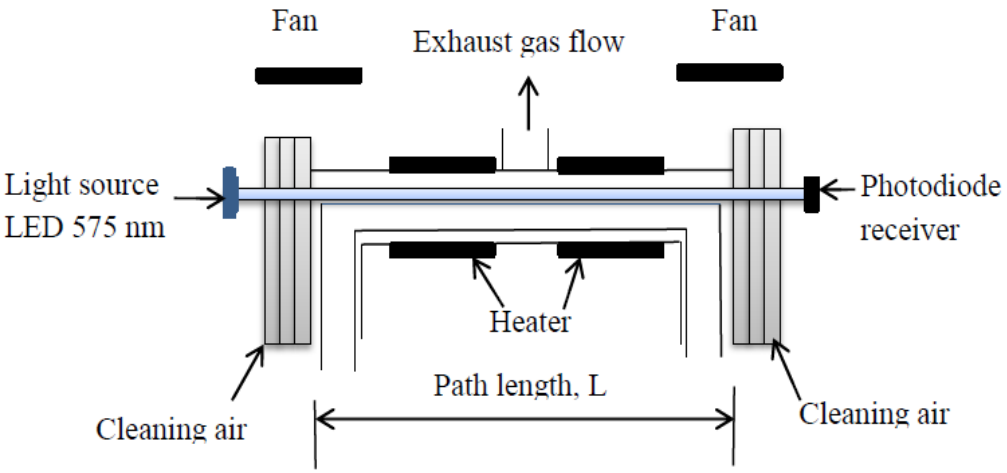

Fig. 3.15. Principle of diesel smoke measurement.

Fig. 3.16. Photograph of the AVL 437C diesel smoke meter.

Calibration of the smoke meter was done periodically. It was done by warming the heating elements up to 70 °C. The pre-heating was carried out to prevent the temperature falling below dew point, and thus, to avoid measurement error or condensation of smoke. Fresh air was allowed to enter the measurement chamber which was drawn through the fitter paper, underwent measurement and set the zero point for calibration. The halogen bulb current irradiated the column of the fresh air volume, and the signals from the detector

were measured by the microprocessor and set as the reference value for 0% opacity. The linearity was checked by gently pushing the linearity check knob down, up to its dead position. The calibration plate was thus measured in front of the detector, and the measured opacity value was indicated and printed on the protocol print out. The probe of the exhaust gas analyzer was inserted at the end of the exhaust pipe during the measurement of emissions. Once the engine reached stable operation, the probe was inserted into the exhaust pipe and the measurements were taken.

3.11. Experimental methodology

3.11.1. Thermodynamic modelling of the ethanol-fueled HCCI engine

Initially, the ethanol-fueled HCCI engine was modelled to determine the auto-ignition temperature, and to check the feasibility of its operation based on its performance and emission parameters. The boundary conditions of the model were taken from the test engine geometric properties. By trial and error method, the intake air temperature was changed to find the minimum operating temperature for the ethanol-fueled HCCI operation.

3.11.2. Engine experimentation with diesel and ethanol

During engine experimentation, initially, the engine was operated with diesel for obtaining the reference data of the combustion, performance and emission parameters. The engine was tested at 20%, 40%, 60%, 80% and 100% loads. For each load condition, the engine was run for at least 3 min after which data were recorded.

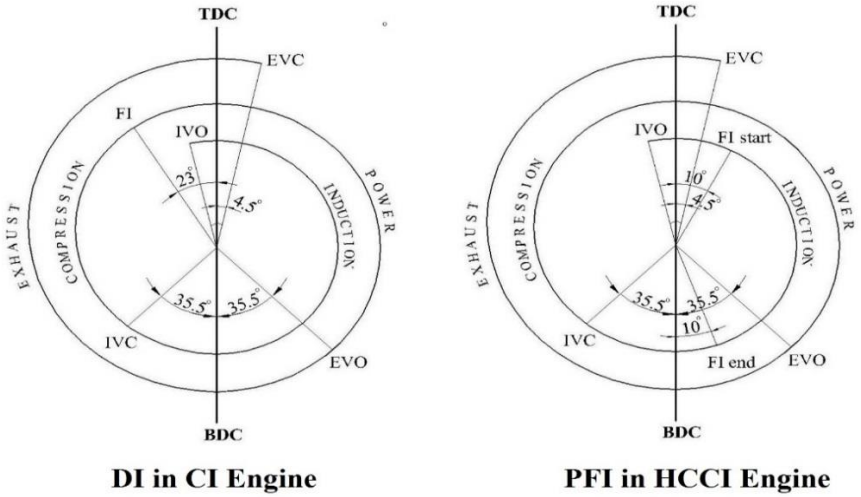

Fig. 3.17. Comparison between the valve timing of CI and HCCI modes.

Further, the diesel engine was converted to run on the HCCI combustion mode by adopting external mixture formation. Port fuel injection technique was used to prepare the homogeneous mixture external to the combustion chamber and allowed to enter inside the cylinder during suction stroke. An electrical fuel pump (12 V DC) was placed inside the fuel tank used to supply ethanol. An electronically controlled port fuel injector (PFI) works on 12 V Transistor-Transistor Logic (TTL) pulse produced by the injector control system. Fig. 3.17 shows the valve timing diagram of port injected HCCI engine and diesel engine.

The auto-ignition temperature of ethanol is relatively higher than that of diesel, due its low cetane number. In order to achieve auto-ignition temperature of the ethanol, the intake air was heated from 130-170 °C using an electric heater. The amount of energy spent was calculated using Eq. 3.17.

$$Q = m_a \times C_{p,air} \times \Delta T \tag{3.17}$$

Where Q is the heat supplied, m_a is the mass of the air, and ΔT is the temperature difference between heated air and ambient air.

The speed of the engine (1500 rpm) was maintained constant by varying the amount of fuel injected per cycle at every load. The ethanol-fueled HCCI combustion, performance and emission parameters were recorded at 20%, 40%, 60%, 80% and 100% loads and compared with the diesel operation.

3.11.3. Multi-Criteria Decision Making – TOPSIS Method

Now a days, a proper decision making is important because it saves time, money and manpower [216–218]. Recently, the Technique for Order of Preference by Similarity to Ideal Solution (TOPSIS) method has been used by researchers for making decision for engine operation [176,219]. The decision of the best/optimum charge temperature plays a major role in cleaner combustion of the ethanol-fueled HCCI engine operation. For this purpose, TOPSIS – a Multi-Criteria Decision Making (MCDM) technique was applied to optimize the charge temperature. The input data/decision matrix was obtained from the experimental results of the ethanol-fueled HCCI engine. The principle component analysis approach was used to evaluate the weights for each response using Minitab software. The optimum operating condition was found from this TOPSIS method based on its performance and emission parameters.

3.11.4. Prediction of HCCI engine output parameters using GRNN

Experiments were conducted at regular intervals of 20% load and 10 °C charge temperature variations. However, the optimum HCCI operating condition may lie in between any interval of load and charge temperature combination. Different computational methods have been used for prediction of engine performance that include artificial neural network [191,194,220], and fuzzy logic [221–223]. For any combination of the input parameters, the output parameters of the HCCI engine was predicted using the GRNN technique. The data sets for GRNN was taken from the experimental results of the ethanol-fueled HCCI engine.

In this study, initially, the neural network was trained with the 60% of the experimental data sets. Further, the validation and testing of the network was done with each 20% data sets. Also, grid search method was used to find the optimized kernel bandwidth to reduce the cross-validation error. The obtained results were validated and tested with the experimental HCCI performance and emission metrics. Accurate prediction of experimental data at unknown operating condition is highly impossible. Finally, the maximum prediction error analysis for any unknown operating condition was determined.

3.11.5. Engine experimentation with charge heating and EGR

The HCCI combustion is practically uncontrolled without using an exhaust gas recirculation (EGR). Hence, EGR was used in this experiment to control the abnormal combustion. Low percentages of EGR viz. 0%, 3%, 5%, and 7% were circulated in this study. The effect of the EGR addition, decreased the NO emission and increased the UHC emission. Hence, the determination of an optimum amount of EGR was essential.

The optimum EGR was determined by plotting the graph between charge temperature (X-axis), and UHC and NO emission (Y-axis). Finally, the final experiment was conducted with optimum EGR circulation and 130–170 °C intake air temperature, to record the combustion, performance and emission parameters at 20%, 40%, 60%, 80% and 100% loads.

3.11.6. Multi-objective optimization using hybrid GRNN−PSO

The optimization of HCCI engine is the difficult task as the output parameters NO−PM−BSFC are in trade-off behaviour. Hence, multiple objective functions were

required to considered optimization of ethanol-fueled HCCI engine. A fitness function was generated and four different cases were chosen for study. The GRNN was trained with the 45 experimental data sets and "newgrnn()" was applied in MATLAB to train the network without any error. The GRNN cannot optimize the solution, and hence swarm based adaptive mechanism was hybridized.

First, the GRNN network evaluate the output parameters of the HCCI engine for the input particle generated by the particle swarm optimization (PSO). The GRNN output was evaluated for its fitness value of the generated particle in the PSO. The best fitness value was stored in the PSO and continues the iteration process. The termination criteria of this hybrid GRNN−PSO algorithm is accuracy of the iteration process reaches 10^{-6} or maximum number of iterations.

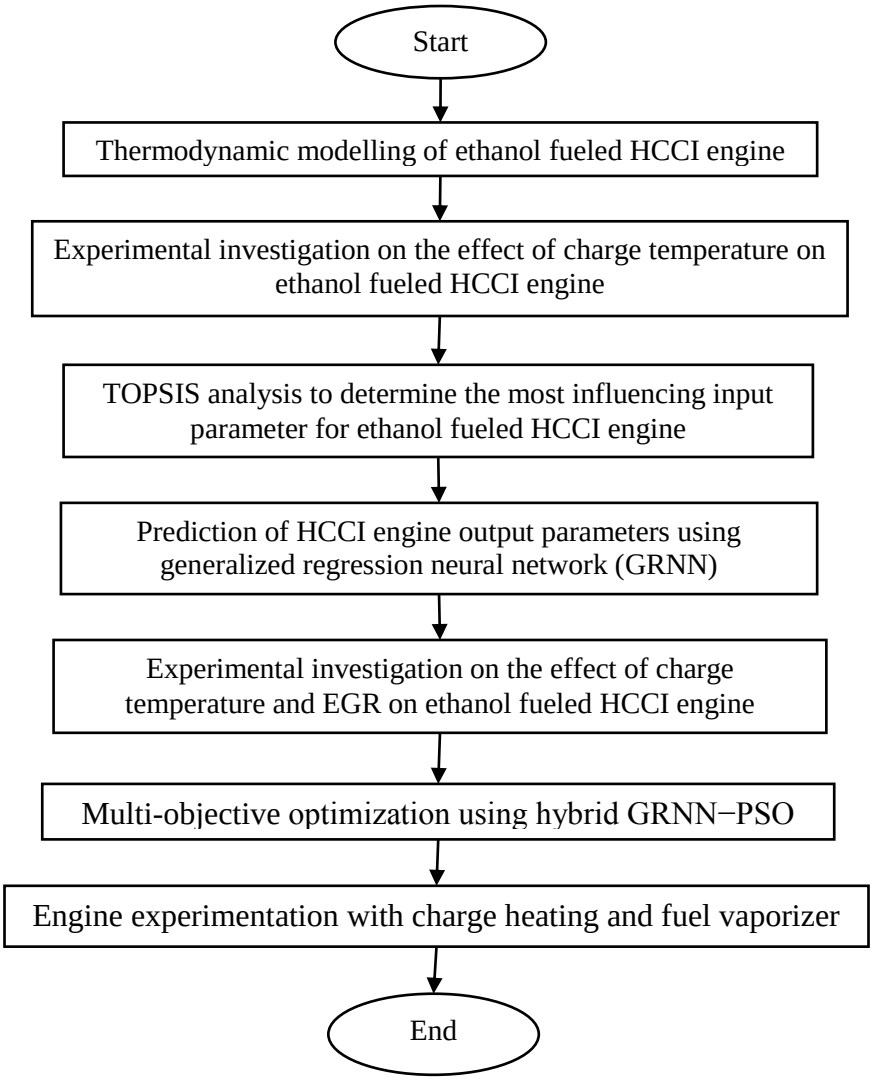

Fig. 3.18. Modules of work presented in the thesis.

3.11.7. Engine experimentation with charge heating and fuel vaporizer

The degree of homogeneity of the fuel-air mixture was further increased with the fuel vaporizer. The custom intake air manifold having the provision to house the fuel vaporizer. The fuel vaporizer (160 mm length) consisted of oven heating element, ceramic beads, SS pipe (ϕ18 mm) and glass wool insulation. Initially, nichrome heating element was inserted inside beads and then wounded over the SS pipe, and finally glass wool was covered over for insulation. The ceramic pipe allowed the heat alone and resisted current whereas glass wool resisted both the heat and current.

The required amount of fuel per cycle was injected by the PFI at 2.5 bar inside the fuel vaporizer. The temperature of the fuel vaporizer was maintained at 110 °C for a complete vaporization of the ethanol. The vaporized ethanol fuel mixed with the fresh intake air and enters inside the cylinder during engine suction. The combustion, performance and emission parameters were recorded at 20%, 40%, 60%, 80% and 100% loads. The technical specifications of the fuel vaporizer is given in Appendix A7.

Fig. 3.18 shows the flowchart that indicates different modules of theoretical and experimental works adopted in this investigation.

3.12. Uncertainty analysis

Uncertainty is a measure of the 'goodness' of a result. Without such a measure, it is impossible to judge the fitness of the value. An uncertainty or error analysis is necessary to establish the bounds on the accuracy of the estimated parameters.The evaluations of some unknown uncertainties from known physical quantities were obtained using Eq. 3.18.

$$\frac{U_Y}{Y} = \left[\sum_{i=1}^{n} \left(\frac{1}{Y} \frac{\partial Y}{\partial xi} U_{xi} \right)^2 \right]^{1/2} \tag{3.18}$$

Where $U_Y$denotes the uncertainty in Y, and Y is the physical parameter that is dependent on the parameters xi. As a result, the maximum uncertainty of the experiment obtained was ±2.6%. Appendix A6 shows the range, accuracy, and uncertainty of the instruments used in this study.

Chapter 4

Prediction and optimization

4.1 General

The efficiency and emission requirements of the HCCI engine are confecting, and hence optimization is extremely significant. This chapter briefly describes the methodologies used for prediction of the output parameters and optimization of the input parameters. This thesis contains four different models that are used for the prediction and optimization of the ethanol fueled HCCI engine which are as follows.

(a) thermodynamic modelling for prediction of auto-ignition temperature and emissions corresponding to different charge temperatures.

(b) Multi-criteria decision making using TOPSIS method for determination of optimal operating conditions based on the experimental results.

(c) GRNN modelling for the prediction of HCCI engine output parameters.

(d) Hybrid GRNN-PSO optimization for the best/optimal operating condition based on the prediction results.

4.2 Thermodynamic modelling

An HCCI engine based system running on natural gas was thermodynamic analysed by Djermouni and Ouadha [224]. They proved that maximum exergy losses occur in the HCI engine.Fathi et al. [225] reviewed cycle-by-cycle combustion control modeling and design architecture for HCCI engines. They addressed control problem issues altogether by introducing HCCI engine control structure in progress and presenting highlights from literature.Soyhan et al. [226] evaluated the heat transfer correlations for HCCI engine modeling. They observed significant differences between the heat transfer results obtained by using Woschni, Assanis and Hohenberg correlations. Shaver et al. [39]modeled cycle-to-cycle dynamics of HCCI engines with variable valve actuation. Their results show that the cyclic dynamics which occur during an SI-to-HCCI mode transition are essentially just an extension of the inherent cycle-to-cycle dynamics of HCCI. Dehghani et al. [227] modeled thermodynamic control of cycle-to-cycle exhaust gas temperature in an HCCI engine. They validated with the experimental results and found good agreement. Gupta et al. [228] analyzed thermodynamically the use of hydrogen enriched compressed natural gas fuelled HCCI engine. They found that there

was an increase in power output from 31.4% to 38.4%.Neshat and Saray [229] studied the effect of different heat transfer models on HCCI engine simulation. They reported multi zone chemical kinetics model to estimate convective heat transfer of HCCI engines more accurately. Trivedi and Haleem [230] thermodynamic analyzethe wet ethanol operated HCCI engineto evaluate its first and second law efficiency. They found the increase of the fuel air mixture intake temperature which finally reduces the work output and efficiency of the engine.

4.2.1 Thermodynamic properties

The assumption of the constant specific heat values is valid only for small temperature differences. This assumption might create a greater error, if the temperature difference is large. Thus, the temperature-dependent specific heat values are incorporated to bring closer predictions to reality [231]. The air-fuel mixture characterization requires the specific heat ratio calculation. Here, the gas is assumed to be thermally prefect i.e. depends only on temperature. Specific heat C_p is expressed in terms of polynomial adjustments. The 7 term NASA polynomial equation as follows [232]:

$$\frac{C_p}{R} = a_1 + a_2 T + a_3 T^2 + a_4 T^3 + a_5 T^4 \tag{4.1}$$

Where R is perfect gas constant and considering its value as 8.314472 J mol^{-1} K^{-1}.

The specific heat ratio expressed as $\gamma = C_p / C_v$.

4.2.2 Thermodynamic analysis of HCCI combustion

In this study, a thermodynamic analysis was used to determine the cylinder pressure P versus crank angle θ. This obtained pressure was used for characterization of the temperature. The following assumptions were made for the modelling of the compression and power strokes:

(a) All thermodynamic variables were assumed to be uniform throughout the engine at any instant of time.

(b) The mixture was considered to be homogeneous, and there was no spatial gradient throughout the combustion chamber.

(c) The compression stroke started at intake valve closing (IVC) and expansion stroke ended at exhaust valve closing (EVO).

(d) Woschni's model was used to compute the heat transfer losses from the cylinder.

(e) Modelling was done only for the compression and expansion strokes only.

Let, the first law of thermodynamics is applied to a closed system, for the trapped mass of homogeneous mixture, a small change in the process is simply written as:

$$\delta Q - \delta W = dU \tag{4.2}$$

From the definition of work, the first law can be expressed as:

$$\delta Q - PdV = dU \tag{4.3}$$

The ideal gas equation can be expressed as:

$$PV = mRT \tag{4.4}$$

Differentiating Eq. (4.4) we get, $PdV + VdP = mRdT$ (4.5)

For an ideal gas with temperature dependent specific heats, the change in internal energy is expressed as:

$$dU = mC_v(\theta)dT \tag{4.6}$$

By substituting dU in Eq. (4.6) into Eq. (4.5) we get

$$dU = \frac{C_v(\theta)}{R}(PdV + VdP) \tag{4.7}$$

By substituting dU in Eq. (4.7) into Eq. (4.3) we get

$$\delta Q - PdV = \frac{C_v(\theta)}{R}(PdV + VdP) \tag{4.8}$$

$$\delta Q_{in} - \delta Q_{loss} - PdV = \frac{C_v(\theta)}{R}(PdV + VdP) \tag{4.9}$$

The amount of heat added per cycle is $\delta Q_{in} = m_f LHV$ (4.10)

The amount of heat added to the system w.r.t. crank angle θ is given as:

$$Q(\theta) = Q_{in} x_b \tag{4.11}$$

The burnt fraction of the fuel at any crank angle θ is expressed using Wibes function:

$$x_b(\theta) = 1 - \exp\left(-a\left(\frac{\theta - \theta_s}{\Delta\theta}\right)^{m+1}\right) \text{ if } (\theta \geq \theta_s) \tag{4.12.a}$$

$$x_b(\theta) = 0 \text{ if } (\theta < \theta_s) \tag{4.12.b}$$

Where Δθ represents the combustion duration, θ_s corresponds to the start of combustion governed by the auto-ignition temperature of the fuel. The start of combustion (SOC)

advances with increase in the intake charge temperature. This indicates the burned fraction of the fuel also advances with increase in the intake charge temperature. In thermodynamic analysis, the mass fraction of the fuel burned curve is adjusted with the parameters of a and m. For curve smoothening, a = 4 and m = 2 were taken. Based on the values of a and m, the curve is showing different pattern. Fig. 4.1 depicts the smoothness of the fuel burned fraction curve versus crank angle.

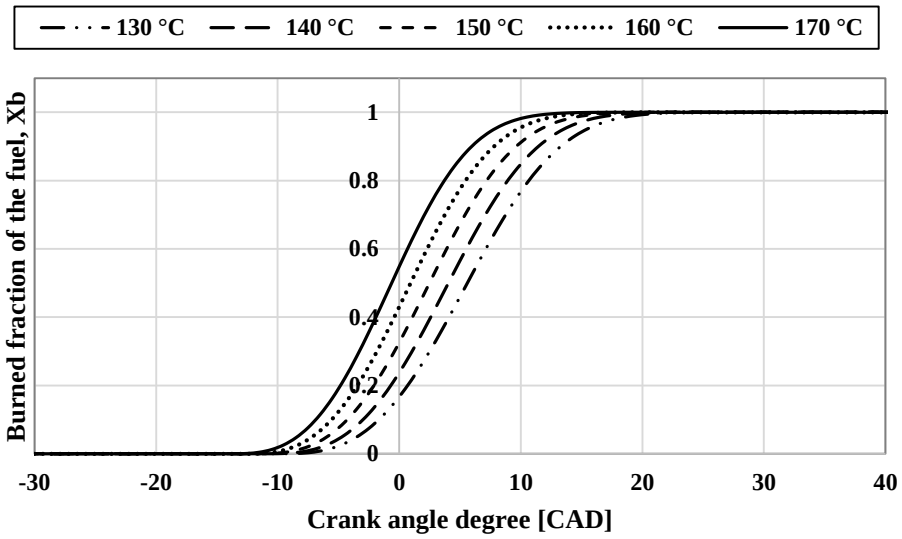

Fig. 4.1. The fraction of the fuel burned versus crank angle θ (with a = 4 and m = 2).

The position of piston at any crank angle is given as:

$$x(\theta) = (L + r) - \left[r\cos\theta + \left(L^2 - r^2 \sin^2\theta \right)^{1/2} \right] \tag{4.13}$$

The instantaneous volume changes in the cylinder can be expressed as:

$$V(\theta) = V_c + \frac{\pi D^2}{4} x(\theta) \tag{4.14}$$

The amount heat losses from the system at any crank angle θ is expressed as:

$$q_{loss} = \frac{\bar{h}A}{w}(T - T_w)\delta\theta \tag{4.15}$$

Where a correlation such as that by Woschni (1967) is used.

$$\bar{h} = 3.26 D^{-0.2} p^{0.8} T^{-0.55} [2.28\overline{V_p} + 0.00324 \frac{V_d T_1}{P_1 V_1}(P - P_{motored})]^{0.8} \tag{4.16}$$

Where D is the cylinder bore and V_p is the mean piston speed. Unit of h is kW/m^2K.

The heat transfer is modelled using a convective heat transfer coefficient and an effective area. The exposed surface area at any crank angle is

$$A = A_{pistonhead} + A_{cylinderhead} + \frac{\pi DL}{2}(\gamma_c + 1 - \cos\theta - (\gamma_c{}^2 - \sin^2\theta)^{1/2}) \quad (4.17)$$

Where γ_c is the ratio of the connecting rod length to the crank radius.

The relation between the crank angle and time is given as;

$$\Delta\theta = 6(rpm)\Delta t \quad (4.18)$$

By substituting the Eqs. (4.11) and (4.15) into Eq. (4.9) followed by differentiation w.r.t. crank angle θ, we get

$$\frac{dP(\theta)}{d\theta} = \frac{k-1}{V(\theta)}\left(Q_{in}\frac{dx_b}{d\theta} - Q_{loss}\right) - k\frac{P(\theta)}{V(\theta)}\frac{dV(\theta)}{d\theta} \quad (4.19)$$

Where, $k = C_p(\theta)/C_v(\theta)$ and $R = C_p(\theta) - C_v(\theta)$.

Upon discretization of the above equation using classical finite difference method, we get:

$$P(\theta+\Delta\theta) = P(\theta) + \frac{k-1}{V(\theta)}Q_{in}\left[x_b(\theta+\Delta\theta) - x_b(\theta)\right] - \Delta\theta\frac{k-1}{V(\theta)}Q_{loss} - k\frac{P(\theta)}{V(\theta)}\left[V(\theta+\Delta\theta) - V(\theta)\right] \quad (4.20)$$

The temperature of the in-cylinder gases can be calculated from the equation of state as:

$$T = \frac{P(\theta)V(\theta)}{mR} \quad (4.21)$$

4.2.3 Kinetics of combustion

4.2.3.1. HCCI combustion mechanism

Ethanol is composed of carbon, hydrogen and oxygen. The reaction for combustion is as follows [233]:

$$C_{\alpha=x+y}H_\beta O_\gamma + \frac{1}{\phi}\left(\alpha + \frac{\beta}{4} - \frac{\gamma}{2}\right)(O_2 + 3.76N_2) \rightarrow n_1CO_2 + n_2H_2O + n_3N_2 + n_4O_2 + n_5CO \quad \text{(R.1)}$$

Where the equivalence ratio is expressed as follows:

$$\phi = \frac{\left(\frac{m_f}{m_{air}}\right)_{actual}}{\left(\frac{m_f}{m_{air}}\right)_{stoichiometric}} = \frac{1}{\phi_s}\left(\frac{m_f}{m_{air}}\right)_{actual} \quad (4.22)$$

Where ϕ_s is the stoichiometric fuel-air mixture.

$$n_1 = x;\ n_2 = \frac{\beta}{2};\ n_3 = \frac{1}{\phi}\left(\alpha + \frac{\beta}{4} - \frac{\gamma}{2}\right)\times 3.76;\ n_4 = \frac{1}{\phi}\left(\alpha + \frac{\beta}{4} - \frac{\gamma}{2}\right) - \left(x + \frac{y}{2} + \frac{\beta}{4} - \frac{\gamma}{2}\right);\ n_5 = y$$

The two-step kinetic reaction of (R.1) was as follows:

- Preliminary step: Production of CO

$$C_\alpha H_\beta O_\gamma + \left(\frac{\alpha}{2} + \frac{\beta}{4} - \frac{\gamma}{2}\right) O_2 \rightarrow \frac{\beta}{2} H_2O + \alpha CO \quad \text{(R.2)}$$

- Secondary step: Production of CO_2

$$CO + \frac{1}{2} O_2 \rightarrow CO_2 \quad \text{(R.3)}$$

Further, the progress of reaction (R.3) was assumed to follow the Arrhenius law [234].

$$k = 2.53 \times 10^{12} \exp\left(-\frac{47700}{T}\right) \quad (4.23)$$

4.2.3.2. Mechanism for NO_x formation

The sources for the formation of NO_x (NO; NO_2; N_2O; N_2O_3; N_2O_4; N_2O_5) during combustion are (i) fuel NO, (ii) prompt NO, and (iii) thermal NO. Ethanol is a clean fuel and doesn't contribute to any "fuel NO", whereas the "prompt NO" is formed in the rich regions that are absent in HCCI combustion as it utilises the lean homogeneous mixture for combustion [235]. The model presented here is only for the formation of "thermal NO" during the combustion of hydrocarbon fuel. The three governing equations (the extended Zeldovich mechanism) that contribute to the formation of thermal oxides of nitrogen can be written as:

$$O + N_2 \leftrightarrow NO + N \quad \text{(R.4)}$$

$$N + O_2 \leftrightarrow NO + O \quad \text{(R.5)}$$

$$N + OH \leftrightarrow NO + H \quad \text{(R.6)}$$

The first two reactions (R.4) and (R.5) are interrelated and considered to be significantly important. Reaction (R.4) was relatively slow, and reaction (R.5) is very fast. The free nitrogen N produces the radical (M) through the formation of N_2O reaction is as follows:

$$N_2O + O \leftrightarrow 2NO \quad \text{(R.7)}$$

$$N_2 + O + M \leftrightarrow N_2O + M \quad \text{(R.8)}$$

The presence of mono-oxygen O is responsible for the formation of NO_x by Zeldovich mechanism which is given below;

$$O_2 + M \rightarrow 2O + M \quad \text{(R.9)}$$

The NO_x formation reactions (R.4) – (R.9) based on Arrhenius laws are given in Table 4.1. The units of the rate constant are given in cm^3, gmol, s, K. The first rate corresponds to the temperature <2000 K while the second rate is for temperature >2000 K.

Table 4.1 NO_x combustion chemistry model with reaction rate constants [233,236,237].

Reaction	**K_f**	**K_r**
$O + N_2 \leftrightarrow NO + N$	15.8E13exp(-38031/T)	35E12exp(-166/T)
	16.3E13exp(-38095/T)	-
$N + O_2 \leftrightarrow NO + O$	26.5E11exp(-3226/T)	56E10exp(-19317/T)
	-	59E10exp(-19430/T)
$N + OH \leftrightarrow NO + H$	73.3E12exp(-564/T)	20.2E13exp(-24725/T)
	-	18.2E13exp(-24528/T)
$N_2O + O \leftrightarrow 2NO$	29E12exp(-11657/T)	-
	-	-
$N_2 + O + M \leftrightarrow N_2O + M$	14.1E12exp(−9505/T)	62E13exp(−28247/T)
	26E12exp(−10672/T)	-
$O_2 + M \rightarrow 2O + M$	83.6E5exp(−61162/T)	-
	10.3E6exp(−61578/T)	-

4.2.4. Numerical procedure

The in-cylinder pressure was calculated numerically by using the discretized Eq. (4.20) for each crack angle θ, in the range -144.5 <θ< 144.5 (i.e., IVC to EVO) with a step size of $\Delta\theta = 1°$. The fraction of the fuel burned $x_b(\theta)$ is given by Eq. (4.12). In a two-step reaction mechanism, the first step is the partial oxidation of the fuel (i.e., production of CO) and then the second step is the complete oxidation (i.e., production of CO_2) from the reaction (R.1). In the preliminary reaction (R.2), the assumption of all fuel burned and produces carbon monoxide (CO). The instantaneous number of moles of each species at every crank angle are defined according to Arrhenius law, given in Table 4.1 and (R.3) – (R.9). The chemical formula of ethanol is C_2H_5OH or C_2H_6O (*i.e.* $\alpha = 2$, $\beta = 6$ and $\gamma = 1$).

The specific heat ratio was calculated at each crank angle by considering the following compounds: ethanol, O_2, N_2, CO_2 and H_2O. The global combustion equation for ethanol is expressed as:

$$C_2H_5OH + 3(O_2 + 3.76N_2) \rightarrow 2CO_2 + 3H_2O + 11.28N_2 \quad \text{(R.10)}$$

$$\gamma(\theta,T) = \frac{C_p(\theta,T)}{C_v(\theta,T)} = \frac{C_p(\theta,T)}{C_p(\theta,T) - R_u}$$

The work from the engine per cycle, W is calculated as follows:

$$W = \oint PdV \quad (4.24)$$

$$W = \sum_{\theta=-144.5^\circ}^{144.5^\circ} \left[P(\theta+\Delta\theta)-P(\theta)\right]\left[\mathrm{V}(\theta+\Delta\theta)-V(\theta)\right] \tag{4.25}$$

The indicated thermal efficiency η_{th} is calculated as follows:

$$\eta_{th} = W/Q_{in} \tag{4.26}$$

4.3. Multi-Criteria Decision Making (MCDM) – TOPSIS Method

The Technique for Order of Preference by Similarity to Ideal Solution (TOPSIS) is a MCDM-based approach to evaluate the best alternative. This technique was introduced by Hwang and Yoon in the year 1995. It includes two artificial alternative results, best and worst. TOPSIS is based on the idea that the selected alternative should have nearest from best (also known as positive ideal) solution and farthest from worst (negative ideal) solution. The steps followed [238] in this approach are given below.

Step 1: Form a decision matrix (Eq. 4.27) that covers the information of all attributes (output characteristics) and alternatives of the process,

$$X = \begin{bmatrix} x_{11} & x_{12} & . & x_{1j} & x_{1n} \\ x_{21} & x_{22} & . & x_{2j} & x_{2n} \\ . & . & . & . & . \\ x_{i1} & x_{i2} & . & x_{ij} & . \\ . & . & . & . & . \\ x_{m1} & x_{m2} & . & x_{mj} & x_{mn} \end{bmatrix} \tag{4.27}$$

the promising alternatives are denoted in the row $(i = 1,2,.....,m)$ and all the qualities associating with each of the alternatives are shown in the column $(j = 1,2,.....,n)$.

Step 2: In the next step, the decision matrix is normalized using the equation given below:

$$x_{ij}^{'} = \frac{x_{ij}}{\sqrt{\sum_{i=1}^{m} x_{ij}^2}} \tag{4.28}$$

where, $x_{ij}^{'}$ represents the normalized value. The normalized decision matrix can be characterized as:

$$X' = \begin{bmatrix} x'_{11} & x'_{12} & . & x'_{1j} & x'_{1n} \\ x'_{21} & x'_{22} & . & x'_{2j} & x'_{2n} \\ . & . & . & . & . \\ x'_{i1} & x'_{i2} & . & x'_{ij} & . \\ . & . & . & . & . \\ x'_{m1} & x'_{m2} & . & x'_{mj} & x'_{mn} \end{bmatrix} \quad (4.29)$$

Step 3: The weighted normalized decision matrix is then calculated by assuming the weight of each quality response (attribute) and multiplying by corresponding normalized value.

$$Y = w_j x'_{ij} \quad (4.30)$$

The weighted normalized decision matrix is as shown below:

$$Y = \begin{bmatrix} y_{11} & y_{12} & . & y_{1j} & y_{1n} \\ y_{21} & y_{22} & . & y_{2j} & y_{2n} \\ . & . & . & . & . \\ y_{i1} & y_{i2} & . & y_{ij} & . \\ . & . & . & . & . \\ y_{m1} & y_{m2} & . & y_{mj} & y_{mn} \end{bmatrix} \quad (4.31)$$

Step 4: Calculate the best (positive ideal) and worst (negative ideal) solution by using the Eq. (4.32) and Eq. (4.33).

(a) Best (positive ideal) solution

$$A^B = \left\{ \left(\max y_{ij} \middle| j \in J \right); \left(\min y_{ij} \middle| j \in J' \right) \right\}$$

$$= \left\{ y_1^B, y_2^{\mathbf{B}}, \ldots\ldots\ldots, y_j^B, \ldots\ldots\ldots, y_n^B \right\} \quad (4.32)$$

(b) Worst (negative ideal) solution

$$A^W = \left\{ \left(\min y_{ij} \middle| j \in J \right); \left(\max y_{ij} \middle| j \in J' \right) \right\}$$

$$= \left\{ y_1^W, y_2^W, \ldots\ldots\ldots, y_j^W, \ldots\ldots\ldots, y_n^W \right\} \quad (4.33)$$

where, J is the set of positive quality features and J' is the set of negative quality features.

Step 5: Then, calculate the separation measure for each alternative using Eq. (4.34) and (4.35).

(a) Separation from the best (positive ideal) solution

$$S_i^B = \sqrt{\sum_{j=1}^{n} \left(y_{ij} - y_j^B\right)^2} \qquad \text{i = 1, 2,……., m} \tag{4.34}$$

(b) Separation from the worst (negative ideal) solution

$$S_i^W = \sqrt{\sum_{j=1}^{n} \left(y_{ij} - y_j^W\right)^2} \quad \text{i = 1, 2,……., m} \tag{4.35}$$

Step 6: At last, compute relative closeness to the ideal solution using the formula given below.

$$C_i^+ = \frac{S_i^W}{S_i^B + S_i^W},\ i = 1, 2, \ldots\ldots, m; 0 \le C_i^+ \le 1 \tag{4.36}$$

Step 7: Assign rank to all the relative closeness value after arranging them in descending order. The highest value of relative closeness indicates the good quality measure.

4.4. GRNN modelling

A mathematical model based on the biological neural networks is ANN model, which was trained from the previously recorded data [239]. The ANN finds the relationship between the input and output variables using a non-linear regression analysis. GRNN algorithm was used in this study, as it uses one-pass learning algorithm for sparse data with an extremely parallel structure for prediction or control. An important step in GRNN prediction process is to pre-process the data set [240]. The dataset pre-processing involves smoothing, omitting outliers, recognizing the missing data, etc. [241]. GRNN is the probabilistic-based network performs regression [242,243]. A GRNN consists of exactly four layers. They are (i) input layer, (ii) radial layer, (iii) regression layer, and a (iv) output layer. The clustering of the input training data is performed in the radial layer. Hence, the number of neurons in the radial layer is exactly equal to the number of data sets used for the training. The regression layer always consists of an extra neuron compared to the output layer. This additional neuron calculates the probability density function, whereas remaining neurons are used for calculation of outputs. The GRNN chooses an approximate function which relates the input and the output parameters directly based on the training data. Thus, the GRNN is less time-consuming than other iterative training networks.

The popular prediction tools existed are genetic programing (GP), fuzzy regression and neural networks. The genetic program involves mutation, crossover and cut-paste

operations. Hence it takes more search time to obtain the relation. Moreover, the GP requires a prior information about the mathematical operations that are used for prediction [244]. Whereas fuzzy regression network is a rule based prediction approach in which the accuracy is dependent on the user defined instructions [245,246]. ANN is composed of simple processors those are extremely interconnected with parallel operating system, mainly learnt from the previous experience. Unlike the other prediction tools like genetic programing and fuzzy regression, ANN does not use any complex mathematical equations/operators for explaining the non-linear and multi-dimensional systems. In HCCI engines, the auto-ignition is purely dependent on time-temperature history of the homogeneous air/fuel mixture. Moreover, HCCI combustion is more sensitive to the intake air temperature. In order to predict the non-linear nature between input and output parameters of HCCI engine, ANN has been implemented.

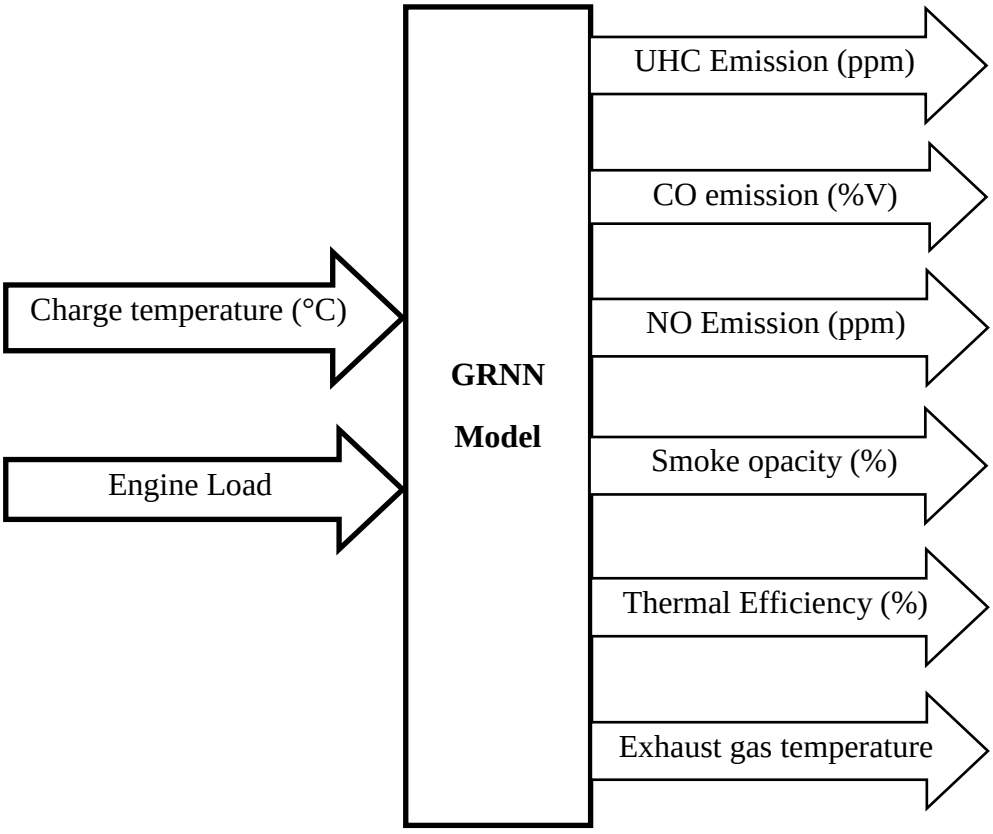

Fig. 4.2. Description of GRNN model.

Back propagation neural networks (BPNN) may face local minima problem instead of finding the global minima surface error. Moreover, BPNN requires long training time to find optimal solution [247]. If the results obtained by BPNN is not comparable with the actual results, the adaptive nature of BPNN should be restarted with different initial conditions till it achieves the accuracy within threshold limit. To overcome this problem,

the linear combination of exponential terms is used to reduce the error at the sample points as in the case of radial basis functions (RBF). But, these RBF neurons are not identical and require global computations to determine their parameters. In GRNN, the estimated output is bounded to the observed data points since the estimation is the weighted average of actual sample points. Moreover, the adaptive parameter σ may be tuned to smooth out any noisy data and approximate closely the actual observed values. The model description is shown in Fig. 4.2.

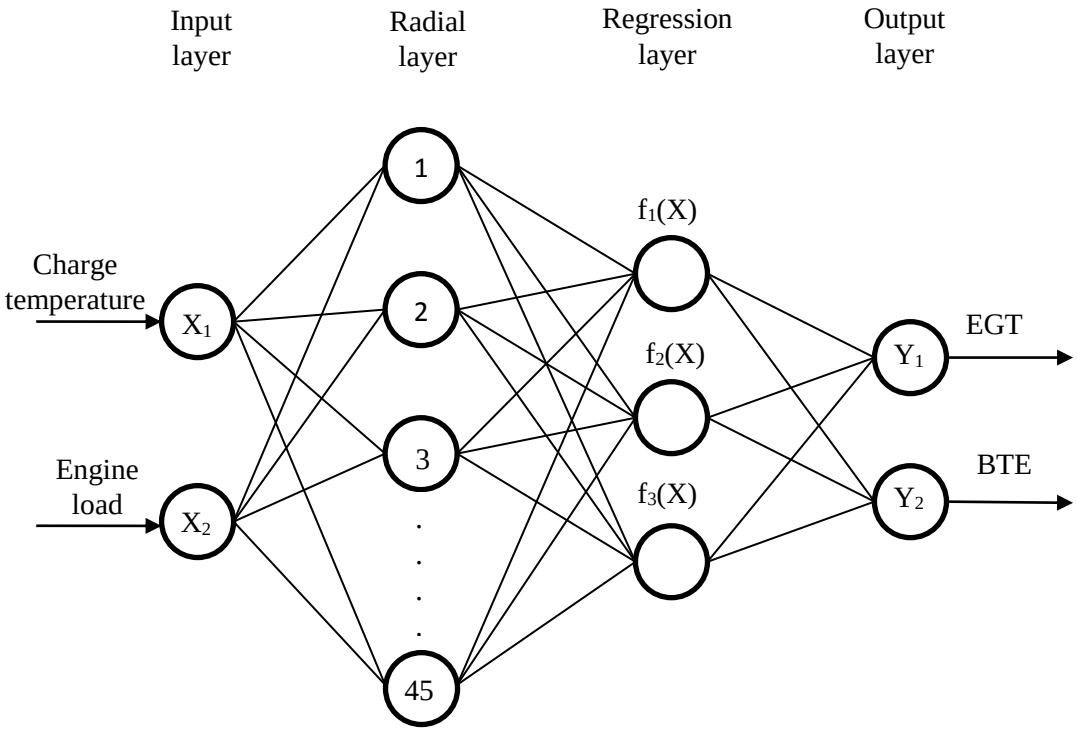

Fig. 4.3. GRNN architecture used for the performance study.

The GRNN model was prepared with the help of existing experimental data. The charge temperature and engine load were used as input parameters, whereas the emission and performance values were considered as output parameters. The engine performance parameters were BTE and EGT; and the exhaust emission parameters were NO, smoke, UHC, and CO considered as output parameters. Fig. 4.3 and Fig. 4.4 show the GRNN architecture used for the performance and emission studies respectively. The GRNN estimated the performance and emission parameters for any combination of charge temperature and engine load.

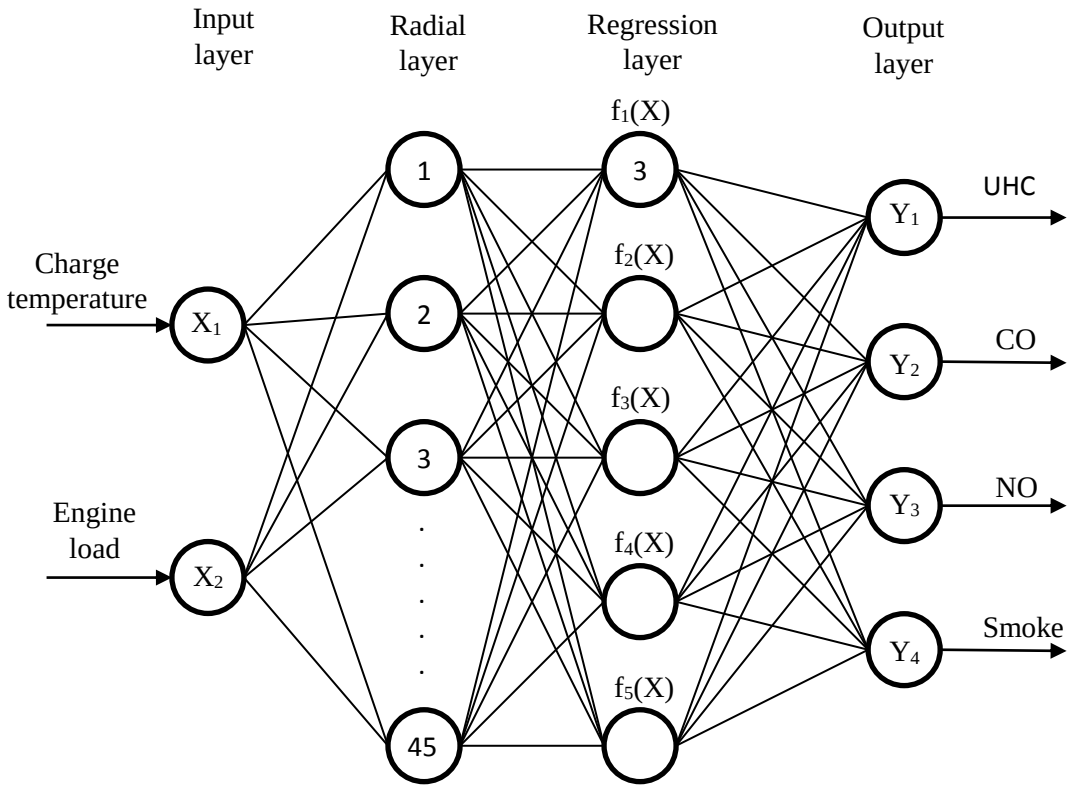

Fig. 4.4. GRNN architecture used for the emission study.

The mathematical basis of GRNN model for the prediction of an HCCI engine performance is a nonlinear regression analysis between HCCI output parameters, and its influencing input parameters. The regression analysis between the HCCI performance parameters (dependent variables) Y relative to its index vector of the influencing input factors (independent variables) X can be calculated by Eq. (4.37).

$$\hat{Y}(X) = \frac{\sum_{i=1}^{n} Y^{i} \exp\left(-\frac{D_i^2}{2\sigma^2}\right)}{\sum_{i=1}^{n} \exp\left(-\frac{D_i^2}{2\sigma^2}\right)} \tag{4.37}$$

Where (X_i, Y_i) is a sample of (X, Y), D_i^2 is the scalar function, and σ^2 is the squared bandwidth of the Gaussian RBF kernel [248].

$$D_i^2 = (X - X_i)^T (X - X_i) \tag{4.38}$$

The steps involved in the GRNN which is implemented for the considered HCCI engine are as follows:

Step 1: Initialize the 45 number of experimental data sets.

Step 2: Among the 45 data points, consider first 60% (27 number) of datasets for training the model.

Step 3: Obtain the smoothening parameter through cross-validation procedure. In this analysis, grid search method is used to find the optimal adaptive parameter σ with minimum cross-validation error.

Step 4: Determine the scalar function D_i^2 (for i = 1 to 27) for i^{th} node and determine the coefficient (exponential term) of equation (4.37) by substituting D_i^2 and σ^2.

Step 5: Multiply the calculated exponential term with the corresponding actual output data point Y_i. This step is processed in radial layer of the GRNN.

Step 6: For the obtained outputs of radial units, regression layer is used. The regression layer contains an extra neuron that calculates the probability density function of the output parameters.

Step 7: The weighted average of the GRNN output parameters are predicted in the observed range.

Step 8: To check the efficiency of the proposed method, the remaining 40% data sets are used for validating and testing.

4.5. Hybrid GRNN−PSO optimization

The GRNN algorithm discussed in the section 4.3 can predict the HCCI engine output parameters but cannot optimize the solution. Hence, a swarm based algorithm is hybridized with GRNN for optimization.

4.5.1. Construction of GRNN model for HCCI performance prediction

Based on GRNN topological structure, the modeling process of GRNN model is given in the following steps;

Step 1: Initialize the index vector (input layer) of the influencing factors of HCCI engine by the input neurons.

Step 2: Calculate the output value of each radial/pattern neuron.

The input index vector can be transferred directly to each radial neuron by setting the weights to 1. The output of each radial neuron uses radial basis function to calculate its output value by Eq. (4.39).

$$f(X, X_i) = \exp\left(-D_i^2 / 2\sigma^2\right) \tag{4.39}$$

Step 3: Calculate the output value of regression/summation neurons.

The number of neurons in the regression layer consists of arithmetic summation (S_s) neurons (equal to output layer neurons) and weighted summation (S_w) neuron. The

arithmetic sum of the radial outputs and the interconnected summation neuron weight equals to 1. The weighted summation S_w computes the weighted sum of the radial layer outputs. The output vector can be calculated by Eq. (4.40) and Eq. (4.41).

$$S_s = \sum_{i=1}^{n} \exp\left(-D_i^2 / 2\sigma^2\right) \tag{4.40}$$

$$S_w = \sum_{i=1}^{n} \left[Y_i \ \exp\left(-D_i^2 / 2\sigma^2\right) \right] \tag{4.41}$$

The architecture of GRNN model used in this study is described in Fig. 4.5.

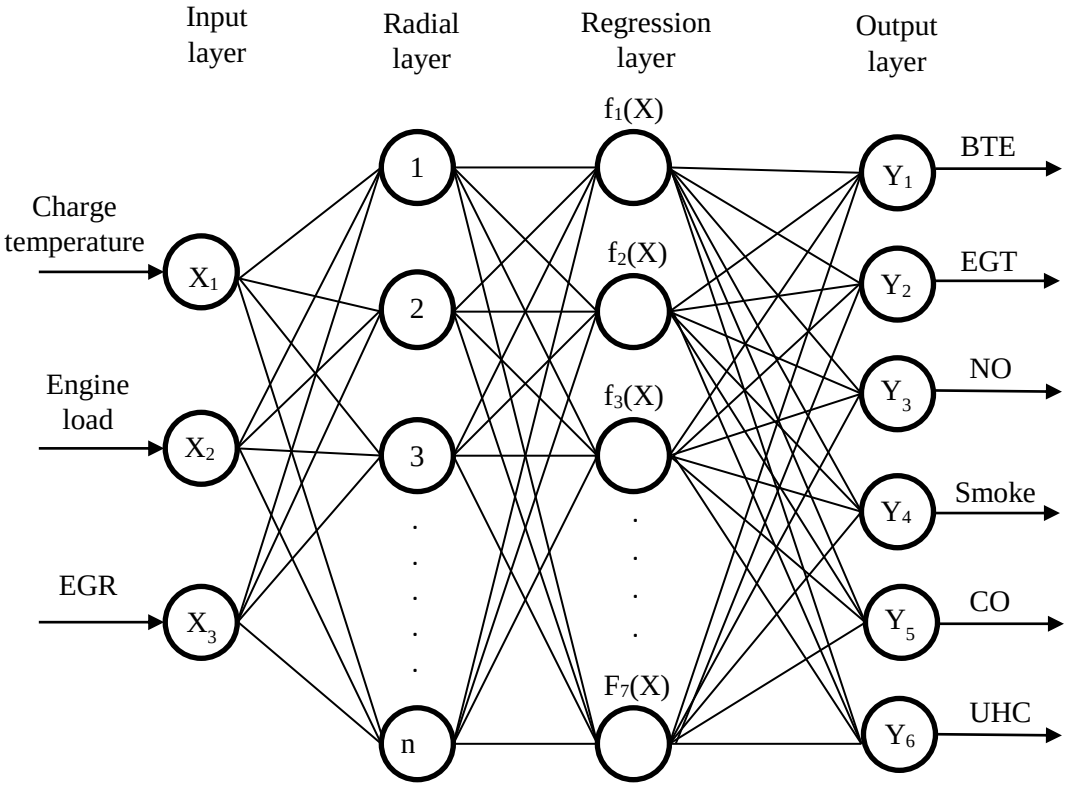

Fig. 4.5. GRNN architecture used in this study.

Step 4: Determine the prediction values of the HCCI engine performance metrics.

The output value of S_w will be divided by the output value of S_s. The predicted values can be gained by Eq. (4.42).

$$\hat{Y}(X) = \frac{S_w}{S_s} = \frac{\sum_{i=1}^{n} \left[Y_i \ \exp\left(-D_i^2 / 2\sigma^2\right) \right]}{\sum_{i=1}^{n} \left[\exp\left(-D_i^2 / 2\sigma^2\right) \right]} \tag{4.42}$$

The smoothening parameter σ needs to be set manually throughout the modeling process. The GRNN prediction accuracy and the generalization ability are very sensitive to the

setting of the smoothening parameter. The optimal smoothening parameter with a minimum cross-validation error was determined using grid search method.

4.5.2. Particle swarm optimization (PSO) algorithm

PSO is one of the swarm intelligence technique motivated from social nature of birds flocking [249]. The birds in PSO is called as a swarm and each bird in the swarm is considered as a particle. Hence, the population in PSO can be identified as a set $S = \{p_1, p_2, p_3, \dots, p_r\}$

Where $p_1, p_2, p_3, \dots, p_r$ represents 'r' number of individual population existing in the swarm.

These individuals are expected to change their position within the workspace. During the movement of the particles, their new positions are renewed with an appropriate velocity. Consider 'r' particles with the positions of $\{x_1, x_2, x_3, \dots, x_r\}$ with their corresponding velocities$\{v_1, v_2, v_3, \dots, v_r\}$ in the swarm. The new position and velocity of every indivisual can be achieved through the conversed information of individuals within the swarm. This can be achieved in terms of commemoration i.e. each individual pillories its best position that, it has ever visited during its search. The best position obtained by every individual is called 'position best' and is denoted by X_{pbest}. Therefore, there exists 'r' number of X_{pbest}values for 'r' individulas in the swarm.

All particles within the swarm are communally shared their experience, and there exists only one global best position, ever visited by any of the individual as represented in Fig. 4.6. The choice of the best particle/position is determined according to the obtained fitness values of every individual in the swarm.

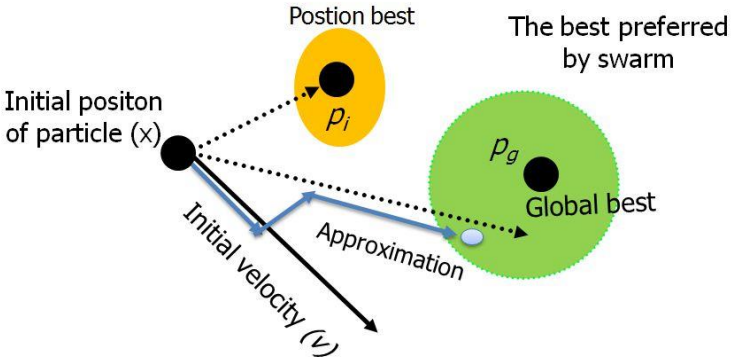

Fig. 4.6. PSO structure for its global best approximation.

The particle in swarm with optimal fitness value is called as global best position and is denoted with X_{gbest}. The selection of X_{gbest} specifies the end of one PSO-iteration. This

procedure will be repeated until it reaches the maximum number of iterations has occurred. The new velocity and the position of each individual is updated according to Eq. (4.43) & (4.44).

$$v_i(z+1) = v_i(z) + C_1 * rand1 * \left(X_{pbest} - x_i\right) + C_2 * rand2 * (X_{gbest} - x_i) \quad (4.43)$$

And $x_i(z+1) = x_i + v_i(z+1)$ (4.44)

Where z = number of iteration; rand1 & rand2 = random parameters ranging between 0 and 1; and C_1& C_2 are cognitive and social parameters.

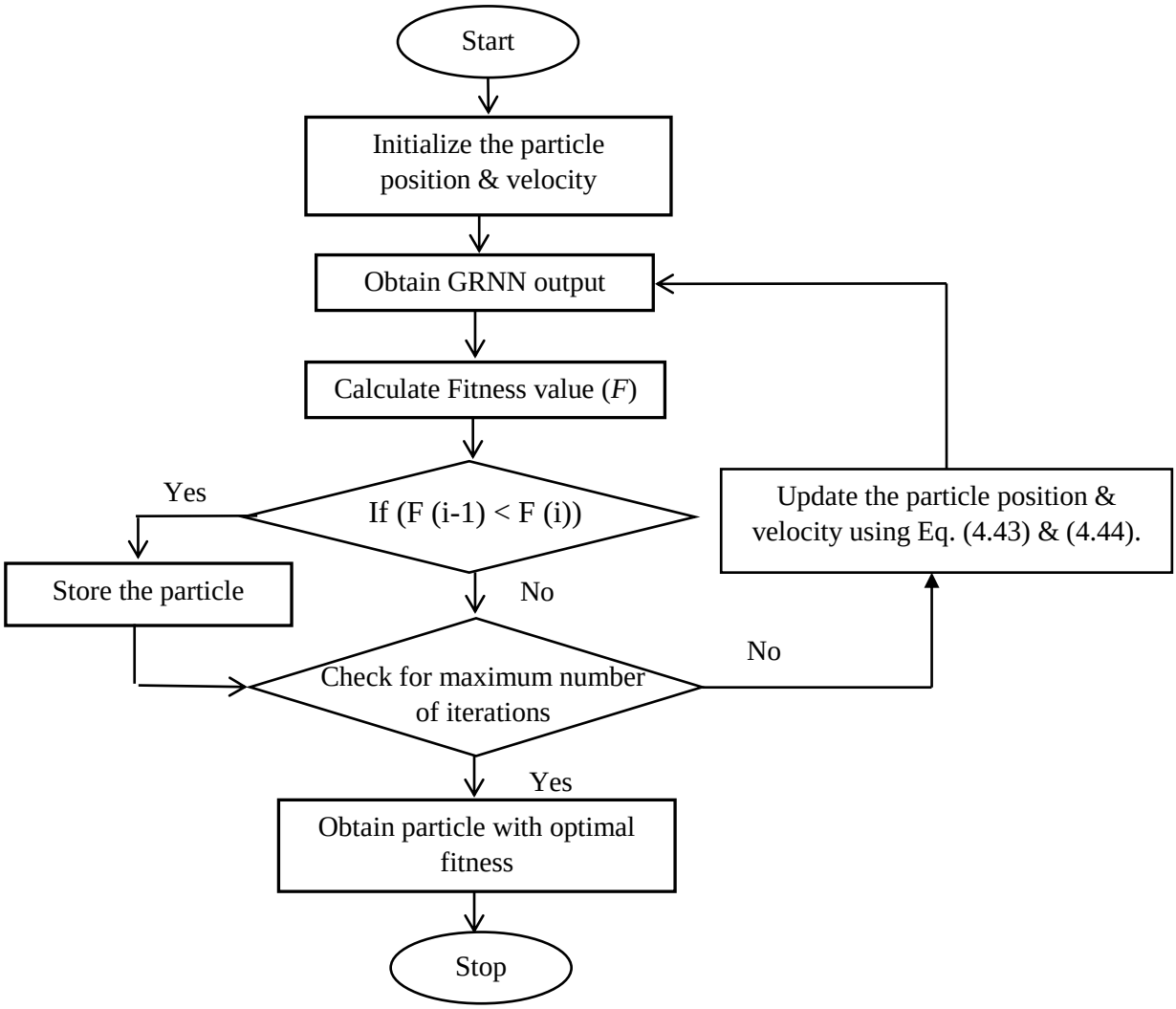

Fig. 4.7. Flow chart of the proposed methodology.

4.5.3. GRNN−PSO Implementation

In this research study, three input parameters of the HCCI engine namely charge temperature, engine load, and EGR were considered. Therefore, the dimension of each swarm particle was three that corresponds to each input parameter. Later, each random particle was given to the developed GRNN tool as an input to obtain six output values as

discussed. For the obtained output values, the fitness of the particle was to be measured. The detailed procedure of the developed strategy is illustrated in Fig. 4.7.

The developed methodology works as per the following steps:

Step 1: Initialise a particle position and velocity (position = velocity) with two dimensions within their input range as given below:

- 130 °C < X_1> 170 °C (first dimension as charge temperature)
- 20% < X_2> 100% (second dimension as engine load)
- 0 < X_3> 7% (third dimension as EGR rate)

Step 2: Send the generated input values to the GRNN tool for predicting six output values as discussed in section 4.5.1.

Step 3: Obtain the fitness value for the generated particle.

Step 4: Store the fitness value of current particle for further comparison.

Step 5: Generate a new particle while updating the position of the current particle as follows:

$$x_{z,j}(z+1) = x_{z,j} + v_{z,j}(z+1) \quad (4.45)$$

Where 'z' is iteration count or particle generation count.

'j' represents the dimension of the particle vary from 1 to 3.

$v_{z,j}$is the velocity or position shift of the particle in the j^{th} dimension is constrained as follows:

- $v_{z,1} = \pm 1.$
- $v_{z,2} = \pm 1.$
- $v_{z,3} = \pm 1.$

Step 6: Send the new particle to GRNN as described in Step 2.

Step 7: Repeat Steps 3, 4 & 5 until the maximum number of iterations reached.

Obtain the particle with an optimal fitness value.

Chapter 5

Results and discussion

5.1. General

The present study establishes the experimental and optimization results obtained from operating an HCCI engine fueled with ethanol. A single cylinder, four stroke, air cooled diesel engine producing 4.4 kW power at 1500 rpm was converted to run on the HCCI mode and used as the test engine. The experimental results of the combustion, performance and emission were analysed and presented in this thesis. The HCCI output parameters were predicted with the GRNN algorithm. Also, the optimum operating conditions of the HCCI engine were evaluated with the hybrid GRNN-PSO technique. All the results of this investigation are presented in the subsequent sections.

5.2. Thermodynamic analysis of ethanol fueled HCCI engine

5.2.1. General

In this chapter, a physical model based on the analysis of a thermodynamic model was developed to assess the combustion, performance and emission parameters of the homogeneous charge compression ignition (HCCI) engine run on ethanol. Fuel and air were assumed to be well mixed and in the gas phase with both the intake and exhaust valves closed at the beginning of the simulation. The charge was modelled in a single zone with the entire contents of the cylinder viewed as a continuum. A very similar approach has been used by Martinez-Frias et al. [41]. The boundary conditions of the model were taken from the test engine geometric properties. The initial conditions were the HCCI engine input parameters (charge temperature and engine load). The requirements of pressure and temperature for the specific heats calculation were obtained by solving the energy conversion equation based on the first law of thermodynamics. Two-step reaction mechanisms were implemented to model the ethanol combustion process for which Woschni reactions model for the heat transfer process was used. The formation of NO_x was also modelled by using an eight species six-step reaction mechanism considering a

phenomenological model based on the combustion speed. The indicated thermal efficiency and the exhaust emissions were also calculated numerically.

5.2.2. Domain of ethanol fueled HCCI operation

The domain/range of HCCI operation is limited [36,250–252]. For the HCCI operation, there are two operating limits; (i) high load knock limit and (ii) low load misfire limit. The upper load limit of HCCI combustion is limited by the high rate of pressure rise, the so-called "knock limit" and the unburned emissions limit the lower limit. Fig. 5.1 depicts the operating regime of HCCI combustion of ethanol. The lower boundary defines, the lower limit of HCCI combustion. At low loads and intake temperatures, the decrease in the requirement of fuel leads to the decrease in the heat release rates. This causes the lower gas temperature that results in the high unburned hydrocarbon (UHC) and carbon monoxide (CO) emissions. At high loads and intake temperatures, the increase in the fuel flow rate leads to high heat release rates. This causes a sudden rise in the cylinder pressure with an unacceptable noise that in turn damages the engine. The acceptable pressure rise limit is approximately 8 bar/CA for noise, which is given in section 2.3.2. The misfire limit was decided from the abnormal HC and CO emission values. Hence, the HCCI operating domain is limited by knock and misfire [253].

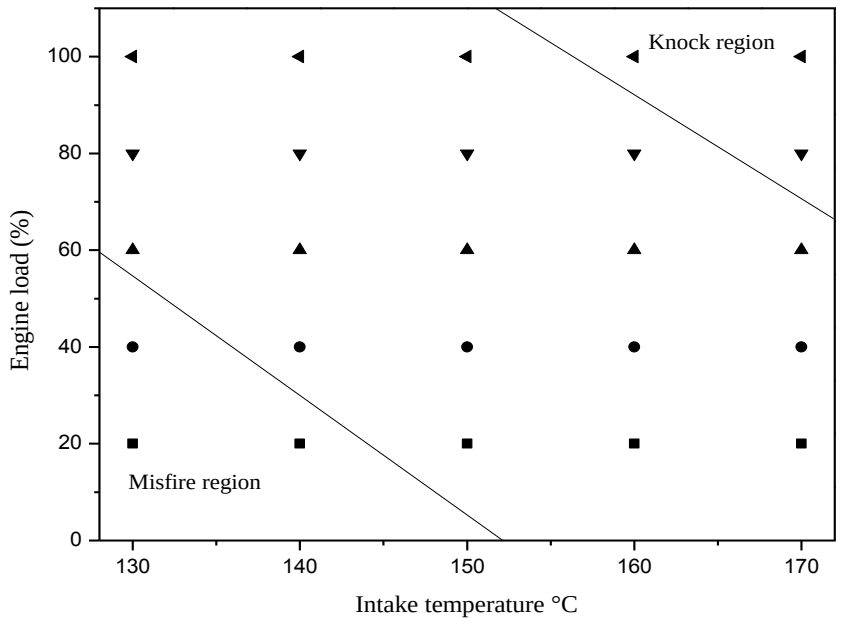

Fig. 5.1. Domain of HCCI operation for ethanol.

5.2.3. Modelling of combustion parameters

The combustion characteristics of the ethanol fueled HCCI engine mainly depends on the cylinder pressure and temperature. Hence, they are necessary to be modelled or predicted before conducting experiments.

5.2.3.1. Cylinder pressure–volume (PV) diagram

Fig. 5.2 portrays the cylinder pressure with cylinder volume using temperature dependent specific heats for the ethanol fueled HCCI engine running at 1500 rpm. It is apparent from the figure that the pressure–volume diagram of the ethanol fueled HCCI combustion is alike to the ideal Otto cycle. The correctly phased HCCI combustion is approaching ideal Otto cycle [254]. The maximum pressure of 79 bar is reported for the intake air temperature of 170 °C. During combustion process of the fuel, the high specific heat species compounds such as CO_2 and H_2O are formed. These species absorb some amount of the heat released during combustion and undergone disassociation of molecules. This absorbed heat causes a reduction in the peak cylinder pressure and temperature in the combustion chamber. The network output of the HCCI engine is estimated using PV curve in the diagram.

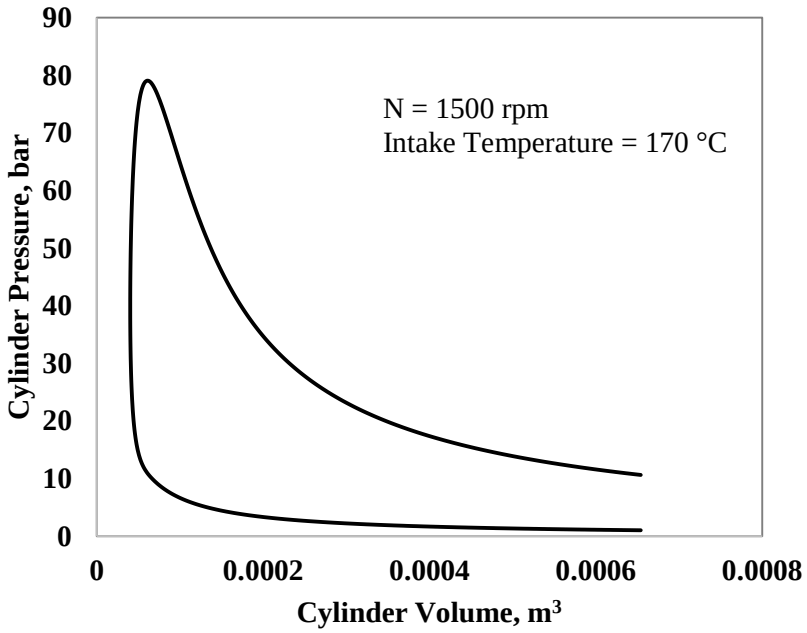

Fig. 5.2. Variation of cylinder pressure versus volume at full load.

5.2.3.2. Cylinder pressure history

Fig. 5.3 depicts the effect of intake air temperature on the cylinder pressure with crank angle at full load. The intake pressure is considered to be 1 bar, while closing the intake valve in this study. The pressure increases slowly with respect to the crank angle due to volume variations during compression stroke until the auto-ignition point of the air/fuel mixture. The pressure obtained follows the Eq. (4.20) for all the intake air temperatures. At full load, the maximum pressure is found to be about 64 bar, 66 bar, 71 bar, 77 bar and 79 bar for the intake temperatures of 130 °C, 140 °C, 150 °C, 160 °C and 170 °C respectively. It is evident from the figure that, the combustion duration increases with the increase in the intake air temperatures.

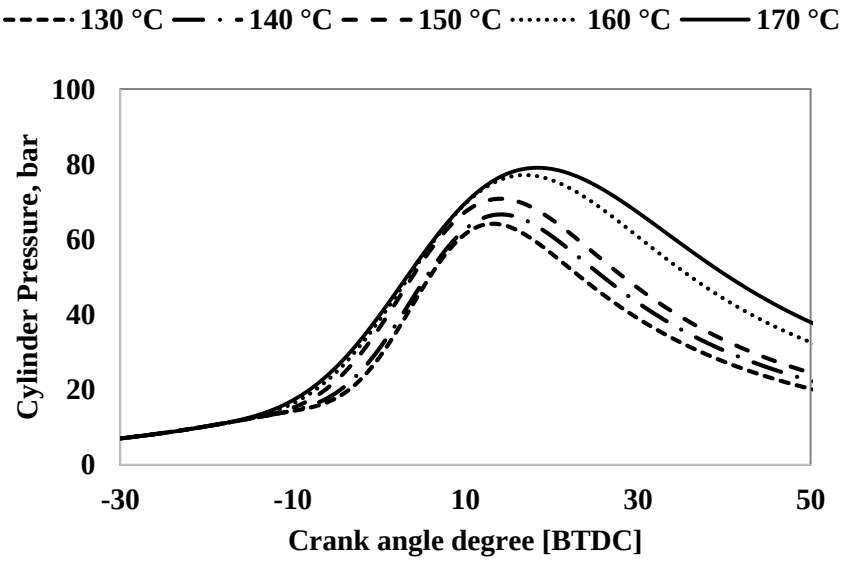

Fig. 5.3. Cylinder pressure versus crank angle degree at full load.

5.2.3.3. Start of combustion

Fig. 5.4 depicts the effect of intake air temperature on the start of combustion with crank angle.The early start of combustion (SOC) is observed with the increase in the intake air temperatures. The SOC of -10.5°CA, -12.5°CA, -15.5°CA, -18.5°CA and -20.5°CA and is observed for the intake temperatures of 130 °C, 140 °C, 150 °C, 160 °C and 170 °C respectively, at full load.The air/fuel mixture reaches the auto-ignition temperature in early crank angles for higher intake temperatures.

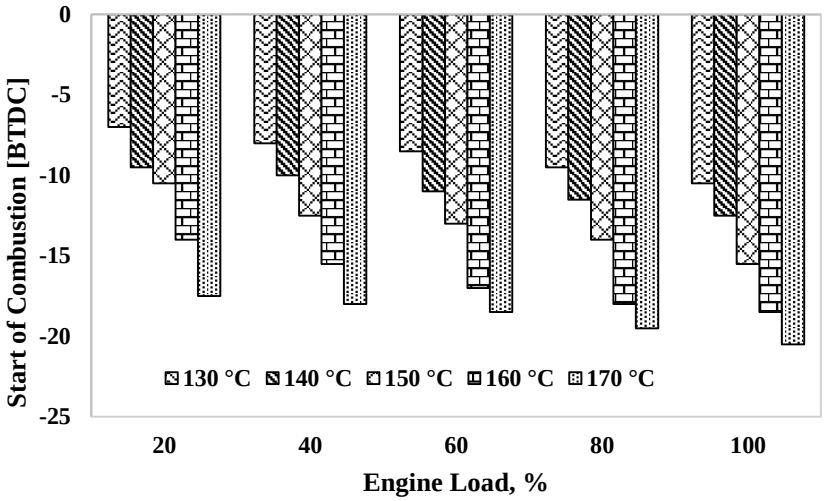

Fig. 5.4. Variation of start of combustion with engine load.

5.2.3.4. Combustion duration

Fig. 5.5 depicts the effect of intake air temperature on the combustion duration with crank angle. The combustion duration also decreases with the increase in the intake air temperature due to increase in the reaction kinetics with temperature.

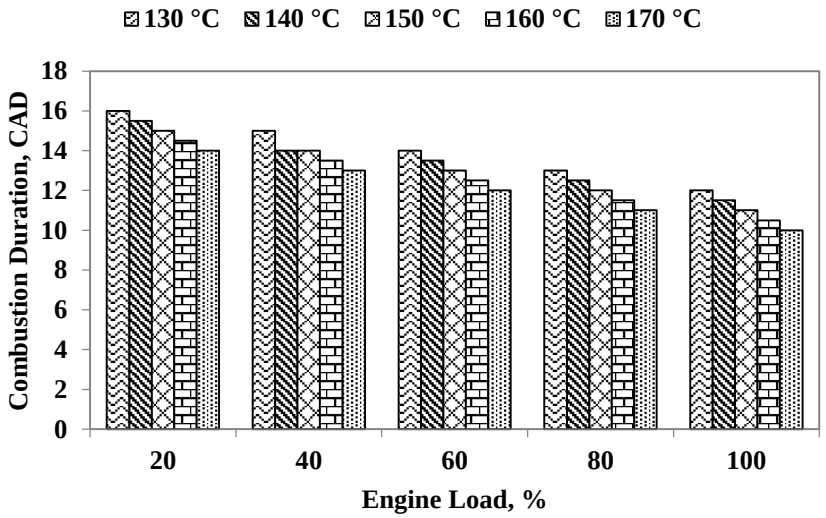

Fig. 5.5. Variation of combustion duration with engine load.

5.2.3.5. Cylinder temperature history

Fig. 5.6 depicts the effect of intake air temperature on the cylinder temperature with respect to crank angle degree at full load. The temperature is calculated based on the ideal gas law, in this work. The maximum in-cylinder temperatures are obtained in the vicinity of maximum in-cylinder pressures. At full load, the peak cylinder temperatures are about

1318 K, 1365 K, 1423 K, 1493 K and 1538 K for the intake temperatures of 130 °C, 140 °C, 150 °C, 160 °C and 170 °C respectively. The in-cylinder temperature increases with the increase in the intake air temperature and the engine load. The higher in-cylinder temperature also indicates the higher indicated thermal efficiency.For a fixed geometry piston and cylinder device, increasing the initial temperature of the system will result in higher temperatures being reached earlier in the stroke. This in turn leads to advanced start of combustion.

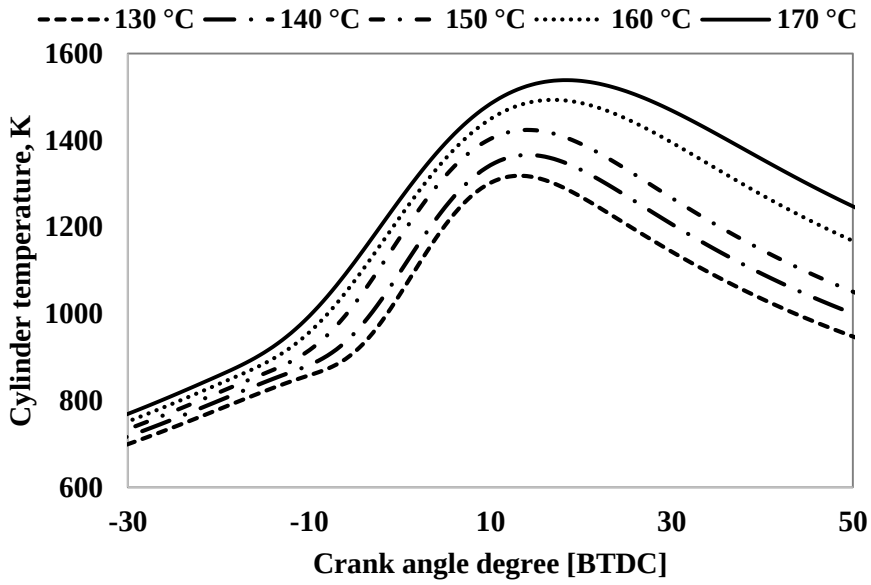

Fig. 5.6. Cylinder temperature versus crank angle degree at full load.

5.2.4. Performance parameters

5.2.4.1. Indicated thermal efficiency

The actual power developed by the piston after combustion process is known as indicated power. The indicated thermal efficiency indicates the actual energy conversion effectiveness. The efficiency of the HCCI can be improved greatly by improving the mixture homogeneity. Thermal efficiency of the engine is depends upon the compression ratio and combustion phasing [128]. Fig. 5.7 portrays the variation of indicated thermal efficiency with engine load for different intake temperatures. The indicated thermal efficiency increases with the increase in the engine load as expected. The indicated thermal efficiency is found to be maximum for 170 °C intake air temperature at all engine loads. This is due to increase in the fuel consumption with the increase in the engine load.

At full load, the indicated thermal efficiency is found to be about 35%, 38%, 41%, 44% and 46% for the intake temperatures of 130 °C, 140 °C, 150 °C, 160 °C and 170 °C respectively. Similarly, the indicated thermal efficiency increases with the increase in the intake air temperature due to increase in the maximum cylinder gas temperature. At very high intake air temperature, two factors namely knocking and drop in volumetric efficiency causes lower indicated thermal efficiency at full load.

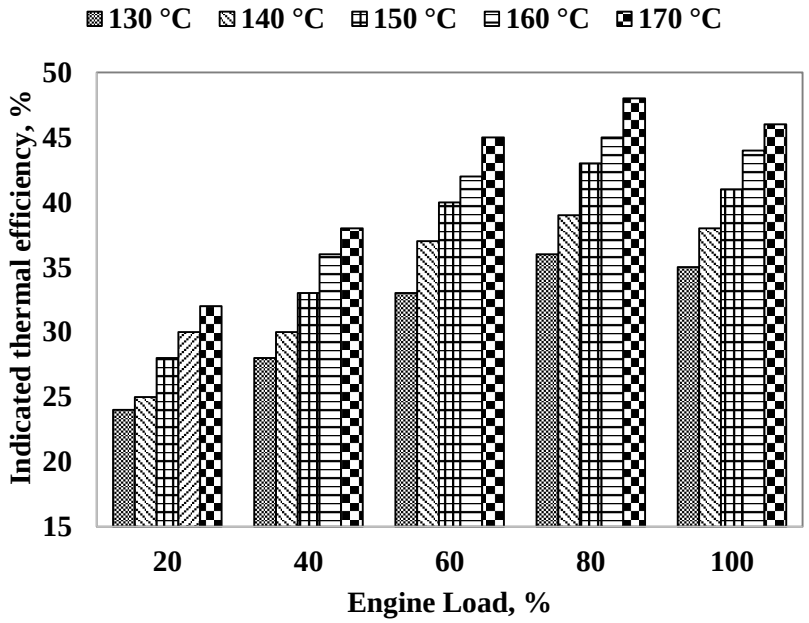

Fig. 5.7. Variation of the indicated thermal efficiency with engine load.

5.2.4.2. Exhaust gas temperature

Fig. 5.8 portrays the variation of the exhaust gas temperature with the engine load and different intake air temperatures. In this work, the exhaust gas temperature is considered to be the temperature at exhaust valve opening. The exhaust gas temperature increases with the increase in the engine load. This is due to the increase in the amount of fuel injected with the increase in the engine load. It can be observed from the figure that, the exhaust gas temperature increases with the increase in the intake air temperature. At full load, the exhaust gas temperatures are 385, 421, 456, 538 and 539 °C for intake temperatures of 130 °C, 140 °C, 150 °C, 160 °C and 170 °C respectively.

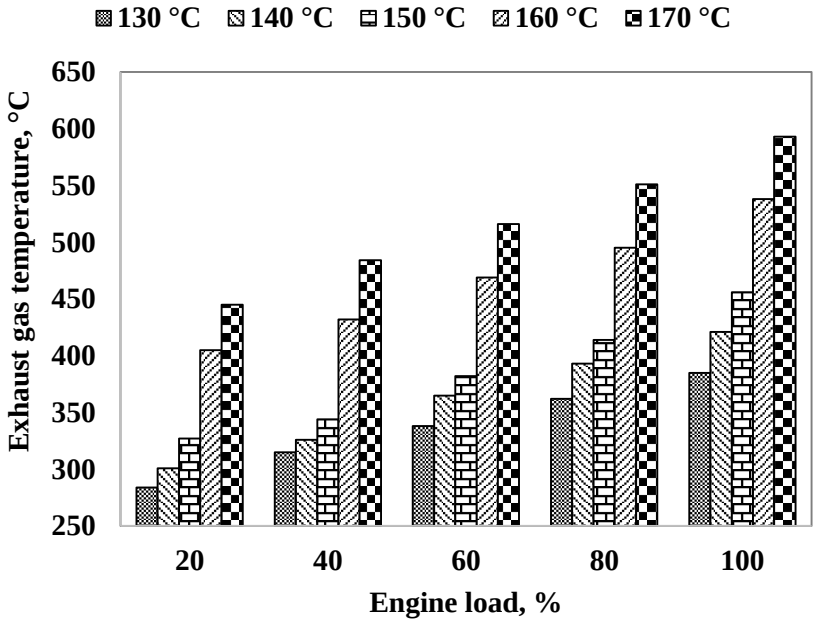

Fig. 5.8. Variation of the exhaust gas temperature with engine load.

5.2.5. Emission parameters

5.2.5.1. Carbon monoxide emission

Fig. 5.9 portrays the variation of the carbon monoxide (CO) emission with the engine load and different intake air temperatures. The CO emission decreases with the increase in the engine load. This is due to the increase in the amount of fuel requirements for the high load operation, causes the increase in the overall cylinder temperature with the engine load. At full load, the CO emission is 0.05, 0.045, 0.04, 0.035 and 0.03 %V for the intake temperatures of 130 °C, 140 °C, 150 °C, 160 °C and 170 °C respectively. The CO emission is formed either due to the lack of oxidation temperature or absence of oxygen. In HCCI engines, lean air/fuel mixtures are used to promote the complete oxidation of the fuel. Hence, the CO emission may be due to the oxidation temperature.

5.2.5.2. Nitric oxide emission

Fig. 5.10 portrays the variation of the NO_x emission with the engine load and intake air temperature. It is evident from the figure that, the NO_x emission increases with the increase in the engine load. This is due to increase in the fuel consumption with the increase in the engine load that causes significant increase in the peak cylinder temperature in the combustion chamber. This shows that the NO_x emission trend in HCCI

is also similar to the trends of SI and CI engines. At full load, the highest NO_x emission is found to be 14 ppm for 170 °C intake temperature. The NO_x emission in the ethanol-HCCI operation corresponds to the thermal nitric oxide alone due to the absence of fuel NO_x in ethanol.

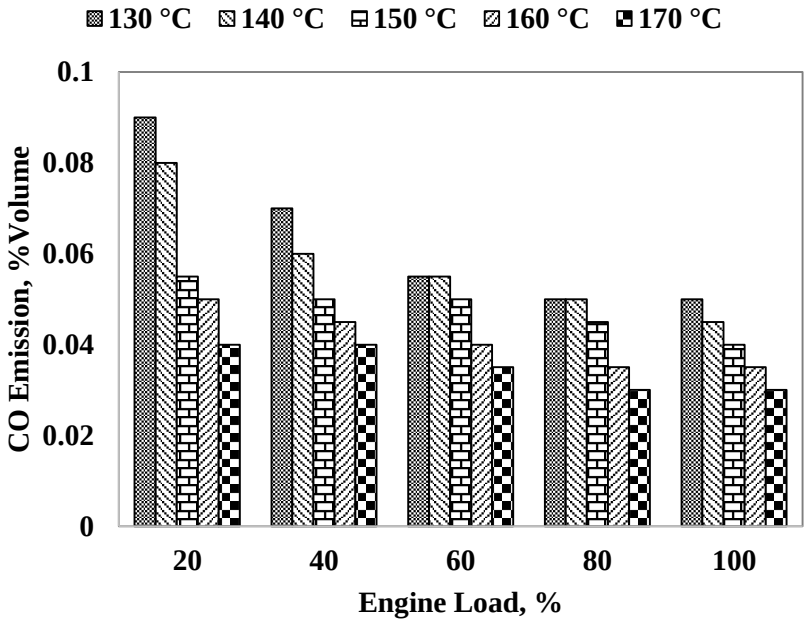

Fig. 5.9. Variation of the carbon monoxide emission with engine load.

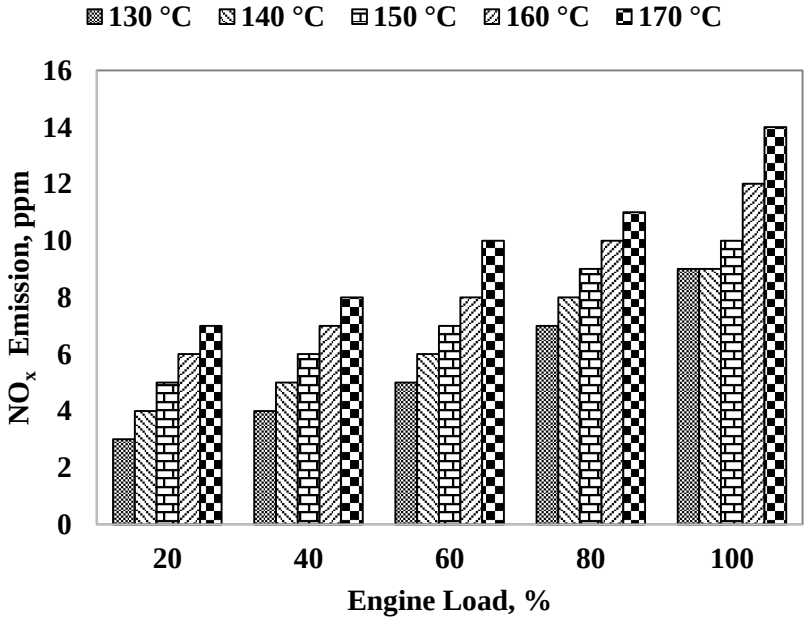

Fig. 5.10. Variation of the nitric oxide emission with engine load.

5.2.6. Summary

This chapter describes the thermodynamic model with temperature dependent specific heats used for the prediction of the combustion, performance and emission parameters the ethanol fueled HCCI engine. This model predicts the in-cylinder pressure and temperature, EGT, indicated thermal efficiency and exhaust emissions at various engine loads. The variation in the pressure and temperature has the direct effect on efficiency, heat losses, EGT and emissions. The obtained numerical results show that, the indicated thermal efficiency increases with the engine load, and advances the SOC with the increase in the intake air temperature. The CO emission decreases with the engine load, while NO_x emission increases with the engine load. The NO_x emissions were found to be below 14 ppm during the entire engine operation.This modelling is expected to provide the valuable guidelines for the researchers and designers regarding the performance evaluation as well as the development of the HCCI engines.

5.3. Effect of charge temperature

5.3.1. General

This chapter presents the experimental results of the combustion, performance, and emission characteristics of the ethanol-fueled HCCI engine at various engine loads by varying the intake air temperature and compared with those of diesel operation. The auto-ignition temperature of ethanol can be achieved with the compression ratios above 24:1 due to its low Cetane number [23]. Therefore, intake air heating system is used to attain ethanol's auto-ignition temperature. Ethanol was injected into the intake manifold by using port fuel injection technique. Due to an adequate mixing time during suction and compression strokes, a complete homogeneous charge was prepared. The intake air was heated from 130 to 170 °C at a step of 10 °C for achieving stable HCCI operation. The load on the engine were represented by the percentage of the rated load (4.4 kW) on the engine. The basis for comparing mineral diesel and ethanol results is to show that ethanol fuelled HCCI engine gives best performance than diesel fuelled CI engine. The comparison is carryout with load on X-axis.

5.3.2. Combustion parameters

5.3.2.1. Cylinder pressure and rate of combustion

The main parameters that influence the cylinder pressure are (i) volume changes, (ii) heat transfer, (iii) combustion, and (iv) leakage past the piston. Fig. 5.11 depicts the effects of intake temperature on the cylinder pressure, and the rate of heat release of the HCCI engine run on ethanol at full load. It can be observed from the figure that, the cylinder pressure data of ethanol HCCI is higher than that of diesel operation at full load. The start of combustion of ethanol occurs earlier by 2–3 °CA than that of diesel due to the high intake air temperatures in the entire load spectrum. The high intake air temperatures are chosen to compensate the lower cetane number for ethanol. Ethanol is a good anti-knocking agent. Ethanol is oxygenated fuel which aids to complete combustion and lower pollution than diesel. The flash point and octane number values are better for ethanol than diesel. Therefore, the chemical reactivity of ethanol is more than mineral diesel. The HCCI combustion of ethanol indicates that as the intake air temperature increases, the reaction rate accelerates. As the intake air temperature increases, the probability of molecular collisions also increases; hence the reaction rate improves, while the reaction time decreases. The advanced start of combustion and increased peak pressure for ethanol

are observed with the temperature increment. The chemical reaction rates are mainly affected by pressure rather than temperature, but the important factor influencing the cylinder peak pressure is still intake temperature [15]. The maximum peak cylinder pressure at full load is found to be about 86 bar, and a mild knock is observed at 170 °C. Similarly, the misfire occurrence (high CO emission) is found at 130 °C. Hence, the HCCI operating regime for each initial condition is limited for knock and misfire [255].

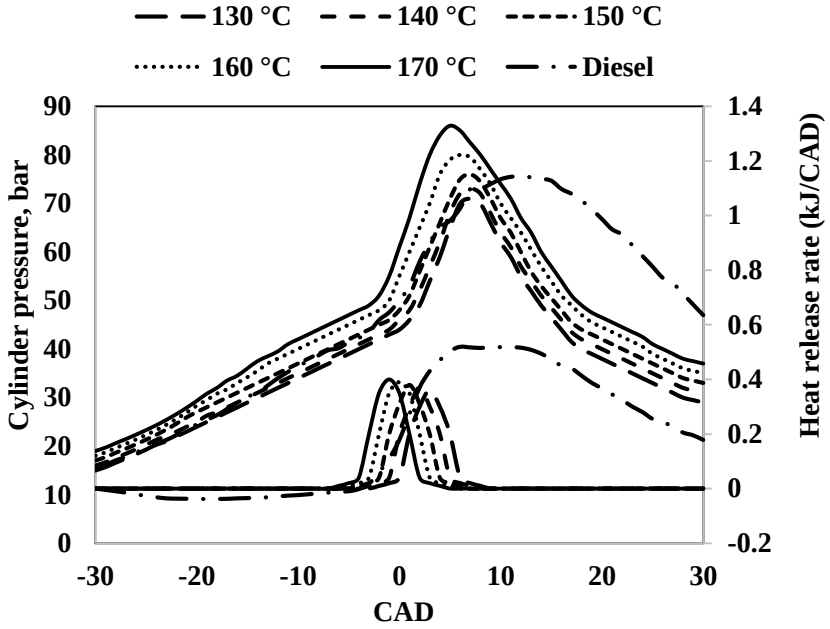

Fig. 5.11. Effects of intake air temperature on cylinder pressure and rate of heat release rate.

The combustion rate is very high in the HCCI, as combustion occurs simultaneously to the whole cylinder charge. The combustion rate largely depends upon the species concentration and temperature. It can be observed from the figure that, the ethanol HCCI operation exhibits a single stage HRR due to its high octane number. Similar results were reported by a few researchers [256–258]. This indicates that, the premixed dominated combustion for the ethanol fuel HCCI combustion. The single boiling point of ethanol fuel with two carbon atoms can produce aldehydes easily; and hence the HRR is higher. As the temperature increases, the reaction rate also increases for combustion of ethanol causing early CAD combustion that in turn increases convective heat transfer losses [255].

5.3.2.2. Ringing intensity (RI) analysis

The upper load of HCCI combustion operating range is limited due to the high HRR resulting in a high-pressure rise rate followed by a heavy knock. This knock creates

unacceptable levels of noise and sometimes damage to engine components. Fig. 5.12 portrays the variation of RI with the engine load and intake air temperature for the ethanol HCCI operation. It can be apparent from the figure that, RI increases with the increase in the engine load and the intake air temperature. As the engine load increases, the combustion chamber temperature increases due to the advanced combustion phase, resulting in a higher HRR, which leads to a higher rate of pressure rise. Intake air temperature has a significant effect on combustion noise, but combustion efficiency improved with the increased intake air temperature.

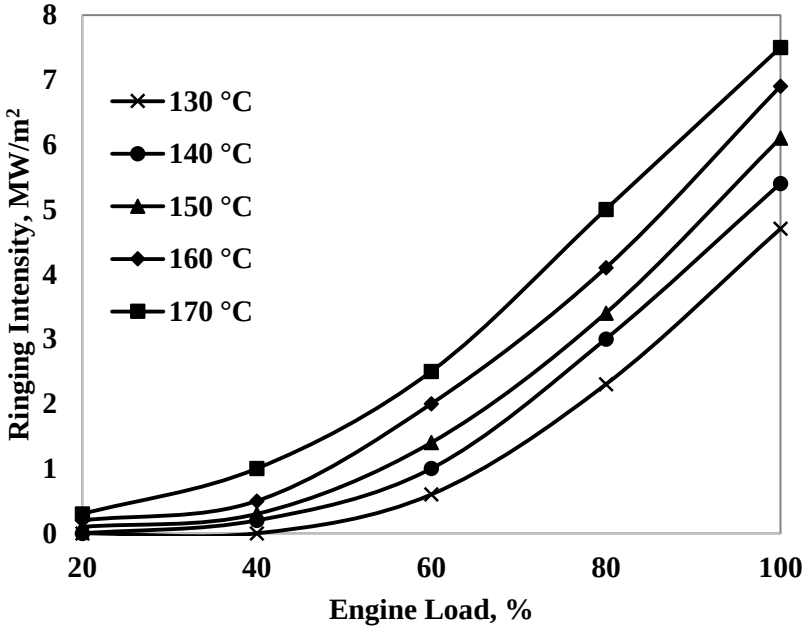

Fig. 5.12. Effects of intake air temperature on ringing intensity.

5.3.2.3. Combustion duration

The time period between the start of combustion and the end of combustion is termed as combustion duration, which is measured in degree crank angle. It is calculated from the cumulative heat release analysis. The start of combustion is taken at which 5% of the total heat energy is released whereas 95% for the end of combustion. Fig. 5.13 shows the variation of the combustion duration as a function of intake air temperatures for the ethanol HCCI operation, and compared with diesel operation. It can be observed that, the combustion duration is very short for the ethanol HCCI operation and has a very less influence on the intake air temperature. The presence of oxygen in ethanol promotes the combustion rate and causes a lower combustion duration. At full load, the combustion duration for ethanol is below 9.5° crank angle, whereas for diesel is 37° crank angle. The

higher combustion duration for diesel is due to direct injection inside the combustion chamber.

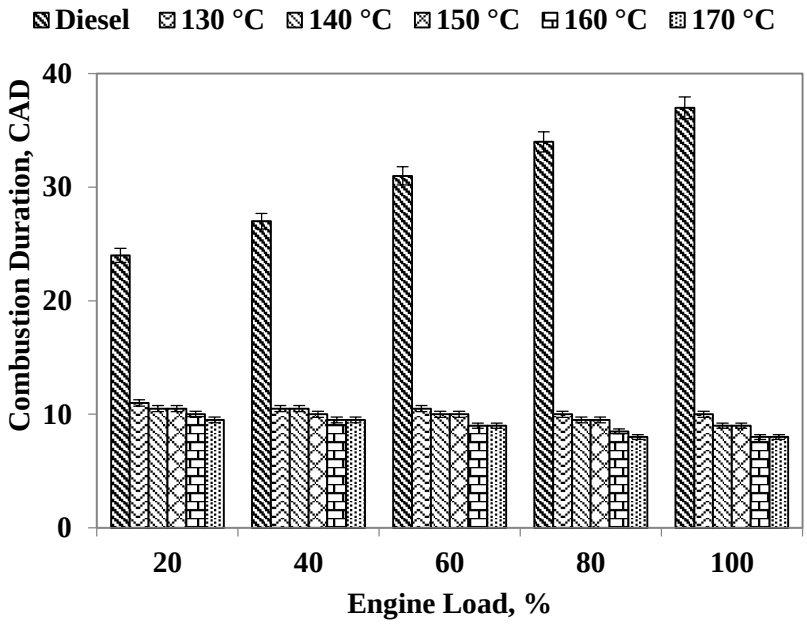

Fig. 5.13. Effects of intake air temperature on combustion duration.

5.3.2.4. Combustion timing (CA50)

The combustion timing is another important factor in the HCCI mode represented by the crank angle of 50% of the heat released. The CA50 needs to be controlled to run the HCCI engine effectively for a better performance. As the load increases the CA50 window for the stable HCCI, the engine operation becomes narrowed making the engine control more challenging [259,260]. The combustion stability and combustion noise are controlled with CA50. Fig. 5.14 shows the variation of the combustion timing as a function of intake air temperatures for the ethanol HCCI operation, and compared with the diesel operation. The CA50 for diesel increases with the increase in the engine load due to increase in the fuel injection quantity with the load. But, for ethanol CA50 advances with the increase in the engine load, and the intake air temperature due to increase in the equivalence ratio of premixed ethanol with the engine load. At full load, the CA50 for ethanol is 1° before the top dead center (TDC) for 170 °C intake air temperature, which tends to a high combustion noise at the high load that limits the operating range of the ethanol HCCI operation. Since there is no direct control for the start of ignition in the port fuel injection technique, the higher load limit of HCCI combustion is limited by knock.

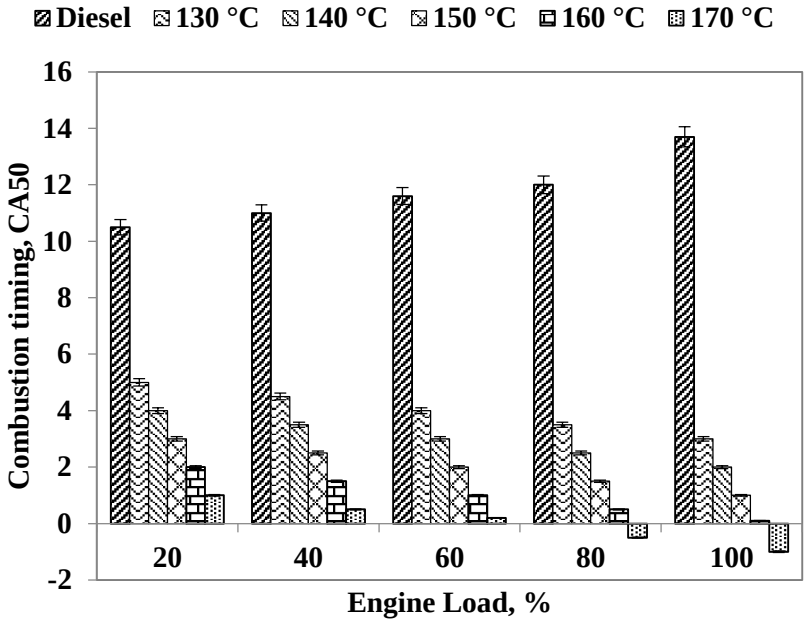

Fig. 5.14. Effects of intake air temperature on combustion timing.

5.3.3. Performance parameters

5.3.3.1. Brake thermal efficiency (BTE)

The HCCI technology offers a higher brake thermal efficiency compared to those of SI and CI engines [30]. The BTE mainly depends on the combustion efficiency, compression ratio and combustion phasing [9]. Fig. 5.15 shows the variation of BTE as a function of intake air temperature for the ethanol HCCI operation, and compared with that of diesel operation. It can be observed from the figure that, at each intake air temperature, lower BTE for the lower engine loads due to the retarded start of combustion. The heat losses from the HCCI engine are expected to be lower due to (i) the lower combustion temperature, (ii) shorter combustion duration, and (iii) little soot formation due to homogeneous mixture preparation. Advanced start of combustion leads to the high HRR and higher combustion temperatures. Therefore, the heat loss from the cylinder walls and piston increases thereby a lesser work done by the piston. On the other hand, retarding the start of combustion results in a poor combustion efficiency due to lower combustion temperature and increased emissions. The maximum thermal efficiency for the ethanol HCCI operation is found to be 43% at 170 °C. As the intake air temperature increases, the BTE also increases for all the engine loads probably due to the higher combustion efficiency.

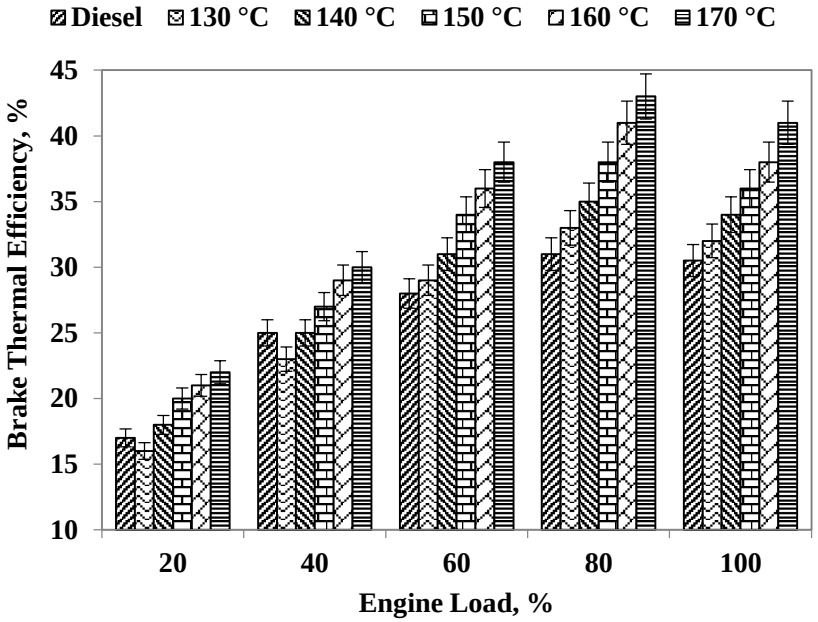

Fig. 5.15. Effects of intake air temperature on brake thermal efficiency.

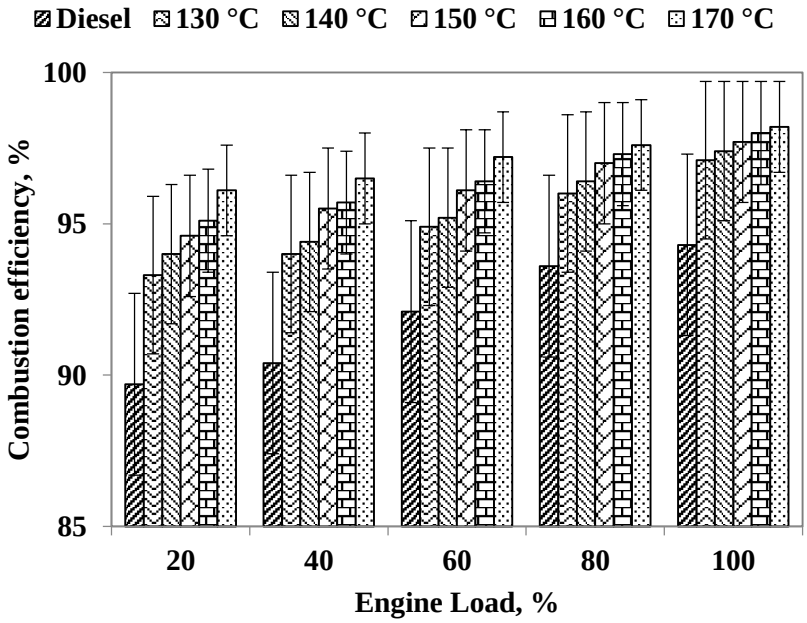

Fig. 5.16. Effect of intake air temperature on combustion efficiency.

5.3.3.2. Combustion efficiency

The effectiveness of fuel burning in the engine is measured by combustion efficiency. This can be calculated as the ratio of cumulative HRR to the total heat energy supplied. Fig. 5.16 illustrates the variation of combustion efficiency as a function of the intake air

temperature for the ethanol HCCI operation, and compared with that of diesel operation. The combustion efficiency increases with the increase in the engine load as well as with the intake air temperature due to an increased overall in-cylinder temperature. At high intake temperatures, the fuel oxidation reactions proceed at faster rates leading to a complete combustion. The combustion efficiency of ethanol is found to be 98.2% for 170 °C. This may be due to the oxygen content in the fuel.

5.3.3.3. Exhaust gas temperature (EGT)

Fig. 5.17 shows the variation of exhaust gas temperature as a function of intake air temperature for the ethanol HCCI operation, and compared with that of diesel operation. The exhaust gas temperature increases with the increase in the engine load for all intake temperatures, as expected. However, the exhaust gas temperature decreases with the increase in the intake temperature. As the intake temperature increases, the start of combustion is advanced which is due to the faster chemical kinetics and reaction rates. An early start of combustion with the short combustion duration increases the convective heat transfer due to the increase in the residence time of burned hot gasses in the cylinder. This in turn reduces the exhaust gas temperature. At higher intake air temperature,dominant premixed combustion may be one of the possible reasons for lower EGT. Fig. 5.18 illustrates the consequences of intake charge temperature on the exhaust gas temperature in HCCI engine.

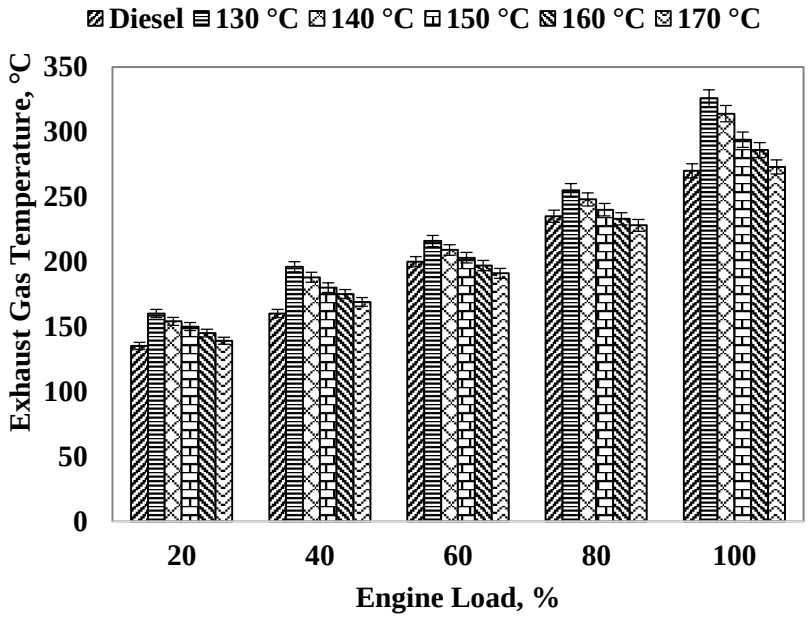

Fig. 5.17. Effects of intake air temperature on the exhaust gas temperature.

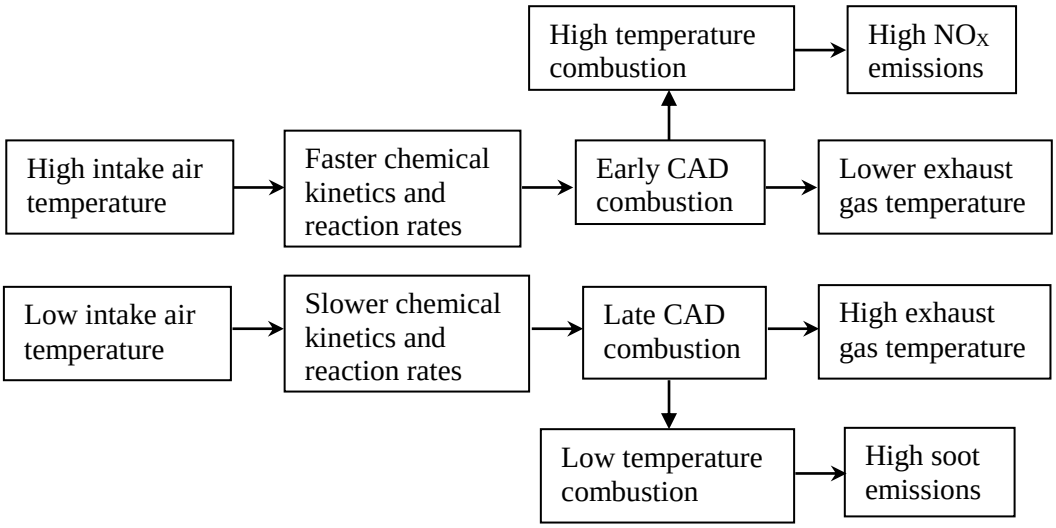

Fig. 5.18. Consequences of intake air temperature on the exhaust gas temperature.

5.3.4. Engine emission analysis

5.3.4.1. Unburned hydrocarbon (UHC)

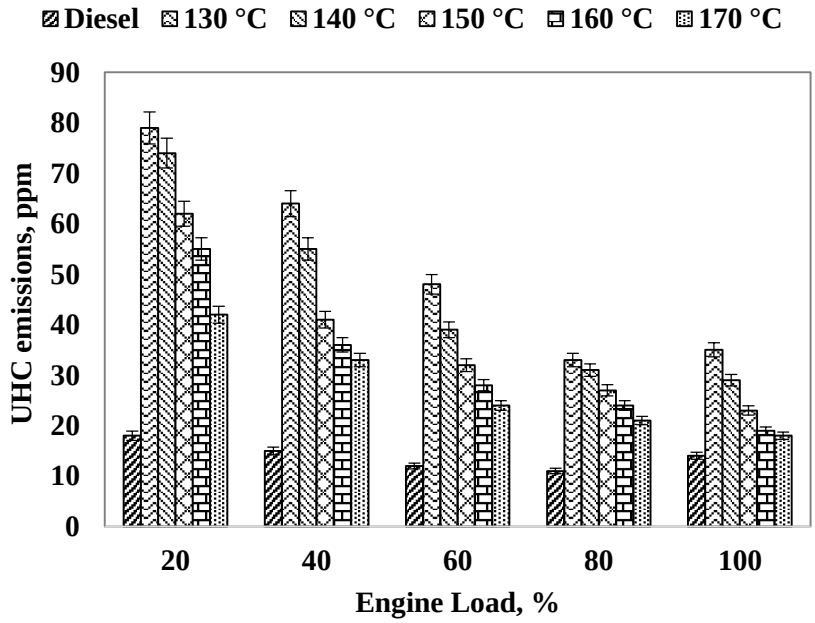

Fig. 5.19. Effects of intake air temperature on UHC emissions for ethanol HCCI combustion.

The formation of UHC emissions in the HCCI engines indicates the incomplete combustion of hydrocarbon fuel due to a low temperature combustion. The combustion temperature is much lower near the walls of the combustion chamber due to heat losses. Greater parts of UHC emissions arise from the combustion chamber wall regions [128]. Fig. 5.19 portrays the variation of the UHC emissions as a function of the intake air

temperature for ethanol HCCI operation, and compared with that of diesel operation. It is evident from the figures that, the UHC emission decreases with the increase in the engine load due to an increase in the equivalence ratio of the mixture with load. The UHC emissions also decreases with the increase in the intake air temperature. In HCCI operation of ethanol, the UHC is higher compared to that of diesel which is due to the low temperature combustion of ethanol.

5.3.4.2. Carbon-monoxide (CO) emissions

The carbon-monoxide (CO) emission in the HCCI engines are formed due to the lack of oxidation temperature caused by the low-temperature combustion. Fig. 5.20 portrays the variation of CO emission as a function of the intake air temperature for the ethanol HCCI operation, and compared with that of diesel operation. The CO emission decreases with the engine load due to an increase in the combustion temperature with load. The early start of combustion phase causes a lower CO emission, while late combustion phasing causes a high CO emission. The CO emission for the ethanol HCCI operation is higher than that of diesel due to the lower combustion temperature. The CO emission is higher at a lower intake air temperature (130 °C) and loads due to misfire. The lower load limit of ethanol-fueled HCCI operation is constrained by the CO emission.

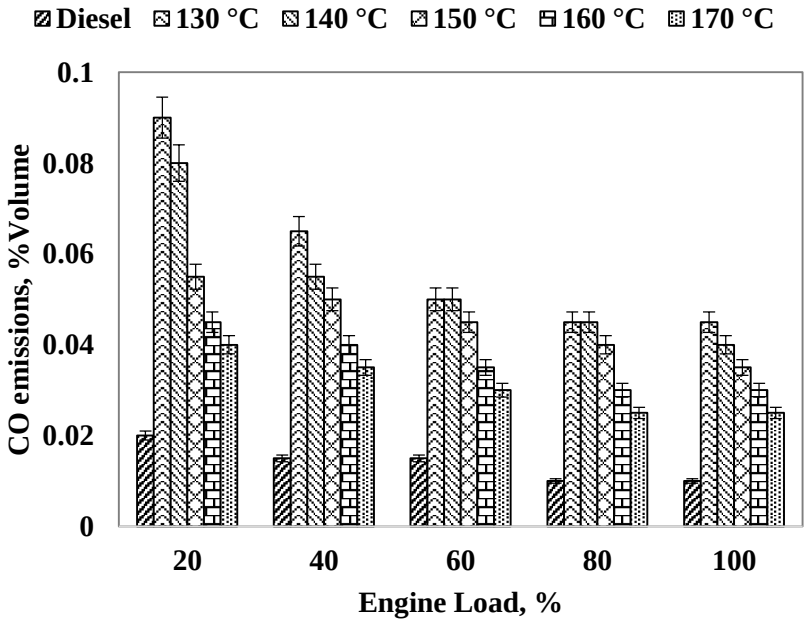

Fig. 5.20. Effects of intake air temperature on CO emissions for ethanol HCCI combustion.

5.3.4.3. Nitric oxide (NO) emission

The three principal factors that affect the formation of nitric oxide (NO) in aa heat engine are (i) availability of oxygen and nitrogen, (ii) temperature favorability of the burned gasses, and (iii) the residence time. The NO is formed inside the combustion chamber during the post-flame combustion process in the region of high temperature. The formation of NO emission from atmospheric nitrogen in any combustor proceeds via extended Zeldovich mechanism [53].

$[NO] \propto [N_2][O_2]^{0.5} e^{(E/RT_f)}$ Where E is the activation energy for the reaction (kJ/kg)

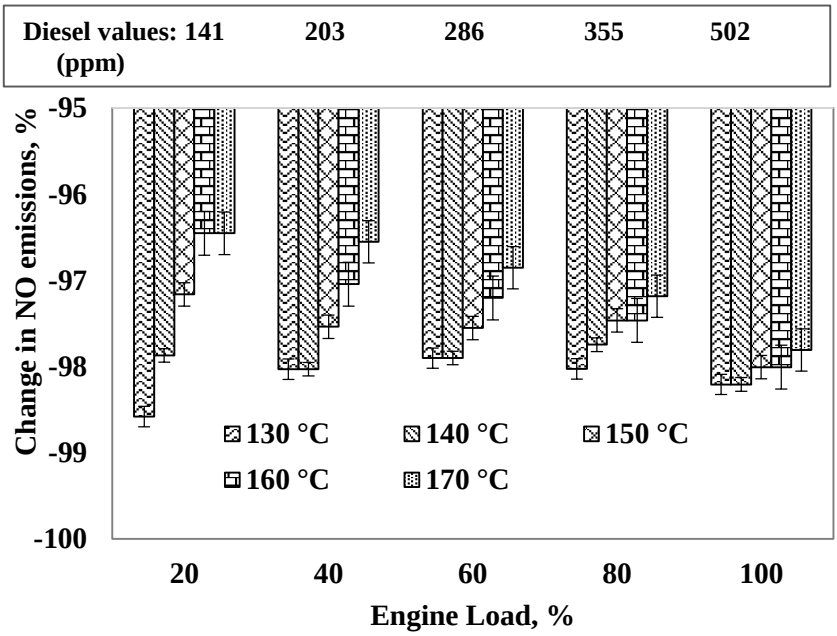

Fig. 5.21. The variation of NO emissions with the engine load and intake temperature compared to diesel.

From the above equation, the NO formation is very sensitive towards the temperature and the oxygen concentration. Since the oxygen concentration is crucial for combustion efficiency, the temperature of combustion has to be reduced in order to suppress nitric oxides formation [261]. Fig. 5.21 depicts the variations of NO emission with the engine load and charge temperature. The NO emission increases with the increase in engine load for the ethanol HCCI operation. It is expected that, the NO emission increases with the increase in the engine load due to the increase in the combustion temperature of the burned gasses. As well as, the NO emission increases with the increase in the intake temperature due to the increase in the residence time caused by the early start of combustion. For diesel, the NO emission is higher compared to that of ethanol due to

diffusion combustion. The NO emission is 96% lower for PFI of ethanol HCCI operation compared to that of diesel operation throughout the load spectrum. At full load, the maximum NO emission is noticed. For 170 °C charge temperature, the highest NO emission of 11 ppm is found for the ethanol fueled HCCI operation at full load condition.

5.3.4.4. Smoke opacity

The three principle factors that affect the formation of smoke in CI engines are (i) presence of soot (solid carbon) in the fuel, (ii) lack of oxidation temperature, and (iii) shorter time availability for mixture preparation [262–266]. Fig. 5.22 portrays the changes in smoke emission with the engine load and intake temperature for the ethanol HCCI operation. It is evident from the figure that, the smoke opacity decreases with the increase in the intake air temperature for all engine loads. The smoke emission is 94% lower for PFI of ethanol HCCI operation compared to that of diesel operation. At full load, almost negligible smoke emission observed for the ethanol HCCI operation. This may be due to the homogeneous charge prepared with the increased ignition delay. The smoke emissions are decreased with the engine load as well as the intake temperature also. At 170 °C, the smoke emissions are found to be near zero due to the increase in oxidation temperature, and residence time of burned gasses of ethanol. At 170 °C, the least value of smoke emissions recorded is about 0.1% for the ethanol HCCI operation at full load. The smoke emissions are less than 0.7% throughout this investigation.

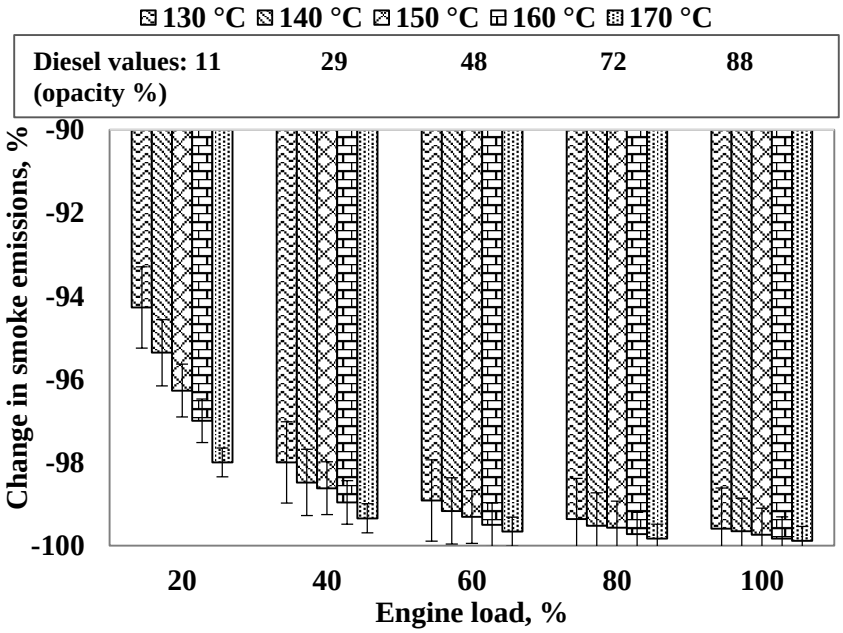

Fig. 5.22. The variation of smoke emissions with the engine load and intake temperature compared to diesel.

5.3.5. Summary

In this investigation, the HCCI engine was examined by applying the charge heating strategy in a single cylinder, four-stroke diesel engine fueled with ethanol at 1500 rpm. The inlet air temperature was increased from 130 to 170 °C at a step of 10 °C, and port fuel injection of ethanolwas used for the homogeneous charge preparation. Since the homogeneous mixture was prepared outside the engine cylinder, wall wetting and mixing did not arise. The effect of intake air temperature on the auto-ignition timing, heat release rate, combustion timing and emissions on the ethanol fueled HCCI engine were analyzed and compared with the standard DI diesel operation. From the results of the investigation, the following conclusions are drawn.

- Increasing the intake air temperature advanced the combustion phase and decreased the exhaust gas temperature.

- The increase in the intake air temperature increased the in-cylinder pressure and ethanol is more sensitive to the intake air temperature.

- The operating regime of HCCI was limited. The higher load was limited by combustion noise and the lower load was limited by the CO emissions.

- Maximum combustion efficiency and thermal efficiency for the ethanol HCCI operation was found 98.2% and 43% respectively for intake temperature of 170 °C.

- The UHC and CO emissions were found to be higher for the ethanol HCCI operation than that of diesel DI operation due to low temperature combustion.
- The NO emission was found to be 11 ppm for ethanol HCCI which was about 97% lower compared to diesel DI operation.

- The smoke opacity for the ethanol HCCI operation was found to be below 0.1% which is negligible compared to that of diesel DI operation.

5.4. Multi-Criteria Decision Making – TOPSIS Method

5.4.1. General

The selection of the best/optimum charge temperature plays a major role in cleaner combustion of ethanol-fueled HCCI engine operation. This chapter discusses the selection of optimum charge temperature for ethanol-fueled HCCI engine using a Multi-Criteria Decision Making (MCDM) method called the Technique for Order of Preference by Similarity to Ideal Solution (TOPSIS). The evaluation of the best charge temperature was based on the exploratory analysis of the HCCI engine performance and emission parameters those were obtained from section 5.2. The weights for each response has been evaluated using principle component analysis approach.

5.4.2. TOPSIS computations

The TOPSIS method was proposed for the selection of the optimum charge temperature during the operation of ethanol-fueled HCCI engine from 130-170 °C. The performance and emission parameters of the engine experimental data was taken from section 5.2. The combination of the input and output parameters were depicted in terms of a decision matrix (Eq. 4.27) and listed in Table 5.1.

The output attributes were normalized using Eq. 4.28. The normalized data matrix has been evaluated and shown in Table 5.2.

The weights for each response were determined using principal component analysis (PCA) approach. The summation of the total weights was equal to unity. Minitab 16.0 software was used to calculate the principal components for HCCI engine performance and emission parameters. The weightage for BTE, EGT, NO smoke, UHC, and CO are 0.19, 0.09, 0.2, 0.15, 0.2, and 0.18 respectively. The weighted normalized matrix was calculated using Eq. 4.30 and displayed in the Table 5.3.

Table 5.1 Experimental performance and emission readings observed from HCCI engine.

Experiment No.	Input parameters		Output parameters					
			Performance		Emission			
	Load (%)	Charge temperature (°C)	BTE (%)	EGT (°C)	NO (ppm)	Smoke (%)	UHC (ppm)	CO (%V)
1	20	130	16	160	2	0.63	79	0.09
2		140	18	154	2	0.51	74	0.08
3		150	20	150	4	0.42	62	0.055
4		160	21	145	5	0.33	55	0.045
5		170	22	139	5	0.22	42	0.04
6	30	130	19	177	3	0.6	68	0.077
7		140	20	169	3	0.46	63	0.07
8		150	23	162	4	0.41	52	0.052
9		160	25	160	6	0.32	43	0.042
10		170	27	154	6	0.21	37	0.037
11	40	130	23	196	4	0.58	64	0.065
12		140	25	188	4	0.44	55	0.055
13		150	27	180	5	0.4	41	0.05
14		160	29	175	6	0.3	36	0.04
15		170	30	169	7	0.19	33	0.035
16	50	130	26	205	5	0.55	51	0.059
17		140	28	203	6	0.42	44	0.053
18		150	30	197	6	0.37	35	0.047
19		160	32	191	7	0.28	31	0.037
20		170	35	186	8	0.18	28	0.033
21	60	130	29	216	6	0.52	48	0.055
22		140	31	209	6	0.4	39	0.05
23		150	34	203	7	0.33	32	0.045
24		160	36	197	8	0.24	28	0.035
25		170	38	191	9	0.16	24	0.03
26	70	130	32	233	6	0.48	45	0.05
27		140	33	225	7	0.38	35	0.047
28		150	35	219	8	0.32	30	0.042
29		160	38	211	8	0.22	26	0.033
30		170	41	203	9	0.14	23	0.029
31	80	130	33	255	7	0.46	41	0.048
32		140	35	248	7	0.34	31	0.045
33		150	38	240	9	0.31	28	0.04
34		160	41	233	9	0.2	24	0.032
35		170	43	228	10	0.12	21	0.027
36	90	130	32.5	281	8	0.41	37	0.047
37		140	34.5	279	8	0.32	30	0.044
38		150	37	271	9	0.26	26	0.037
39		160	39	265	9	0.18	22	0.031
40		170	42	256	10	0.11	20	0.026
41	100	130	32	326	9	0.36	35	0.045
42		140	34	314	9	0.3	29	0.04
43		150	36	294	10	0.23	23	0.035
44		160	38	286	10	0.15	19	0.03
45		170	41	273	11	0.1	18	0.025

Table 5.2 Normalized data matrix for performance and emission parameters.

Load (%)	Charge temperature (°C)	BTE	EGT	NO	Smoke	UHC	CO
20	130	0.0748	0.1090	0.0415	0.2627	0.2853	0.2837
	140	0.0842	0.1049	0.0415	0.2126	0.2672	0.2522
	150	0.0935	0.1022	0.0830	0.1751	0.2239	0.1734
	160	0.0982	0.0988	0.1037	0.1376	0.1986	0.1419
	170	0.1029	0.0947	0.1037	0.0917	0.1517	0.1261
30	130	0.0888	0.1206	0.0622	0.2502	0.2456	0.2427
	140	0.0935	0.1151	0.0622	0.1918	0.2275	0.2207
	150	0.1076	0.1103	0.0830	0.1709	0.1878	0.1639
	160	0.1169	0.1090	0.1244	0.1334	0.1553	0.1324
	170	0.1263	0.1049	0.1244	0.0876	0.1336	0.1166
40	130	0.1076	0.1335	0.0830	0.2418	0.2311	0.2049
	140	0.1169	0.1280	0.0830	0.1835	0.1986	0.1734
	150	0.1263	0.1226	0.1037	0.1668	0.1481	0.1576
	160	0.1356	0.1192	0.1244	0.1251	0.1300	0.1261
	170	0.1403	0.1151	0.1452	0.0792	0.1192	0.1103
50	130	0.1216	0.1396	0.1037	0.2293	0.1842	0.1860
	140	0.1309	0.1383	0.1244	0.1751	0.1589	0.1671
	150	0.1403	0.1342	0.1244	0.1543	0.1264	0.1482
	160	0.1496	0.1301	0.1452	0.1167	0.1120	0.1166
	170	0.1637	0.1267	0.1659	0.0750	0.1011	0.1040
60	130	0.1356	0.1471	0.1244	0.2168	0.1733	0.1734
	140	0.1450	0.1424	0.1244	0.1668	0.1408	0.1576
	150	0.1590	0.1383	0.1452	0.1376	0.1156	0.1419
	160	0.1683	0.1342	0.1659	0.1001	0.1011	0.1103
	170	0.1777	0.1301	0.1867	0.0667	0.0867	0.0946
70	130	0.1496	0.1587	0.1244	0.2001	0.1625	0.1576
	140	0.1543	0.1533	0.1452	0.1584	0.1264	0.1482
	150	0.1637	0.1492	0.1659	0.1334	0.1083	0.1324
	160	0.1777	0.1437	0.1659	0.0917	0.0939	0.1040
	170	0.1917	0.1383	0.1867	0.0584	0.0831	0.0914
80	130	0.1543	0.1737	0.1452	0.1918	0.1481	0.1513
	140	0.1637	0.1689	0.1452	0.1418	0.1120	0.1419
	150	0.1777	0.1635	0.1867	0.1292	0.1011	0.1261
	160	0.1917	0.1587	0.1867	0.0834	0.0867	0.1009
	170	0.2011	0.1553	0.2074	0.0500	0.0758	0.0851
90	130	0.1520	0.1914	0.1659	0.1709	0.1336	0.1482
	140	0.1613	0.1900	0.1659	0.1334	0.1083	0.1387
	150	0.1730	0.1846	0.1867	0.1084	0.0939	0.1166
	160	0.1824	0.1805	0.1867	0.0750	0.0795	0.0977
	170	0.1964	0.1744	0.2074	0.0459	0.0722	0.0820
100	130	0.1496	0.2220	0.1867	0.1501	0.1264	0.1419
	140	0.1590	0.2139	0.1867	0.1251	0.1047	0.1261
	150	0.1683	0.2002	0.2074	0.0959	0.0831	0.1103
	160	0.1777	0.1948	0.2074	0.0625	0.0686	0.0946
	170	0.1917	0.1859	0.2281	0.0417	0.0650	0.0788

Table 5.3 Weighted normalized data matrix for performance and emission parameters.

Load (%)	Charge temperature (°C)	BTE	EGT	NO	Smoke	UHC	CO
20	130	0.0140	0.0094	0.0082	0.0406	0.0565	0.0508
	140	0.0157	0.0090	0.0082	0.0328	0.0529	0.0451
	150	0.0175	0.0088	0.0164	0.0270	0.0443	0.0310
	160	0.0183	0.0085	0.0204	0.0213	0.0393	0.0254
	170	0.0192	0.0081	0.0204	0.0142	0.0300	0.0226
30	130	0.0166	0.0103	0.0123	0.0386	0.0486	0.0434
	140	0.0175	0.0099	0.0123	0.0296	0.0451	0.0395
	150	0.0201	0.0095	0.0164	0.0264	0.0372	0.0293
	160	0.0218	0.0094	0.0245	0.0206	0.0308	0.0237
	170	0.0236	0.0090	0.0245	0.0135	0.0265	0.0209
40	130	0.0201	0.0115	0.0164	0.0373	0.0458	0.0367
	140	0.0218	0.0110	0.0164	0.0283	0.0393	0.0310
	150	0.0236	0.0105	0.0204	0.0258	0.0293	0.0282
	160	0.0253	0.0102	0.0245	0.0193	0.0257	0.0226
	170	0.0262	0.0099	0.0286	0.0122	0.0236	0.0197
50	130	0.0227	0.0120	0.0204	0.0354	0.0365	0.0333
	140	0.0244	0.0119	0.0245	0.0270	0.0315	0.0299
	150	0.0262	0.0115	0.0245	0.0238	0.0250	0.0265
	160	0.0279	0.0112	0.0286	0.0180	0.0222	0.0209
	170	0.0305	0.0109	0.0327	0.0116	0.0200	0.0186
60	130	0.0253	0.0126	0.0245	0.0335	0.0343	0.0310
	140	0.0271	0.0122	0.0245	0.0258	0.0279	0.0282
	150	0.0297	0.0119	0.0286	0.0213	0.0229	0.0254
	160	0.0314	0.0115	0.0327	0.0155	0.0200	0.0197
	170	0.0332	0.0112	0.0368	0.0103	0.0172	0.0169
70	130	0.0279	0.0136	0.0245	0.0309	0.0322	0.0282
	140	0.0288	0.0132	0.0286	0.0245	0.0250	0.0265
	150	0.0305	0.0128	0.0327	0.0206	0.0215	0.0237
	160	0.0332	0.0123	0.0327	0.0142	0.0186	0.0186
	170	0.0358	0.0119	0.0368	0.0090	0.0164	0.0164
80	130	0.0288	0.0149	0.0286	0.0296	0.0293	0.0271
	140	0.0305	0.0145	0.0286	0.0219	0.0222	0.0254
	150	0.0332	0.0140	0.0368	0.0200	0.0200	0.0226
	160	0.0358	0.0136	0.0368	0.0129	0.0172	0.0180
	170	0.0375	0.0133	0.0409	0.0077	0.0150	0.0152
90	130	0.0284	0.0164	0.0327	0.0264	0.0265	0.0265
	140	0.0301	0.0163	0.0327	0.0206	0.0215	0.0248
	150	0.0323	0.0158	0.0368	0.0167	0.0186	0.0209
	160	0.0340	0.0155	0.0368	0.0116	0.0157	0.0175
	170	0.0367	0.0150	0.0409	0.0071	0.0143	0.0147
100	130	0.0279	0.0191	0.0368	0.0232	0.0250	0.0254
	140	0.0297	0.0184	0.0368	0.0193	0.0207	0.0226
	150	0.0314	0.0172	0.0409	0.0148	0.0164	0.0197
	160	0.0332	0.0167	0.0409	0.0097	0.0136	0.0169
	170	0.0358	0.0160	0.0450	0.0064	0.0129	0.0141

Table 5.4 Distance of alternatives from PIS and NIS (S_i^B, S_i^W).

Load (%)	Charge temperature (°C)	S_i^B	S_i^W
20	130	0.07049	0.0381
	140	0.06116	0.0395
	150	0.04660	0.0407
	160	0.03957	0.0452
	170	0.03020	0.0542
30	130	0.06030	0.0357
	140	0.05138	0.0393
	150	0.03994	0.0445
	160	0.03359	0.0487
	170	0.02727	0.056
40	130	0.05412	0.0352
	140	0.04228	0.0422
	150	0.03455	0.0473
	160	0.02871	0.0531
	170	0.02702	0.0579
50	130	0.04637	0.0382
	140	0.03837	0.0427
	150	0.03181	0.0498
	160	0.02803	0.0557
	170	0.02750	0.0608
60	130	0.04376	0.039
	140	0.03452	0.0467
	150	0.03067	0.0521
	160	0.02854	0.0586
	170	0.02981	0.0641
70	130	0.03950	0.0428
	140	0.03386	0.0486
	150	0.03223	0.0531
	160	0.02741	0.0611
	170	0.02934	0.0662
80	130	0.03894	0.0439
	140	0.03098	0.0523
	150	0.03433	0.0549
	160	0.03046	0.0629
	170	0.03323	0.0683
90	130	0.03862	0.0453
	140	0.03336	0.0521
	150	0.03303	0.0575
	160	0.03052	0.064
	170	0.03347	0.0689
100	130	0.03983	0.0469
	140	0.03584	0.053
	150	0.03611	0.0596
	160	0.03437	0.0658
	170	0.03766	0.07

Table 5.5 Relative closeness and ranking of the alternatives at each load.

Load (%)	Charge temperature (°C)	Relative closeness	Rank
20	130	0.351	5
	140	0.393	4
	150	0.466	3
	160	0.533	2
	170	0.642	1
30	130	0.372	5
	140	0.433	4
	150	0.527	3
	160	0.592	2
	170	0.673	1
40	130	0.394	5
	140	0.499	4
	150	0.578	3
	160	0.649	2
	170	0.682	1
50	130	0.452	5
	140	0.527	4
	150	0.610	3
	160	0.665	2
	170	0.689	1
60	130	0.471	5
	140	0.575	4
	150	0.629	3
	160	0.672	2
	170	0.683	1
70	130	0.520	5
	140	0.589	4
	150	0.622	3
	160	0.690	2
	170	0.693	1
80	130	0.530	5
	140	0.628	3
	150	0.615	4
	160	0.674	1
	170	0.673	2
90	130	0.540	5
	140	0.610	4
	150	0.635	3
	160	0.677	1
	170	0.673	2
100	130	0.541	5
	140	0.598	4
	150	0.623	3
	160	0.657	1
	170	0.650	2

Table 5.6 Relative closeness and ranking of the alternatives.

Experiment No.	Load (%)	Charge temperature (°C)	Relative closeness	Rank
1	20	130	0.351	45
2		140	0.393	43
3		150	0.466	39
4		160	0.533	32
5		170	0.642	16
6	30	130	0.372	44
7		140	0.433	41
8		150	0.527	34
9		160	0.592	26
10		170	0.673	10
11	40	130	0.394	42
12		140	0.499	37
13		150	0.578	28
14		160	0.649	15
15		170	0.682	5
16	50	130	0.452	40
17		140	0.527	35
18		150	0.610	23
19		160	0.665	12
20		170	0.689	3
21	60	130	0.471	38
22		140	0.575	29
23		150	0.629	18
24		160	0.672	11
25		170	0.683	4
26	**70**	130	0.520	36
27		140	0.589	27
28		150	0.622	21
29		160	0.690	2
30		**170**	**0.693**	**1**
31	80	130	0.530	33
32		140	0.628	19
33		150	0.615	22
34		160	0.674	7
35		170	0.673	9
36	90	130	0.540	31
37		140	0.610	24
38		150	0.635	17
39		160	0.677	6
40		170	0.673	8
41	100	130	0.541	30
42		140	0.598	25
43		150	0.623	20
44		160	0.657	13
45		170	0.650	14

The relative closeness to the ideal solution at each load was calculated using Eq. 4.36. Table 5.5 gives the relative closeness and rank for each alternative with respect to each load. The ranking preference was given to all the relative closeness values in the descending order to obtain the optimal input parameters. Therefore, the alternatives with the largest relative closeness value was identified as near to the optimal solution. The charge temperature 170 °C was positioned at first ranking in 20-70% load conditions. Therefore, the preference of the alternative charge temperatures would be 170 °C > 160 °C > 150 °C > 140 °C > 130 °C.

The optimal engine operating load can be found by ranking all the alternatives with respect to the relative closeness values. Table 5.6 provides the relative closeness and ranking of the alternatives for the studied range of engine load and charge temperature. It can be observed from the table, that the first rank is positioned in 70% load and 170 °C charge temperature. The first rank corresponds to the optimum operating condition for ethanol-fueled HCCI engine.

5.4.3. ANOVA testing

The analysis of variance (ANOVA) test was carried out to determine the significance level of the HCCI engine operating parameters. The most influencing input parameter was determined using this test. In ANOVA table, the numerical value of 'P' is less than 0.05 then that model is identified as statistically significant with 95% confidence level. The level of significance of each operating parameter from the results of the ANOVA test are given in Table 5.7. The aforesaid table confirms that both charge temperature and load are significant as the 'P' value is less than 0.05. From the table, it is also revealed that the charge temperature is the most significant parameter than engine load with a contribution of 63.04% and 27.89% respectively.

Table 5.7 ANOVA table for relative closeness.

Source	Degree of freedom	Sum of Squares	Mean Squares	F-value	P-value	% Contribution
Charge temperature	4	0.25453	0.063633	55.68	0.000	63.04
Load	8	0.11260	0.014076	12.32	0.000	27.89
Error	32	0.03657	0.001143			
Total	44	0.40371				
S = 0.03381		R-Sq = 87.5%				

Furthermore, a response table was also drawn to identify the most influencing parameters of HCCI engine. Response table for means of relative closeness is listed in Table 5.8. The higher the value of delta (max-min) indicates the influence of the corresponding parameter is higher. From the table, it is evident that, the charge temperature is the most influencing parameter of the HCCI engine as it contains the highest delta value.

Table 5.8 Response table for means.

Level	Charge temperature	Load
1	0.4633	0.4770
2	0.5391	0.5193
3	0.5896	0.5604
4	0.6455	0.5886
5	0.6729	0.6061
6	0.6230	
7	0.6239	
8	0.6271	
9	0.6137	
Delta	0.2096	0.1500
Rank	1	2

Fig. 5.23 depicts the 3D surface plots and contour plots for the relative closeness values. These plots are helpful in identifying the trend of variation of input parameters with respect to output responses. It is evident from the figure that, the relative closeness value increases with the increase in the charge temperature and engine load. Thus, it can be concluded that, the charge temperature is most influencing parameter than load for the studied range of HCCI operation.

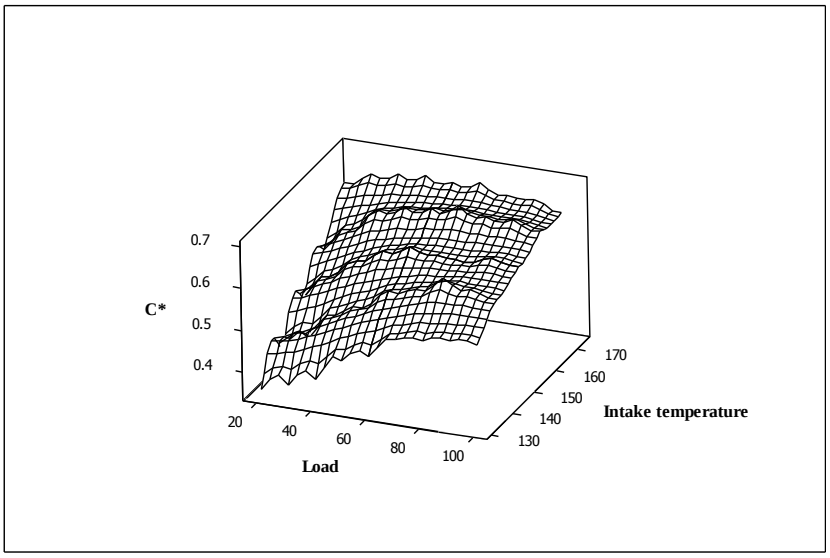

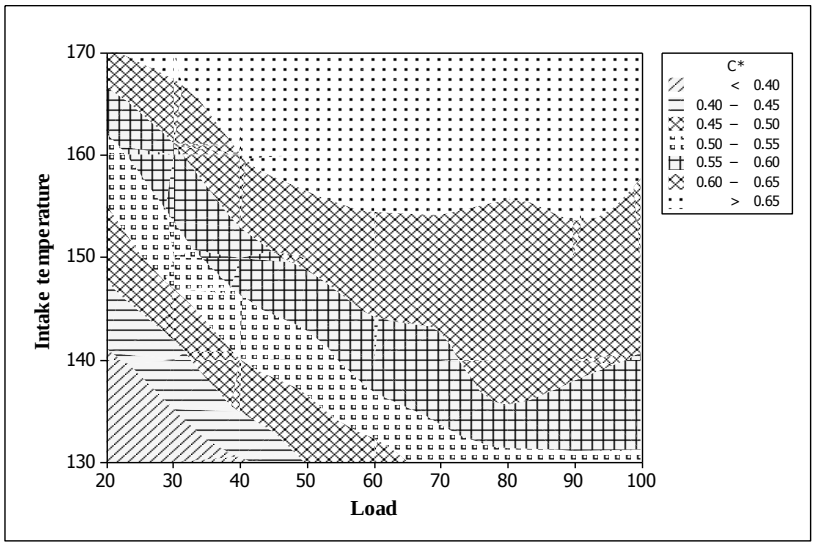

Fig. 5.23. Contour and surface plot for relative closeness Vs intake temperature and load.

5.4.4. Summary

The selection of best charge temperature plays an important role for the ethanol-fueled HCCI engines. There are 45 number of performance and emission experimental data sets that were considered before choosing the best operating charge temperature which involves a multidimensional perspective. Therefore, an effective decision-making approach is essential to resolve the problem. In this study, TOPSIS decision making was used to evaluate the optimum operating conditions. The principal component analysis approach was used to compute the weights and given as input for TOPSIS to determine the priorities of the alternatives. The proposed MCDM method could help the engine manufacturers to choose the best alternative. The optimal HCCI operating condition was found at 70% load and 170 °C charge temperature. The ANOVA test results reveal that the charge temperature is the most significant parameter followed by the engine load. The percentage contribution of charge temperature and load are 63.04% and 27.89% respectively.

5.5. Prediction of HCCI engine output parameters using GRNN

5.5.1. General

The evaluation of the performance and emission parameters of an ethanol-fueled HCCI engine is a challenging one, because of non-linear nature of the parameters. In this chapter, a smart prediction tool was developed for measuring the performance, and emission characteristics of the ethanol-fueled HCCI engine. For this purpose, a study was conducted through a combination of experimental data analysis and generalized regression neural network (GRNN) modelling. This study used a set of experimental data (from Table 5.4.1) obtained from the ethanol HCCI engine to characterize variations in performance measures such as brake thermal efficiency (BTE), and exhaust gas temperature (EGT), and the emission parameters such as unburned hydrocarbons (UHC), carbon monoxide (CO), nitric oxide (NO), and smoke opacity. The neural network was trained, validated and tested with the experimental data sets. Also, grid search method was used to find the optimized kernel bandwidth to reduce the cross-validation error. The obtained results were validated and tested with the experimental HCCI performance and emission metrics.

5.5.2. GRNN trainee using cross validation

By observing the Eq. (4.37) the only adaptive parameter in the GRNN model is Kernel width (σ). Higher values of σ lead to over smoothening of the data while smaller values of σ lead to over-fitting of the data. In order to find the optimal Kernel width, a grid search method is used in this investigation. Hence, it is required to define a range for σ values [σ_{low}, σ_{high}] with 'N' number of iterations. Therefore, the implementation of the cross-validation for the obtained 'N' values of Kernel width is performed using the Eq. (5.1).

$$\sigma = \sigma_{low} + (i - 1)\frac{\sigma_{high} - \sigma_{low}}{N} \qquad I = 1,2,\ldots..,M \tag{5.1}$$

The optimal value of the Kernel width (σ) corresponds to the model with the lowest cross-validation error. For the optimal/minimum value of the error, the interval and the number of iterations need to be consistent (i.e., the effective interval is much smaller). In the current study, the initial search interval for the optimal Kernel bandwidth (σ value) is considered as [1; 10], and search iterations equal to 10. The cross-validation curve for the kernel bandwidth search is shown in Fig. 5.24. The curve has well-defined minima, with an optimal value of σ at 3.73.

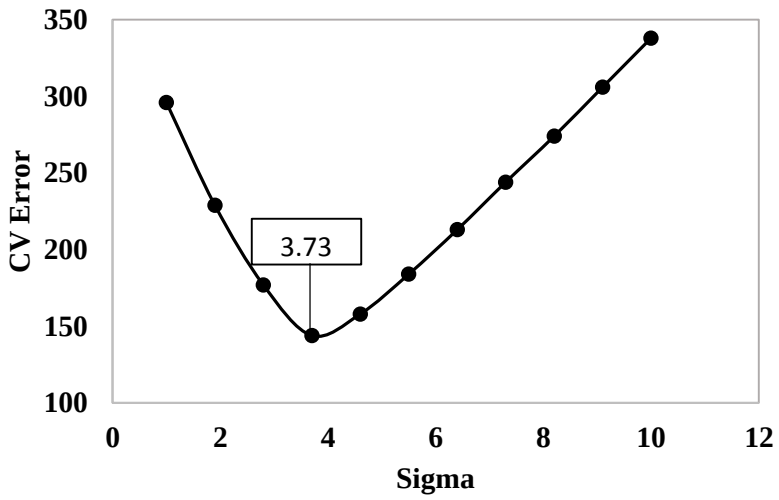

Fig. 5.24. Cross-validation curve for GRNN model. Optimal σ = 3.73.

5.5.3. GRNN training, validation, and testing

Initially, the neural network was trained with 27 data sets (60%) from the available experimental results. The developed tool was validated with 9 data sets (20%) and tested with the remaining 9 data sets (20%) to improve the generalization of the network. Fig. 5.25 shows the experimentally measured EGT and BTE values versus GRNN training data. Fig. 5.26 shows the experimentally measured NO, smoke, UHC and CO values versus GRNN training data. The linear approximation is observed between the trained GRNN and experimental data with minimal error. The graphical representation of the percentage error during GRNN training is depicted in Fig. 5.27. It is observed from the figure that, a maximum of 2.5% error during GRNN training.

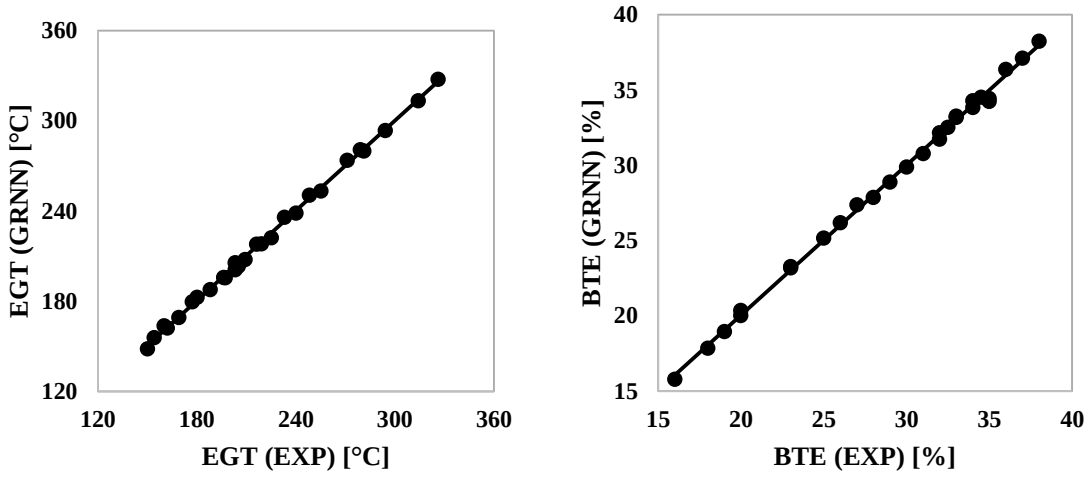

Fig. 5.25. GRNN trained versus experimental (EXP) values for the engine performance data.

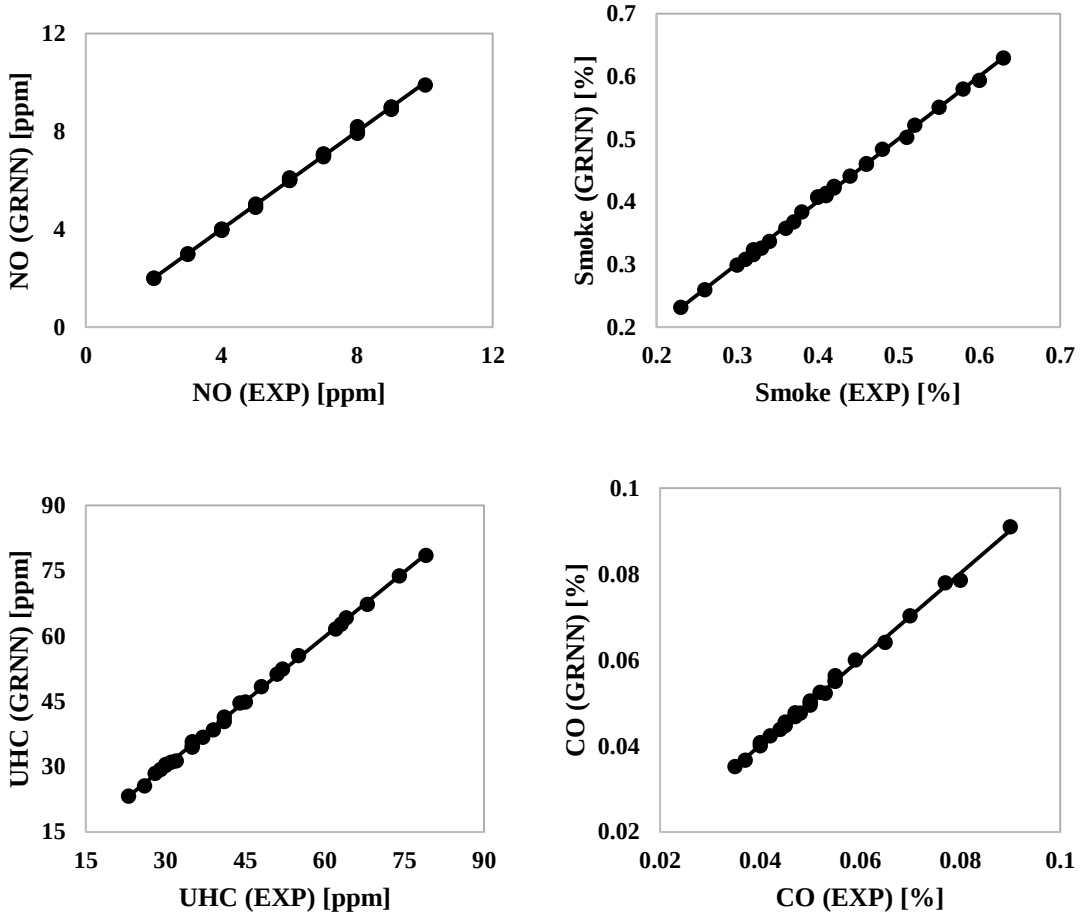

Fig. 5.26. GRNN trained versus experimental (EXP) values for the engine emission data.

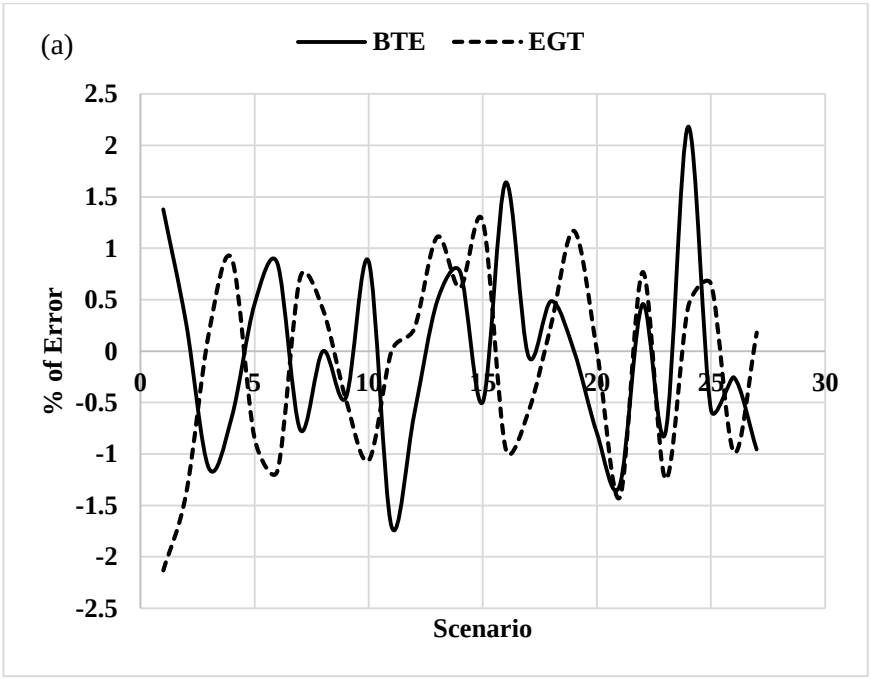

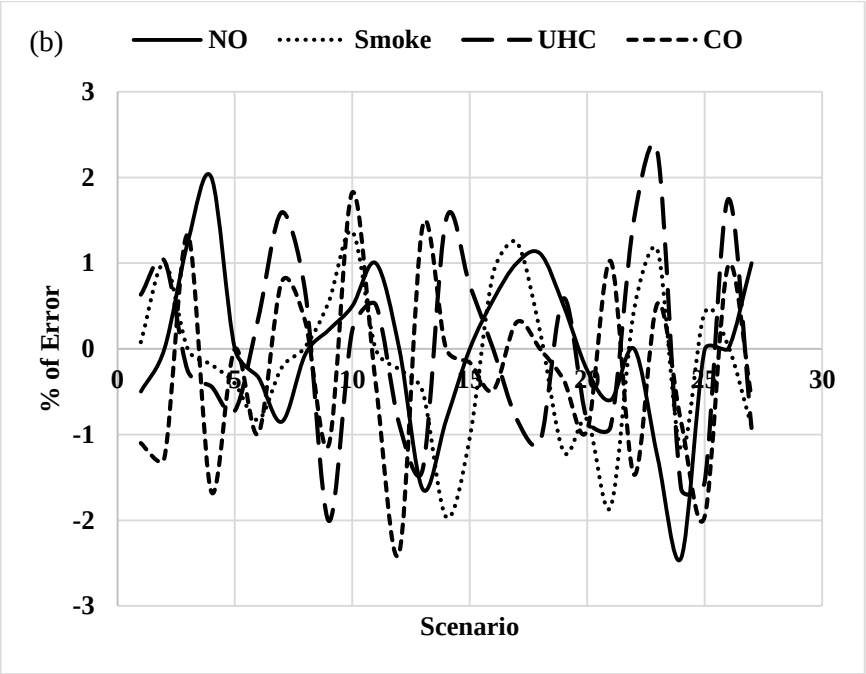

Fig. 5.27. Graphical representation of error percentage for trainee data. (a) Performance parameters, (b) Emission parameters.

The developed GRNN prediction tool was validated and tested and compared with the experimental data sets.The graphical representation of the percentage error during GRNN validation is shown in Fig. 5.28. It is evident from the figure that, a maximum of 2% error found during GRNN validation. Also, the proposed methodology is in good agreement with the GRNN predicted and experimentally measured performance and emission parameters. The graphical representation of the percentage error during GRNN testing is depicted in Fig. 5.29. It is evident from the figure that, a maximum of 2% error found during GRNN network testing. The GRNN requires a less training data compared with other ANN models. The proposed GRNN approach can be used to predict/calibrate the performance and emission parameters of the HCCI engine within ±2 % accuracy.

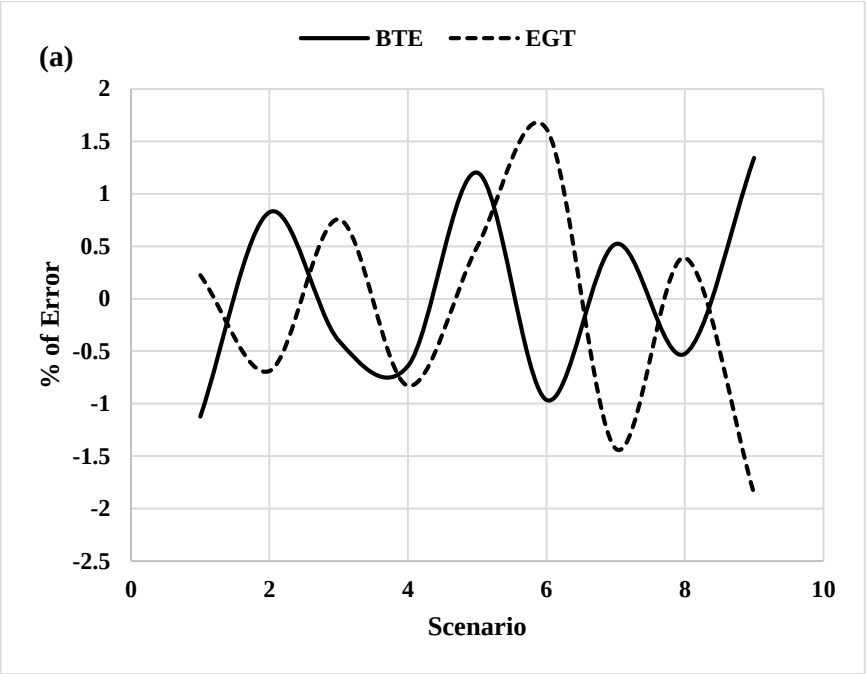

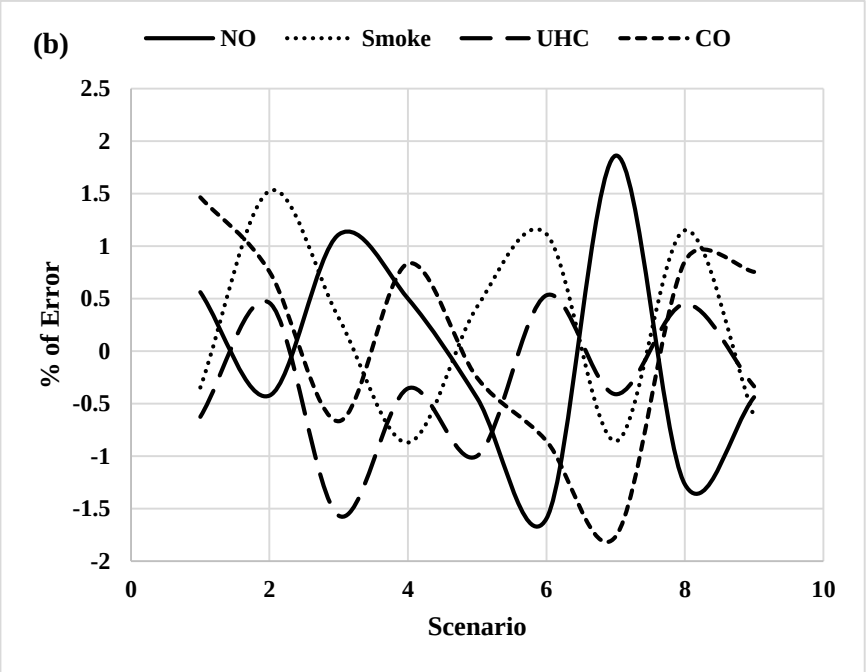

Fig. 5.28. Graphical representation of error percentage for validation data. (a) Performance parameters, (b) Emission parameters.

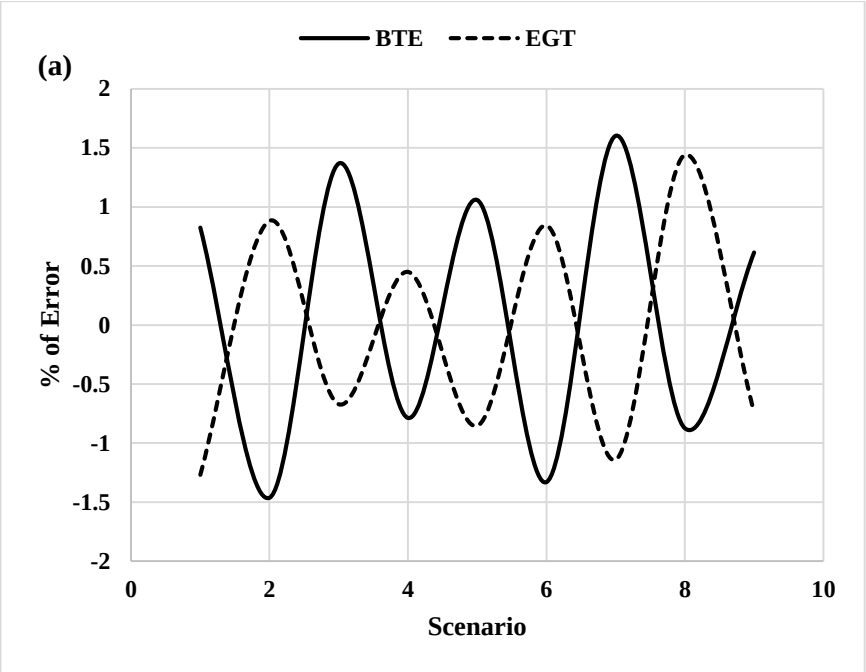

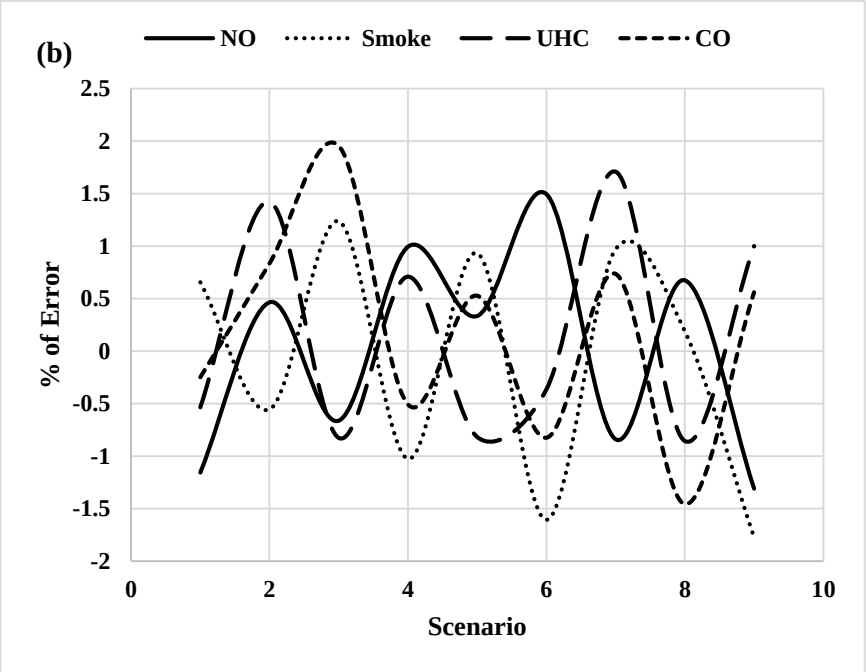

Fig. 5.29. Graphical representation of error percentage for test data. (a) Performance parameters, (b) Emission parameters.

5.5.4. Summary

The prediction of the ethanol-fueled HCCI engine output parameters for any combination of input parameters using GRNN was done. The existing experimental data sets from Table 5.4.1 is used for the network training, validation, and testing. Initially, the network is trained with the 60% of the experimental data sets. Further, the validation and testing of the network done with each 20% data sets. The developed GRNN tool could predict the performance parameters of BTE and EGT within ±2% error. Similarly, prediction of the emission parameters including NO, smoke, UHC and CO within ±2% error. The validation results predicted that, the output parameters those lie within 2% error. The results also showed that the GRNN models are advantageous for network simplicity and require less sparse data. The developed new tool efficiently predicts the relation between the input and output parameters. The new GRNN model can also be used for the HCCI engine control and testing.

5.6. Effect of charge temperature and EGR

5.6.1. General

This chapter presents the experimental results of the combustion, performance, and emission characteristics of ethanol-fueled HCCI engine at various engine loads by varying the intake air temperature and exhaust gas recirculation (EGR). Port fuel injection technique was used to inject the fuel into the intake manifold. The intake air was heated from 130 to 170 °C at a regular interval of 10 °C for achieving stable HCCI operation. Also, the EGR up to 7% was used to control the abnormal combustion. The present research engine is a natural aspirated engine. Further increase in the EGR results in a lower fresh intake charge that causes decrease in the brake power. The two main reasons for EGR up to 7% are fixed valve timing and lower volumetric efficiency. The load on the engine were represented by the percentage of the rated load on the engine.

5.6.2. Determination of optimum EGR

The utilization of EGR is to control the abnormal combustion at high operating load conditions. This abnormal combustion is due to sudden pressure rise rate caused by high heat release rate (HRR). Therefore, the HRR needs to be controlled for the smooth operation of the engine [267]. The smooth combustion has advantages of great engine life and less noise operation. In this regard, EGR is a useful tool, cheaply available next to the engine and reduces nitric oxide emissions [36,268,269]. But adopting high levels of EGR has an adverse effect on engine performance as it increases the UHC emissions. The amount of EGR dilution limits the maximum power density of HCCI engines. Hence, an optimum EGR was circulated for better performance and emissions. Fig. 5.30 portrays the effect of intake air temperature and EGR dilution on the NO and UHC emissions. The NO emission increases with the intake air temperature, probably due to the early start of combustion whereas the UHC emission decreases due to oxidation at a high temperature. As the EGR increases, the NO emission suppresses, while the UHC emissions increase due to the dilution effect [255]. There was a significant drop in the NO emission with 7% EGR compared to that of 0% EGR operation, but the increase in the UHC emissions showed a misfire existence. Hence, an optimum of 5% EGR was used for achieving the low NO emissions, and smooth running of the ethanol-fueled HCCI engine.

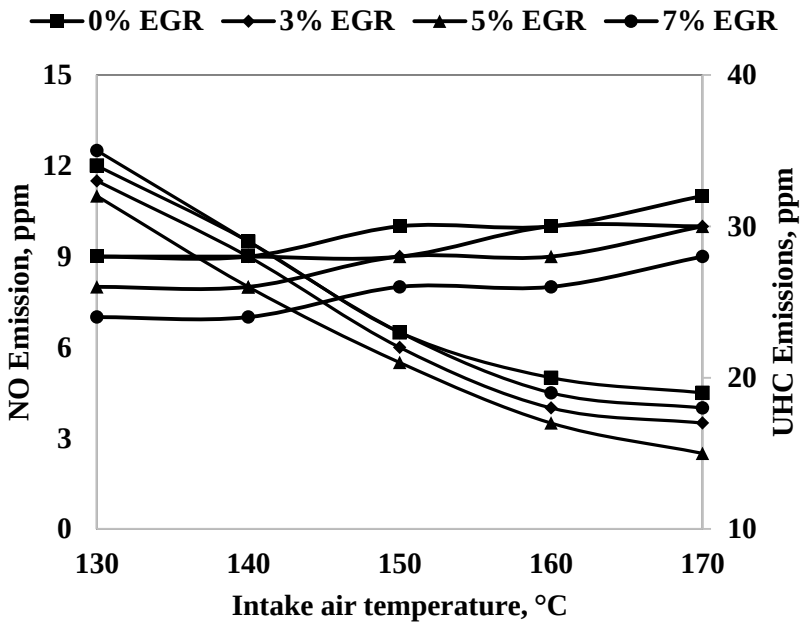

Fig. 5.30. Effect of intake air temperature and EGR dilution on NO and UHC emissions.

5.6.3. Combustion parameters

5.6.3.1. Cylinder pressure

The pressure crank angle diagram at full load for ethanol HCCI engine with charge heating and EGR is depicted in Fig. 5.31. It can be observed that the increase in the charge temperature causes advancing the start of combustion (SOC) as expected. The advanced SOC and increased peak pressure are observed with the temperature increment. This is due to the high reaction rates with an increase in the charge temperature. For high charge temperatures, the fuel/air mixture reaches the auto-ignition temperature in early crank angles. The cylinder pressure data is high for 170 °C charge temperature at full load. The peak cylinder pressure is found to be 81 bar for 170 °C charge temperature.

5.6.3.2. Heat release rate

Chemical kinetics mainly governs the HCCI combustion. In this study, the heat release rate of the ethanol fueled HCCI engine was controlled with the use of EGR. The addition of EGR is advantageous in controlling the combustion phase. Fig. 5.32 portrays the heat release rate with respect to the crank angle at full load. It is apparent from the figure that, the heat release rate is the highest for 170 °C charge temperature and lowest for 130 °C charge temperature at full load. The maximum heat release rate for 170 °C charge temperature is recorded as 48.8 J/CAD at full load.

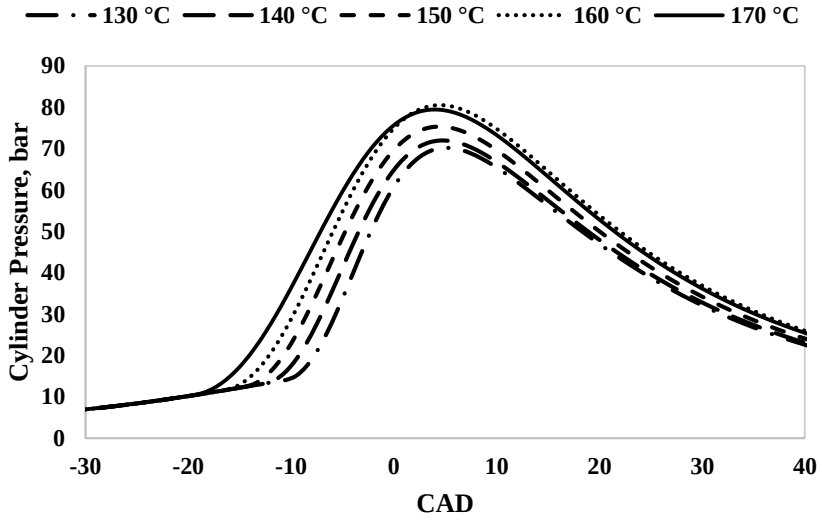

Fig. 5.31. Variation of cylinder pressure with crank angle.

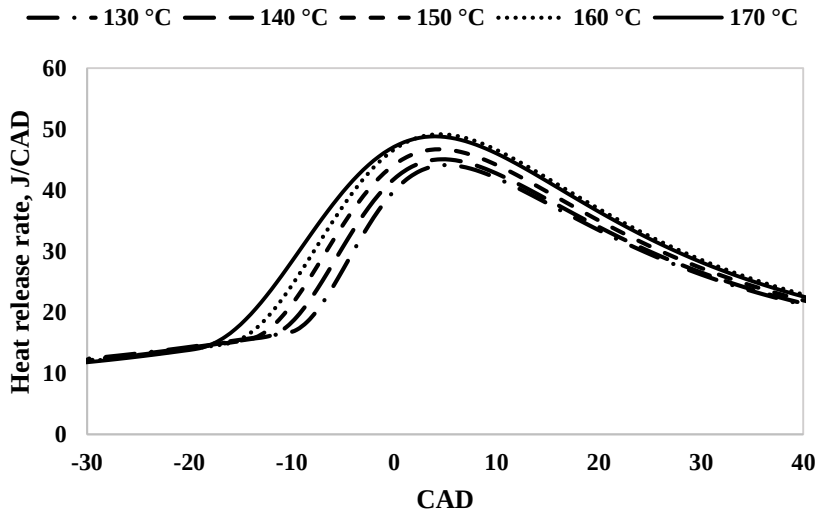

Fig. 5.32. Variation of heat release rate with crank angle.

5.6.3.3. Combustion duration

Fig. 5.33 depicts the variation of the combustion duration with engine load for ethanol fueled HCCI engine. It can be observed from the figure that, the combustion duration increases with the increase in the engine load for all the charge temperatures due to an increase in the equivalence ratio with load increment. Also, the decrease in the combustion duration is observed with the increase in the charge temperature. At 20% load, the shorter combustion duration of 14 CAD is observed for 170 °C charge temperature.

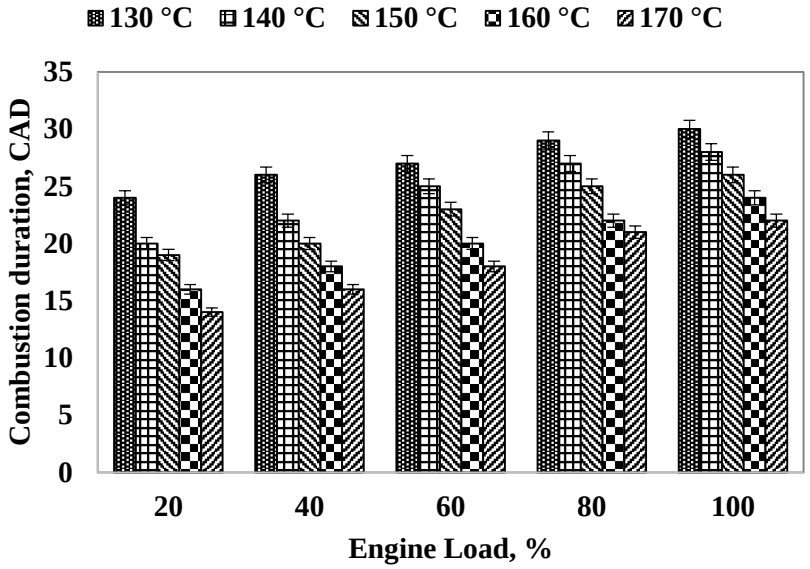

Fig. 5.33. Variation of combustion duration with load.

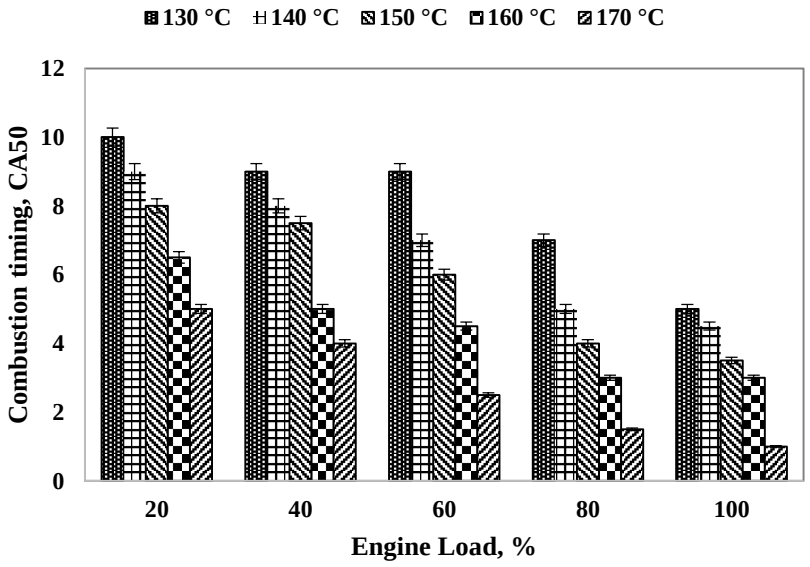

Fig. 5.34. Variation of combustion timing with load.

5.6.3.4. Combustion timing (CA50)

The crank angle/position at which 50% of the total heat release occurs is termed as combustion timing (CA50). Fig. 5.34 shows the variation of the combustion timing (CA50) with engine load for ethanol fueled HCCI engine. It is evident from the figure that, the CA50 decreases with the increase in the engine load due to increase in the equivalence ratio with load. As the charge temperature increases, the CA50 decreases due to the early SOC. At full load, the CA50 is 1° after TDC for 170 °C charge temperature.

5.6.4. Performance parameters

5.6.4.1. Thermal efficiency

Fig. 5.35 shows the variation of BTE with engine load for the ethanol fueled HCCI operation. The BTE increases with the charge temperature due to the advanced start of combustion (SOC) due to high charge temperature. For PFI applications, the advanced SOC leads to an overall increase in the peak in-cylinder gas temperature. A similar trend for an increase in the BTE is also observed with the engine load. At 170 °C charge temperature, a maximum of 45% BTE was found for the ethanol HCCI operation. The BTE increases with the increase in the charge temperature and engine load probably due to the higher combustion efficiency [270].

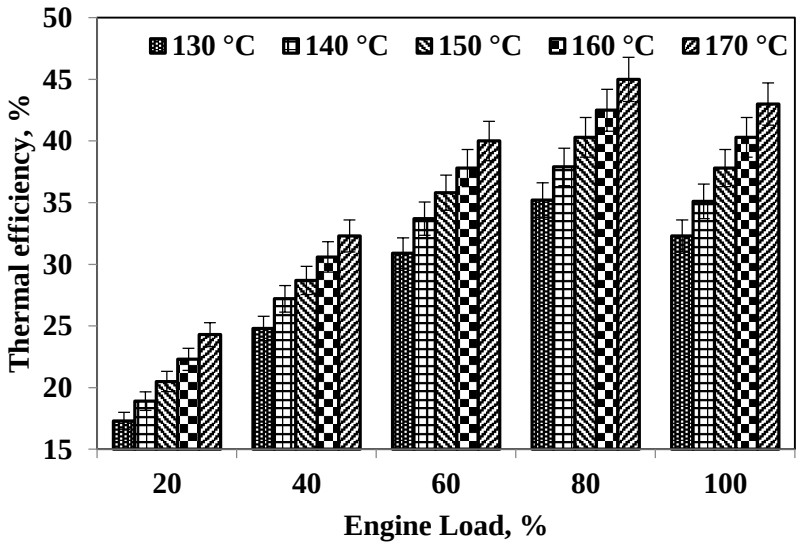

Fig. 5.35. Variation of thermal efficiency with load.

5.6.4.2. Exhaust gas temperature

Fig. 5.36 depicts the trend of EGT with engine load for the ethanol fueled HCCI operation. It can be observed from the figure that the EGT increases with the entire load spectrum. At 130 °C charge temperature, a maximum of 318 °C EGT is noticed. However, the decrease in EGT was observed with an increase in the charge temperature is noticed. A similar trend of decrease in EGT with charge temperature is also observed by Saxena et al. [20]. As the charge temperature increases then the SOC also advances due to the increase in the chemical kinetics and rate of reactions during combustion. Also, the heat transfer

losses from the cylinder also increase for the advanced SOC due to an increase in the residence time of burned hot gasses.

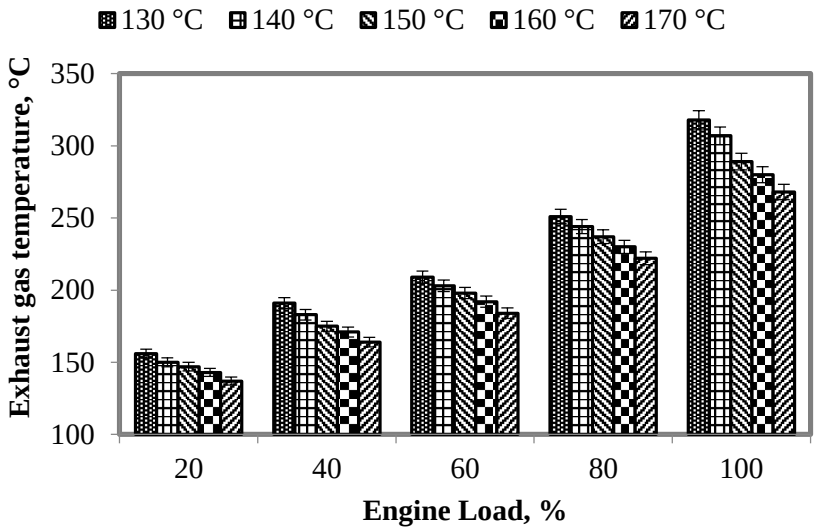

Fig. 5.36. Variation of exhaust gas temperature with load.

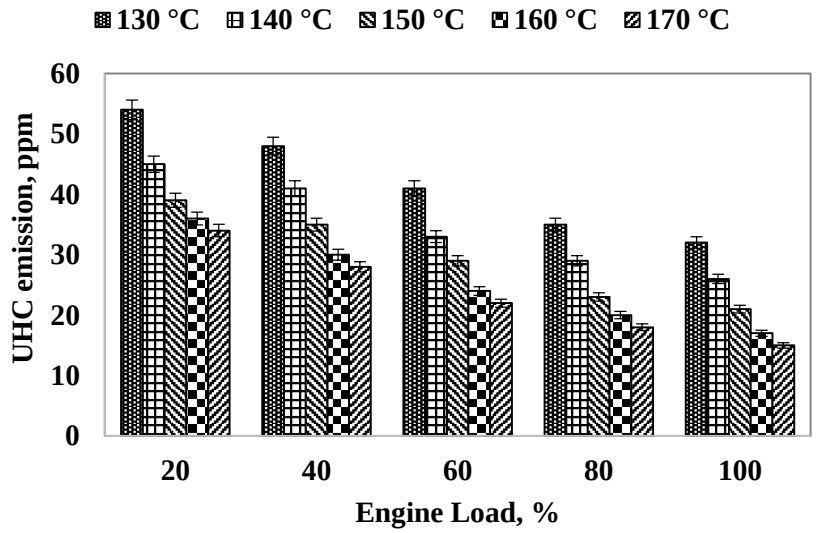

Fig. 5.37. Variation of unburned hydrocarbon emission with load.

5.6.5. Emission parameters

5.6.5.1. UHC emission

Fig. 5.37 depicts the variation of UHC emission with engine load for the ethanol fueled HCCI operation.The UHC emission is the indication of the rate of unburned fuel. As the load increases, the equivalence ratio of the air/fuel mixture also increases which causes a

decrease in the UHC emissions. A maximum UHC emission of 54 ppm is found for 130 °C charge temperature and 20% engine load operation. At 170 °C charge temperature, the lowest UHC emission of 15 ppm is observed during full load operation. The decrease of UHC emission in the range from 37% to 53% is observed from 20% load to full load operation in this study.

5.6.5.2. CO emission

Fig. 5.38 shows the variation of CO emission with engine load for the ethanol fueled HCCI operation.The CO emission indicates the rate of incomplete combustion [271–274]. As the engine load increases, the peak in-cylinder gas temperature also increases that causes a reduction in the CO emission. As the charge temperature increases, the decrease in the CO emission was observed due to the advanced SOC with an increase in the charge temperature. The maximum CO emission of 0.08% is exhibited for 130 °C charge temperature and 20% load operating condition. Similarly, the lowest CO emission of 0.01% is found at full load and 170 °C charge temperature. The decrease of CO emission in the range from 56% to 71% is noticed from 20% load to full load operation in this study.

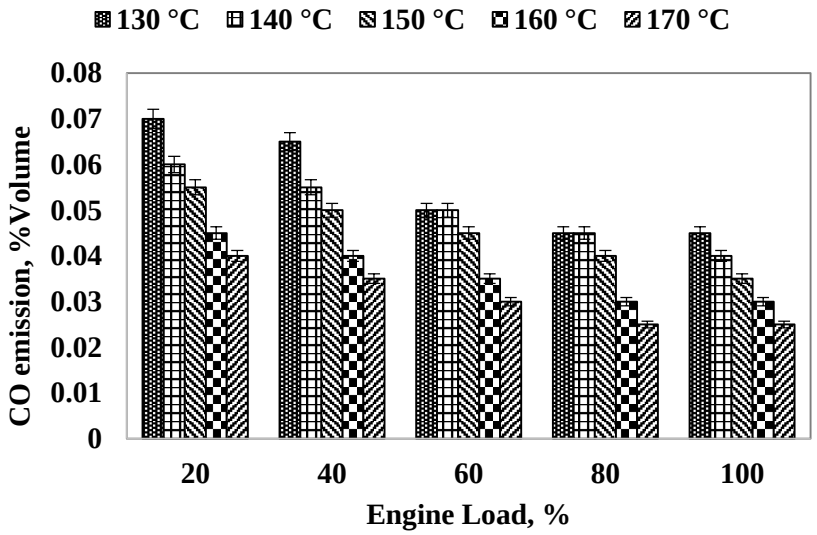

Fig. 5.38. Variation of carbon monoxide emission with load.

5.6.5.3. NO emission

The nitric oxide emissions are produced during the process of combustion only in the presence of nitrogen and oxygen at 1800K [275]. The predominant factors affecting the NO emission are (i) in-cylinder pressure and (ii) oxygen availability [8,276]. Fig. 5.39

shows the variation of NO emission with engine load for the ethanol fueled HCCI operation. The lowest NO emission is found to be 3 ppm at 20% load and 130 °C charge temperature. Whereas, the highest NO emission of 10 ppm is observed for 170 °C charge temperature at full load condition. The increase in the engine load also causes an increase in the NO emission. This may be probably due to increase in the peak in-cylinder temperature. The early SOC also causes the increase in the burned gases residence time might also increase in the NO emission.

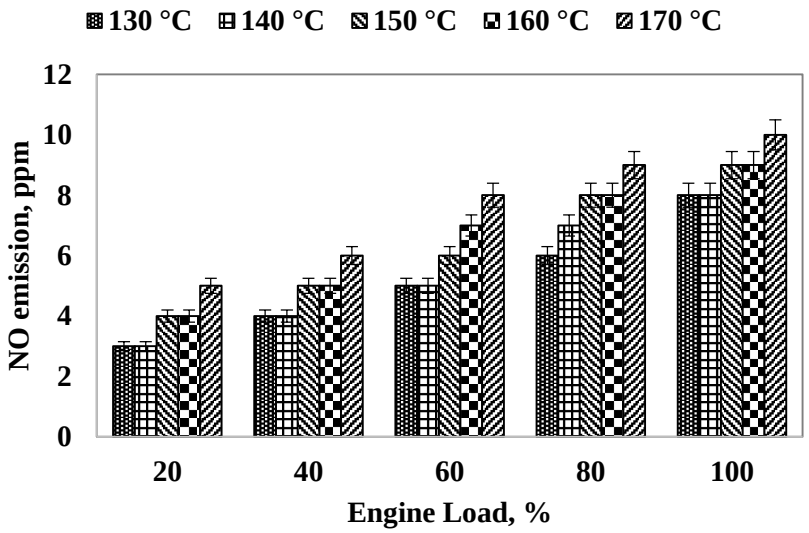

Fig. 5.39. Variation of nitric oxide emission with load.

5.6.5.4. Smoke opacity

Fig. 5.40 portrays the variations of smoke opacity with the engine load for the ethanol fueled HCCI operation. The formation of smoke occurs at extreme air/oxygen deficiency [277]. But, in the port injected HCCI engines, the utilization of the lean homogeneous air/fuel mixture causes negligible smoke due to the oxygen availability. As the charge temperature increases, the decrease in the smoke opacity is observed in the entire load spectrum. It can also be observed from the figure that, the smoke emissions are almost negligible for the ethanol HCCI operation at full load. The increase in the mixture homogeneity of port injected ethanol fuel might be the reason for lower smoke opacity. At 170 °C, the lowest smoke opacity of 0.1% is observed at full load condition due to the increase in oxidation temperature. The decrease of smoke emission in the range from 67% to 70% is observed from 20% load to full load operation. The smoke opacity is below 0.6% throughout this investigation.

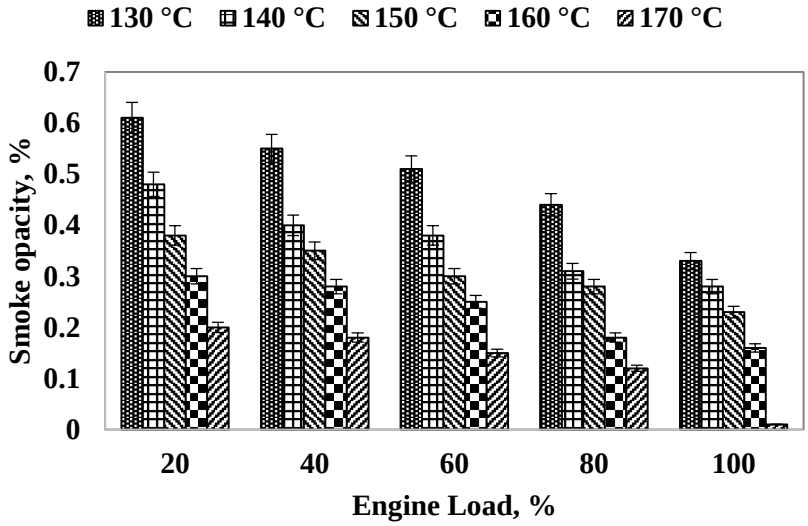

Fig. 5.40. Variation of smoke opacity with load.

5.6.6. Summary

In this investigation, the charge heating and EGR strategy was applied to characterize the ethanol-fueled HCCI engine combustion, performance and emission parameters. The inlet air temperature was increased from 130 to 170 °C at a step of 10 °C, and port fuel injection of ethanol was used for the homogeneous charge preparation. Since the homogeneous mixture was prepared outside the engine cylinder, wall wetting and mixing did not arise. An optimum EGR of 5% was used throughout this investigation. From the results of the investigation, the following conclusions were drawn.

- As the charge temperature increased, the in-cylinder pressure also increased due to early SOC.
- The maximum brake thermal efficiency of 45% was found for 170 °C charge temperature at 80% engine load.
- The UHC emissions decreased with increase in the charge temperature. At 170 °C charge temperature, the lowest UHC emissions were found to be 15 ppm at full load.
- The CO emission decreased with increase in the charge temperature. At 170 °C charge temperature, the lowest CO emission were found to be 0.025 %V at full load.
- The NO emission was found to be below 10 ppm for the entire engine operation.
- The maximum smoke opacity was found to be 0.61% for 130 °C charge temperature at 20% engine load.

5.7. Hybrid optimization of the test engine using GRNN-PSO

5.7.1. General

The optimization of an ethanol-fueled HCCI engine is essential to run at its best operating condition. However, the optimization objective function is different from user to user. In this study, there were three main criteria for the HCCI engine optimization was considered. They are (a) performance optimization, (b) emission optimization, and (c) both performance and emission optimization. Hence, the objective function must have flexibility for any user defined weights based on the choice of the optimizer.

5.7.2. Fitness function evaluation

The HCCI engine having multiple objective/fitness functions. Each output parameter of the engine is one objective that might either maximize or minimize function. However, all the output parameters considered were not having single objective of either maximization or minimization of the problem. Therefore, a single fitness function was developed in this chapter to satisfy all the criteria's. The developed fitness function must have high brake thermal efficiency (BTE) and low exhaust emissions. Therefore, the fitness function (F) was directly proportional to BTE and inversely proportional to the exhaust emissions (UHC, CO, NO, and smoke) and EGT.

$$\Rightarrow \mathrm{F} \propto \mathrm{BTE} \text{ and } \mathrm{F} \propto \left\{ \begin{matrix} {}^{1}/_{\mathrm{UHC}} \\ {}^{1}/_{\mathrm{CO}} \\ {}^{1}/_{\mathrm{smoke}} \\ {}^{1}/_{\mathrm{NO}} \\ {}^{1}/_{\mathrm{EGT}} \end{matrix} \right\} \tag{5.2}$$

$$\mathrm{F} = \frac{\mathrm{w_1} * \mathrm{BTE}}{\mathrm{w_2} * \mathrm{UHC} + \mathrm{w_3} * \mathrm{CO} + \mathrm{w_4} * \mathrm{smoke} + \mathrm{w_5} * \mathrm{NO} + \mathrm{w_6} * \mathrm{EGT}} \tag{5.3}$$

Where w_1, w_2, w_3, w_4, w_5 and w_6 are the weighing parameters corresponds to the BTE, EGT, NO, smoke, CO and UHC respectively.

However, the increase in the BTE led to an increase in the NO emission. On the other hand, the decrease in the BTE led to the increase in the UHC, CO, and smoke emissions. Therefore, it is required to optimize the BTE, while maintaining the lower exhaust

emissions. Therefore, the weights (w_1 to w_6) are to be decided based on the emission legislations. The present study deals with specific four cases as follows.

Case 1: Equal priority to all the engine output parameters.

$w_1 = w_2 = w_3 = w_4 = w_5 = w_6 = 1/6$ (5.4)

Case 2: Full priority to exhaust emissions.

$w_1 = 0, w_2 = 0, w_3 = w_4 = w_5 = w_6 = 0.25$ (5.5)

Case 3: Full priority to performance.

$w_1 = 0.7, w_2 = 0.3, w_3 = w_4 = w_5 = w_6 = 0$ (5.6)

Case 4: High priority to BTE, NO and smoke. Low priority to EGT, UHC and CO.

$w_1 = 0.3, w_3 = w_4 = 0.2, w_2 = w_5 = w_6 = 0.1$ (5.7)

Note: The detailed explanation for the above four cases are addressed in the section 5.7.4.

5.7.3. GRNN trainee using cross validation

In this study, Matlab R2015b was used to carry out the simulation by HP desktop with Intel Core i7-3770 3.4 GHz CPU and 8 GB RAM. First, GRNN model was trained to complete the prediction simulation, in which "newgrnn()" was applied by Matlab to construct a GRNN without training error. The optimal smoothing parameter σ was chosen from the experimental trainee datasets with a minimum cross-validation error.

The smoothing parameter σ was the only adaptive parameter in the Eq. 4.42 of the GRNN model. High σ values lead to the data over smoothening, while low σ values lead to the data over-fitting. Hence, optimum σ needs to be chosen for effective prediction of the GRNN model. The optimal σ was found from grid search method in this investigation. The σ values [σ_{low}, σ_{high}] were defined in a range with 'N' number of iterations. Thus, the cross-validation was implemented with the obtained 'N' values of Kernel width was performed using Eq. 5.8.

$$\sigma = \sigma_{low} + (i-1)\frac{\sigma_{high}-\sigma_{low}}{N} \qquad i = 1,2,\ldots..,M \tag{5.8}$$

The optimal σ was chosen based on the lowest cross-validation error of the model. The total number of iterations and the interval both needs to be constrained for the minimum error (i.e., the effective search interval was much smaller). In this study, the initial search interval for the optimal σ value was considered as [1; 10], and search iterations was equal

to 10. Fig. 5.41 shows the influence of smoothening parameter on GRNN model.The curve has well-defined minima, with an optimal σ at 4.42.

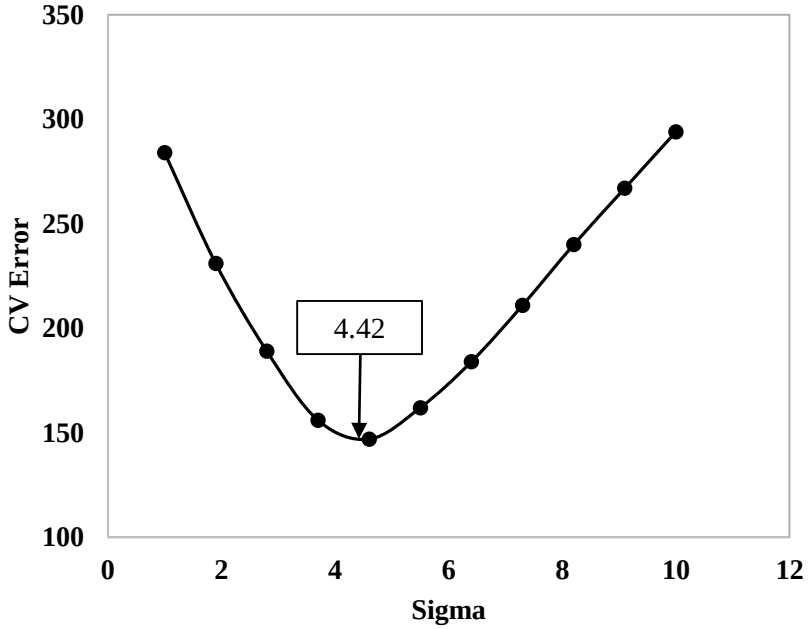

Fig. 5.41. Cross-validation curve for GRNN model. Optimal σ = 4.42.

5.7.4. Hybrid GRNN-PSO optimization

The objective of the proposed PSO-GRNN algorithm in this study was to find the optimum operating conditions of HCCI engine based on its best performance while minimizing hazardous air pollution. The optimization procedure was initialized with the solutions generated by random and searches for global optima by updating the generations. The developed model had a high flexibility such that the output weights of the model were user defined. The optimization can be performed for any user defined values based on their priority of the output criterion. The termination accuracy of the iteration process is 10^{-6}. In this paper, four different cases were studied to optimize the HCCI engine based on its performance and emission parameters.

5.7.4.1. Equal priority to all the engine output parameters

The optimization was initially performed by considering all the engine output parameters which were equally given priority. This case is the preliminary investigation of any engine study that can be carried out by keeping equal priority to all the outputs. Fig. 5.42 shows the best fitness of the generated swarm on the iteration process for equal priority to the engine output parameters. It can be observed from the figure that the optimal solution is

found at 127th iteration with the fitness value of 0.1867. The maximum fitness value obtained by the 127th particle having values in three dimensions of [170 °C, 62%, 6%].

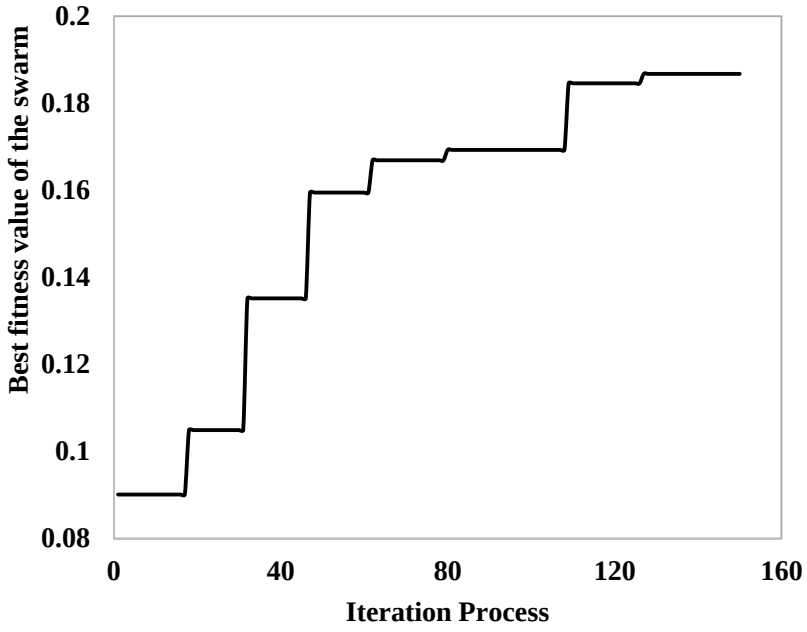

Fig. 5.42. The global best fitness value in every iteration for case 1.

5.7.4.2. Full priority to exhaust emissions

The increase in the emission legislations with an increase in the automobile air pollution demands that the priority was mainly given to the exhaust emissions. The emissions considered in this study were NO, smoke, UHC, and CO. These emissions are the primary cause of atmospheric pollution. The nitric oxide emissions in the engine exhaust cause acid rains, ground-level ozone, and peroxyacetyl nitride (PAN) formation in the photochemical smog. Hence, the NO emission levels must be low as possible.The human health problems caused by smoke (particulate matter) emissions are respiratory morbidity, deficiencies in pulmonary, and lung cancer. The environmental effects like accelerated metal corrosion, and damage to paints, sculptures, etc. with smoke emissions in the atmosphere. Hence, these emissions were minimized to its greater extent as possible. The emissions of CO and UHC indicate low combustion efficiency of the fuel. This can be achieved by avoiding misfire, wall wetting, and peak cylinder temperature above 1400 K for oxidation of the fuel. Therefore, CO and UHC emissions are also minimized for an efficient HCCI operation.

This case describes the engine with maximum weights to the emission rates and minimum weight to the thermal efficiency. Therefore, it is suggested that the researchers and engine manufacturers should not choose this criterion with a full priority to the exhaust emissions. From the fitness function, it is evident that this criterion obtained a fitness value of "0" due to the reason of neglecting thermal efficiency parameter.

5.7.4.3. Full priority to performance

The performance of the engine is vital to be considered due to the involvement of its running cost. The low-performance vehicle not only consumes more fuel but also causes huge air pollution compared to high-performance vehicle. The effectiveness of the engine is measured with BTE (ratio of power output to fuel input energy). Hence, high BTE is desired for an efficient HCCI engine operation. The amount of heat energy going as waste without converting into engine power/work is measured with exhaust gas temperature. Thus, lower EGT is desired. Fig. 5.43 shows the best fitness of the generated swarm on the iteration process for full priority to the performance parameters. It can be observed from the figure that the optimal solution is found at 147th iteration with the fitness value of 0.4821. The maximum fitness value obtained by the 147th particle having values in three dimensions of [170 °C, 76%, 5%].

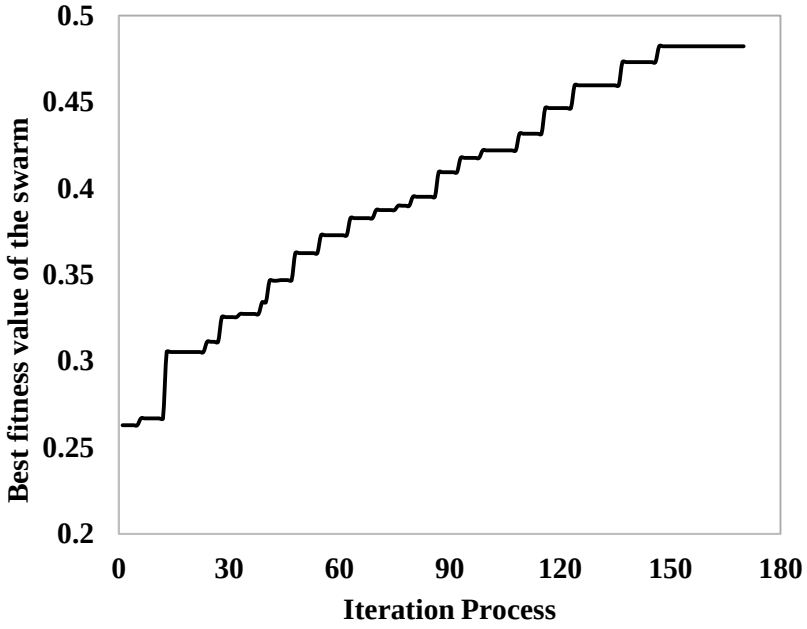

Fig. 5.43. The global best fitness value in every iteration for case 3.

5.7.4.4. High priority to BTE, NO and smoke. Low priority to EGT, UHC and CO.

It is understood that, the full priority cannot be given to either performance and emission parameters. Hence, the highly influencing parameters will be given high priority corresponding to the HCCI engine performance and emissions. The increase in the performance of IC engine is measured with its BTE and hence it is given a high priority. The emissions of NO and smoke emissions having greater influence as they cause acid rain and public health issues respectively. Fig. 5.44 depicts the best fitness of the generated swarm on the iteration process for general criteria. It can be observed from the figure that, the optimal solution is found at 129th iteration with the fitness value of 0.5348. The maximum fitness value obtained by the 129th particle having values in three dimensions of [170 °C, 72%, 4%].

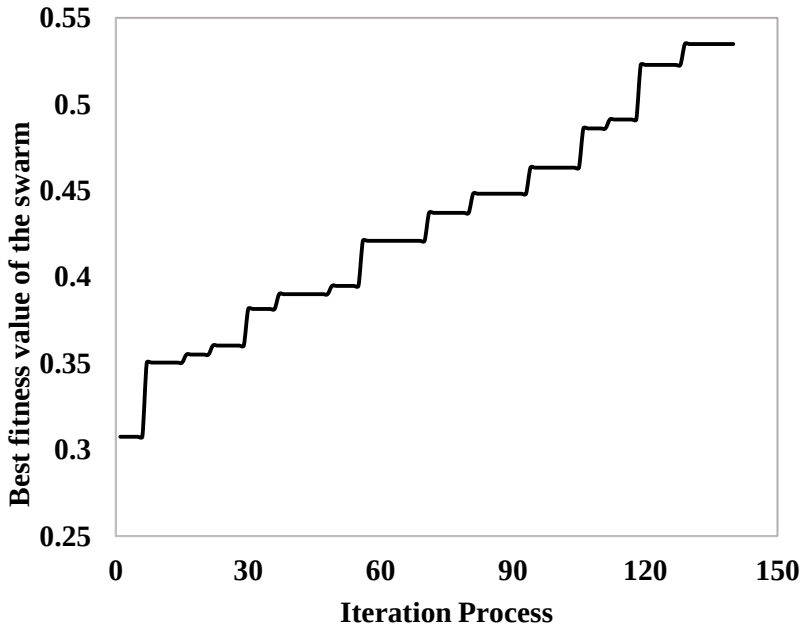

Fig. 5.44. The global best fitness value in every iteration for case 4.

All the above four cases considered are mutually diverse in nature, and the algorithm is flexible for any user-defined weights. The weights of this algorithm are chosen by the user based on the individual nations' regulations and legislations. Table 5.9 compares the results obtained with the hybrid GRNN-PSO for the four cases considered in section 5.6.4. Among all the four cases, the most general criteria is case 4 commonly chosen by engine manufacturers with little modification in the weights. This algorithm consumed very less

time to converge its optimum fitness value, and hence it can be used for rapid engine prototyping.

Table 5.9 Analysis of results obtained by hybrid GRNN-PSO.

Case	Iteration No.	Best output swarm						Time taken (s)
		BTE (%)	EGT (°C)	NO (ppm)	Smoke (%)	UHC (ppm)	CO (%V)	
1	127	40	184	8	0.15	22	0.025	0.063
3	147	45	222	9	0.12	18	0.02	0.073
4	129	42.3	200	8	0.13	21	0.023	0.064

5.7.5. Summary

In this study, a hybrid GRNN-PSO model was developed to optimize the ethanol-fueled HCCI engine based on the output performance and emission parameters. The model fits the complicated nonlinear relationship among the input and output parameters of the HCCI engine. A total of 45 steady state experimental data sets were considered for training the GRNN, and "newgrnn()" was applied in MATLAB to train the network without any error. The GRNN network interpretive of the probability estimate such that it can predict the performance and emission parameters of HCCI engine within the range of input parameters. Since GRNN cannot optimize the solution, and hence swarm based adaptive mechanism was hybridized. A new fitness function was developed by considering the six engine output parameters. For the developed fitness function, constrained optimization criteria were implemented in four cases. The optimum HCCI engine operating conditions for the general criteria were found to be 170 °C charge temperature, 72% engine load, and 4% EGR. This model consumed about 60-75 ms for HCCI engine optimization. The main advantage of the developed fitness function is that a user can define the weights as per the emission norms and fuel economy standards.

5.8. Effect of charge temperature and fuel vaporizer

5.8.1. General

This chapter presents the experimental results of the combustion, performance, and emission characteristics of ethanol-fueled HCCI engine at various engine loads by varying the intake air temperature using external fuel vaporizer. The custom intake manifold consists of fuel vaporizer, in which the fuel was injected with port fuel injection technique. The intake air was heated from 100 to 140 °C at a regular interval of 10 °C for achieving stable HCCI operation. The load on the engine were represented by the percentage of the rated load on the engine.

5.8.2. Combustion parameters

5.8.2.1. Cylinder pressure

The analysis of in-cylinder pressure data is important to analyse the combustion behaviour as it influences the power and emissions [82]. Fig. 5.45 depicts the pressure crank angle diagram at full load for ethanol HCCI engine with charge heating using vaporizer. It is observed that the start of combustion (SOC) shifted towards top dead centre due to early SOC during compression stroke. The increase in the charge temperature causes the probability of molecular collisions increases. Therefore, the reaction rates accelerate for higher charge temperatures causing early SOC. The presence of higher temperature favorsearly auto-ignition of the homogenous charge. The peak cylinder pressure is found to be 79 bar for 140 °C charge temperature.

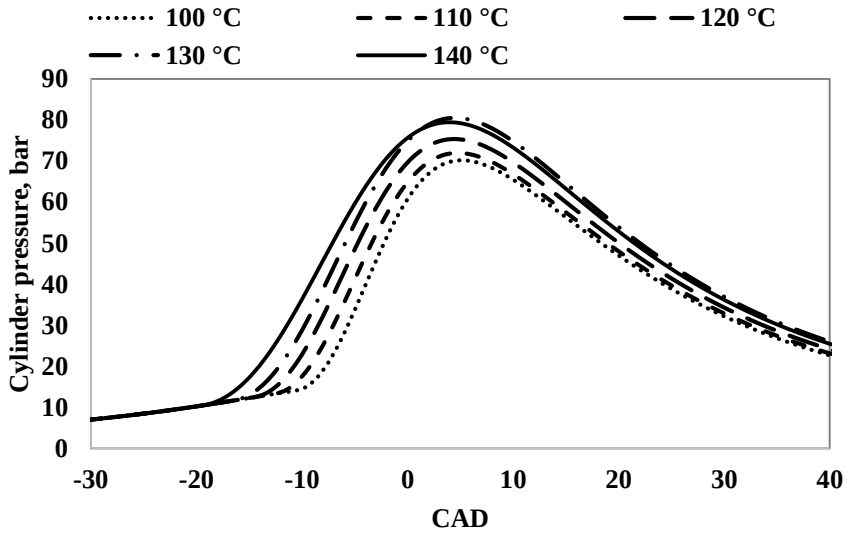

Fig. 5.45. Variation of cylinder pressure with crank angle.

5.8.2.2. Heat release rate

The heat release rate is calculated from the acquired in-cylinder pressure data. Fig. 5.46 portrays the heat release rate with respect to the crank angle at full load. The highest heat release rate was observed for 140 °C charge temperature and lowest for 100 °C charge temperature at full load. The maximum heat release rate for 140 °C charge temperature is recorded as 46.4 J/CAD at full load.

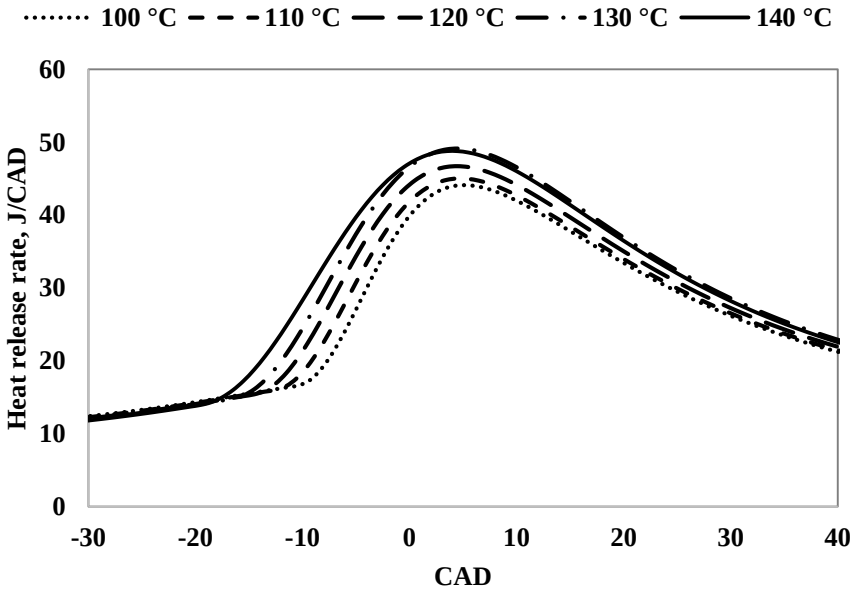

Fig. 5.46. Variation of heat release rate with crank angle.

5.8.2.3. Combustion duration

Fig. 5.47 shows the variation of the combustion duration with engine load for ethanol fueled HCCI engine.It can be observed from the figure that the combustion duration increases with the increase in the engine load for all the charge temperatures due to an increase in the equivalence ratio with load increment. Also, the decrease in the combustion duration is observed with the increase in the charge temperature. At 20% load, the shorter combustion duration of 13 CAD is observed for 140 °C charge temperature. At full load, the maximum combustion duration of 27 CAD is observed for 100 °C charge temperature.

5.8.2.4. Combustion timing (CA50)

Combustion timing (CA50) refers to the crank angle at which 50% of the cumulative heat was released. Fig. 5.48 shows the variation of the combustion timing with engine load for ethanol fueled HCCI engine.Fig. 5.46 shows the variation of the combustion timing (CA50) with engine load for ethanol fueled HCCI engine. As the charge temperature

increases, the CA50 is closer to before TDC due to the early SOC. It is evident from the figure that the CA50 decreases with the increase in the engine load due to increase in the equivalence ratio with load. At full load, the CA50 is 3° after TDC for 140 °C charge temperature.

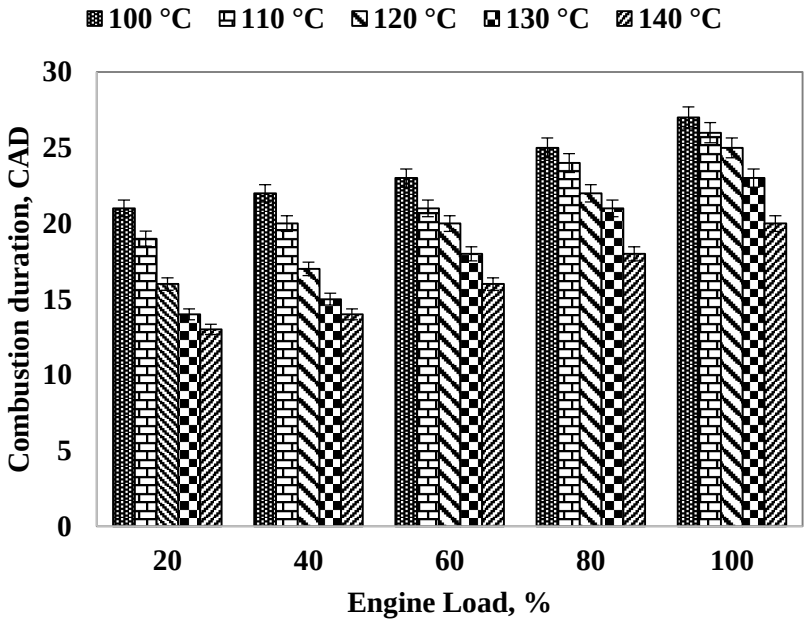

Fig. 5.47. Variation of combustion duration with load.

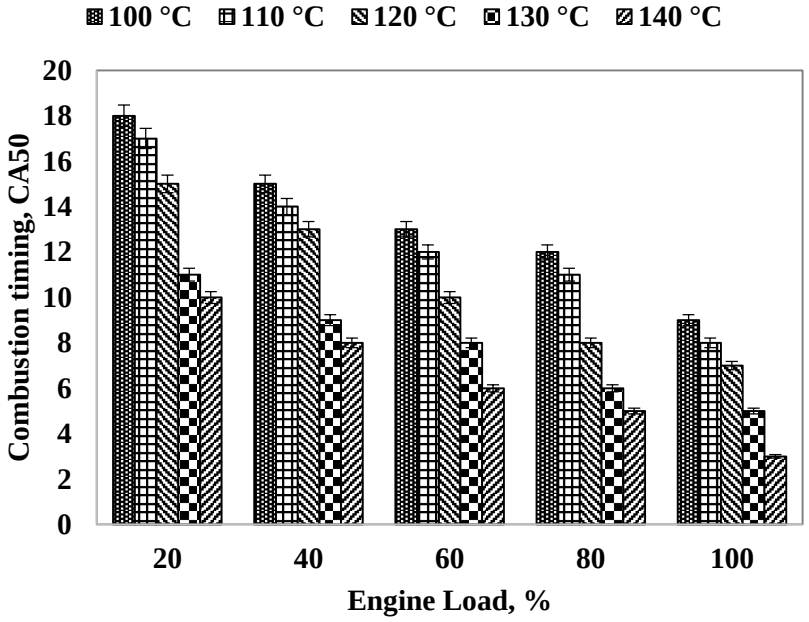

Fig. 5.48. Variation of combustion timing with load.

5.8.3. Performance parameters

5.8.3.1. Brake thermal efficiency

Fig. 5.49 shows the variation of BTE with engine load for the ethanol fueled HCCI operation. The BTE increases with the charge temperature due to the advanced start of combustion (SOC) at high charge temperature. The advanced SOC leads to an overall increase in the peak in-cylinder gas temperature. A similar trend for an increase in the BTE is also observed with the engine load. At 140 °C charge temperature, a maximum of 46% BTE was found for the ethanol HCCI operation.

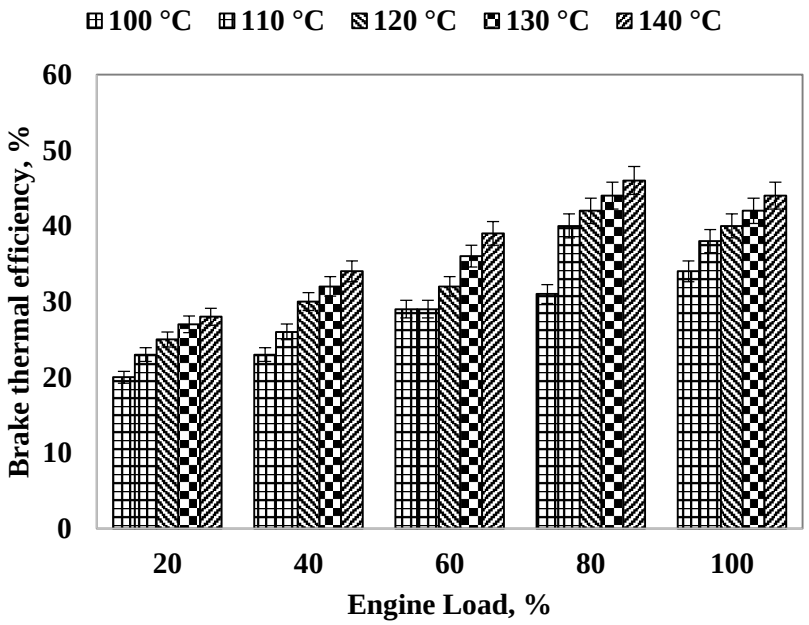

Fig. 5.49. Variation of thermal efficiency with load.

5.8.3.2. Exhaust gas temperature

Fig. 5.50 depicts the trend of EGT with engine load for the ethanol fueled HCCI operation. It can be observed from the figure that the EGT increases with the entire load spectrum. At 100 °C charge temperature, a maximum of 326 °C EGT is noticed at full load. However, the decrease in EGT was observed with an increase in the charge temperature is noticed. As the charge temperature increases then the SOC also advances due to the increase in the chemical kinetics and rate of reactions during combustion. Also, the heat transfer losses from the cylinder also increase for the advanced SOC due to an increase in the residence time of burned hot gasses.

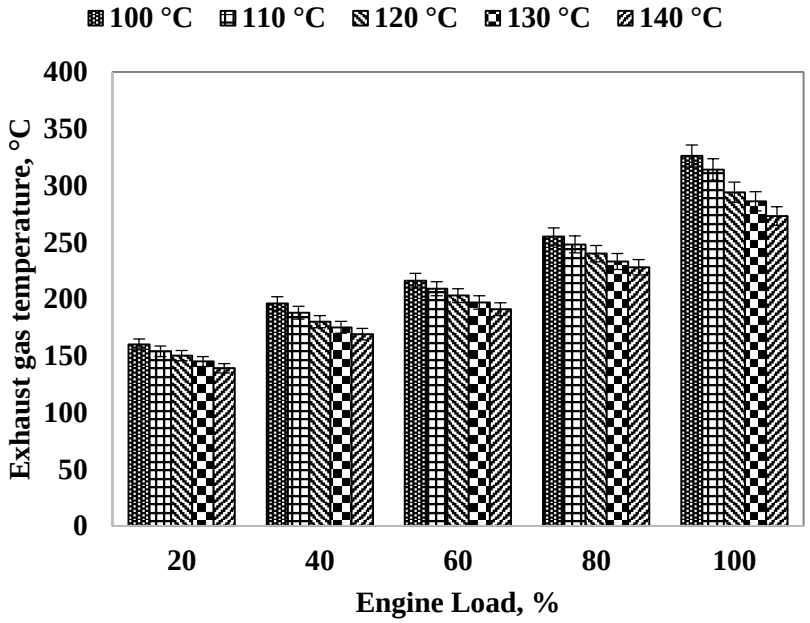

Fig. 5.50. Variation of exhaust gas temperature with load.

5.8.4. Emission parameters

5.8.4.1. UHC emission

Fig. 5.51 depicts thevariation of UHCemission with engine load for the ethanol fueledHCCI operation.The UHC emission is the indication of the rate of unburned fuel. As the load increases, the equivalence ratio of the air/fuel mixture also increases which causes a decrease in the UHC emissions. A maximum UHC emission of 44 ppmis found for 100 °C charge temperature and 20%engine load operation. At 140 °C charge temperature, the lowest UHC emission of 15 ppmis observed during fullload operation. The decrease of UHC emission in the range from 32% to 52% is observed from 20% load to full load operation in this study.

5.8.4.2. CO emission

Fig.5.52 shows thevariation of CO emissionwith engine load for the ethanol fueledHCCI operation.The CO emission indicates the rate of incomplete combustion [271–274]. As the engine loadincreases, the peak in-cylinder gas temperature also increases that causes a reduction in the CO emission. As the charge temperature increases, the decreasein the CO emissionwas observed due to the advanced SOC with an increase in the charge temperature. The maximum CO emission of 0.07% is exhibitedfor 100 °C charge temperature and 20% load operating condition. Similarly, the lowest CO emission of

0.025% is found at full loadand 140 °Ccharge temperature. The decrease of CO emission in the range from 36% to 38% is noticed from20% load to full load operation in this study.

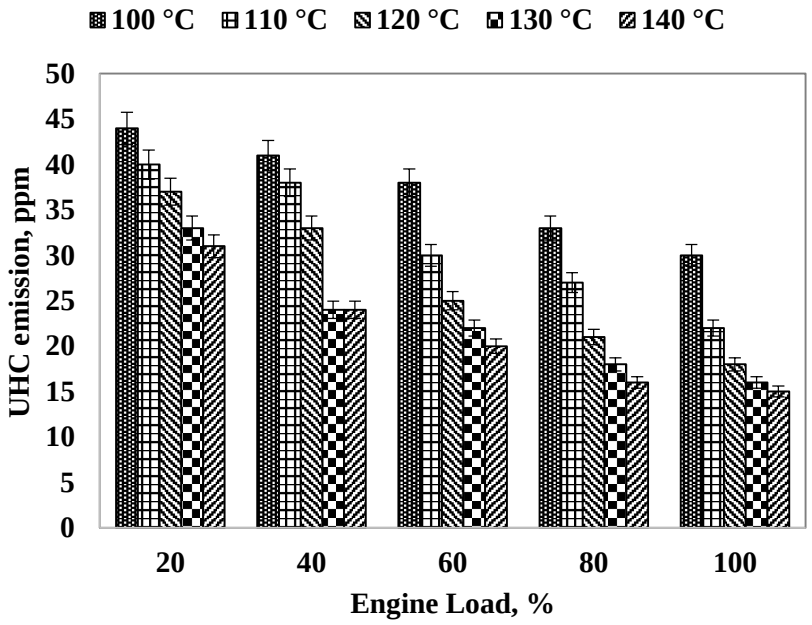

Fig. 5.51. Variation of unburned hydrocarbon emission with load.

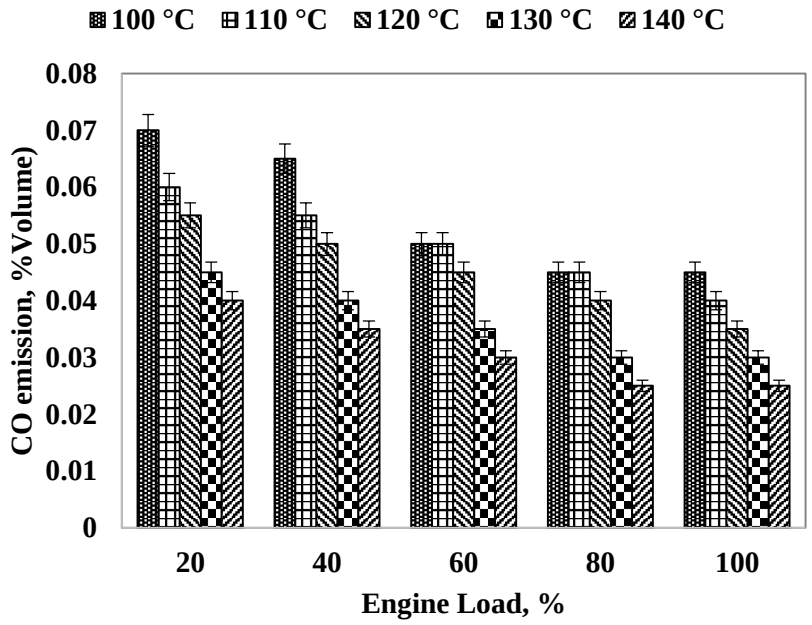

Fig. 5.52. Variation of carbon monoxide emission with load.

5.8.4.3. NO emission

Fig.5.53 shows the variation of NO emission with engine load for the ethanol fueledHCCI operation. The NO emission increases with increase in the engine load. This may be

probably due to increase in the peak in-cylinder temperature. Also, the NO emission increases with increase in the charge temperature due to early SOC that causes the increase in the burned gasesresidence time might also increase in the NOemission. The highest NO emission of 5 ppm is observed for 140 °Ccharge temperature at full load condition.

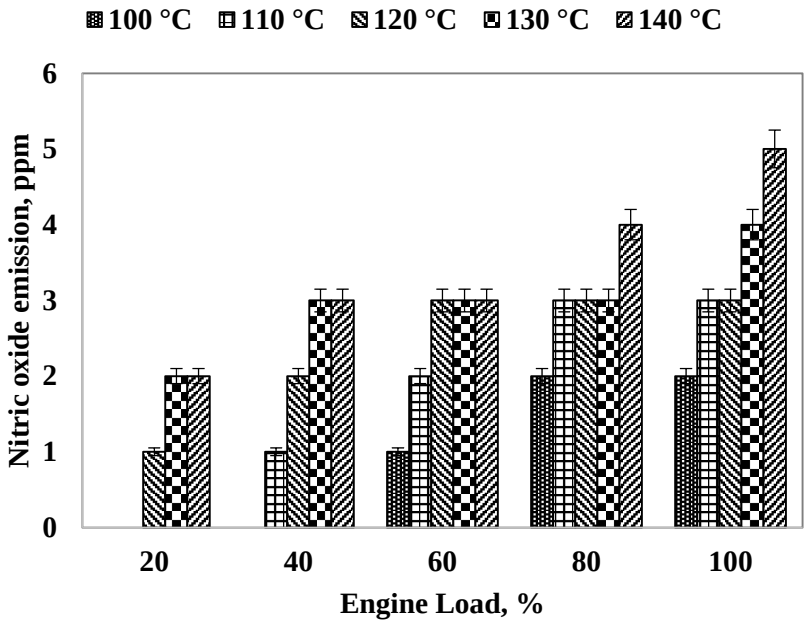

Fig. 5.53. Variation of nitric oxide emission with load.

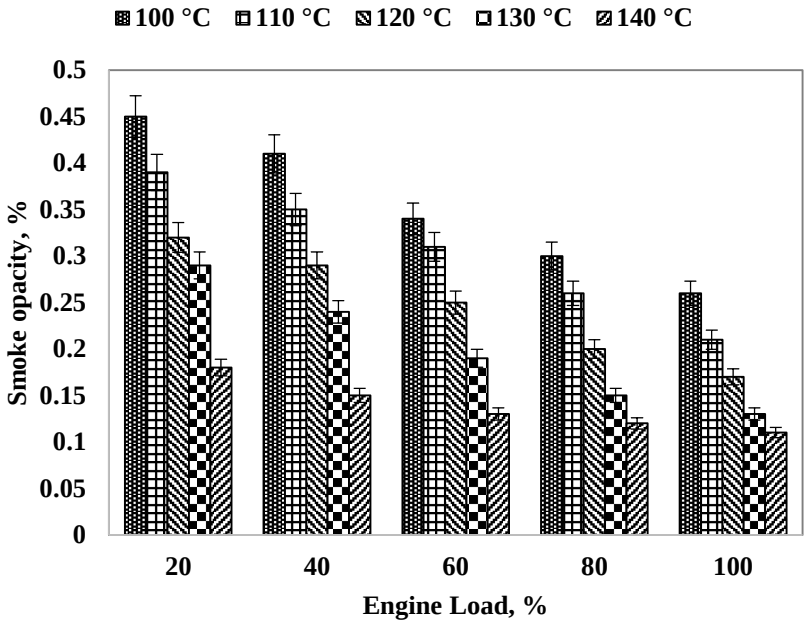

Fig. 5.54. Variation of Smoke opacity with load.

5.8.4.4. Smoke opacity

Fig.5.54 portrays thevariation of smoke opacitywith engine load for the ethanol fueledHCCI operation. The utilization of the lean homogeneous air/fuel mixture causes negligible smoke due to the oxygen availability. As the charge temperature increases, the decrease in the smoke opacity is observed in the entire load spectrum. It can be observed from the figure that, the smoke opacity is almost negligiblefor theethanol HCCI operation at full load. The increase in the mixture homogeneity of vaporized ethanol fuel might be the reason for lower smoke opacity. At 140 °C, the lowest smoke opacity of 0.11% is observed at full load condition due to the increase in oxidation temperature. The decrease of smoke emission in the range from 42% to 39% is observedfrom 20% load to full loadoperation. Thesmoke opacity is below 0.5% throughout this investigation.

Table 5.10 Comparision of HCCI performance and emissions of manifold injection and fuel vaporizer at full load.

Parameter value at 170 °C	**Manifold injection**	**Fuel vaporizer**
Brake thermal efficiency (%)	41	44
Exhaust gas temperature (°C)	273	273
Hydrocarbon emission (ppm)	18	15
Carbon monoxide emission (%)	0.025	0.025
Nitric oxide emission (ppm)	11	5
Smoke opacity (%)	0.1	0.11

The results obtained with manifold injection and fuel vaporizer are compared in Table 5.10 at full load condition. From the comparision, the utilization of fuel vaporizer is advantageous as it offers better brake thermal efficiency and low nitric oxide emission.

5.8.5. Summary

In this investigation, the fuel vaporizeris used to prepare fuel vapour and inducted into the intake manifold during suction stroke. The vaporized ethanol fuel mixed with air and forms homogeneous charge. The inlet air temperature was increased from 100 to 140 °C at a step of 10 °C to characterize the ethanol-fueled HCCI engine combustion, performance and emission parameters.The preparation of the homogeneous mixture outside the engine cylinder eliminates the problems of wall wetting, and under mixing. From the results of the investigation, the following conclusions were drawn.

- The increase in the charge temperature causes increased in-cylinder pressure due to early SOC.
- The maximum brake thermal efficiency of 46% was found for 140 °C charge temperature at 80% engine load.

- The UHC emissions decreased with the increase in the charge temperature. At 140 °C charge temperature, the lowest UHC emissions were found to be 15 ppm at full load.

- The CO emission decreased with the increase in the charge temperature. At 140 °C charge temperature, the lowest CO emission were found to be 0.025 %V at full load.

- The NO emission was found to be below 5 ppm for the entire engine operation.

- The maximum smoke opacity was found to be 0.45% for 100 °C charge temperature at 20% engine load.

Chapter 6

Conclusion and scope for further work

6.1. Conclusion

From the theoritical and experimental analysis of the combustion, performance and emission parameters of the ethanol fueled HCCI engine by adopting different techniques, the following conclusions are drawn;

6.1.1. Thermodynamic analysis of ethanol fueled HCCI engine

- The obtained numerical results show that the indicated thermal efficiency increases with the engine load, and advances the SOC with the increase in the intake air temperature.
- The CO emission decreases with the engine load while NO_x emission increases with the engine load.
- The NO_x emissions were found to be below 14 ppm during the entire engine operation.
- The intake air temperature requirements for successful operation of ethanol fueled HCCI engine was found. The minimum intake air temperature required to auto-ignite the air-fuel mixture was found to be 130 °C. Whereas, at 170 °C knocking limits the maximum intake air requirement for the existing engine configuration.
- This modelling is expected to provide the valuable guidelines for the researchers and designers regarding the performance evaluation as well as the development of the HCCI engines.

6.1.2. Effect of charge temperature

- Increasing the intake air temperature advanced the combustion phase and decreased the exhaust gas temperature.
- The increase in the intake air temperature increased the in-cylinder pressure and ethanol is more sensitive to the intake air temperature.
- The operating regime of HCCI was limited. The higher load was limited by combustion noise and the lower load was limited by the CO emissions.

- Maximum combustion efficiency and thermal efficiency for the ethanol HCCI operation was found 98.2% and 43% respectively for intake temperature of 170 °C.

- The UHC and CO emissions were found to be higher for the ethanol HCCI operation than that of diesel DI operation due to low temperature combustion.

- The NO emission was found to be 11 ppm for ethanol HCCI which was about 97% lower compared to diesel DI operation.

- The smoke opacity for the ethanol HCCI operation was found to be below 0.1% which is negligible compared to that of diesel DI operation.

6.1.3. Multi-Criteria Decision Making – TOPSIS Method

- The optimal HCCI operating condition was found at 70% load and 170 °C charge temperature.

- The ANOVA test results reveal that the charge temperature is the most significant parameter followed by the engine load.

- The percentage contribution of charge temperature and load are 63.04% and 27.89% respectively.

6.1.4. Prediction of HCCI engine output parameters using GRNN

- The GRNN network was trained with the 60% of the experimental data sets. Further, the validation and testing of the network done with each 20% data sets.

- The developed GRNN tool could predict the performance parameters of BTE and EGT within ±2% error.

- Similarly, prediction of the emission parameters including NO, smoke, UHC and CO within ±2% error.

- The validation results predicted that the output parameters those lie within 2% error. The results also showed that the GRNN models are advantageous for network simplicity and require less sparse data.

- The developed new tool efficiently predicts the relation between the input and output parameters.

6.1.5. Effect of charge temperature and EGR

- An optimum of 5% EGR was found to be optimum for controlling the HCCI engine.
- As the charge temperature increased, the in-cylinder pressure also increased due to early SOC.
- The maximum brake thermal efficiency of 45% was found for 170 °C charge temperature at 80% engine load.
- The UHC emissions decreased with the increase in the charge temperature. At 170 °C charge temperature, the lowest UHC emissions were found to be 15 ppm at full load.
- The CO emission decreased with the increase in the charge temperature. At 170 °C charge temperature, the lowest CO emission were found to be 0.025 %V at full load.
- The NO emission was found to be below 10 ppm for the entire engine operation.
- The maximum smoke opacity was found to be 0.61% for 130 °C charge temperature at 20% engine load.

6.1.6. Hybrid optimization of the test engine using GRNN-PSO

- This model fits the complicated nonlinear relationship among the input and output parameters of the HCCI engine.
- A new fitness function was developed by considering the six engine output parameters. For the developed fitness function, constrained optimization criteria were implemented in four cases.
- The optimum HCCI engine operating conditions for the general criteria were found to be 170 °C charge temperature, 72% engine load, and 4% EGR.
- This model consumed about 60–75 ms for HCCI engine optimization.

6.1.7. Effect of charge temperature and fuel vaporizer

- The maximum brake thermal efficiency of 46% was found for 170 °C charge temperature at 80% engine load.
- The NO emission and smoke emission were found to be below 5 ppm and 0.45% respectively.

Overall it is concluded that, the HCCI combustion of sole ethanol fuel is possible with the charge heating only. The high load limit of HCCI can be extended with ethanol fuel. High thermal efficiency and low emissions were possible with ethanol fueled HCCI to meet the current demand.

6.2. Scope for further work

- Supercharged and turbocharged HCCI research required to extend the operating regime to higher and lower loads.
- Similar investigations on HCCI need to be explored on other alcohols.
- The ethanol fueled HCCI need to be tested in automotive engines and in gensets.
- Kinetic and computational studies need to be conducted for better understanding.
- Experimental investigations are required for variable speed engine and gensets.

References

[1] International Energy Agency. Energy and Air Pollution. 2016. doi:10.1021/ac00256a010.

[2] BP Energy Outlook - 2016 edition. 2016.

[3] IPCC 2014. Climate Change 2014: Synthesis Report. Contribution of Working Groups I, II and III to the Fifth Assessment Report of the Intergovernmental Panel on Climate Change. IPCC, Geneva, Switzerland: 2014.

[4] Wu HW, Wang RH, Ou DJ, Chen YC, Chen TY. Reduction of smoke and nitrogen oxides of a partial HCCI engine using premixed gasoline and ethanol with air. Appl Energy 2011;88:3882–90. doi:10.1016/j.apenergy.2011.03.027.

[5] Vehicular Pollution - water, effects, environmental, pollutants, impact, EPA, chemicals, toxic, human, power, sources, use, life, health, oil 2016. http://www.pollutionissues.com/Ve-Z/Vehicular-Pollution.html (accessed August 29, 2016).

[6] Dieselnet. EU Emission Standards for Passenger Cars n.d. https://www.dieselnet.com/standards/eu/ld.php (accessed July 6, 2016).

[7] U.S. Environmental Protection Agency. Nitrogen Oxides (NOx), Why and How They Are Controlled. Research Triangle Park, North Carolina 27711: 1999.

[8] Sharma A, Sivalingam M. Impact of Fuel Injection Pressure on Performance and Emission Characteristics of a Diesel Engine Fueled with Jatropha Methyl Ester Tyre Pyrolysis Blend. SAE Tech Pap 2014;2014–Octob. doi:10.4271/2014-01-2650.

[9] Prakash R, Singh RK, Murugan S. Use of biodiesel and bio-oil emulsions as an alternative fuel for direct injection diesel engine. Waste and Biomass Valorization 2013;4:475–84. doi:10.1007/s12649-012-9182-y.

[10] Agarwal AK. Biofuels (alcohols and biodiesel) applications as fuels for internal combustion engines. Prog Energy Combust Sci 2007;33:233–71. doi:10.1016/j.pecs.2006.08.003.

[11] P Richards. Automotive Fuels Reference Book, Third Edition. SAE International; 2014.

[12] World fuel ethanol production. Renew Fuels Assoc n.d. http://www.ethanolrfa.org/resources/industry/statistics/#1454099081080-c193f577-ec5e (accessed July 2, 2016).

[13] Yamada H, Suzaki K, Sakanashi H, Choi N, Tezaki A. Kinetic measurements in homogeneous charge compression of dimethyl ether: role of intermediate formaldehyde controlling chain branching in the low-temperature oxidation mechanism. Combust Flame 2005;140:24–33. doi:10.1016/j.combustflame.2004.09.009.

[14] Flowers D, Aceves S, Westbrook CK, Smith JR, Dibble R. Detailed Chemical Kinetic Simulation of Natural Gas HCCI Combustion: Gas Composition Effects and Investigation of Control Strategies. J Eng Gas Turbines Power 2001;123:433. doi:10.1115/1.1364521.

[15] Zhang CH, Pan JR, Tong JJ, Li J. Effects of intake temperature and excessive air coefficient on combustion characteristics and emissions of HCCI combustion. Procedia Environ Sci 2011;11:1119–27. doi:10.1016/j.proenv.2011.12.169.

[16] Amnéus P. Homogeneous Ignition - Chemical Kinetic Studies for IC-Engine Applications. ISSN 1102-8718 2002.

[17] ECOpoint Inc. DieselNet: Diesel Exhaust Emission Standards 2016. https://www.dieselnet.com//standards/ (accessed August 9, 2016).

[18] EPA U. Regulations & Standards: Transportation and Climate 2016. https://www3.epa.gov/otaq/climate/regulations.htm (accessed August 9, 2016).

[19] Bendu H, Murugan S. Homogeneous charge compression ignition (HCCI) combustion: Mixture preparation and control strategies in diesel engines. Renew Sustain Energy Rev 2014;38:732–46.

doi:10.1016/j.rser.2014.07.019.

[20] Saxena S, Schneider S, Aceves S, Dibble R. Wet ethanol in HCCI engines with exhaust heat recovery to improve the energy balance of ethanol fuels. Appl Energy 2012;98:448–57. doi:10.1016/j.apenergy.2012.04.007.

[21] Onishi S, Jo SH, Shoda K, Jo P Do, Kato S. Active Thermo-Atmosphere Combustion (ATAC) - A New Combustion Process for Internal Combustion Engines. SAE 790501, 1979. doi:10.4271/790501.

[22] Noguchi M, Tanaka Y, Tanaka T, Takeuchi Y. A Study on Gasoline Engine Combustion by Observation of Intermediate Reactive Products during Combustion. SAE 790840, 1979. doi:10.4271/790840.

[23] Christensen M, Hultqvist A, Johansson B. Demonstrating the Multi Fuel Capability of a Homogeneous Charge Compression Ignition Engine with Variable Compression Ratio. SAE Tech Pap 1999:SAE 1999-01-3679. doi:10.4271/1999-01-3679.

[24] Haraldsson G., Tunestål P., Johansson B., Hyvönen J. HCCI combustion phasing with closed-loop combustion control using variable compression ratio in a multi cylinder engine. SAE Tech Pap 2003. doi:10.4271/2003-01-1830.

[25] Hyvönen J, Haraldsson G, Johansson B. Operating range in a Multi Cylinder HCCI engine using Variable Compression Ratio. SAE Tech Pap 2003-01-1829 2003. doi:10.4271/2003-01-1829.

[26] Hyvönen J, Haraldsson G, Johansson B. Supercharging HCCI to Extend the Operating Range in a Multi-Cylinder VCR-HCCI Engine, 2003. doi:10.4271/2003-01-3214.

[27] Swami Nathan S, Mallikarjuna JM, Ramesh a. Effects of charge temperature and exhaust gas re-circulation on combustion and emission characteristics of an acetylene fuelled HCCI engine. Fuel 2010;89:515–21. doi:10.1016/j.fuel.2009.08.032.

[28] Liu H, Zheng Z, Yao M, Zhang P, Zheng Z, He B, et al. Influence of temperature and mixture stratification on HCCI combustion using chemiluminescence images and CFD analysis. Appl Therm Eng 2012;33:135–43. doi:10.1016/j.applthermaleng.2011.09.026.

[29] Canakci M. An experimental study for the effects of boost pressure on the performance and exhaust emissions of a DI-HCCI gasoline engine. Fuel 2008;87:1503–14. doi:10.1016/j.fuel.2007.08.002.

[30] Canakci M. Combustion characteristics of a DI-HCCI gasoline engine running at different boost pressures. Fuel 2012;96:546–55. doi:10.1016/j.fuel.2012.01.042.

[31] Olsson J-O, Tunestål P, Johansson B. Boosting for High Load HCCI. SAE Pap 2004-01-0940 2004. doi:10.4271/2004-01-0940.

[32] Wildman C, Scaringe RJ, Cheng W. On the Maximum Pressure Rise Rate in Boosted HCCI Operation. SAE Tech. Pap. 2009-01-2727, 2009. doi:10.4271/2009-01-2727.

[33] Bogin G, Chen JY, Dibble RW. The effects of intake pressure, fuel concentration, and bias voltage on the detection of ions in a Homogeneous Charge Compression Ignition (HCCI) engine. Proc Combust Inst 2009;32 II:2877–84. doi:10.1016/j.proci.2008.08.012.

[34] Martinez-Frias J, Aceves SM, Flowers D, Smith JR, Dibble R. Equivalence ratio-EGR control of HCCI engine operation and the potential for transition to spark-ignited operation. SAE World Congr 2001. doi:10.4271/2001-01-3613.

[35] Bhave A, Kraft M, Mauss F, Oakley A, Zhao H. Evaluating the EGR-AFR operating range of a HCCI engine. SAE Pap. 2005-01-0161, 2005. doi:10.4271/2005-01-0161.

[36] Shi L, Cui Y, Deng K, Peng H, Chen Y. Study of low emission homogeneous charge compression ignition (HCCI) engine using combined internal and external exhaust gas recirculation (EGR). Energy 2006;31:2329–40. doi:10.1016/j.energy.2005.12.005.

[37] Ravi N, Liao H-H, Jungkunz AF, Widd A, Gerdes JC. Model predictive control of HCCI using variable valve actuation and fuel injection. Control Eng Pract 2012;20:421–30. doi:10.1016/j.conengprac.2011.12.002.

[38] Mahrous A-FM, Potrzebowski A, Wyszynski ML, Xu HM, Tsolakis A, Luszcz P. A modelling study into the effects of variable valve timing on the gas exchange process and performance of a 4-valve DI homogeneous charge compression ignition (HCCI) engine. Energy Convers Manag 2009;50:393–8. doi:10.1016/j.enconman.2008.09.018.

[39] Shaver GM, Roelle MJ, Christian Gerdes J. Modeling cycle-to-cycle dynamics and mode transition in HCCI engines with variable valve actuation. Control Eng Pract 2006;14:213–22. doi:10.1016/j.conengprac.2005.04.009.

[40] Milovanovic N, Chen R. Influence of the Variable Valve Timing Strategy on the Control of a Homogeneous Charge Compression (HCCI) Engine. SAE Tech. Pap. 2004-01-1899, 2004. doi:10.4271/2004-01-1899.

[41] Martinez-Frias J, Aceves SM, Flowers DL. Improving Ethanol Life Cycle Energy Efficiency by Direct Utilization of Wet Ethanol in HCCI Engines. J Energy Resour Technol 2007;129:332. doi:10.1115/1.2794768.

[42] Canova M, Garcin R, Midlam-Mohler S, Guezennec Y, Rizzoni G. A control - oriented model of combustion process in a HCCI diesel engine. Proc. 2005, Am. Control Conf. 2005., IEEE; 2005, p. 4446–51. doi:10.1109/ACC.2005.1470696.

[43] Maurya RK, Agarwal AK. Experimental study of combustion and emission characteristics of ethanol fuelled port injected homogeneous charge compression ignition (HCCI) combustion engine. Appl Energy 2011;88:1169–80. doi:10.1016/j.apenergy.2010.09.015.

[44] Iida N. Combustion Analysis of Methanol-Fueled Active Thermo-Atmosphere Combustion (ATAC) Engine Using a Spectroscopic Observation. SAE Pap. 940684, 1994. doi:10.4271/940684.

[45] Dunn-Rankin D. Lean combustion : technology and control. Academic Press; 2008.

[46] Yao M, Zheng Z, Liu H. Progress and recent trends in homogeneous charge compression ignition (HCCI) engines. Prog Energy Combust Sci 2009;35:398–437. doi:10.1016/j.pecs.2009.05.001.

[47] Dec JE, Sjöberg M. Isolating the Effects of Fuel Chemistry on Combustion Phasing in an HCCI Engine and the Potential of Fuel Stratification for Ignition Control, 2004. doi:10.4271/2004-01-0557.

[48] Angelos JP, Puignou M, Andreae MM, Cheng WK, Green WH, Singer MA. Detailed chemical kinetic simulations of homogeneous charge compression ignition engine transients. Int J Engine Res 2008;9:149–64. doi:10.1243/14680874JER02207.

[49] Lü X, Hou Y, Zu L, Huang Z. Experimental study on the auto-ignition and combustion characteristics in the homogeneous charge compression ignition (HCCI) combustion operation with ethanol/n-heptane blend fuels by port injection. Fuel 2006;85:2622–31. doi:10.1016/j.fuel.2006.05.003.

[50] Sjöberg M, Dec JE. Comparing late-cycle autoignition stability for single- and two-stage ignition fuels in HCCI engines. Proc Combust Inst 2007;31:2895–902. doi:10.1016/j.proci.2006.08.010.

[51] Olsson J-O, Tunestål P, Johansson B. Closed-Loop Control of an HCCI Engine. SAE Pap 2001-01-1031 2001:1076–85. doi:10.4271/2001-01-1031.

[52] Olsson J-O, Tunestål P, Haraldsson G, Johansson B. A turbocharged dual-fuel HCCI engine. SAE Tech. Pap. 2001-01-1896, Society of Automotive Engineers; 2001.

[53] Heywood J. Internal Combustion Engine Fundamentals. McGraw-Hill Education; 1988.

[54] Kraft M, Maigaard P, Mauss F, Christensen M, Johansson B. Investigation of combustion emissions in a homogeneous charge compression injection engine: Measurements and a new computational model. Proc Combust Inst 2000;28:1195–201. doi:10.1016/S0082-0784(00)80330-6.

[55] Thring RH. Homogeneous-Charge Compression-Ignition (HCCI) Engines. SAE 892068, 1989. doi:10.4271/892068.

[56] Ishibashi Y, Asai M. Improving the Exhaust Emissions of Two-Stroke Engines by Applying the Activated Radical Combustion. SAE 960742, 1996. doi:10.4271/960742.

[57] Gatellier B, Walter B, Miche M. New diesel combustion process to achieve near zero NOx and particulates emissions. Proc. IFP Int. Congr., France: 2001.

[58] Kimura S, Aoki O, Ogawa H, Muranaka S, Enomoto Y. New Combustion Concept for Ultra-Clean and High-Efficiency Small DI Diesel Engines. SAE 1999-01-3681, 1999. doi:10.4271/1999-01-3681.

[59] Takeda Y, Keiichi N, Keiichi N. Emission Characteristics of Premixed Lean Diesel Combustion with Extremely Early Staged Fuel Injection. SAE Tech. Pap. 961163, 1996. doi:10.4271/961163.

[60] Hashizume T, Miyamoto T, Hisashi A, Tsujimura K. Combustion and Emission Characteristics of Multiple Stage Diesel Combustion. SAE 980505, 1998. doi:10.4271/980505.

[61] Yokota H, Kudo Y, Nakajima H, Kakegawa T, Suzuki T. A New Concept for Low Emission Diesel Combustion. SAE 970891, 1997. doi:10.4271/970891.

[62] Hasegawa R, Yanagihara H. HCCI Combustion in DI Diesel Engine. SAE 2003-01-0745, 2003. doi:10.4271/2003-01-0745.

[63] Iwabuchi Y, Kawai K, Shoji T, Takeda Y. Trial of New Concept Diesel Combustion System - Premixed Compression-Ignited Combustion. SAE 1999-01-0185, 1999. doi:10.4271/1999-01-0185.

[64] Aoyama T, Hattori Y, Mizuta J, Sato Y. An Experimental Study on Premixed-Charge Compression Ignition Gasoline Engine. SAE 960081, 1996. doi:10.4271/960081.

[65] Lakshmanan T, Nagarajan G. Experimental investigation of port injection of acetylene in DI diesel engine in dual fuel mode. Fuel 2011;90:2571–7. doi:10.1016/j.fuel.2011.03.039.

[66] Swami Nathan S, Mallikarjuna JM, Ramesh A. An experimental study of the biogas–diesel HCCI mode of engine operation. Energy Convers Manag 2010;51:1347–53. doi:10.1016/j.enconman.2009.09.008.

[67] Sudheesh K, Mallikarjuna JM. Diethyl ether as an ignition improver for biogas homogeneous charge compression ignition (HCCI) operation - An experimental investigation. Energy 2010;35:3614–22. doi:10.1016/j.energy.2010.04.052.

[68] Morsy MH. Ignition control of methane fueled homogeneous charge compression ignition engines using additives. Fuel 2007;86:533–40. doi:10.1016/j.fuel.2006.08.006.

[69] Ibrahim MM, Ramesh A. Experimental investigations on a hydrogen diesel homogeneous charge compression ignition engine with exhaust gas recirculation. Int J Hydrogen Energy 2013;38:10116–25. doi:10.1016/j.ijhydene.2013.05.092.

[70] Saravanan N, Nagarajan G, Dhanasekaran C, Kalaiselvan KM. Experimental investigation of hydrogen port fuel injection in DI diesel engine. Int J Hydrogen Energy 2007;32:4071–80. doi:10.1016/j.ijhydene.2007.03.036.

[71] Saravanan N, Nagarajan G. Performance and emission studies on port injection of hydrogen with varied flow rates with Diesel as an ignition source. Appl Energy 2010;87:2218–29. doi:10.1016/j.apenergy.2010.01.014.

[72] Kamil M, Rahman MM, Bakar RA. Performance evaluation of external mixture formation strategy in hydrogen fueled engine. J Mech Eng Sci 2011;1:2231–8380.

[73] Oguma H, Ichikura T, Iida N. A Study on Adaptability of Alternative Fuels for Lean-Burn Two-Stroke Atac Engine. SAE 972097, 1997.

[74] lida N. Alternative Fuels and Homogeneous Charge Compression Ignition Combustion Technology. SAE Pap. 978449, 1999.

[75] Esterlingot E, Guibert P, Lavy J, Raux S. Thermodynamical and optical analyses of controlled autoignition combustion in two-stroke engines. SAE Pap. 978473, 1997.

[76] Ishibashi Y, Asai M, Nishida K. An experimental study of stratified scavenging activated radical combustion engine. SAE Pap. 978454, 1997.

[77] Ishibashi Y, Sakuyama H. An Application Study of the Pneumatic Direct Injection Activated Radical Combustion Two-Stroke Engine to Scooter. SAE Tech. Pap. 2004-01-1870, 2004. doi:10.4271/2004-01-1870.

[78] Ishibashi Y, Asai M. A Low Pressure Pneumatic Direct Injection Two-Stroke Engine by Activated Radical Combustion Concept. SAE 980757, 1998. doi:10.4271/980757.

[79] Ishibashi Y. Basic Understanding of Activated Radical Combustion and Its Two-Stroke Engine Application and Benefits. SAE Tech. Pap. 2000-01-1836, 2000. doi:10.4271/2000-01-1836.

[80] Ganesh D, Nagarajan G, Mohamed Ibrahim M. Study of performance, combustion and emission characteristics of diesel homogeneous charge compression ignition (HCCI) combustion with external mixture formation. Fuel 2008;87:3497–503. doi:10.1016/j.fuel.2008.06.010.

[81] Ganesh D, Nagarajan G. Homogeneous charge compression ignition (HCCI) combustion of diesel fuel with external mixture formation. Energy 2010;35:148–57. doi:10.1016/j.energy.2009.09.005.

[82] Singh AP, Agarwal AK. Combustion characteristics of diesel HCCI engine: An experimental investigation using external mixture formation technique. Appl Energy 2012;99:116–25. doi:10.1016/j.apenergy.2012.03.060.

[83] Ganesh D, Nagarajan G. Homogeneous Charge Compression Ignition (HCCI) Combustion of Diesel Fuel with External Mixture Formation. SAE Tech. Pap. 2009-01-0924, 2009. doi:10.4271/2009-01-0924.

[84] S G, Ganesh PhD D, Nagarajan PhD G. Performance and Emission Analysis on Mixed-Mode Homogeneous Charge Compression Ignition (HCCI) Combustion of Biodiesel Fuel with External Mixture Formation. SAE Tech. Pap., 2012. doi:10.4271/2011-01-2450.

[85] Kim DS, Lee CS. Improved emission characteristics of HCCI engine by various premixed fuels and cooled EGR. Fuel 2006;85:695–704. doi:10.1016/j.fuel.2005.08.041.

[86] Liu H, Zhang P, Li Z, Luo J, Zheng Z, Yao M. Effects of temperature inhomogeneities on the HCCI combustion in an optical engine. Appl Therm Eng 2011;31:2549–55. doi:10.1016/j.applthermaleng.2011.04.020.

[87] Bahri B, Aziz AA, Shahbakhti M, Muhamad Said MF. Understanding and detecting misfire in an HCCI engine fuelled with ethanol. Appl Energy 2013;108:24–33. doi:10.1016/j.apenergy.2013.03.004.

[88] Lee CS, Lee KH, Kim DS. Experimental and numerical study on the combustion characteristics of partially premixed charge compression ignition engine with dual fuel☆. Fuel 2003;82:553–60. doi:10.1016/S0016-2361(02)00319-8.

[89] Soloiu V, Duggan M, Harp S, Vlcek B, Williams D. PFI (port fuel injection) of n-butanol and direct injection of biodiesel to attain LTC (low-temperature combustion) for low-emissions idling in a compression engine. Energy 2013;52:143–54. doi:10.1016/j.energy.2013.01.023.

[90] Padala S, Woo C, Kook S, Hawkes ER. Ethanol utilisation in a diesel engine using dual-fuelling technology. Fuel 2013;109:597–607. doi:10.1016/j.fuel.2013.03.049.

[91] Kelly-Zion PL, Dec JE. A computational study of the effect of fuel type on ignition time in homogenous charge compression ignition engines. Proc Combust Inst 2000;28:1187–94. doi:10.1016/S0082-0784(00)80329-X.

[92] Li T, Deng K, Peng H, Wu C. Effect of partial-heating of the intake port on the mixture preparation and combustion of the first cranking cycle during the cold-start stage of port fuel injection engine. Exp Therm Fluid Sci 2013;49:14–21. doi:10.1016/j.expthermflusci.2013.03.001.

[93] Panão MRO, Moreira ALN. Interpreting the influence of fuel spray impact on mixture preparation for HCCI combustion with port-fuel injection. Proc Combust Inst 2007;31:2205–13. doi:10.1016/j.proci.2006.07.050.

[94] Padala S, Le MK, Kook S, Hawkes ER. Imaging diagnostics of ethanol port fuel injection sprays for automobile engine applications. Appl Therm Eng 2013;52:24–37.

doi:10.1016/j.applthermaleng.2012.11.007.

[95] Brusstar M, Stuhldreher M, Swain D, Pidgeon W. High Efficiency and Low Emissions from a Port-Injected Engine with Neat Alcohol Fuels. Powertrain Fluid Syst Conf Exhib 2002;111. doi:10.4271/2002-01-2743.

[96] Megaritis a., Yap D, Wyszynski ML. Effect of inlet valve timing and water blending on bioethanol HCCI combustion using forced induction and residual gas trapping. Fuel 2008;87:732–9. doi:10.1016/j.fuel.2007.05.007.

[97] Fathi M, Saray RK, Checkel MD. The influence of Exhaust Gas Recirculation (EGR) on combustion and emissions of n-heptane/natural gas fueled Homogeneous Charge Compression Ignition (HCCI) engines. Appl Energy 2011;88:4719–24. doi:10.1016/j.apenergy.2011.06.017.

[98] Yao M, Chen Z, Zheng Z, Zhang B, Xing Y. Study on the controlling strategies of homogeneous charge compression ignition combustion with fuel of dimethyl ether and methanol. Fuel 2006;85:2046–56. doi:10.1016/j.fuel.2006.03.016.

[99] Saqaff A.Al-Kaf, Ahamad Suhaimi HAA. Radical combustion: new concept for two stroke engines. ASEAN J Sci Technol Dev 2000;17:91–9.

[100] Baumgarten C. Mixture Formation in Internal Combustion Engine. Springer Berlin Heidelberg; 2006. doi:10.1007/3-540-30836-9.

[101] Shimazaki N, Akagawa H, Tsujimura K. An Experimental Study of Premixed Lean Diesel Combustion, 1999. doi:10.4271/1999-01-0181.

[102] Miyamoto T, Hayashi A K, Harada A, Sasaki S, Akgarwa H TK. Numerical simulation of premixed lean diesel combustion in a DI engine. Fourth Int. Symp. COMODIA 98, Kyoto, Japan: 1998, p. 179–84.

[103] Nishijima Y, Asaumi Y, Aoyagi Y. Impingement Spray System with Direct Water Injection for Premixed Lean Diesel Combustion Control. SAE 2002-01-0109, 2002. doi:10.4271/2002-01-0109.

[104] Su W, Lin T, Pei Y. A Compound Technology for HCCI Combustion in a DI Diesel Engine Based on the Multi-Pulse Injection and the BUMP Combustion Chamber. SAE 2003-01-0741, 2003. doi:10.4271/2003-01-0741.

[105] Su W, Wang H, Liu B. Injection Mode Modulation for HCCI Diesel Combustion. SAE Tech. Pap., 2005. doi:10.4271/2005-01-0117.

[106] Kimura S, Aoki O, Kitahara Y, Aiyoshizawa E. Ultra-Clean Combustion Technology Combining a Low-Temperature and Premixed Combustion Concept for Meeting Future Emission Standards. SAE 2001-01-0200, 2001. doi:10.4271/2001-01-0200.

[107] Walter B, Gatellier B. Near Zero NO x Emissions and High Fuel Efficiency Diesel Engine: the NADI TM Concept Using Dual Mode Combustion. Oil Gas Sci Technol – Rev IFP 2003;58:101–14.

[108] Walter B, Gatellier B. Development of the High Power NADI™ Concept Using Dual Mode Diesel Combustion to Achieve Zero NOx and Particulate Emissions. SAE 2002-01-1744, 2002. doi:10.4271/2002-01-1744.

[109] Kawashima J, Ogawa H, Tsuru Y. Research on a Variable Swirl Intake Port for 4-Valve High-Speed DI Diesel Engines, 1998. doi:10.4271/982680.

[110] Kimura S, Ogawa H, Matsui Y, Enomoto Y. An experimental analysis of low-temperature and premixed combustion for simultaneous reduction of NOx and particulate emissions in direct injection diesel engines. Int J Engine Res 2002;3:249–59. doi:10.1243/146808702762230932.

[111] Kawamoto K, Araki T, Shinzawa M, Kimura S, Koide S, Shibuya M. Combination of Combustion Concept and Fuel Property for Ultra-Clean DI Diesel, 2004. doi:10.4271/2004-01-1868.

[112] Kimura S, Matsui Y, Itoh T. Effects of Combustion Chamber Insulation on the Heat Rejection and Thermal Efficiency of Diesel Engines. SAE Pap. 920543, 1992. doi:10.4271/920543.

[113] Kim MY, Lee CS. Effect of a narrow fuel spray angle and a dual injection configuration on the

improvement of exhaust emissions in a HCCI diesel engine. Fuel 2007;86:2871–80. doi:10.1016/j.fuel.2007.03.016.

[114] Fang T, Coverdill RE, Lee CF, White RA. Effects of injection angles on combustion processes using multiple injection strategies in an HSDI diesel engine. Fuel 2008;87:3232–9. doi:10.1016/j.fuel.2008.05.012.

[115] Reveille B, Kleemann A, Knop V, Habchi C. Potential of Narrow Angle Direct Injection Diesel Engines for Clean Combustion: 3D CFD Analysis. SAE Tech. Pap. 2006-01-1365, 2006. doi:10.4271/2006-01-1365.

[116] Stanglmaier RH, Roberts CE. Homogeneous Charge Compression Ignition (HCCI): Benefits, Compromises, and Future Engine Applications. SAE Tech. Pap. 1999-01-3682, 1999. doi:10.4271/1999-01-3682.

[117] Wang X, Huang Z, Zhang W, Kuti OA, Nishida K. Effects of ultra-high injection pressure and micro-hole nozzle on flame structure and soot formation of impinging diesel spray. Appl Energy 2011;88:1620–8. doi:10.1016/j.apenergy.2010.11.035.

[118] Christensen M, Johansson B, Amneus P, Mauss F. Supercharged homogeneous charge compression ignition. SAE Tech. Pap. 980787, 1998. doi:10.4271/980787.

[119] Law D, Kemp D, Allen J, Kirkpatrick G, Copland T. Controlled Combustion in an IC-Engine with a Fully Variable Valve Train. SAE 2001-01-0251, 2001. doi:10.4271/2001-01-0251.

[120] Flowers D, Aceves S, Smith R, Au M, Girard J, Dibble R. Operation of a Four-cylinder 1 . 9L Propane Fueled Homogeneous Charge Compression Ignition Engine : Basic Operating Characteristics and Cylinder-to Cylinder Effects. SAE 2001-01-1895, 2001.

[121] Machrafi H, Cavadiasa S. An experimental and numerical analysis of the influence of the inlet temperature, equivalence ratio and compression ratio on the HCCI auto-ignition process of Primary Reference Fuels in an engine. Fuel Process Technol 2008;89:1218–26. doi:10.1016/j.fuproc.2008.05.019.

[122] Aceves SM, Flowers D, Smith JR, Dibble R. HCCI . Engine Control by Thermal Management. SAE 2000-01-2869, 2000.

[123] Valentino G, Corcione FE, Iannuzzi SE, Serra S. Experimental study on performance and emissions of a high speed diesel engine fuelled with n-butanol diesel blends under premixed low temperature combustion. Fuel 2012;92:295–307. doi:10.1016/j.fuel.2011.07.035.

[124] Xie F-X, Li X-P, Wang X-C, Su Y, Hong W. Research on using EGR and ignition timing to control load of a spark-ignition engine fueled with methanol. Appl Therm Eng 2013;50:1084–91. doi:10.1016/j.applthermaleng.2012.08.003.

[125] Olsson J, Tunestål P, Ulfvik J, Johansson B. The Effect of Cooled EGR on Emissions and Performance of a Turbocharged HCCI Engine. SAE Tech. Pap. 2003-01-0743, 2003. doi:10.4271/2003-01-0743.

[126] Hiraya K, Hasegawa K, Urushihara T, Iiyama A, Itoh T. A Study on Gasoline Fueled Compression Ignition Engine ～ A Trial of Operation Region Expansion. SAE 2002-01-0416, 2002. doi:10.4271/2002-01-0416.

[127] Murase E, Hanada K. Control of the Start of HCCI Combustion by Pulsed Flame Jet. SAE 2002-01-2867, 2002. doi:10.4271/2002-01-2867.

[128] Christensen M, Johansson B. Homogeneous Charge Compression Ignition with Water Injection. SAE Pap 1999;1999-01–01. doi:10.4271/1999-01-0182.

[129] Christensen M, Johansson B. Supercharged Homogeneous Charge Compression Ignition (HCCI) with Exhaust Gas Recirculation and Pilot Fuel. SAE Tech. Pap. 2000-01-1835, 2000. doi:10.4271/2000-01-1835.

[130] Au MY, Girard JW, Dibble R, Flowers D, Aceves SM, Martinez-Frias J, et al. 1.9-Liter Four-Cylinder HCCI Engine Operation with Exhaust Gas Recirculation. SAE Tech. Pap. 2001-01-1894, 2001. doi:10.4271/2001-01-1894.

[131] LEE T, REITZ RD. The Effect of Intake Boost Pressure on MK (Modulated Kinetics) Combustion. JSME Int J Ser B 2003;46:451–9. doi:10.1299/jsmeb.46.451.

[132] Bengtsson J, Gafvert M, Strandh P. Modeling of HCCI engine combustion for control analysis. 2004 43rd IEEE Conf. Decis. Control (IEEE Cat. No.04CH37601), vol. 2, IEEE; 2004, p. 1682–1687 Vol.2. doi:10.1109/CDC.2004.1430286.

[133] Tanaka S, Ayala F, Keck JC, Heywood JB. Two-stage ignition in HCCI combustion and HCCI control by fuels and additives. Combust Flame 2003;132:219–39. doi:10.1016/S0010-2180(02)00457-1.

[134] Saxena S, Vuilleumier D, Kozarac D, Krieck M, Dibble R, Aceves S. Optimal operating conditions for wet ethanol in a HCCI engine using exhaust gas heat recovery. Appl Energy 2014;116:269–77. doi:10.1016/j.apenergy.2013.11.033.

[135] Sjöberg M, Dec JE. Effects of EGR and its constituents on HCCI autoignition of ethanol. Proc Combust Inst 2011;33:3031–8. doi:10.1016/j.proci.2010.06.043.

[136] Willand J, Nieberding R-G, Vent G, Enderle C. The Knocking Syndrome - Its Cure and Its Potential, 1998. doi:10.4271/982483.

[137] Christensen M, Johansson B, Einewall P. Homogeneous Charge Compression Ignition (HCCI) Using Isooctane, Ethanol and Natural Gas - A Comparison with Spark Ignition Operation. 1997. doi:10.4271/972874.

[138] Epping K, Aceves S, Bechtold R, Dec JE. The Potential of HCCI Combustion for High Efficiency and Low Emissions, 2002. doi:10.4271/2002-01-1923.

[139] Ryan TW, Matheaus AC. Fuel Requirements for HCCI Engine Operation, 2003. doi:10.4271/2003-01-1813.

[140] Kalghatgi G, Risberg P, Ångstrom H-E. A Method of Defining Ignition Quality of Fuels in HCCI Engines, 2003. doi:10.4271/2003-01-1816.

[141] Kalghatgi GT. Auto-Ignition Quality of Practical Fuels and Implications for Fuel Requirements of Future SI and HCCI Engines. 2005. doi:10.4271/2005-01-0239.

[142] Shibata G, Oyama K, Urushihara T, Nakano T. The Effect of Fuel Properties on Low and High Temperature Heat Release and Resulting Performance of an HCCI Engine 2004.

[143] Shibata G, Oyama K, Urushihara T, Nakano T. Correlation of Low Temperature Heat Release With Fuel Composition and HCCI Engine Combustion, 2005. doi:10.4271/2005-01-0138.

[144] Hosseini V, Neill WS, Guo H, Chippior WL, Fairbridge C, Mitchell K. Effects of different cetane number enhancement strategies on HCCI combustion and emissions n.d. doi:10.1177/1468087410395873.

[145] Ickes AM, Bohac S V, Assanis DN, Lay WE. Effect of fuel cetane number on a premixed diesel combustion mode n.d. doi:10.1243/14680874JER03809.

[146] Szybist JP, Bunting BG. Cetane Number and Engine Speed Effects on Diesel HCCI Performance and Emissions, 2005. doi:10.4271/2005-01-3723.

[147] Risberg P, Kalghatgi G, Ångstrom H-E, Wåhlin F. Auto-ignition quality of Diesel-like fuels in HCCI engines, 2005. doi:10.4271/2005-01-2127.

[148] Li T, Okabe Y, Izumi H, Shudo T, Ogawa H. Dependence of Ultra-High EGR Low Temperature Diesel Combustion on Fuel Properties, 2006. doi:10.4271/2006-01-3387.

[149] Aroonsrisopon T, Foster DE, Morikawa T, Iida M. Comparison of HCCI Operating Ranges for Combinations of Intake Temperature, Engine Speed and Fuel Composition, 2002. doi:10.4271/2002-01-1924.

[150] Maurya RK, Agarwal AK. Experimental study of combustion and emission characteristics of ethanol fuelled port injected homogeneous charge compression ignition (HCCI) combustion engine. Appl Energy 2011;88:1169–80. doi:10.1016/j.apenergy.2010.09.015.

[151] Bunting BG, Crawford RW, Wolf LR, Xu Y. The Relationships of Diesel Fuel Properties, Chemistry, and HCCI Engine Performance as Determined by Principal Components Analysis, 2007. doi:10.4271/2007-01-4059.

[152] Bunting BG, Wildman CB, Szybist JP, Lewis S, Storey J. Fuel chemistry and cetane effects on diesel homogeneous charge compression ignition performance, combustion, and emissions. Int J Engine Res 2007;8:15–27. doi:10.1243/14680874JER01306.

[153] Bunting BG, Eaton SJ, Crawford RW. Performance Evaluation and Optimization of Diesel Fuel Properties and Chemistry in an HCCI Engine. SAE Tech Pap 2009-01-2645 2009;4970. doi:10.4271/2009-01-2645.

[154] Sato S, Iida N. Analysis of DME Homogeneous Charge Compression Ignition Combustion. SAE Tech. Pap. 2003-01-1825, 2003. doi:10.4271/2003-01-1825.

[155] Mosbach S, Kraft M, Bhave A, Mauss F, Mack JH, Dibble RW. Simulating a Homogeneous Charge Compression Ignition Engine Fuelled with a DEE/EtOH Blend. SAE Tech. Pap. 2006-01-1362, 2006. doi:10.4271/2006-01-1362.

[156] Konno M, Chen Z. Ignition Mechanisms of HCCI Combustion Process Fueled With Methane/DME Composite Fuel. SAE Tech. Pap. 2005-01-0182, 2005. doi:10.4271/2005-01-0182.

[157] Aceves S, Dibble R, Flowers D, Smith JR, Westbrook CK. Sensitivity of natural gas HCCI combustion to fuel and operating parameters using detailed kinetic modeling. Int. Mech. Eng. Congr. Expo. Nashville, TN (US), 11/14/1999, Lawrence Livermore National Laboratory; 1999.

[158] Nagarajan G, MillerJothi NK, Renganarayanan S. A NEW APPROACH FOR UTILISATION OF LPG - DEE IN HOMOGENEOUS CHARGE COMPRESSION IGNITION (HCCI) ENGINE. SAE Tech. Pap. 2004-28-0020, 2004. doi:10.4271/2004-28-0020.

[159] Yeom K, Jang J, Bae C. Homogeneous charge compression ignition of LPG and gasoline using variable valve timing in an engine. Fuel 2007;86:494–503. doi:10.1016/j.fuel.2006.07.027.

[160] Oh C, Jang J, Bae C. The Effect of LPG Composition on Combustion and Performance in a DME-LPG Dual-fuel HCCI Engine. SAE Tech. Pap. 2010-01-0336, 2010. doi:10.4271/2010-01-0336.

[161] Shibata G, Ogawa H. HCCI Combustion Control by DME-Ethanol Binary Fuel and EGR. SAE Tech. Pap. 2012-01-1577, 2012. doi:10.4271/2012-01-1577.

[162] Mack JH, Aceves SM, Dibble RW. Demonstrating direct use of wet ethanol in a homogeneous charge compression ignition (HCCI) engine. Energy 2009;34:782–7. doi:10.1016/j.energy.2009.02.010.

[163] Zhang H, Hasegawa R, Ogawa H. Improvement in DME-HCCI Combustion with Ethanol as a Low-Temperature Oxidation Inhibitor. SAE Int J Fuels Lubr 2011;5:2011-01–1791. doi:10.4271/2011-01-1791.

[164] Lü X, Ji L, Zu L, Hou Y, Huang C, Huang Z. Experimental study and chemical analysis of n-heptane homogeneous charge compression ignition combustion with port injection of reaction inhibitors. Combust Flame 2007;149:261–70. doi:10.1016/j.combustflame.2007.01.002.

[165] Clothier PQE, Moise A, Pritchard HO. Effect of free-radical release on diesel ignition delay under simulated cold-starting conditions. Combust Flame 1990;81:242–50. doi:10.1016/0010-2180(90)90022-J.

[166] Khaliq A, Trivedi SK, Dincer I. Investigation of a wet ethanol operated HCCI engine based on first and second law analyses. Appl Therm Eng 2011;31:1621–9. doi:10.1016/j.applthermaleng.2011.02.001.

[167] Rashedul HK, Kalam MA, Masjuki HH, Ashraful AM, Imtenan S, Sajjad H, et al. Numerical study on convective heat transfer of a spark ignition engine fueled with bioethanol. Int Commun Heat Mass Transf 2014;58:33–9. doi:10.1016/j.icheatmasstransfer.2014.08.019.

[168] Sakhrieh A, Abu-Nada E, Al-Hinti I, Al-Ghandoor A, Akash B. Computational thermodynamic analysis of compression ignition engine. Int Commun Heat Mass Transf 2010;37:299–303. doi:10.1016/j.icheatmasstransfer.2009.11.002.

[169] Ge Y, Chen L, Sun F, Wu C. Effects of heat transfer and friction on the performance of an irreversible air-standard miller cycle. Int Commun Heat Mass Transf 2005;32:1045–56. doi:10.1016/j.icheatmasstransfer.2005.02.002.

[170] Akash BA. Effect of heat transfer on the performance of an ait-standard diesel cycle. Int Commun Heat Mass Transf 2001;28:87–95. doi:10.1016/S0735-1933(01)00216-0.

[171] Ozsoysal OA. Heat loss as a percentage of fuel's energy in air standard Otto and Diesel cycles. Energy Convers Manag 2006;47:1051–62. doi:10.1016/j.enconman.2005.06.020.

[172] Al-Sarkhi A, Jaber JO, Abu-Qudais M, Probert SD. Effects of friction and temperature-dependent specific-heat of the working fluid on the performance of a Diesel-engine. Appl Energy 2006;83:153–65. doi:10.1016/j.apenergy.2005.01.001.

[173] Al-Sarkhi A, Jaber JO, Probert SD. Efficiency of a Miller engine. Appl Energy 2006;83:343–51. doi:10.1016/j.apenergy.2005.04.003.

[174] Ge Y, Chen L, Sun F, Wu C. Thermodynamic simulation of performance of an Otto cycle with heat transfer and variable specific heats of working fluid. Int J Therm Sci 2005;44:506–11. doi:10.1016/j.ijthermalsci.2004.10.001.

[175] Sakthivel G, Ilangkumaran M, Nagarajan G, Shanmugam P. Selection of best biodiesel blend for IC engines: an integrated approach with FAHP-TOPSIS and FAHP-VIKOR. Int J Oil, Gas Coal Technol 2013;6:581–96. doi:10.1504/ijogct.2013.056153.

[176] Sakthivel G, Ilangkumaran M, Gaikwad A. A hybrid multi-criteria decision modeling approach for the best biodiesel blend selection based on ANP-TOPSIS analysis. Ain Shams Eng J 2015;6:239–56. doi:10.1016/j.asej.2014.08.003.

[177] Garcia MS, Lamata MT, Verdegay JL. PC-TOPSIS Method for the Selection of a Cleaning System for Engine Maintenance. Anal. Des. Intell. Syst. using Soft Comput. Tech., Berlin, Heidelberg: Springer Berlin Heidelberg; 2007, p. 519–29. doi:10.1007/978-3-540-72432-2_53.

[178] Soufi MD, Ghobadian B, Najafi G, Sabzimaleki MR, Yusaf T. TOPSIS multi-criteria decision modeling approach for biolubricant selection for two-stroke petrol engines. Energies 2015;8:13960–70. doi:10.3390/en81212408.

[179] Etghani MM, Shojaeefard MH, Khalkhali A, Akbari M. A hybrid method of modified NSGA-II and TOPSIS to optimize performance and emissions of a diesel engine using biodiesel. Appl Therm Eng 2013;59:309–15. doi:10.1016/j.applthermaleng.2013.05.041.

[180] Garcia-Cascales MS, Lamata MT. Multi-criteria analysis for a maintenance management problem in an engine factory: Rational choice. J. Intell. Manuf., vol. 22, 2011, p. 779–88. doi:10.1007/s10845-009-0290-x.

[181] Sarkar A. A TOPSIS method to evaluate the technologies. Int J Qual Reliab Manag 2013;31:2–13. doi:10.1108/IJQRM-03-2013-0042.

[182] Rezaei J, Shahbakhti M, Bahri B, Aziz AA. Performance prediction of HCCI engines with oxygenated fuels using artificial neural networks. Appl Energy 2015;138:460–73. doi:10.1016/j.apenergy.2014.10.088.

[183] Taghavifar H, Taghavifar H, Mardani A, Mohebbi A, Khalilarya S, Jafarmadar S. Appraisal of artificial neural networks to the emission analysis and prediction of CO2, soot, and NOx of n-heptane fueled engine. J Clean Prod 2015. doi:10.1016/j.jclepro.2015.03.035.

[184] Soufi MD, Ghobadian B, Najafi G, Sabzimaleki M, Jaliliantabar F. Performance and Exhaust Emissions of a SI Two-stroke Engine with Biolubricants Using Artificial Neural Network. Energy Procedia 2015;75:3–9. doi:10.1016/j.egypro.2015.07.127.

[185] Haghighi EA, Jafarmadar S, Taghavifar H. Application of ANN-ICA Hybrid Algorithm toward Prediction of Engine Power and Exhaust Emissions 2013;3.

[186] Özener O, Yüksek L, Özkan M. Artificial neural network approach to predicting engine-out emissions and performance parameters of a turbo charged diesel engine. Therm Sci 2013;17:153–66. doi:10.2298/TSCI120321220O.

[187] Yusaf TF, Buttsworth DR, Saleh KH, Yousif BF. CNG-diesel engine performance and exhaust emission analysis with the aid of artificial neural network. Appl Energy 2010;87:1661–9. doi:10.1016/j.apenergy.2009.10.009.

[188] Najafi G, Ghobadian B, Tavakoli T, Buttsworth DR, Yusaf TF, Faizollahnejad M. Performance and exhaust emissions of a gasoline engine with ethanol blended gasoline fuels using artificial neural network. Appl Energy 2009;86:630–9. doi:10.1016/j.apenergy.2008.09.017.

[189] Sayin C, Ertunc HM, Hosoz M, Kilicaslan I, Canakci M. Performance and exhaust emissions of a gasoline engine using artificial neural network. Appl Therm Eng 2007;27:46–54. doi:10.1016/j.applthermaleng.2006.05.016.

[190] Hossein Soukht Saraee, Samad Jafarmadar, Elnaz Alizadeh-Haghighi and SJA. Experimental Investigation of Pollution and Fuel Consumption on a CI Engine Operated on Alumina Nanoparticles—Diesel Fuel with the Aid of Artificial Neural Network. Environ Prog Sustain Energy 2015;0. doi:DOI 10.1002/ep.12233.

[191] Roy S, Banerjee R, Bose PK. Performance and exhaust emissions prediction of a CRDI assisted single cylinder diesel engine coupled with EGR using artificial neural network. Appl Energy 2014;119:330–40. doi:10.1016/j.apenergy.2014.01.044.

[192] Çay Y, Çiçek A, Kara F, Sağiroğlu S. Prediction of engine performance for an alternative fuel using artificial neural network. Appl Therm Eng 2012;37:217–25. doi:10.1016/j.applthermaleng.2011.11.019.

[193] Mohamed Ismail H, Ng HK, Queck CW, Gan S. Artificial neural networks modelling of engine-out responses for a light-duty diesel engine fuelled with biodiesel blends. Appl Energy 2012;92:769–77. doi:10.1016/j.apenergy.2011.08.027.

[194] Çay Y, Korkmaz I, Çiçek A, Kara F. Prediction of engine performance and exhaust emissions for gasoline and methanol using artificial neural network. Energy 2013;50:177–86. doi:10.1016/j.energy.2012.10.052.

[195] Deh Kiani MK, Ghobadian B, Tavakoli T, Nikbakht AM, Najafi G. Application of artificial neural networks for the prediction of performance and exhaust emissions in SI engine using ethanol-gasoline blends. Energy 2010;35:65–9. doi:10.1016/j.energy.2009.08.034.

[196] Hosoz M, Ertunc HM, Karabektas M, Ergen G. ANFIS modelling of the performance and emissions of a diesel engine using diesel fuel and biodiesel blends. Appl Therm Eng 2013;60:24–32. doi:10.1016/j.applthermaleng.2013.06.040.

[197] Oğuz H, Sarıtas I, Baydan HE. Prediction of diesel engine performance using biofuels with artificial neural network. Expert Syst Appl 2010;37:6579–86. doi:10.1016/j.eswa.2010.02.128.

[198] Zurita G V., Peña JC. Vibration based reconstruction of the cylinder pressure in diesel engines by using neural networks. Investig Y Desarro 2005;60:53–60.

[199] Choi Y, Chen J-Y. Fast prediction of start-of-combustion in HCCI with combined artificial neural networks and ignition delay model. Proc Combust Inst 2005;30:2711–8. doi:10.1016/j.proci.2004.08.143.

[200] Piloto-Rodríguez R, Sánchez-Borroto Y, Lapuerta M, Goyos-Pérez L, Verhelst S. Prediction of the cetane number of biodiesel using artificial neural networks and multiple linear regression. Energy Convers Manag 2013;65:255–61. doi:10.1016/j.enconman.2012.07.023.

[201] Jabbr AI, Vaz WS, Khairallah HA, Koylu UO. Multi-objective optimization of operating parameters for hydrogen-fueled spark-ignition engines. Int J Hydrogen Energy 2016;41:18291–9. doi:10.1016/j.ijhydene.2016.08.016.

[202] De Risi A, Donateo T, Laforgia D. Optimization of the combustion chamber of direct injection diesel engines. SAE Tech Pap 2003. doi:10.4271/2003-01-1064.

[203] Park SW. Optimization of combustion chamber geometry for stoichiometric diesel combustion using a micro genetic algorithm. Fuel Process Technol 2010;91:1742–52. doi:10.1016/j.fuproc.2010.07.015.

[204] Wickman DD, Senecal PK, Reitz RD. Diesel engine combustion chamer geometry optimization using genetic algorithms and multi-dimensional spray and combustion modeling. SAE Tech Pap 2001-01-0547 2001. doi:10.4271/2001-01-0547.

[205] Kesgin U. Genetic algorithm and artificial neural network for engine optimisation of efficiency and NOx emission. Fuel 2004;83:885–95. doi:10.1016/j.fuel.2003.10.025.

[206] Hiroyasu T, Miki M, Kamiura J, Watanabe S, Hiroyasu H. Multi-Objective Optimization of Diesel Engine Emissions and Fuel Economy using Genetic Algorithms and Phenomenological Model. SAE Tech. Pap. 2002-01-2778, 2002. doi:10.4271/2002-01-2778.

[207] Mohammadhassani J, Dadvand A, Khalilarya S, Solimanpur M. Prediction and reduction of diesel engine emissions using a combined ANN – ACO method. Appl Soft Comput J 2015;34:139–50. doi:10.1016/j.asoc.2015.04.059.

[208] Mousa AA, El-Shorbagy MA, Abd-El-Wahed WF. Local search based hybrid particle swarm optimization algorithm for multiobjective optimization. Swarm Evol Comput 2012;3:1–14. doi:10.1016/j.swevo.2011.11.005.

[209] Mozaffari A, Azad NL. An ensemble neuro-fuzzy radial basis network with self-adaptive swarm based supervisor and negative correlation for modeling automotive engine coldstart hydrocarbon emissions: A soft solution to a crucial automotive problem. Appl Soft Comput 2015;32:449–67. doi:10.1016/j.asoc.2015.04.009.

[210] Roy S, Das AK, Bose PK, Banerjee R. ANN metamodel assisted Particle Swarm Optimization of the performance-emission trade-off characteristics of a single cylinder CRDI engine under CNG dual-fuel operation. J Nat Gas Sci Eng 2014;21:1156–62. doi:10.1016/j.jngse.2014.11.013.

[211] Burgess WA, Ellenbecker MJ, Treitman RD. Ventilation for control of the work environment. Wiley-Interscience; 2004.

[212] Anemometer 2016. https://en.wikipedia.org/wiki/Anemometer (accessed October 26, 2016).

[213] Nondispersive infrared sensor 2016. https://en.wikipedia.org/wiki/Nondispersive_infrared_sensor (accessed September 26, 2016).

[214] NDIR Gas Sensor Light Sources | ILT. Int Light Technol 2016. http://www.intl-lighttech.com/applications/light-sources/ndir-gas-sensor-lamps (accessed August 28, 2016).

[215] How to Design Electronic Sensors Incorporating Electrochemical Gas Sensors 2016. http://www.azosensors.com/article.aspx?ArticleID=543 (accessed August 28, 2016).

[216] Chou T-Y, Chou ST, Tzeng G-H. Evaluating IT/IS investments: A fuzzy multi-criteria decision model approach. Eur J Oper Res 2006;173:1026–46. doi:10.1016/j.ejor.2005.07.003.

[217] The decision making process 2016. http://www.quesucede.com/page/show/id/decision-making (accessed October 2, 2016).

[218] Chandwani RK, Dwivedi YK. Telemedicine in India: current state, challenges and opportunities. Transform Gov People, Process Policy 2015;9:393–400. doi:10.1108/TG-07-2015-0029.

[219] Velasquez M, Hester PT. An Analysis of Multi-Criteria Decision Making Methods. Int J Oper Res 2013;10:56–66.

[220] Cay Y. Prediction of a gasoline engine performance with artificial neural network. Fuel 2013;111:324–31. doi:10.1016/j.fuel.2012.12.040.

[221] Tasdemir S, Saritas I, Ciniviz M, Allahverdi N. Artificial neural network and fuzzy expert system comparison for prediction of performance and emission parameters on a gasoline engine. Expert Syst Appl 2011;38:13912–23. doi:10.1016/j.eswa.2011.04.198.

[222] Al-Hinti I, Samhouri M, Al-Ghandoor A, Sakhrieh A. The effect of boost pressure on the performance characteristics of a diesel engine: A neuro-fuzzy approach. Appl Energy 2009;86:113–21. doi:10.1016/j.apenergy.2008.04.015.

[223] Rai A, Kumar NS, P. SP, Rao BRS. Fuzzy Logic Based Prediction of Performance and Emission

Parameters of a LPG-Diesel Dual Fuel Engine. Procedia Eng 2012;38:280–92. doi:10.1016/j.proeng.2012.06.036.

[224] Djermouni M, Ouadha A. Thermodynamic analysis of an HCCI engine based system running on natural gas. Energy Convers Manag 2014;88:723–31. doi:10.1016/j.enconman.2014.09.033.

[225] Fathi M, Jahanian O, Shahbakhti M. Modeling and controller design architecture for cycle-by-cycle combustion control of homogeneous charge compression ignition (HCCI) engines – A comprehensive review. Energy Convers Manag 2017;139:1–19. doi:10.1016/j.enconman.2017.02.038.

[226] Soyhan HS, Yasar H, Walmsley H, Head B, Kalghatgi GT, Sorusbay C. Evaluation of heat transfer correlations for HCCI engine modeling. Appl Therm Eng 2009;29:541–9. doi:10.1016/j.applthermaleng.2008.03.014.

[227] Dehghani Firoozabadi M, Shahbakhti M, Koch CRR, Jazayeri SA a. Thermodynamic control-oriented modeling of cycle-to-cycle exhaust gas temperature in an HCCI engine. Appl Energy 2013;110:236–43. doi:10.1016/j.apenergy.2013.04.055.

[228] Gupta DK, Goyal R, Kumar R, Nadim Shams M. A thermodynamic analysis of a hydrogen enriched compressed natural gas fuelled HCCI engine. Int J Appl Eng Res 2013;8:2051–5.

[229] Neshat E, Saray RK. Effect of different heat transfer models on HCCI engine simulation. Energy Convers Manag 2014;88:1–14. doi:10.1016/j.enconman.2014.07.075.

[230] Trivedi SK, Haleem A. Thermodynamic analysis and utilisation of wet ethanol in homogeneous charge compression ignition engine. Int J Sustain Energy 2016;35:33–46. doi:10.1080/14786451.2013.858718.

[231] Abu-Nada E, Al-Hinti I, Al-Sarkhi a., Akash B. Thermodynamic modeling of spark-ignition engine: Effect of temperature dependent specific heats. Int Commun Heat Mass Transf 2006;33:1264–72. doi:10.1016/j.icheatmasstransfer.2006.06.014.

[232] Burcat a, Branko R. Third millennium ideal gas and condensed phase thermochemical database for combustion with updates from active thermochemical tables. Tech Rep 2005;ANL-05/20:ANL-05/20 TAE 960. doi:10.2172/925269.

[233] Hedfi H, Jedli H, Jbara A, Slimi K. Modeling of a bioethanol combustion engine under different operating conditions. Energy Convers Manag 2014;88:808–20. doi:10.1016/j.enconman.2014.09.035.

[234] Davis SG, Joshi A V., Wang H, Egolfopoulos F. An optimized kinetic model of H2/CO combustion. Proc Combust Inst 2005;30:1283–92. doi:10.1016/j.proci.2004.08.252.

[235] Singh AP, Agarwal AK. An experimental investigation of combustion, emissions and performance of a diesel fuelled HCCI engine. SAE Tech Pap 2012-28-0005 2012:DOI: 10.4271/2012-28-0005. doi:10.4271/2012-28-0005.

[236] Aithal SM. Modeling of NOx formation in diesel engines using finite-rate chemical kinetics. Appl Energy 2010;87:2256–65. doi:10.1016/j.apenergy.2010.01.011.

[237] Mellor AM, Mello JP, Duffy KP, Easley WL, Faulkner JC. Skeletal Mechanism for NOx Chemistry in Diesel Engines, 1998. doi:10.4271/981450.

[238] Khan A, Maity K. Application of MCDM-Based TOPSIS Method for the Optimization of Multi Quality Characteristics of Modern Manufacturing Processes. Int J Eng Res Africa 2016;23:33–51. doi:10.4028/www.scientific.net/JERA.23.33.

[239] Renno C, Petito F, Gatto A. Artificial neural network models for predicting the solar radiation as input of a concentrating photovoltaic system. Energy Convers Manag 2015;106:999–1012. doi:10.1016/j.enconman.2015.10.033.

[240] Janakiraman VM, Nguyen X, Assanis D. Nonlinear identification of a gasoline HCCI engine using neural networks coupled with principal component analysis. Appl Soft Comput 2013;13:2375–89. doi:10.1016/j.asoc.2013.01.006.

[241] Nawi NM, Atomi WH, Rehman MZ. The Effect of Data Pre-processing on Optimized Training of Artificial Neural Networks. Procedia Technol 2013;11:32–9. doi:10.1016/j.protcy.2013.12.159.

[242] Ramsami P, Oree V. A hybrid method for forecasting the energy output of photovoltaic systems. Energy Convers Manag 2015;95:406–13. doi:10.1016/j.enconman.2015.02.052.

[243] Ibrić S, Djuriš J, Parojčić J, Djurić Z. Artificial neural networks in evaluation and optimization of modified release solid dosage forms. Pharmaceutics 2012;4:531–50. doi:10.3390/pharmaceutics4040531.

[244] Demirhan H, Kayhan Atilgan Y. New horizontal global solar radiation estimation models for Turkey based on robust coplot supported genetic programming technique. Energy Convers Manag 2015;106:1013–23. doi:10.1016/j.enconman.2015.10.038.

[245] Taylan O, Kaya D, Demirbas A. An integrated multi attribute decision model for energy efficiency processes in petrochemical industry applying fuzzy set theory. Energy Convers Manag 2016;117:501–12. doi:10.1016/j.enconman.2016.03.048.

[246] Wu Y, Zhang J, Yuan J, Geng S, Zhang H. Study of decision framework of offshore wind power station site selection based on ELECTRE-III under intuitionistic fuzzy environment: A case of China. Energy Convers Manag 2016;113:66–81. doi:10.1016/j.enconman.2016.01.020.

[247] Specht D, Shapiro PD. Training Speed Comparison of Probabilistic Neural Networks with Back-Propagation Networks. Proc. Int. Neural Netw. Conf., Paris, France: 1990, p. 440–3.

[248] Specht DF. A general regression neural network. Neural Networks, IEEE Trans 1991;2:568–76. doi:10.1109/72.97934.

[249] Kennedy J, Eberhart R. Particle swarm optimization. Proc. ICNN'95 - Int. Conf. Neural Networks, vol. 4, IEEE; 1995, p. 1942–8. doi:10.1109/ICNN.1995.488968.

[250] Lacey J, Kameshwaran K, Filipi Z, Cannella W, Fuentes-Afflick P. Influence of ethanol addition in refinery stream fuels and the HCCI combustion. Fuel 2014;126:122–33. doi:10.1016/j.fuel.2014.02.041.

[251] Benajes J, Molina S, Novella R, Amorim R. Study on Low Temperature Combustion for Light-Duty Diesel Engines. Energy {&} Fuels 2010;24:355–64. doi:10.1021/ef900832c.

[252] Saxena S, Bedoya ID. Fundamental phenomena affecting low temperature combustion and HCCI engines, high load limits and strategies for extending these limits. Prog Energy Combust Sci 2013;39:457–88. doi:10.1016/j.pecs.2013.05.002.

[253] Bendu H, Murugan S. Homogeneous charge compression ignition (HCCI) combustion: Mixture preparation and control strategies in diesel engines. Renew Sustain Energy Rev 2014;38:732–46. doi:10.1016/j.rser.2014.07.019.

[254] Aceves SM, Flowers DL, Martinez-Frias J, Smith JR, Dibble R, Au M, et al. HCCI Combustion: Analysis and Experiments. SAE Tech Pap 2001-01- 2001. doi:10.4271/2001-01-2077.

[255] Bendu H, Murugan S. Homogeneous charge compression ignition (HCCI) combustion: Mixture preparation and control strategies in diesel engines. Renew Sustain Energy Rev 2014;38:732–46.

[256] Sjoberg M, Dec JE. Ethanol Autoignition Characteristics and HCCI Performance for Wide Ranges of Engine Speed, Load and Boost. SAE Int J Engines 2010;3:84–106. doi:10.4271/2010-01-0338.

[257] Yang Y, Dec JE, Dronniou N, Sjöberg M. Tailoring HCCI heat-release rates with partial fuel stratification: Comparison of two-stage and single-stage-ignition fuels. Proc Combust Inst 2011;33:3047–55. doi:10.1016/j.proci.2010.06.114.

[258] Sjöberg M, Dec JE. Smoothing HCCI Heat-Release Rates Using Partial Fuel Stratification with Two-Stage Ignition Fuels, 2006. doi:10.4271/2006-01-0629.

[259] Xu M, Gui Y, Deng K. Fuel injection and EGR control strategy on smooth switching of CI/HCCI mode in a diesel engine. J Energy Inst 2015;88:157–68. doi:10.1016/j.joei.2014.06.005.

[260] Maurya RK, Agarwal AK. Statistical analysis of the cyclic variations of heat release parameters in

HCCI combustion of methanol and gasoline. Appl Energy 2012;89:228–36. doi:10.1016/j.apenergy.2011.07.002.

[261] Sharma A, Murugan S. Investigation on the behaviour of a DI diesel engine fueled with Jatropha Methyl Ester (JME) and Tyre Pyrolysis Oil (TPO) blends. Fuel 2013;108:699–708. doi:10.1016/j.fuel.2012.12.042.

[262] Kent JH, Wagner HG. Why do Diffusion flames Emit smoke. Combust Sci Technol 1984;41:245–69. doi:10.1080/00102208408923834.

[263] Drysdale D. Smoke: Its Formation, Composition and Movement. An Introd to Fire Dyn 2011:441–74. doi:10.1002/9781119975465.ch11.

[264] Chen H, Shuai SJ, Wang JX. Study on combustion characteristics and PM emission of diesel engines using ester-ethanol-diesel blended fuels. Proc Combust Inst 2007;31 II:2981–9. doi:10.1016/j.proci.2006.07.130.

[265] Kim D, Gautam M, Gera D. Parametric studies on the formation of diesel particulate matter via nucleation and coagulation modes. J Aerosol Sci 2002;33:1609–21. doi:10.1016/S0021-8502(02)00119-2.

[266] Yao Q, Li SQ, Xu HW, Zhuo JK, Song Q. Reprint of: Studies on formation and control of combustion particulate matter in China: A review. Energy 2010;35:4480–93. doi:10.1016/j.energy.2010.08.009.

[267] Chen R, Milovanovic N. A computational study into the effect of exhaust gas recycling on homogeneous charge compression ignition combustion in internal combustion engines fuelled with methane. Int J Therm Sci 2002;41:805–13. doi:10.1016/S1290-0729(02)01375-3.

[268] Pradeep V, Sharma RP. Use of HOT EGR for NOx control in a compression ignition engine fuelled with bio-diesel from Jatropha oil. Renew Energy 2007;32:1136–54. doi:10.1016/j.renene.2006.04.017.

[269] Alger T, Mangold B. Dedicated EGR : A New Concept in High Efficiency Engines. Sae 2013;2:620–31. doi:2009-01-0694.

[270] Bendu H, Deepak BBVL, Murugan S. Application of GRNN for the prediction of performance and exhaust emissions in HCCI engine using ethanol. Energy Convers Manag 2016;122:165–73. doi:10.1016/j.enconman.2016.05.061.

[271] Chichkova RI. Carbon monoxide intoxication: An updated review. J Neurol Sci 2007;262:122–30. doi:10.1016/j.jns.2007.06.037.

[272] Thom SR. Hyperbaric-Oxygen Therapy for Acute Carbon Monoxide Poisoning. N Engl J Med 2002;347:1105–6. doi:10.1056/NEJMe020103.

[273] Venkataraman C, Rao GUM. Emission Factors of Carbon Monoxide and Size-Resolved Aerosols from Biofuel Combustion. Environ Sci Technol 2001;35:2100–7. doi:10.1021/es001603d.

[274] Piantadosi CA. Carbon Monoxide Poisoning. N Engl J Med 2002;347:1054–5. doi:10.1056/NEJMp020104.

[275] Habib MA, Elshafei M, Dajani M. Influence of combustion parameters on NOx production in an industrial boiler. Comput Fluids 2008;37:12–23. doi:10.1016/j.compfluid.2007.04.006.

[276] Monyem A, H. Van Gerpen J. The effect of biodiesel oxidation on engine performance and emissions. Biomass and Bioenergy 2001;20:317–25. doi:10.1016/S0961-9534(00)00095-7.

[277] Srinivasa Pai P, Shrinivasa Rao BR. Artificial Neural Network based prediction of performance and emission characteristics of a variable compression ratio CI engine using WCO as a biodiesel at different injection timings. Appl Energy 2011;88:2344–54. doi:10.1016/j.apenergy.2010.12.030.

Appendix A1

Test engine technical specifications

Engine parameters	
Model	TAF 1
Make	Kirloskar
Maximum power	4.4 kW
Rated speed	1500 rpm
Bore x stroke	87.5 mm x 110 mm
Piston type	Bowl-in-piston
Compression ratio	17.5:1
Connecting rod length	220 mm
Cooling system	Air cooling
Number of valves	2
Intake valve opening/closing	4.5° bTDC/35.5º aBDC
Exhaust valve opening/closing	35.5° bBDC/4.5º aTDC
Weight	163 kg

Appendix A2

Technical specifications of the pressure transducer

Description	Data
Make	KISTLER, Switzerland
Model	5395A
Colling type	Air cooled
Range	0-100 bar
Sensitivity	25 mV/bar
Linearity	0.1 <+ % FSO
Acceleration sensitivity	< 0.001 bar / g
Operating temperature range	-196 to 200 ºC
Capacitance	5 PF
Weight	1.7 g
Connector, Teflon insulator	M4 x 0.35

Appendix A3

Technical specifications of the charge amplifier

Description	Data
Make	KISLTER instruments, Switzerland
Measuring ranges	12 stages graded pC 10-50000 1:2:5 and stepless 1 to 10
Accuracy of two most sensitive rangesAccuracy of other range stages	<± 3% <± 1%
Linearity, of Transducer sensitivity	<±0.5%
Calibration capacitor	1000 ± 0.5pF
Operating temperature range	-196 to 200 ^{o}C
Calibration input sensitivity	1±0.5 pC/mV
Input voltage, maximum with pulses	+ 12V
Connector, Teflon insulator	M4 x 0.35

Appendix A4

Technical specification of AVL 444 Digas analyser

Measured quantity	Measuring range	Accuracy
CO	0-10%	< 0.6% vol: ±0.03% vol ≥ 0.6% vol: ± 5% of initial value
HC	0-20000 ppm vol	< 200 ppm vol: ± 10 ppm vol ≥ 200 ppmvol: ± 5% of initial value
NO	0-5000 ppm vol	< 500 ppm vol: ± 50 ppm vol ≥ 500 ppmvol: ± 10% of initial value

Specification	Range
Voltage	11-22 V DC
Power consumption	≈25W
Warm up time	≈ 7 min
Operating temperature	5-45 ^{o}C
Dimensions (WxDxH)	270x320x85
Weight	4.5 kg net weight without accessories

Appendix A5

Technical specification of AVL 437C diesel smoke meter

Description	Data
Measuring chamber	0-100% opacity
Accuracy and repeatability	±1 % of full scale
Alarming signal temperature	Lights up when temperature of measuring chamber is below 70 ^{o}C
Linearity check	48.4% - 53.1% or 1.54 m^{-1} - 1.54 m^{-1} of measurement range
Measuring chamber length	430 ± 5 mm
Light source	Halogen lamp, 12V
Sensor	Selenium Photocell
Weight	24 kg

Appendix A6

Range, accuracy, and uncertainty of the instruments

Instrument used	Range		Accuracy	% uncertainties
Gas analyzer	CO	0−10 %	±0.03%	±1
	UHC	0−20000 ppm	±10 ppm	±0.5
	NO	0−5000 ppm	±50 ppm	±1
Smoke meter	0−100 % opacity		±1	±1
EGT indicator (K-type chromel – alumel thermocouples)	0–900 °C		±1 °C	±0.15
Pressure transducer	0−110 bar		±0.1	±0.1
Speed sensor	0−10000 rpm		±10 rpm	±1
Crank angle encoder	0−720 °CA		±0.5°	±0.01
Charge amplifier			±1	±0.1
Load indicator	250–6000 W		±10	±0.2

Appendix A7

Technical specification of fuel vaporizer

Description	Data
Material	SS pipe
Vaporizer length	160 mm
Diameter	18 mm
Heating element	Nichrome
Current resistant material	Ceremic beads over heating element
Insulation material	Glasswool
Vaporizer temperature	110±10 °C
Power supply to the heater	500 W
Warm-up time	5 min
Ethanol injection pressure	2.5 bar

Appendix A8

Matlab program for thermodynamic modelling

```
clc; clear all;
N = 1500;   % speed min RPM
D = 87.5e-3; % Bore diameter
Ac = (pi/4)*D^2; % Area of cylinder
ls = 110e-3; % length of the stroke
Vs = Ac*ls; % Swept volume
r = 55e-3;   % Radius of crank = half of stroke length
l = 220e-3; % length of the connecting rod
d = D-1;  % diameter of piston
Ap = (pi/4)*d^2;  % Area of piston
gc = (l/r); % ratio of connecting rod to radius of crank
CR = 17.5; % compression ratio
Vc = Vs/(CR-1); % Clearance volume
Vd = Vc+Vs; % Total volume
mf = 300e-3;   % mass of fuel per cycle
LHV = 26e6;   % Calorific value of the fuel
Qin = mf*LHV;
Vp = 2*ls*N/60; % mean piston speed
w = 6*N;
Tw = 350; % wall temperature in K
dt = 1;   % step angle
%gama = 1.4;         % gas constant
%density = 1.225;    % Density of air 1.225 kg/m3 at sea level and 15 degree centigrade
%m = density*V0;     % mass of air = 26.6 kg/hr
thetaS = deg2rad(-20.5);
CD = deg2rad(60);
CA = -144.5:1:144.5;

fori=1:1:290
theta = deg2rad(-144.5:1:144.5);
Xtm = (l+r)-((r*cos(theta))+sqrt(l^2-((r^2)*(sin(theta).^2))));
Vtm = Vc+(Ac)*Xtm;
Vm0 = 6.5408e-04;
Vtm(i) = Vc+(Ac)*Xtm(i);
%%%%% motoring pressure and temperature
Tm0 = 443;  Pm0 = 1.01325;       % intake temperarure and pressure for motoring
Pr = 1.01325;
Ru = 8.314472;    % Universal gas constant
Cpm = (2.506e-11*Tm0^2)+(1.454e-7*Tm0^1.5)-(4.246e-7.*Tm0)+(3.162e-
5*Tm0^0.5)+(1.3303)-(1.512e4*Tm0-1.5)+(3.063e5*Tm0^-2)-(2.212e7*Tm0-3);
Cvm = Cpm + Ru;  k = Cpm/Cvm;
%Pm(i) = Pr-k.*(Pr./Vtm(i)).*(Vtm(i)-Vm0);
Tm(i) = Tm0.*(6.5408e-04/Vtm(i))^(0.4);
Pm(i) = Pr.*(Tm(i)/413)^(1.2/0.2);
%Pm(i) = (Ru*Tm(i))./Vtm(i);
%Tm(i) = Tm0*(Pm(i)/Pm0)^(0.4/1.4);
Pr = Pm(i);
Tm0 = Tm(i);  Vm0 = Vtm(i);
%%%%%% Cylinder pressure and temperature
Xt = (l+r)-((r*cos(theta))+sqrt(l^2-((r^2)*(sin(theta).^2))));
Vt = Vc+(Ac)*Xt;    V0 = 6.5408e-04;
```

```
Vt(i) = Vc+(Ac)*Xt(i);
T01 = 443;   V01 = 6.5408e-04;  P01 = 1.01325;
Pt(1) = 1.01325;
T0 = 443;  P0 = 1.01325;
Xb0 = 0;   Qloss0 = 0;
if theta(i) >= thetaS
Xb(i) = 1-exp(-4*((theta(i)-thetaS)./CD).^3);
else
Xb(i) = 0.0;
end
Ah = Ap+Ac+(pi*D*ls/2)*(gc+1-cos(theta)-sqrt(gc^2-sin(theta).^2));
if theta(i) >= thetaS
   H = 3.26*(D^-0.2).*(P0.^0.8).*(T0^-0.55).*(2.28*Vp+0.00324*(Vd.*T01/(P01*V01)).*(Pt-
Pm(i))).^0.8;
else
   H = 0.0;
end
Qloss = ((H.*Ah(i))/w)*(T0-Tw)*dt;
Cp = (2.506e-11*T0^2)+(1.454e-7*T0^1.5)-(4.246e-7*T0)+(3.162e-5*T0^0.5)+(1.3303)-
(1.512e4*T0-1.5)+(3.063e5*T0^-2)-(2.212e7*T0-3);
Cv = Cp + Ru;  n(i) = Cp/Cv;
Pt(i) =  P0+((n(i)-1)./Vt(i))*Qin.*(Xb(i)-Xb0)-(dt.*((n(i)-1)./Vt(i)).*Qloss0)-
n(i).*(P0./Vt(i)).*(Vt(i)-V0);
T(i) = T0*(Pt(i)/P0)^(0.4/1.4);
P0 = Pt(i);   T0 = T(i);
Xb0 = Xb;     Qloss0 = Qloss;
V0 = Vt(i);
end
```

Appendix A9

Program to control ECU

```
int analogpin=3;
int data=10;
float rpm;
void setup() {
  // put your setup code here, to run once:
pinMode(11,OUTPUT);

}

void loop() {
  // put your main code here, to run repeatedly:
  rpm=(analogRead(analogpin))*2*3.14;
  if(rpm>1500)
  data-=10;
  else
  data+=10;
digitalWrite(11,HIGH);
delay(data);
digitalWrite(11,LOW);
```

Dissemination

Internationally indexed journals (SCI)

- **Harisankar Bendu**, S Murugan, "Homogeneous charge compression ignition (HCCI) combustion: Mixture preparation and control strategies in diesel engines", Renewable and Sustainable Energy Reviews 38 (2014) 732–746. http://dx.doi.org/10.1016/j.rser.2014.07.019

- **Harisankar Bendu**, Deepak BBVL, S Murugan, "Application of GRNN for the prediction of performance and exhaust emissions in HCCI engine using ethanol", Energy Conversion and Management 122 (2016): 165-173. http://dx.doi.org/10.1016/j.enconman.2016.05.061

- **Harisankar Bendu**, S Murugan, "Experimental investigation on the effect of charge temperature on ethanol fueled HCCI combustion engine", Journal of Mechanical Science and Technology 30 (10) (2016) 4791–4799. http://dx.doi.org/10.1007/s12206-016-0951-6

- **Harisankar Bendu**, Deepak BBVL, S Murugan, "Multi-objective optimization of ethanol fuelled HCCI engine performance using hybrid GRNN−PSO", Applied Energy 187 (2017), 601-611. http://dx.doi.org/10.1016/j.apenergy.2016.11.072.

Conference publications

- "A study on performance and emission characteristics of HCCI engine fueled with ethanol", International conference on mechanical, material and manufacturing systems (ICMMMS16), Sri Sairam Engineering College, Chennai.

- "Performance and emission studies on HCCI combustion engine fueled with ethanol and diethyl ether blends", International conference on Emerging Trends in Mechanical Engineering, Technocrats Institute of Technology, Bhopal, held during May 27-28, 2016.

Article under preperation

- **Harisankar Bendu**, S Murugan, " Thermodynamic modelling of ethanol fueled HCCI engine under different operating conditions". (Submitted to the conference)
- **Harisankar Bendu**, S Murugan, "A multi-criteria decision modelling approach for the best charge temperature selection based on TOPSIS analysis". (Article under preperation)

CURRICULUM VITAE

HARISANKAR BENDU

Contact information

Permanent address

H.No 2-93,
Muddada village & post,
Gujarathi peta,
Srikakulam District,
Andhra Pradesh.
PIN 532005

Present address

Room No-D105, Vikram Sarabhai Hall of Residence, NIT Rourkela, Rourkela, India, 769008.

Mobile No +917008035481.

E-mail

sankar340@gmail.com

hsbendu@gmail.com

Objective

A challenging research oriented, high performance technology driven with an intellectual, team spirit in which I can make the bright carrier of students.

Qualifications

- **Ph.D.** (2012–2016)
  (Department of Mechanical Engineering)

  National Institute of Technology Rourkela.

- **M.Tech** (2008–2010)
  (Department of Mechanical Engineering)

  Specialization: Thermal Engineering

  National Institute of Technology Rourkela.

- **B.Tech** (2004–2008)
  (Department of Mechanical Engineering)

  GMR Institute of Technology, under JNTU Hyderabad.

- **Intermediate** (2002–2004)
  Sri Chaitanya junior college, Vishakhapatnam.

- **High School (**2002)
  Vivekavardhani School, Srikakulam.

Teaching experience

- 2011–2012
  Assistant Professor at GMR Institute of Technology, Andhra Pradesh.
- 2010–2011
  Assistant Professor at YSR Engineering college of YVU, Andhra Pradesh, India.
- 2016–Present
  Associate Professor at Sri Sivani College of Engineering, Andhra Pradesh.